




16

Spectroscopy 1: rotational and vibrational spectra



General features of spectroscopy

- 16.1 Experimental techniques
- 16.2 The intensities of spectral lines
- 16.3 Linewidths

Pure rotation spectra

- 16.4 Moments of inertia
- 16.5 The rotational energy levels
- 16.6 Rotational transitions
- 16.7 Rotational Raman spectra
- 16.8 Nuclear statistics and rotational states

The vibrations of diatomic molecules

- 16.9 Molecular vibrations
- 16.10 Selection rules
- 16.11 Anharmonicity
- 16.12 Vibration-rotation spectra
- 16.13 Vibrational Raman spectra of diatomic molecules

The vibrations of polyatomic molecules

- 16.14 Normal modes
- 16.15 The vibrational spectra of polyatomic molecules
- 16.16 Vibrational Raman spectra of polyatomic molecules

Checklist of key ideas

Further reading

Exercises

Problems

The general strategy we adopt in the chapter is to set up expressions for the energy levels of molecules, and then to apply selection rules and considerations of populations to infer the form of spectra. Rotational energy levels are considered first, and we see how to derive expressions for their values and then how to interpret rotational spectra in terms of molecular dimensions. Not all molecules can occupy all rotational states: we see the experimental evidence for this restriction and its explanation in terms of nuclear spin and the Pauli principle. Next, we consider the vibrational energy levels of diatomic molecules, and see that we can use the properties of harmonic oscillators developed in Chapter 12. Then we consider polyatomic molecules and find that their vibrations may be discussed as though they consisted of a set of independent harmonic oscillators, so the same approach as that employed for diatomic molecules may be used. We also see that the symmetry properties of the vibrations of polyatomic molecules are helpful for deciding which modes can be studied spectroscopically.

The origin of spectral lines in molecular spectroscopy is the emission or absorption of a photon when the energy of a molecule changes. The difference from atomic spectroscopy is that the energy of a molecule can change not only as a result of electronic transitions but also because it can undergo changes of rotational and vibrational state. Molecular spectra are therefore more complex than atomic spectra. However, they also contain information relating to more properties, and their analysis leads to values of bond strengths, lengths, and angles. They also provide a way of determining a variety of molecular properties, particularly molecular dimensions, shapes, and dipole moments.

Pure rotational spectra, in which only the rotational state of a molecule changes, can be observed in the gas phase. Vibrational spectra of gaseous samples show features that arise from rotational transitions that accompany the excitation of vibration. Electronic spectra, which are described in Chapter 17, show features arising from simultaneous vibrational and rotational transitions. The simplest way of dealing with these complexities is to tackle each type of transition in turn, and then to see how simultaneous changes affect the appearance of spectra.

General features of spectroscopy

All types of spectra have some features in common, and we examine these first. We shall often need to use the relations between the frequency, ν , wavelength, λ , and wavenumber, $\tilde{\nu}$, of electromagnetic radiation that were first mentioned in the *Introduction*:

$$\lambda = \frac{c}{\nu} \quad \tilde{\nu} = \frac{\nu}{c} \quad (1)$$

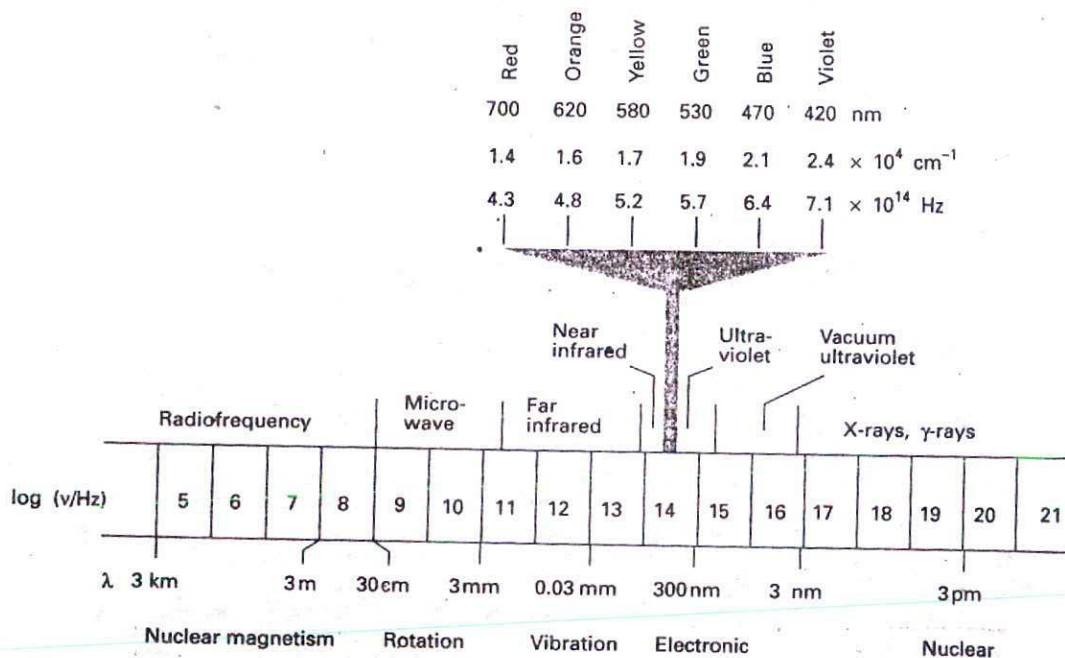
The units of wavenumber are almost always chosen as reciprocal centimetres (cm^{-1}).

Figure 16.1 summarizes the frequencies, wavelengths, and wavenumbers of the various regions of the electromagnetic spectrum and anticipates the type of molecular excitation that is characteristic of each region.

16.1 Experimental techniques

In emission spectroscopy, a molecule undergoes a transition from a state of high energy E_1 to a state of lower energy E_2 and emits the excess energy as a photon. In absorption spectroscopy, the net absorption¹ of nearly monochromatic (single-frequency) incident radiation is monitored as the radiation is swept over a range of frequencies. The energy, $h\nu$, of the photon emitted or absorbed, and therefore the frequency, ν , of the radiation emitted or absorbed, is given by the Bohr frequency condition

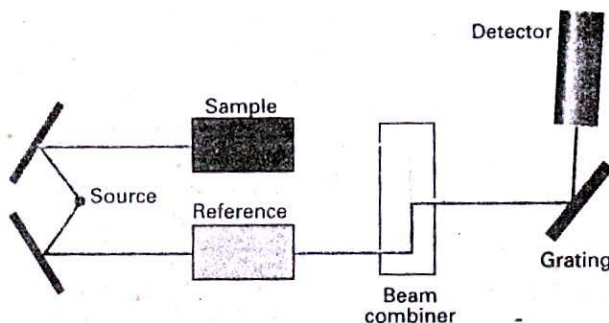
$$h\nu = E_1 - E_2 \quad (2)$$



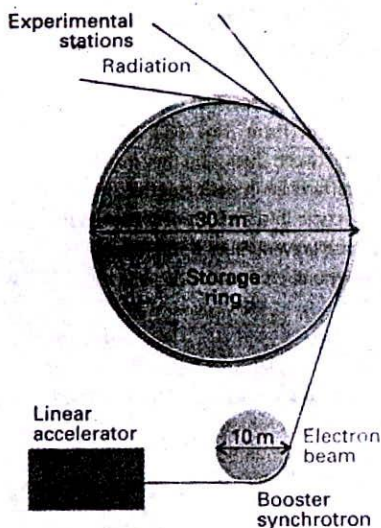
16.1 The electromagnetic spectrum and the classification of the spectral regions. The band at the bottom of the illustration indicates the types of transitions that absorb or emit in the various regions. ('Nuclear magnetism' refers to the types of transitions discussed in Chapter 18; 'nuclear' on the right refers to transitions within the nucleus.)

¹ We say *net* absorption, because it will become clear that, when a sample is irradiated, both absorption and emission at a given frequency are stimulated, and the detector measures the difference, the net absorption.

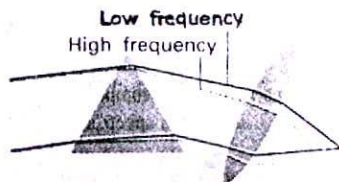
16.2 The layout of a typical absorption spectrometer. The beams pass alternately through the sample and reference cells, and the detector is synchronized with them so that the relative absorption can be determined.



Emission and absorption spectroscopy give the same information about energy level separations, but practical considerations generally determine which technique is employed. Emission spectroscopy, if it is used at all, is normally used only for visible and ultraviolet spectroscopy; absorption spectroscopy is much more widely employed, and we shall concentrate on it. Absorption spectra are also often easier to interpret than emission spectra.



16.3 A synchrotron storage ring. The electrons injected into the ring from the linear accelerator and booster synchrotron are accelerated to high speed in the main ring. An electron in a curved path is subject to constant acceleration, and an accelerated charge radiates electromagnetic energy.



16.4 One simple dispersing element is a prism, which separates frequencies spatially by making use of the higher refractive index of matter for high-frequency radiation. The shortest wavelength for which a glass prism can be used is about 400 nm, but quartz can be used down to 180 nm.

(a) Sources of radiation

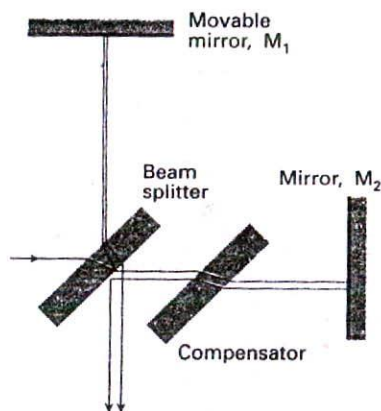
The general layout of a spectrometer is summarized in Fig. 16.2. The source generally produces radiation spanning a range of frequencies. For the far infrared, the source is a mercury arc inside a quartz envelope, most of the radiation being generated by the hot quartz. A *Nernst filament* is used to generate radiation in the near infrared. This device consists of a heated ceramic filament containing rare-earth (lanthanide) oxides, which emits radiation closely resembling that of a true black body. For the visible region of the spectrum, a tungsten/iodine lamp is used, which gives out intense white light. A discharge through deuterium gas or xenon in quartz is still widely used for the near ultraviolet. In a few cases, the source generates monochromatic radiation which can be swept over a range of values. One such generator is the *klystron*, an electronic device used to generate microwaves. Lasers, which are discussed in more detail in Chapter 17, generate monochromatic electromagnetic radiation that can often be tuned over a range of frequencies; different types of laser are used to cover different regions of the electromagnetic spectrum.

For certain applications, synchrotron radiation from a *synchrotron storage ring* is appropriate. A synchrotron storage ring consists of an electron beam (actually a series of closely spaced packets of electrons) travelling in a circular path of several metres in diameter. As electrons travelling in a circle are constantly accelerated by the forces that constrain them to their path, they generate radiation (Fig. 16.3). Synchrotron radiation spans a wide range of frequencies, including the far ultraviolet and beyond to X-rays, and in all except the microwave region is much more intense than can be obtained by most conventional sources. The disadvantage of the source is that it is so large and costly that it is essentially a national facility, and not a laboratory commonplace.

(b) The dispersing element

In all but specialized techniques using monochromatic microwave radiation and lasers, absorption spectrometers include a component for separating the frequencies of the radiation so that the variation of the absorption with frequency can be monitored. In conventional spectrometers, this component is a dispersing element that separates radiation with different frequencies into different spatial directions.

The simplest dispersing element is a glass or quartz prism, which utilizes the variation of refractive index with the frequency of the incident radiation (Fig. 16.4). Materials generally



16.5 A Michelson interferometer. The beam-splitting element divides the incident beam into two beams with a path difference that depends on the location of the mirror M_1 . The compensator ensures that both beams pass through the same thickness of material.

have a higher refractive index for high-frequency radiation than low-frequency radiation, and therefore high-frequency radiation undergoes a greater deflection when passing through a prism. Problems of absorption by the prism can be avoided by replacing it by a *diffraction grating*. A diffraction grating consists of a glass or ceramic plate into which fine grooves have been cut about 1000 nm apart (a separation comparable to the wavelength of visible light) and covered with a reflective aluminium coating. The grating causes interference between waves reflected from its surface, and constructive interference occurs at specific angles that depend on the wavelength of the radiation.

(c) Fourier transform techniques

Modern spectrometers, particularly those operating in the infrared, now almost always use **Fourier transform** techniques of spectral detection and analysis. The heart of a Fourier transform spectrometer is a *Michelson interferometer*, a device for analysing the frequencies present in a composite signal. The total signal from a sample is like a chord played on a piano, and the Fourier transform of the signal is equivalent to the separation of the chord into its individual notes, its spectrum.

A Michelson interferometer works by splitting the beam from the sample into two and introducing a varying path difference, p , into one of them (Fig. 16.5). When the two components recombine, there is a phase difference between them, and they interfere either constructively or destructively depending on the difference in path lengths. The detected signal oscillates as the two components alternately come into and out of phase as the path difference is changed (Fig. 16.6). If the radiation has wavenumber $\tilde{\nu}$, the intensity of the detected signal due to radiation in the range of wavenumbers $\tilde{\nu}$ to $\tilde{\nu} + d\tilde{\nu}$, which we denote $\mathcal{I}(p, \tilde{\nu}) d\tilde{\nu}$, varies with p as

$$\mathcal{I}(p, \tilde{\nu}) d\tilde{\nu} = \mathcal{I}(\tilde{\nu})(1 + \cos 2\pi\tilde{\nu}p) d\tilde{\nu} \quad (3)$$

Hence, the interferometer converts the presence of a particular wavenumber component in the signal into a variation in intensity of the radiation reaching the detector. An actual signal consists of radiation spanning a large number of wavenumbers, and the total intensity at the detector, which we write $\mathcal{I}(p)$, is the sum of contributions from all the wavenumbers present in the signal (Fig. 16.7):

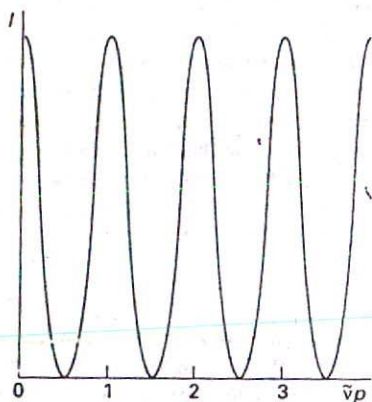
$$\mathcal{I}(p) = \int_0^{\infty} \mathcal{I}(p, \tilde{\nu}) d\tilde{\nu} = \int_0^{\infty} \mathcal{I}(\tilde{\nu})(1 + \cos 2\pi\tilde{\nu}p) d\tilde{\nu} \quad (4)$$

The problem is to find $\mathcal{I}(\tilde{\nu})$, the variation of intensity with wavenumber, which is the spectrum we require, from the record of values of $\mathcal{I}(p)$. This step is a standard technique of mathematics, and is the 'Fourier transformation' step from which this form of spectroscopy takes its name. Specifically:

$$\mathcal{I}(\tilde{\nu}) = 4 \int_0^{\infty} \{\mathcal{I}(p) - \frac{1}{2}\mathcal{I}(0)\} \cos 2\pi\tilde{\nu}p dp \quad (5)$$

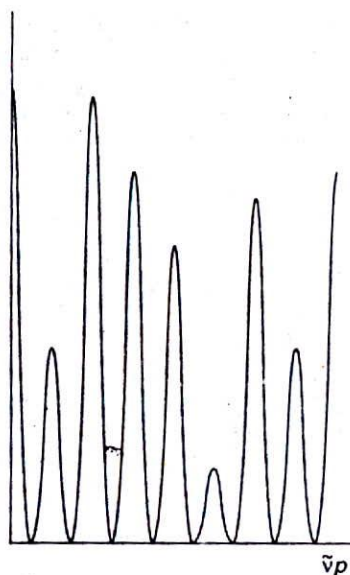
Where $\mathcal{I}(0)$ is given by eqn 4 with $p = 0$. This integration is carried out in a computer that is interfaced to the spectrometer, and the output, $\mathcal{I}(\tilde{\nu})$, is the absorption spectrum of the sample (Fig. 16.8).²

A major advantage of the Fourier transform procedure is that all the radiation emitted by the source is monitored continuously. This is in contrast to a spectrometer in which a monochromator discards most of the generated radiation. As a result, Fourier transform spectrometers have a higher sensitivity than conventional spectrometers. The resolution

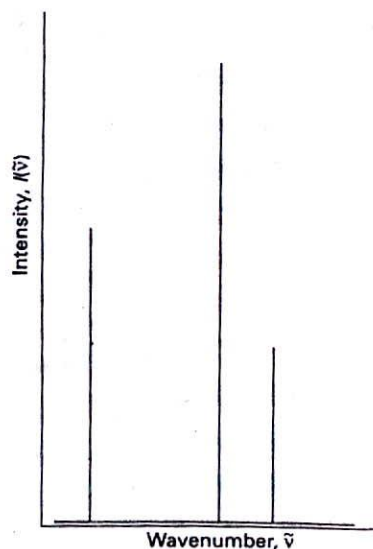


16.6 An interferogram produced as the path length p is changed in the interferometer shown in Fig. 16.5. Only a single frequency component is present in the radiation.

² More precisely, it is the *transmission spectrum*, for the signal depends on the transmitted intensity. However, the absorption and transmission spectra carry the same information and the former term is normally employed.



16.7 An interferogram obtained when several (in this case, three) frequencies are present in the radiation.



16.8 The three frequency components and their intensities that account for the appearance of the interferogram in Fig. 16.7. This spectrum is the Fourier transform of the interferogram, and is a depiction of the contributing frequencies.

they can achieve is determined by the maximum path length difference, p_{\max} , of the interferometer:

$$\Delta\bar{\nu} = \frac{1}{2p_{\max}} \quad (6)$$

To achieve a resolution of 0.1 cm^{-1} requires a maximum path length difference of 5 cm.

(d) Detectors

The third component of a spectrometer is the **detector**, the device that converts incident radiation into an electric current for the appropriate signal processing or plotting. Radiation-sensitive semiconductor devices, such as a *charge-coupled device* (CCD), are increasingly dominating this role in the spectrometer. A microwave detector is typically a *crystal diode* consisting of a tungsten tip in contact with a semiconductor, such as germanium, silicon, or gallium arsenide.

The intensity of the radiation arriving at the detector is usually modulated, because alternating signals are easier to amplify than a steady signal. In some cases the beam is chopped by a rotating shutter. In other cases, the absorption characteristics of the sample itself are modulated. Ways of achieving the latter kind of modulation are described later in the chapter and in Chapter 18.

(e) The sample

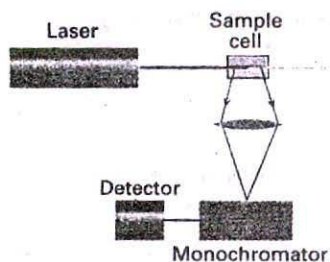
The highest resolution is obtained when the sample is gaseous and at such low pressure that collisions between the molecules are infrequent. Gaseous samples are essential for rotational (microwave) spectroscopy, for only then can molecules rotate freely. To achieve sufficient absorption, the path lengths through gaseous samples must be very long, of the order of metres; long path lengths are achieved by multiple passage of the beam between parallel mirrors at each end of the sample cavity.

The most common range for infrared spectroscopy is from 4000 cm^{-1} to 625 cm^{-1} . Ordinary glass and quartz absorb over most of this range, so some other material must be used as windows. Thus, the sample is typically a liquid held between windows of sodium chloride (which is transparent down to 625 cm^{-1}) or potassium bromide (which is transparent down to 400 cm^{-1}). Other ways of preparing the sample include grinding it into a paste with 'Nujol', a hydrocarbon oil, or pressing it into a solid disk (with powdered potassium bromide, for example).

(f) Raman spectroscopy

In **Raman spectroscopy**, the energy levels of molecules are explored by examining the frequencies present in the radiation scattered by molecules. In a typical experiment, a monochromatic incident beam is passed through the sample and the radiation scattered perpendicular to the beam is monitored (Fig. 16.9). About 1 in 10^7 of the incident photons collide with the molecules, give up some of their energy, and emerge with a lower energy. These scattered photons constitute the lower-frequency Stokes radiation from the sample. Other incident photons may collect energy from the molecules (if they are already excited), and emerge as higher-frequency anti-Stokes radiation. The component of radiation scattered into the forward direction without change of frequency is called Rayleigh radiation.

The shifts in frequency of the scattered radiation from the incident radiation are quite small, and the latter must be very monochromatic if the shifts are to be observed. Moreover,



16.9 The arrangement adopted in Raman spectroscopy. The scattered radiation is monitored at right angles to the incident radiation.

the intensity of scattered radiation is low, so intense incident beams are needed. Lasers are ideal in both respects, and have entirely displaced the mercury arcs used originally. Although laser Raman spectra were originally examined using visible and ultraviolet incident radiation, radiation in the near infrared is now commonly used because its use avoids complications arising from the stimulation of fluorescence (Section 17.3). Detection is usually with a semiconductor device. Raman spectroscopy is often complementary to infrared spectroscopy because, as we shall see, different selection rules are obeyed.

16.2 The intensities of spectral lines

The ratio of the transmitted intensity, \mathcal{I} , to the incident intensity, \mathcal{I}_0 , at a given frequency is called the transmittance, T , of the sample at that frequency:

$$T = \frac{\mathcal{I}}{\mathcal{I}_0} \quad [7]$$

It is found empirically that the transmitted intensity varies with the length, l , of the sample and the molar concentration, $[J]$, of the absorbing species J in accord with the Beer-Lambert law:

$$\mathcal{I} = \mathcal{I}_0 10^{-\varepsilon[J]l} \quad (8)$$

The quantity ε is called the molar absorption coefficient (formerly, and still widely, the 'extinction coefficient'). The molar absorption coefficient depends on the frequency of the incident radiation and is greatest where the absorption is most intense. Its dimensions are $1/(\text{concentration} \times \text{length})$, and it is normally convenient to express it in litres per mole per centimetre ($\text{L mol}^{-1} \text{cm}^{-1}$).³ The form of eqn 7 suggests that it is sensible to introduce the absorbance, A , of the sample at a given wavenumber as

$$A = \log \frac{\mathcal{I}_0}{\mathcal{I}} \quad \text{or} \quad A = -\log T \quad [9]$$

Then the Beer-Lambert law becomes

$$A = \varepsilon[J]l \quad (10)$$

The product $\varepsilon[J]l$ was known formerly as the *optical density* of the sample.

Justification 16.1

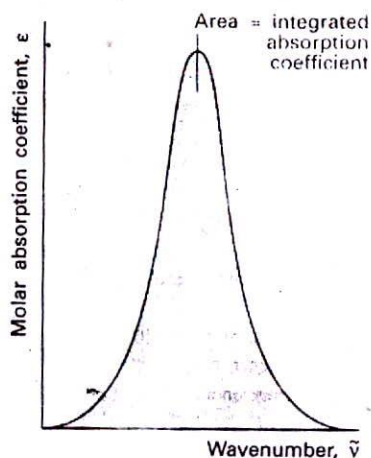
The Beer-Lambert law is an empirical result. However, it is simple to account for its form. The reduction in intensity, $d\mathcal{I}$, that occurs when light passes through a layer of thickness dl containing an absorbing species J at a molar concentration $[J]$ is proportional to the thickness of the layer, the concentration of J , and the intensity, \mathcal{I} , incident on the layer (because the rate of absorption is proportional to the intensity, see below). We can therefore write

$$d\mathcal{I} = -\kappa[J]\mathcal{I} dl$$

where κ (kappa) is the proportionality coefficient, or equivalently

$$\frac{d\mathcal{I}}{\mathcal{I}} = -\kappa[J] dl$$

³ Alternative units are $\text{cm}^2 \text{mol}^{-1}$. This change of units emphasizes the point that ε is a molar cross-section for absorption and, the greater the cross-section of the molecule for absorption, the greater its ability to block the passage of the incident radiation.



16.10 The intensity of a transition is the area under a plot of the molar absorption coefficient against the wavenumber of the incident radiation.

This expression applies to each successive layer into which the sample can be regarded as being divided. Therefore, to obtain the intensity that emerges from a sample of thickness l when the intensity incident on one face of the sample is I_0 , we sum all the successive changes:

$$\int_{I_0}^I \frac{dI}{I} = -\kappa \int_0^l [J] dl$$

If the concentration is uniform, $[J]$ is independent of location, and the expression integrates to

$$\ln \frac{I}{I_0} = -\kappa [J] l$$

This expression gives the Beer-Lambert law when the logarithm is converted to base 10 by using $\ln x = (\ln 10) \log x$ and replacing κ by $\epsilon \ln 10$.

Illustration

The Beer-Lambert law implies that the intensity of electromagnetic radiation transmitted through a sample at a given wavenumber decreases exponentially with the sample thickness and the molar concentration. If the transmittance is 0.1 for a path length of 1 cm (corresponding to a 90 per cent reduction in intensity), then it would be $(0.1)^2 = 0.01$ for a path of double the length (corresponding to a 99 per cent reduction in intensity overall).

The maximum value of the molar absorption coefficient, ϵ_{\max} , is an indication of the intensity of a transition. However, as absorption bands generally spread over a range of wavenumbers, quoting the absorption coefficient at a single wavenumber might not give a true indication of the intensity of a transition. The integrated absorption coefficient, A , is the sum of the absorption coefficients over the entire band (Fig. 16.10), and corresponds to the area under the plot of the molar absorption coefficient against wavenumber:

$$A = \int_{\text{band}} \epsilon(\bar{\nu}) d\bar{\nu} \quad [11]$$

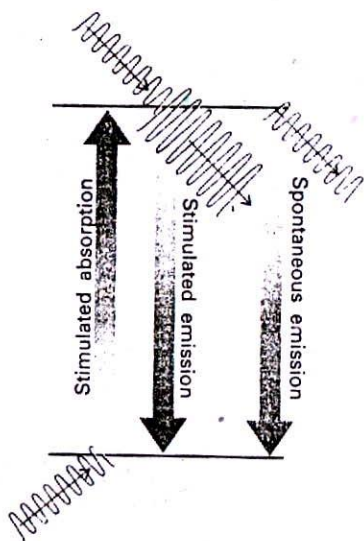
For lines of similar widths, the integrated absorption coefficients are proportional to the heights of the lines.

(a) Absorption intensities

Einstein identified three contributions to the transitions between states. Stimulated absorption is the transition from a low energy state to one of higher energy that is driven by the electromagnetic field oscillating at the transition frequency. The more intense the electromagnetic field (the more intense the incident radiation), the greater the rate at which transitions are induced and hence the stronger the absorption by the sample (Fig. 16.11). Einstein wrote the transition rate, w , from the lower to the upper state as⁴

$$w = B\rho \quad [12]$$

The constant B is the Einstein coefficient of stimulated absorption and $\rho d\nu$ is the energy density of radiation in the frequency range ν to $\nu + d\nu$, where ν is the frequency of the



16.11 The processes that account for absorption and emission of radiation and the attainment of thermal equilibrium. The excited state can return to the lower state spontaneously as well as by a process stimulated by radiation already present at the transition frequency.

⁴ Specifically, w is the rate of change of probability of the molecule being found in the upper state: $w = dP/dt$.

transition. When the molecule is exposed to black-body radiation from a source of temperature T , ρ is given by the Planck distribution (eqn 11.5):⁵

$$\rho = \frac{8\pi h\nu^3/c^3}{e^{h\nu/kT} - 1} \quad (13)$$

For the time being, we can treat B as an empirical parameter that characterizes the transition: if B is large, then a given intensity of incident radiation will induce transitions strongly and the sample will be strongly absorbing. The total rate of absorption, W , the number of molecules excited during an interval divided by the duration of the interval, is the transition rate of a single molecule multiplied by the number of molecules N in the lower state: $W = Nw$.

Einstein considered that the radiation was also able to induce the molecule in the upper state to undergo a transition to the lower state, and hence to generate a photon of frequency ν . Thus, he wrote the rate of this stimulated emission as

$$w' = B'\rho \quad (14)$$

where B' is the Einstein coefficient of stimulated emission. Note that only radiation of the same frequency as the transition can stimulate an excited state to fall to a lower state. However, Einstein realized that stimulated emission was not the only means by which the excited state could generate radiation and return to the lower state, and suggested that an excited state could undergo spontaneous emission at a rate that was independent of the intensity of the radiation (of any frequency) that is already present. He therefore wrote the total rate of transition from the upper to the lower state as

$$w' = A + B'\rho \quad (15)$$

The constant A is the Einstein coefficient of spontaneous emission. The overall rate of emission is

$$W' = N'(A + B'\rho) \quad (16)$$

where N' is the population of the upper state.

As demonstrated in the *Justification* below, Einstein was able to show that the two coefficients of stimulated absorption and emission are equal, and that the coefficient of spontaneous emission is related to them by

$$A = \left(\frac{8\pi h\nu^3}{c^3}\right)B \quad (17)$$

Justification 16.2

At thermal equilibrium, the total rates of emission and absorption are equal, so

$$NB\rho = N'(A + B'\rho)$$

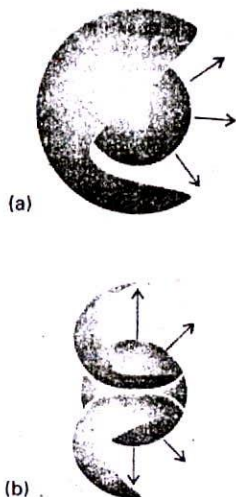
This expression rearranges into

$$\rho = \frac{N'A}{NB - N'B'} = \frac{A/B}{N/N' - B'/B} = \frac{A/B}{e^{h\nu/kT} - B'/B}$$

We have used the Boltzmann expression (see the *Introduction*) for the ratio of populations of states of energies E and E' in the last step:

$$\frac{N'}{N} = e^{-h\nu/kT} \quad h\nu = E' - E$$

⁵ The slightly different form of the distribution stems from the fact that the ρ in eqn 11.5 is for the energy density written as $\rho d\lambda$, whereas here it is written as $\rho d\nu$, and $|d\lambda| = (c/\nu^2) d\nu$.



16.12 (a) When a $1s$ electron becomes a $2s$ electron, there is a spherical migration of charge; there is no dipole moment associated with this migration of charge; this transition is electric-dipole forbidden. (b) In contrast, when a $1s$ electron becomes a $2p$ electron, there is a dipole associated with the charge migration; this transition is allowed. (There are subtle effects arising from the sign of the wavefunction that give the charge migration a dipolar character, which this diagram does not attempt to convey.)

This result has the same form as the Planck distribution (eqn 13), which describes the radiation density at thermal equilibrium. Indeed, when we compare the two expressions for ρ , we can conclude that $B' = B$ and that A is related to B by eqn 17.

The growth of the importance of spontaneous emission with increasing frequency is a very important conclusion, as we shall see when we consider the operation of lasers (Section 17.5). The equality of the coefficients of stimulated emission and absorption implies that, if two states happen to have equal populations, then the rate of stimulated emission is equal to the rate of stimulated absorption, and there is then no net absorption.

Spontaneous emission can be largely ignored at the relatively low frequencies of rotational and vibrational transitions, and the intensities of these transitions can be discussed in terms of stimulated emission and absorption. Then the net rate of absorption is given by

$$W_{\text{net}} = NB\rho - N'B'\rho = (N - N')B\rho \quad (18)$$

and is proportional to the population difference of the two states involved in the transition.

(b) Selection rules and transition moments

We met the concept of a 'selection rule' in Sections 13.3 and 15.6 as a statement about whether a transition is forbidden or allowed. Selection rules also apply to molecular spectra, and the form they take depends on the type of transition. The underlying classical idea is that, for the molecule to be able to interact with the electromagnetic field and absorb or create a photon of frequency ν , it must possess, at least transiently, a dipole oscillating at that frequency. This transient dipole is expressed quantum mechanically in terms of the transition dipole moment, μ_{fi} , between states $|i\rangle$ and $|f\rangle$:

$$\mu_{fi} = \langle f|\mu|i\rangle = \int \psi_f^* \mu \psi_i d\tau \quad (19)$$

where μ is the electric dipole moment operator. The size of the transition dipole can be regarded as a measure of the charge redistribution that accompanies a transition: a transition will be active (and generate or absorb photons) only if the accompanying charge redistribution is dipolar (Fig. 16.12).

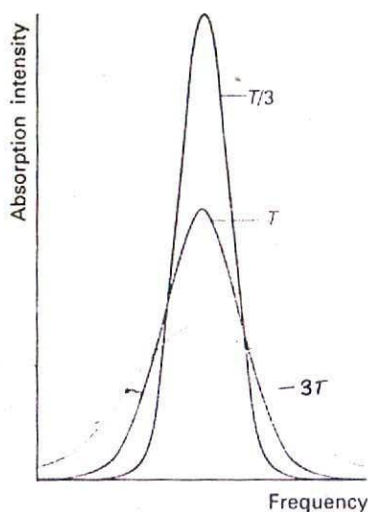
The coefficient of stimulated absorption (and emission), and therefore the intensity of the transition, is proportional to the square of the transition dipole moment, and a detailed analysis gives

$$B = \frac{|\mu_{fi}|^2}{6\epsilon_0\hbar^2} \quad (20)$$

Only if the transition moment is nonzero does the transition contribute to the spectrum. We see that, to identify the selection rules, we must establish the conditions for which $\mu_{fi} \neq 0$.

A gross selection rule specifies the general features a molecule must have if it is to have a spectrum of a given kind. For instance, we shall see that a molecule gives a rotational spectrum only if it has a permanent electric dipole moment. This rule, and others like it for other types of transition, will be explained in the relevant sections of the chapter.

A detailed study of the transition moment leads to the specific selection rules that express the allowed transitions in terms of the changes in quantum numbers. We have already encountered examples of specific selection rules when discussing atomic spectra (Section 13.3), such as the rule $\Delta l = \pm 1$ for the angular momentum quantum number. Specific selection rules can often be interpreted in terms of the changes of angular momentum when a photon (with its intrinsic spin angular momentum $s = 1$) enters or



16.13 The shape of a Doppler-broadened spectral line reflects the Maxwell distribution of speeds in the sample at the temperature of the experiment. Notice that the line broadens as the temperature is increased.

leaves a molecule, and we shall discuss them once we have set up the quantum numbers needed to describe rotation and vibration.

16.3 Linewidths

A number of effects contribute to the widths of spectroscopic lines. Some contributions to linewidth can be modified by changing the conditions, and to achieve high resolutions we need to know how to minimize these contributions. Other contributions cannot be changed, and represent an inherent limitation on resolution.

(a) Doppler broadening

One important broadening process in gaseous samples is the Doppler effect, in which radiation is shifted in frequency when the source is moving towards or away from the observer. When a source emitting electromagnetic radiation of frequency ν moves with a speed s relative to an observer, the observer detects radiation of frequency

$$\nu_{\text{receding}} = \nu \left(\frac{1 - s/c}{1 + s/c} \right)^{1/2} \quad \nu_{\text{approaching}} = \nu \left(\frac{1 + s/c}{1 - s/c} \right)^{1/2} \quad (21)$$

where c is the speed of light. For nonrelativistic speeds ($s \ll c$), these expressions simplify to

$$\nu_{\text{receding}} \approx \frac{\nu}{1 + s/c} \quad \nu_{\text{approaching}} \approx \frac{\nu}{1 - s/c} \quad (22)$$

Molecules reach high speeds in all directions in a gas, and a stationary observer detects the corresponding Doppler-shifted range of frequencies. Some molecules approach the observer, some move away; some move quickly, others slowly. The detected spectral 'line' is the absorption or emission profile arising from all the resulting Doppler shifts. The profile reflects the distribution of molecular velocities parallel to the line of sight (Section 1.3), which is a bell-shaped Gaussian curve (of the form e^{-x^2}). The Doppler line shape is therefore also a Gaussian (Fig. 16.13), and calculation shows that, when the temperature is T and the mass of the molecule is m , the width of the line at half-height (in terms of frequency or wavelength) is

$$\delta\nu = \frac{2\nu}{c} \left(\frac{2kT \ln 2}{m} \right)^{1/2} \quad \delta\lambda = \frac{2\lambda}{c} \left(\frac{2kT \ln 2}{m} \right)^{1/2} \quad (23)$$

For a molecule like N_2 at room temperature ($T \approx 300$ K), $\delta\nu/\nu \approx 2.3 \times 10^{-6}$. For a typical rotational transition wavenumber of 1 cm^{-1} (corresponding to a frequency of 30 GHz), the linewidth is about 70 kHz.

Doppler broadening increases with temperature because the molecules acquire a wider range of speeds. Therefore, to obtain spectra of maximum sharpness, it is best to work with cold samples.

(b) Lifetime broadening

It is found that spectroscopic lines from gas-phase samples are not infinitely sharp even when Doppler broadening has been largely eliminated by working at low temperatures. The same is true of the spectra of samples in condensed phases and solution. This residual broadening is due to quantum mechanical effects. Specifically, when the Schrödinger equation is solved for a system that is changing with time, it is found that it is impossible to specify the energy levels exactly. If on average a system survives in a state for a time τ , the lifetime of the state, then its energy levels are blurred to an extent of order δE , where

$$\delta E \approx \frac{h}{\tau} \quad (24)$$

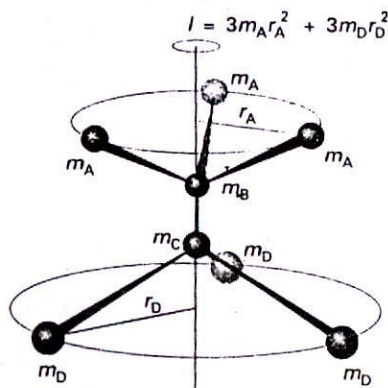
This expression is reminiscent of the Heisenberg uncertainty principle (eqn 11.46), and consequently this lifetime broadening is often called 'uncertainty broadening'. When the energy spread is expressed as a wavenumber through $\delta E = hc\delta\bar{\nu}$, and the values of the fundamental constants are introduced, this relation becomes

$$\delta\bar{\nu} \approx \frac{5.3 \text{ cm}^{-1}}{\tau/\text{ps}} \quad (25)$$

No excited state has an infinite lifetime; therefore, all states are subject to some lifetime broadening and, the shorter the lifetimes of the states involved in a transition, the broader the corresponding spectral lines.

Two processes are responsible for the finite lifetimes of excited states. The dominant one for low-frequency transitions is collisional deactivation, which arises from collisions between molecules or with the walls of the container. If the collisional lifetime, the mean time between collisions, is τ_{col} , the resulting collisional linewidth is $\delta E_{\text{col}} \approx \hbar/\tau_{\text{col}}$. Because $\tau_{\text{col}} = 1/z$, where z is the collision frequency, and from the kinetic model of gases (Section 1.3) we know that z is proportional to the pressure, p , we see that the collisional linewidth is proportional to the pressure. The collisional linewidth can therefore be minimized by working at low pressures.

The rate of spontaneous emission cannot be changed. Hence it is a natural limit to the lifetime of an excited state, and the resulting lifetime broadening is the natural linewidth of the transition. The natural linewidth is an intrinsic property of the transition, and cannot be changed by modifying the conditions. Natural linewidths depend strongly on the transition frequency (they increase with the coefficient of spontaneous emission A and therefore as ν^3), so low-frequency transitions (such as the microwave transitions of rotational spectroscopy) have very small natural linewidths, and collisional and Doppler line-broadening processes are dominant. The natural lifetimes of electronic transitions are very much shorter than for vibrational and rotational transitions, so the natural linewidths of electronic transitions are much greater than those of vibrational and rotational transitions. For example, a typical electronic excited state natural lifetime is about 10^{-8} s (10 ns), corresponding to a natural width of about $5 \times 10^{-4} \text{ cm}^{-1}$ (15 MHz). A typical rotational state natural lifetime is about 10^3 s, corresponding to a natural linewidth of only $5 \times 10^{-15} \text{ cm}^{-1}$ (of the order of 10^{-4} Hz).



16.14 The definition of moment of inertia. In this molecule there are three identical atoms attached to the B atom and three different but mutually identical atoms attached to the C atom. In this example, the centre of mass lies on the C_3 axis, and the perpendicular distances are measured from the axis passing through the B and C atoms.

Pure rotation spectra

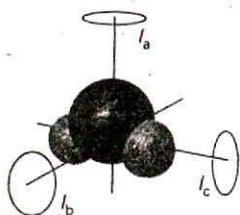
The general strategy we adopt for discussing molecular spectra and the information they contain is to find expressions for the energy levels of molecules and then to calculate the transition frequencies by applying the selection rules. We then predict the appearance of the spectrum by taking into account the transition moments and the populations of the states. In this section we illustrate the strategy by considering the rotational states of molecules.

16.4 Moments of inertia

The key molecular parameter we shall need is the moment of inertia, I , of the molecule (Section 12.6). The moment of inertia of a molecule is defined as the mass of each atom multiplied by the square of its distance from the rotational axis through the centre of mass of the molecule (Fig. 16.14):

$$I = \sum_i m_i r_i^2 \quad [26]$$

where r_i is the perpendicular distance of the atom i from the axis of rotation. The moment of inertia depends on the masses of the atoms present and the molecular geometry, so we can



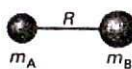
16.15 An asymmetric rotor has three different moments of inertia; all three rotation axes coincide at the centre of mass of the molecule.

suspect (and later shall see explicitly) that rotational spectroscopy will give information about bond lengths and bond angles.

In general, the rotational properties of any molecule can be expressed in terms of the moments of inertia about three perpendicular axes set in the molecule (Fig. 16.15). The convention is to label the moments of inertia I_a , I_b , and I_c , with the axes chosen so that $I_c \geq I_b \geq I_a$. For linear molecules, the moment of inertia around the internuclear axis is zero. The explicit expressions for the moments of inertia of some symmetrical molecules are given in Table 16.1.

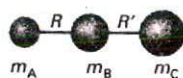
Table 16.1 Moments of inertia†

1. Diatomics

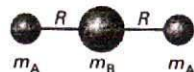


$$I = \frac{m_A m_B}{m} R^2 = \mu R^2$$

2. Linear rotors

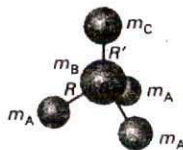


$$I = m_A R^2 + m_C R'^2 - \frac{(m_A R - m_C R')^2}{m}$$

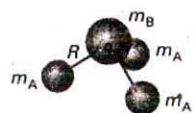


$$I = 2m_A R^2$$

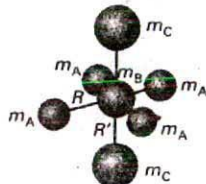
3. Symmetric rotors



$$\begin{aligned} I_{\parallel} &= 2m_A R^2 (1 - \cos \theta) \\ I_{\perp} &= m_A R^2 (1 - \cos \theta) \\ &\quad + \frac{m_A}{m} (m_B + m_C) R^2 (1 + 2 \cos \theta) \\ &\quad + \frac{m_C R'}{m} \{ (3m_A + m_B) R' \\ &\quad \quad + 6m_A R [\frac{1}{3} (1 + 2 \cos \theta)]^{1/2} \} \end{aligned}$$

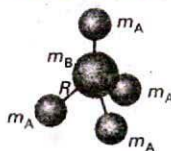


$$\begin{aligned} I_{\parallel} &= 2m_A R^2 (1 - \cos \theta) \\ I_{\perp} &= m_A R^2 (1 - \cos \theta) \\ &\quad + \frac{m_A m_B}{m} R^2 (1 + 2 \cos \theta) \end{aligned}$$

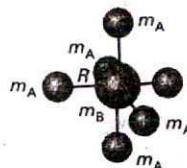


$$\begin{aligned} I_{\parallel} &= 4m_A R^2 \\ I_{\perp} &= 2m_A R^2 + 2m_C R'^2 \end{aligned}$$

4. Spherical rotors

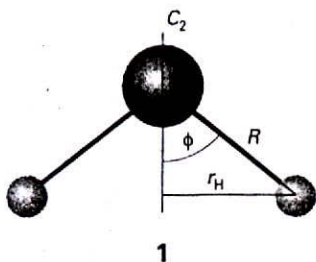


$$I = \frac{8}{3} m_A R^2$$



$$I = 4m_A R^2$$

† In each case m is the total mass of the molecule.


Example 16.1 Calculating the moment of inertia of a molecule

Calculate the moment of inertia of an H_2O molecule around its twofold axis (the bisector of the HOH angle (1)). The HOH bond angle is 104.5° and the bond length is 95.7 pm .

Method According to eqn 26, the moment of inertia is the sum of the masses multiplied by the squares of their distances from the axis of rotation. The latter can be expressed by using trigonometry and the bond angle and bond length.

Answer From eqn 26,

$$I = \sum_i m_i r_i^2 = m_{\text{H}} r_{\text{H}}^2 + 0 + m_{\text{H}} r_{\text{H}}^2 = 2m_{\text{H}} r_{\text{H}}^2$$

If the bond angle of the molecule is denoted 2ϕ and the bond length is R , trigonometry gives $r_{\text{H}} = R \sin \phi$. It follows that

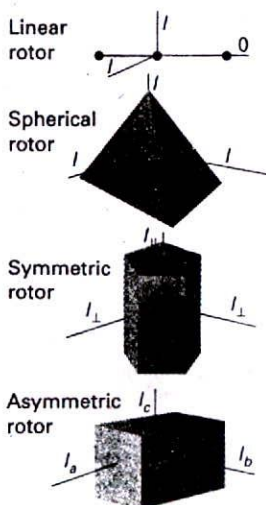
$$I = 2m_{\text{H}} R^2 \sin^2 \phi$$

Substitution of the data gives

$$\begin{aligned} I &= 2 \times (1.67 \times 10^{-27} \text{ kg}) \times (9.57 \times 10^{-11} \text{ m})^2 \times \sin^2 52.3^\circ \\ &= 1.91 \times 10^{-47} \text{ kg m}^2 \end{aligned}$$

Comment The mass of the O atom makes no contribution to the moment of inertia for this mode of rotation, as the atom is immobile while the H atoms circulate around it.

Self-test 16.1 Calculate the moment of inertia of a $\text{CH}_3^{35}\text{Cl}$ molecule around its threefold axis. The C–Cl bond length is 177 pm and the HCl angle is 107° ; $m(^{35}\text{Cl}) = 34.97 \text{ u}$.
[$4.99 \times 10^{-45} \text{ kg m}^2$]



16.16 A schematic illustration of the classification of rigid rotors.

We shall suppose initially that molecules are rigid rotors, bodies that do not distort under the stress of rotation. Rigid rotors can be classified into four types (Fig. 16.16):

Spherical rotors have three equal moments of inertia (examples: CH_4 , SiH_4 , and SF_6).

Symmetric rotors have two equal moments of inertia (examples: NH_3 , CH_3Cl , and CH_3CN).

Linear rotors have one moment of inertia (the one about the axis) equal to zero (examples: CO_2 , HCl , OCS , and $\text{HC}\equiv\text{CH}$).

Asymmetric rotors have three different moments of inertia (H_2O , H_2CO , and CH_3OH are examples).

In group theoretical language, a spherical rotor is a molecule that belongs to a cubic or icosahedral point group; a symmetric rotor is a molecule with at least a threefold axis of symmetry. All diatomic molecules are linear rotors. An asymmetric rotor is a molecule without a threefold (or higher) axis: it may have other elements of symmetry, such as a twofold axis or mirror planes. The energy levels of asymmetric rotors are complicated and we shall not consider them.

16.5 The rotational energy levels

The rotational energy levels of a rigid rotor may be obtained by solving the appropriate Schrödinger equation. Fortunately, however, there is a much less onerous short cut to the exact expressions that depends on noting the classical expression for the energy of a rotating body, expressing it in terms of the angular momentum, and then importing the quantum mechanical properties of angular momentum into the equations.

The classical expression for the energy of a body rotating about an axis a is

$$E_a = \frac{1}{2} I_a \omega_a^2 \quad (27)$$

where ω_a is the angular velocity (in radians per second, rad s^{-1}) about that axis and I_a is the corresponding moment of inertia. A body free to rotate about three axes has an energy

$$E = \frac{1}{2} I_a \omega_a^2 + \frac{1}{2} I_b \omega_b^2 + \frac{1}{2} I_c \omega_c^2$$

Because the classical angular momentum about the axis a is $J_a = I_a \omega_a$, with similar expressions for the other axes, it follows that

$$E = \frac{J_a^2}{2I_a} + \frac{J_b^2}{2I_b} + \frac{J_c^2}{2I_c} \quad (28)$$

This is the key equation. We described the quantum mechanical properties of angular momentum in Section 12.7b, and can now make use of them in conjunction with this equation to obtain the rotational energy levels.

(a) Spherical rotors

When all three moments of inertia are equal to some value I , as in CH_4 and SF_6 , the classical expression for the energy is

$$E = \frac{J_a^2 + J_b^2 + J_c^2}{2I} = \frac{\mathcal{J}^2}{2I}$$

where \mathcal{J} is the magnitude of the angular momentum. We can immediately find the quantum expression by making the replacement

$$\mathcal{J}^2 \rightarrow J(J+1)\hbar^2 \quad J = 0, 1, 2, \dots$$

Therefore, the energy of a spherical rotor is confined to the values

$$E_J = J(J+1) \frac{\hbar^2}{2I} \quad J = 0, 1, 2, \dots \quad (29)$$

The resulting ladder of energy levels is illustrated in Fig. 16.17. The energy is normally expressed in terms of the rotational constant, B , of the molecule, where

$$hcB = \frac{\hbar^2}{2I} \quad \text{so } B = \frac{\hbar}{4\pi cI} \quad (30)$$

The expression for the energy is then

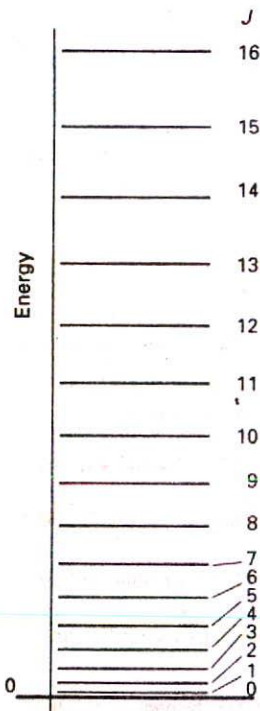
$$E_J = hcB J(J+1) \quad J = 0, 1, 2, \dots \quad (31)$$

The rotational constant as defined by eqn 31 is a wavenumber.⁶ The energy of a rotational state is normally reported as the rotational term, $F(J)$, a wavenumber, by division by hc :

$$F(J) = BJ(J+1) \quad (32)$$

The separation of adjacent levels is

$$F(J) - F(J-1) = 2BJ \quad (33)$$



16.17 The rotational energy levels of a linear or spherical rotor. Note that the energy separation between neighbouring levels increases as J increases.

6 The definition of B as a wavenumber is convenient when we come to vibration-rotation spectra. However, for pure rotational spectroscopy it is more common to define B as a frequency. Then $B = \hbar/4\pi I$ and the energy is $E = \hbar B J(J+1)$.

Because the rotational constant decreases as I increases, we see that large molecules have closely spaced rotational energy levels. We can estimate the magnitude of the separation by considering CCl_4 : from the bond lengths and masses of the atoms we find $I = 4.85 \times 10^{-45} \text{ kg m}^2$, and hence $B = 0.0577 \text{ cm}^{-1}$.

(b) Symmetric rotors

In symmetric rotors, two moments of inertia are equal but different from the third (as in CH_3Cl , NH_3 , and C_6H_6); the unique axis of the molecule is its principal axis (or figure axis). We shall write the unique moment of inertia (that about the principal axis) as I_{\parallel} and the other two as I_{\perp} . If $I_{\parallel} > I_{\perp}$, the rotor is classified as oblate (like a pancake, and C_6H_6); if $I_{\parallel} < I_{\perp}$ it is classified as prolate (like a cigar, and CH_3Cl). The classical expression for the energy, eqn 28, becomes

$$E = \frac{J_b^2 + J_c^2}{2I_{\perp}} + \frac{J_a^2}{2I_{\parallel}}$$

This expression can be written in terms of $\mathcal{J}^2 = J_a^2 + J_b^2 + J_c^2$:

$$E = \frac{\mathcal{J}^2 - J_a^2}{2I_{\perp}} + \frac{J_a^2}{2I_{\parallel}} = \frac{\mathcal{J}^2}{2I_{\perp}} + \left(\frac{1}{2I_{\parallel}} - \frac{1}{2I_{\perp}} \right) J_a^2 \quad (34)$$

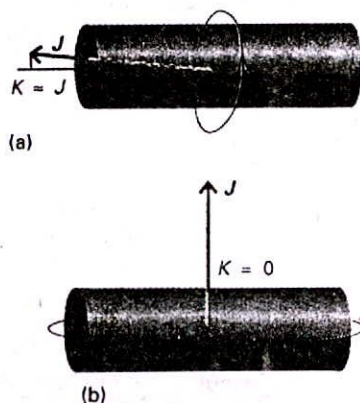
Now we generate the quantum expression by replacing \mathcal{J}^2 by $J(J+1)\hbar^2$, where J is the angular momentum quantum number. We also know from the quantum theory of angular momentum (Section 12.7b) that the component of angular momentum about any axis is restricted to the values $K\hbar$, with $K = 0, \pm 1, \dots, \pm J$. (K is the quantum number used to signify a component on the principal axis; M_J is reserved for a component on an externally defined axis.) Therefore, we also replace J_a^2 by $K^2\hbar^2$. It follows that the rotational terms are

$$F(J, K) = BJ(J+1) + (A-B)K^2 \quad J = 0, 1, 2, \dots \quad K = 0, \pm 1, \dots, \pm J \quad (35)$$

with

$$A = \frac{\hbar^2}{4\pi c I_{\parallel}} \quad B = \frac{\hbar^2}{4\pi c I_{\perp}} \quad (36)$$

Equation 35 matches what we should expect for the dependence of the energy levels on the two distinct moments of inertia of the molecule. When $K = 0$, there is no component of angular momentum about the principal axis, and the energy levels depend only on I_{\perp} (Fig. 16.18). When $K = \pm J$, almost all the angular momentum arises from rotation around the principal axis, and the energy levels are determined largely by I_{\parallel} . The sign of K does not affect the energy because opposite values of K correspond to opposite senses of rotation, and the energy does not depend on the sense of rotation.



16.18 The significance of the quantum number K . (a) When $|K|$ is close to its maximum value, J , most of the molecular rotation is around the principal axis. (b) When $K = 0$ the molecule has no angular momentum about its principal axis: it is undergoing end-over-end rotation.

Example 16.2 Calculating the rotational energy levels of a molecule

An $^{14}\text{NH}_3$ molecule is a symmetric rotor with bond length 101.2 pm and HNH bond angle 106.7° . Calculate its rotational terms.

Method Begin by calculating the rotational constants A and B by using the expressions for moments of inertia given in Table 16.1. Then use eqn 35 to find the rotational terms.

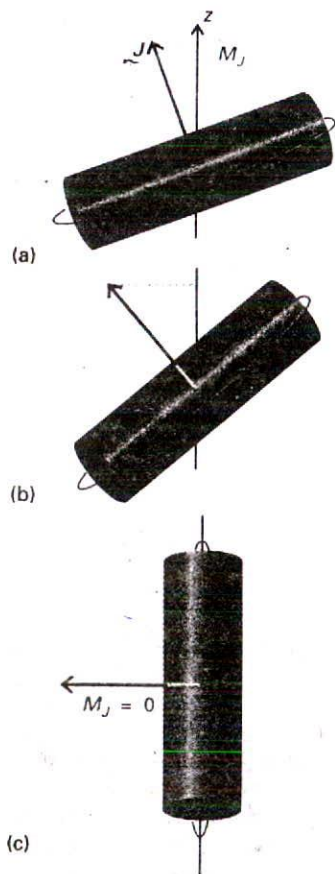
Answer Substitution of $m_A = 1.0078$ u, $m_B = 14.0031$ u, $R = 101.2$ pm, and $\theta = 106.7^\circ$ into the second of the symmetric rotor expressions in Table 16.1 gives $I_{\parallel} = 4.4128 \times 10^{-47}$ kg m² and $I_{\perp} = 2.8059 \times 10^{-47}$ kg m². Hence, $A = 6.344$ cm⁻¹ and $B = 9.977$ cm⁻¹. It follows from eqn 35 that

$$F(J, K)/\text{cm}^{-1} = 9.977J(J+1) - 3.633K^2$$

Comment For $J = 1$, the energy needed for the molecule to rotate mainly about its figure axis ($K = \pm J$) is equivalent to 16.32 cm⁻¹, but end-over-end rotation ($K = 0$) corresponds to 19.95 cm⁻¹.

Self-test 16.2 A CH₃³⁵Cl molecule has a C-Cl bond length of 178 pm, a C-H bond length of 111 pm, and an HCH angle of 110.5°. Calculate its rotational energy terms.

$$[F(J, K)/\text{cm}^{-1} = 0.444J(J+1) + 4.58K^2]$$



16.19 The significance of the quantum number M_J . (a) When M_J is close to its maximum value, J , most of the molecular rotation is around the laboratory z -axis. (b) An intermediate value of M_J . (c) When $M_J = 0$ the molecule has no angular momentum about the z -axis. All three diagrams correspond to a state with $K = 0$; there are corresponding diagrams for different values of K , in which the angular momentum makes a different angle to the molecule's principal axis.

(c) Linear rotors

For a linear rotor (such as CO₂, HCl, and C₂H₂), in which the nuclei are regarded as mass points, the rotation occurs only about an axis perpendicular to the line of atoms and there is zero angular momentum around the line. Therefore, the component of angular momentum around the figure axis of a linear rotor is identically zero, and $K \equiv 0$ in eqn 35. The rotational terms of a linear molecule are therefore

$$F(J) = BJ(J+1) \quad J = 0, 1, 2, \dots \quad (37)$$

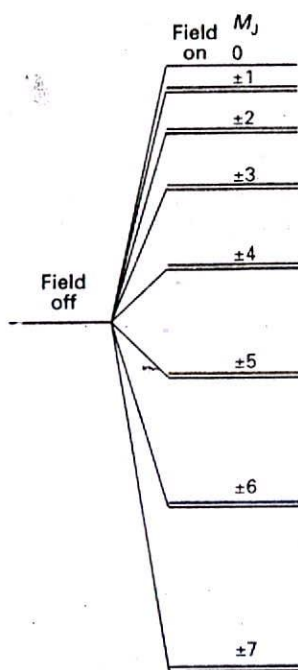
This expression is the same as eqn 32 but we have arrived at it in a significantly different way: here $K \equiv 0$ but for a spherical rotor $A = B$.

(d) Degeneracies and the Stark effect

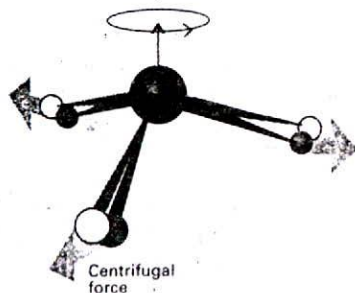
The energy of a symmetric rotor depends on J and K , and each level except those with $K = 0$ is doubly degenerate: the states with K and $-K$ have the same energy. However, we must not forget that the angular momentum of the molecule has a component on an external, laboratory-fixed axis. This component is quantized, and its permitted values are $M_J\hbar$, with $M_J = 0, \pm 1, \dots, \pm J$, giving $2J + 1$ values in all (Fig. 16.19). The quantum number M_J does not appear in the expression for the energy, but it is necessary for a complete specification of the state of the rotor. Consequently, all $2J + 1$ orientations of the rotating molecule have the same energy. It follows that a symmetric rotor level is $2(2J + 1)$ -fold degenerate for $K \neq 0$ and $(2J + 1)$ -fold degenerate for $K = 0$. A linear rotor has K fixed at 0, but the angular momentum may still have $2J + 1$ components on the laboratory axis, so its degeneracy is $2J + 1$.

A spherical rotor can be regarded as a version of a symmetric rotor in which A is equal to B . The quantum number K may still take any one of $2J + 1$ values, but the energy is independent of which value it takes. Therefore, as well as having a $(2J + 1)$ -fold degeneracy arising from its orientation in space, the rotor also has a $(2J + 1)$ -fold degeneracy arising from its orientation with respect to an arbitrary axis in the molecule. The overall degeneracy of a symmetric rotor with quantum number J is therefore $(2J + 1)^2$. This degeneracy increases very rapidly: when $J = 10$, for instance, there are 441 states of the same energy.

The degeneracy associated with the quantum number M_J (the orientation of the rotation in space) is partly removed when an electric field is applied to a polar molecule (for example, HCl or NH₃), as illustrated in Fig. 16.20. The splitting of states by an electric field is called the



16.20 The effect of an electric field on the energy levels of a polar linear rotor. All levels are doubly degenerate except that with $M_J = 0$.



16.21 The effect of rotation on a molecule. The centrifugal force arising from rotation distorts the molecule, opening out bond angles and stretching bonds slightly. The effect is to increase the moment of inertia of the molecule and hence to decrease its rotational constant.

Stark effect. For a linear rotor in an electric field \mathcal{E} , the energy of the state $|J, M_J\rangle$ is given by

$$E(J, M_J) = hcBJ(J+1) + a(J, M_J)\mu^2\mathcal{E}^2 \quad (38a)$$

where

$$a(J, M_J) = \frac{\{J(J+1) - 3M_J^2\}}{2hcBJ(J+1)(2J-1)(2J+3)} \quad (38b)$$

Note that the energy of a state with quantum number M_J depends on the square of the permanent electric dipole moment, μ . The observation of the Stark effect can therefore be used to measure this property, but the technique is limited to molecules that are sufficiently volatile to be studied by microwave spectroscopy. However, as spectra can be recorded for samples at pressures of only about 1 Pa, even some quite nonvolatile substances may be studied. Sodium chloride, for example, can be studied as diatomic NaCl molecules at high temperatures.

(e) Centrifugal distortion

We have treated molecules as rigid rotors. However, the atoms of rotating molecules are subject to centrifugal forces that tend to distort the molecular geometry and change the moments of inertia (Fig. 16.21). The effect of centrifugal distortion on a diatomic molecule is to stretch the bond and hence to increase the moment of inertia. As a result, centrifugal distortion reduces the rotational constant and consequently the energy levels are slightly closer than the rigid-rotor expressions predict. The effect is usually taken into account largely empirically by subtracting a term from the energy and writing

$$F(J) = BJ(J+1) - D_J J^2(J+1)^2 \quad (39)$$

The parameter D_J is the centrifugal distortion constant. It is large when the bond is easily stretched. The centrifugal distortion constant of a diatomic molecule is related to the vibrational wavenumber of the bond, $\tilde{\nu}$ (which, as we shall see later, is a measure of its stiffness), through the approximate relation

$$D_J = \frac{4B^3}{\tilde{\nu}^2} \quad (40)$$

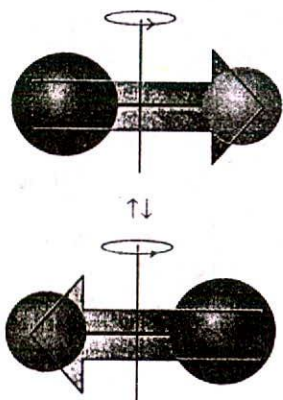
Hence the observation of the convergence of the rotational levels as J increases can be interpreted in terms of the rigidity of the bond.

16.6 Rotational transitions

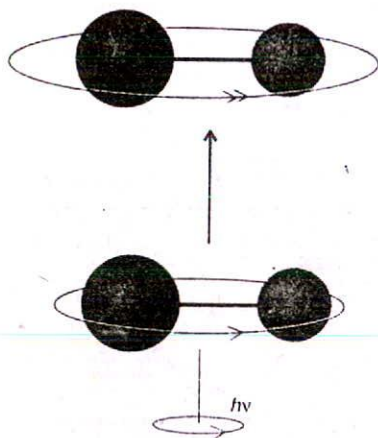
Typical values of B for small molecules are in the region of 0.1 to 10 cm^{-1} (for example, 0.356 cm^{-1} for NF_3 and 10.59 cm^{-1} for HCl), so rotational transitions lie in the microwave region of the spectrum. The transitions are detected by monitoring the net absorption of microwave radiation. Modulation of the transmitted intensity can be achieved by varying the energy levels with an oscillating electric field. In this **Stark modulation**, an electric field of about 10^5 V m^{-1} and a frequency of between 10 and 100 kHz is applied to the sample.

(a) Rotational selection rules

We have already remarked (Section 16.2) that the gross selection rule for the observation of a pure rotational spectrum is that a molecule must have a permanent electric dipole moment. That is, *for a molecule to give a pure rotational spectrum, it must be polar*. The classical basis of this rule is that a polar molecule appears to possess a fluctuating dipole when rotating, but a nonpolar molecule does not (Fig. 16.22). The permanent dipole can be regarded as a handle with which the molecule stirs the electromagnetic field into oscillation



16.22 To a stationary observer, a rotating polar molecule looks like an oscillating dipole which can stir the electromagnetic field into oscillation. This picture is the classical origin of the gross selection rule for rotational transitions.



16.23 When a photon is absorbed by a molecule, the angular momentum of the combined system is conserved. If the molecule is rotating in the same sense as the spin of the incoming photon, then J increases by 1.

(and vice versa for absorption). Homonuclear diatomic molecules and symmetrical ($D_{\infty h}$) linear molecules such as CO_2 are rotationally inactive. Spherical rotors cannot have electric dipole moments unless they become distorted by rotation, so they are also inactive except in special cases. An example of a spherical rotor that does become sufficiently distorted for it to acquire a dipole moment is SiH_4 , which has a dipole moment of about $8.3 \mu\text{D}$ by virtue of its rotation when $J \approx 10$ (for comparison, HCl has a permanent dipole moment of 1.1 D ; molecular dipole moments and their units are discussed in Section 22.1). The pure rotational spectrum of SiH_4 has been detected by using long path lengths (10 m) through high-pressure (4 atm) samples.

Illustration

Of the molecules N_2 , CO_2 , OCS , H_2O , $\text{CH}_2=\text{CH}_2$, C_6H_6 , only OCS and H_2O are polar, so only these two molecules have microwave spectra.

Self-test 16.3 Which of the molecules H_2 , NO , N_2O , CH_4 can have a pure rotational spectrum?

[NO , N_2O]

The specific rotational selection rules are found by evaluating the transition dipole moment between rotational states. For a linear molecule, the transition moment vanishes unless the following conditions are fulfilled:

$$\Delta J = \pm 1 \quad \Delta M_J = 0, \pm 1 \quad (41)$$

The transition $\Delta J = +1$ corresponds to absorption and the transition $\Delta J = -1$ corresponds to emission. The allowed change in J in each case arises from the conservation of angular momentum when a photon, a spin-1 particle, is emitted or absorbed (Fig. 16.23). The change in M_J is also a consequence of the conservation of angular momentum, and takes into account the direction in which the photon leaves or enters the molecule.

When the transition moment is evaluated for all possible relative orientations of the molecule to the line of flight of the photon, it is found that the total $J + 1 \leftrightarrow J$ transition intensity is proportional to

$$|\mu_{J+1, J}|^2 = \left(\frac{J+1}{2J+1} \right) \mu^2 \rightarrow \frac{1}{2} \mu^2 \text{ for } J \gg 1 \quad (42)$$

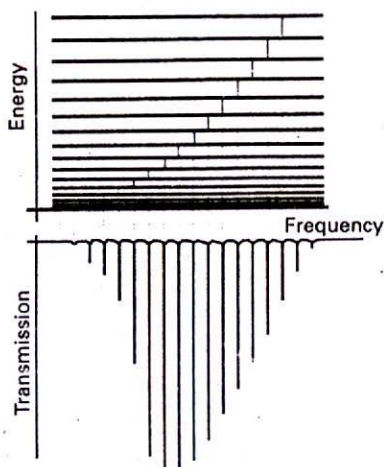
where μ is the permanent electric dipole moment of the molecule. Although the intensity of the absorption varies with J , the dependence is weak and the dominant effect on intensities is the population of the states. It should be noted that the intensity is proportional to the square of the permanent electric dipole moment, so strongly polar molecules give rise to much more intense rotational lines than less polar molecules.

A selection rule for K is needed for symmetric rotors. Any electric dipole moment possessed by a symmetric rotor must lie parallel to the principal axis, as in NF_3 (recall Fig. 15.16). Such a molecule cannot be accelerated into different states of rotation around the figure axis by the absorption of radiation, so $\Delta K = 0$ for a symmetric rotor.

(b) The appearance of rotational spectra

When these selection rules are applied to the expressions for the energy levels of a rigid rotor, it follows that the wavenumbers of the allowed $J + 1 \leftrightarrow J$ absorptions are

$$\tilde{\nu} = 2B(J+1) \quad J = 0, 1, 2, \dots \quad (43)$$



16.24 The rotational energy levels of a linear rotor, the transitions allowed by the selection rule $\Delta J = \pm 1$, and a typical pure rotational absorption spectrum (displayed here in terms of the radiation transmitted through the sample). The intensities reflect the populations of the initial level in each case and the strengths of the transition dipole moments.

When centrifugal distortion is taken into account, the corresponding expression is

$$\tilde{\nu} = 2B(J+1) - 4D_J(J+1)^3 \quad (44)$$

However, because the second term is typically very small compared with the first, the appearance of the spectrum closely resembles that predicted from eqn 43.

Example 16.3 Predicting the appearance of a rotational spectrum

Predict the form of the rotational spectrum of NH_3 .

Method We calculated the energy levels in Example 16.2. The NH_3 molecule is a polar symmetric rotor, so the selection rules $\Delta J = \pm 1$ and $\Delta K = 0$ apply. For absorption, $\Delta J = +1$ and we can use eqn 43. Because $B = 9.977 \text{ cm}^{-1}$, we can draw up the following table for the $J+1 \leftarrow J$ transitions.

J	0	1	2	3	...
$\tilde{\nu}/\text{cm}^{-1}$	19.95	39.91	59.86	79.82	...

The line spacing is 19.95 cm^{-1} .

Self-test 16.4 Repeat the problem for $\text{C}^{35}\text{ClH}_3$ (see Self-test 16.2 for details).

[Lines of separation 0.888 cm^{-1}]

The form of the spectrum predicted by eqn 43 is shown in Fig. 16.24. The most significant feature is that it consists of a series of lines with wavenumbers $2B, 4B, 6B, \dots$ and of separation $2B$. The intensities increase with increasing J and pass through a maximum before tailing off as J becomes large. It should be recalled from Section 16.2 that the observed absorption is the net outcome of the stimulated absorption less the stimulated emission, and that the intensity of each transition depends on the value of J . Hence the value of J corresponding to the most intense line is not quite the same as the value of J for the most highly populated level. The value of J for the most highly populated rotational energy level in a linear molecule is

$$J_{\max} \approx \left(\frac{kT}{2hcB} \right)^{1/2} - \frac{1}{2} \quad (45)$$

For a typical molecule (for example, OCS , with $B = 0.2 \text{ cm}^{-1}$) at room temperature, $kT \approx 1000hcB$, so $J_{\max} \approx 30$.

Justification 16.3

There is a maximum in population because the Boltzmann distribution decays exponentially with increasing J , but the degeneracy of the levels, the number of states with a given energy, increases. Specifically, the population of a rotational energy level J is given by the Boltzmann expression

$$N_J \propto N g_J e^{-E_J/kT}$$

where N is the total number of molecules and g_J is the degeneracy of the level J . The value of J corresponding to a maximum of this expression is found by treating J as a continuous variable, differentiating with respect to J , and then setting the result equal to zero. The result is eqn 45.

The measurement of the line spacing gives B , and hence the moment of inertia perpendicular to the principal axis of the molecule. Because the masses of the atoms are known, it is a simple matter to deduce the bond length of a diatomic molecule. However, in the case of a polyatomic molecule such as OCS or NH_3 , the analysis gives only a single quantity, I_{\perp} , and it is not possible to infer both bond lengths (in OCS) or the bond length and bond angle (in NH_3). This difficulty can be overcome by using isotopically substituted molecules, such as ABC and A'BC; then, by assuming that $R(\text{A}-\text{B}) = R(\text{A}'-\text{B})$, both A-B and B-C bond lengths can be extracted from the two moments of inertia. A famous example of this procedure is the study of OCS; the actual calculation is worked through in Problem 16.12. The assumption that bond lengths are unchanged by isotopic substitution is only an approximation, but it is a good approximation in most cases.

16.7 Rotational Raman spectra

The gross selection rule for rotational Raman transitions is that *the molecule must be anisotropically polarizable*. We begin by explaining what this means.

The distortion of a molecule in an electric field is determined by its polarizability, α (Section 22.1c). More precisely, if the strength of the field is \mathcal{E} , then the molecule acquires an induced dipole moment of magnitude

$$\mu = \alpha \mathcal{E} \quad (46)$$

in addition to any permanent dipole moment it may have. An atom is isotropically polarizable. That is, the same distortion is induced whatever the direction of the applied field. The polarizability of a spherical rotor is also isotropic. However, nonspherical rotors have polarizabilities that do depend on the direction of the field relative to the molecule, so these molecules are anisotropically polarizable (Fig. 16.25). The electron distribution in H_2 , for example, is more distorted when the field is applied parallel to the bond than when it is applied perpendicular to it, and we write $\alpha_{\parallel} > \alpha_{\perp}$.

All linear molecules and diatomics (whether homonuclear or heteronuclear) have anisotropic polarizabilities, and so are rotationally Raman active. This activity is one reason for the importance of rotational Raman spectroscopy, for the technique can be used to study many of the molecules that are inaccessible to microwave spectroscopy. Spherical rotors such as CH_4 and SF_6 , however, are rotationally Raman inactive as well as microwave inactive.⁷

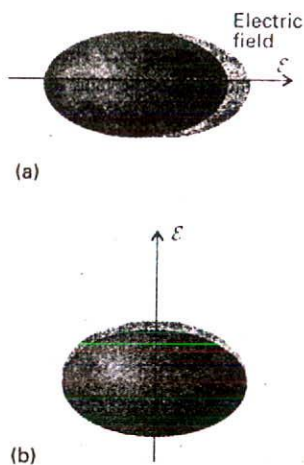
The specific rotational Raman selection rules are

$$\begin{aligned} \text{Linear rotors: } \Delta J &= 0, \pm 2 \\ \text{Symmetric rotors: } \Delta J &= 0, \pm 1, \pm 2; \Delta K = 0 \end{aligned} \quad (47)$$

The classical origin of the ± 2 in these selection rules is outlined in the *Justification* below. The $\Delta J = 0$ transitions do not lead to a shift of the scattered photon's frequency in pure rotational Raman spectroscopy, and contribute to the unshifted Rayleigh radiation observed in the forward direction.⁸

⁷ This inactivity does not mean that such molecules are never found in rotationally excited states. Molecular collisions do not have to obey such restrictive selection rules, and hence collisions between molecules can result in the population of any rotational state.

⁸ See Section 23.5 for the information present in this component under different circumstances.



16.25 An electric field applied to a molecule results in its distortion, and the distorted molecule acquires a contribution to its dipole moment (even if it is nonpolar initially). The polarizability may be different when the field is applied (a) parallel or (b) perpendicular to the molecular axis (or, in general, in different directions relative to the molecule); if that is so, then the molecule has an anisotropic polarizability.

Justification 16.4

If the incident electric field is that of a light wave of frequency ω_i , the induced dipole moment of a molecule is

$$\mu = \alpha \mathcal{E}(t) = \alpha \mathcal{E} \cos \omega_i t$$

If the molecule is rotating at a circular frequency ω_R , to an external observer its polarizability is also time-dependent (if it is anisotropic), and we can write

$$\alpha = \alpha_0 + \Delta\alpha \cos 2\omega_R t$$

where $\Delta\alpha = \alpha_{\parallel} - \alpha_{\perp}$ and α ranges from $\alpha_0 + \Delta\alpha$ to $\alpha_0 - \Delta\alpha$ as the molecule rotates. The 2 appears because the polarizability returns to its initial value twice each revolution (Fig. 16.26). Substituting this expression into the expression for the induced dipole moment gives

$$\begin{aligned} \mu &= (\alpha_0 + \Delta\alpha \cos 2\omega_R t) \times (\mathcal{E} \cos \omega_i t) \\ &= \alpha_0 \mathcal{E} \cos \omega_i t + \mathcal{E} \Delta\alpha \cos 2\omega_R t \cos \omega_i t \\ &= \alpha_0 \mathcal{E} \cos \omega_i t + \frac{1}{2} \mathcal{E} \Delta\alpha \{ \cos(\omega_i + 2\omega_R)t + \cos(\omega_i - 2\omega_R)t \} \end{aligned}$$

This calculation shows that the induced dipole has a component oscillating at the incident frequency (which generates Rayleigh radiation), and that it also has two components at $\omega_i \pm 2\omega_R$, which give rise to the shifted Raman lines. Note that these lines appear only if $\Delta\alpha \neq 0$; hence the polarizability must be anisotropic for there to be Raman lines.

The selection rules can also be explained in terms of the conservation of angular momentum, but the details are tricky because the incoming and scattered photons travel at right angles to each other. However, it should be clear that, because two photons are involved, and each one is a spin-1 particle, a maximum change in angular momentum quantum number of ± 2 is possible.

We can predict the form of the Raman spectrum of a linear rotor by applying the selection rule $\Delta J = \pm 2$ to the rotational energy levels (Fig. 16.27). When the molecule makes a transition with $\Delta J = +2$, the scattered radiation leaves it in a higher rotational state, so the wavenumber of the incident radiation, initially $\bar{\nu}_i$, is decreased. These transitions account for the Stokes lines in the spectrum:

$$\bar{\nu}(J + 2 \leftarrow J) = \bar{\nu}_i - \{F(J + 2) - F(J)\} = \bar{\nu}_i - 2B(2J + 3) \quad (48a)$$

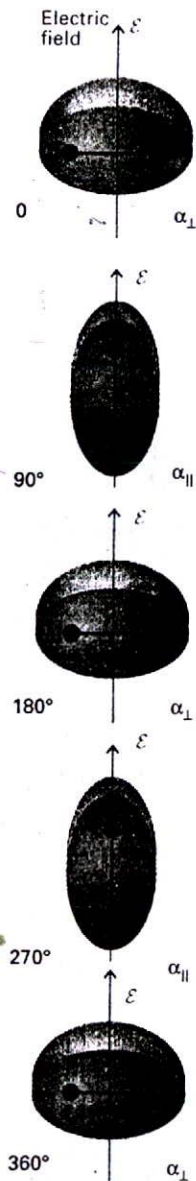
The Stokes lines appear to low frequency of the incident radiation and at displacements $6B, 10B, 14B, \dots$ from $\bar{\nu}_i$ for $J = 0, 1, 2, \dots$. When the molecule makes a transition with $\Delta J = -2$, the scattered photon emerges with increased energy. These transitions account for the anti-Stokes lines of the spectrum:

$$\bar{\nu}(J - 2 \leftarrow J) = \bar{\nu}_i + \{F(J) - F(J - 2)\} = \bar{\nu}_i + 2B(2J - 1) \quad (48b)$$

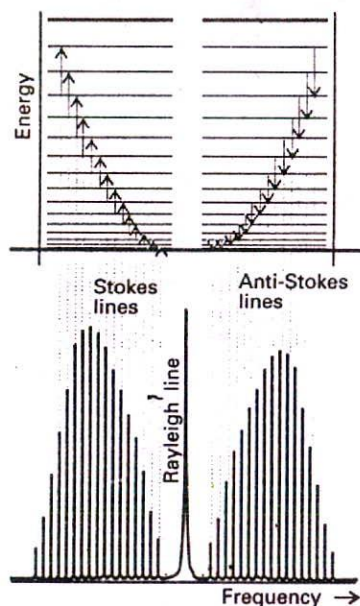
The anti-Stokes lines occur at displacements of $6B, 10B, 14B, \dots$ (for $J = 2, 3, 4, \dots$; $J = 2$ is the lowest state that can contribute under the selection rule $\Delta J = -2$) to high frequency of the incident radiation. The separation of adjacent lines in both the Stokes and the anti-Stokes regions is $4B$, so from its measurement I_{\perp} can be determined and then used to find the bond lengths exactly as in the case of microwave spectroscopy.

Example 16.4 Predicting the form of a Raman spectrum

Predict the form of the rotational Raman spectrum of $^{14}\text{N}_2$, for which $B = 1.99 \text{ cm}^{-1}$, when it is exposed to monochromatic 336.732 nm laser radiation.



16.26 The distortion induced in a molecule by an applied electric field returns to its initial value after a rotation of only 180° (that is, twice a revolution). This is the origin of the $\Delta J = \pm 2$ selection rule in rotational Raman spectroscopy.



16.27 The rotational energy levels of a linear rotor and the transitions allowed by the $\Delta J = \pm 2$ Raman selection rules. The form of a typical rotational Raman spectrum is also shown.

Method The molecule is rotationally Raman active because end-over-end rotation modulates its polarizability as viewed by a stationary observer. The Stokes and anti-Stokes lines are given by eqn 48.

Answer Because $\lambda_i = 336.732 \text{ nm}$ corresponds to $\bar{\nu}_i = 29\,697.2 \text{ cm}^{-1}$, eqns 48a and 48b give the following line positions:

J	0	1	2	3
Stokes lines				
$\bar{\nu}/\text{cm}^{-1}$	29 685.3	29 677.3	29 669.3	29 661.4
λ/nm	336.868	336.958	337.048	337.139
Anti-Stokes-lines				
$\bar{\nu}/\text{cm}^{-1}$			29 709.1	29 717.1
λ/nm			336.597	336.507

Comment There will be a strong central line at 336.732 nm accompanied on either side by lines of increasing and then decreasing intensity (as a result of transition moment and population effects). The spread of the entire spectrum is very small, so the incident light must be highly monochromatic.

Self-test 16.5 Repeat the calculation for the rotational Raman spectrum of NH_3 ($B = 9.977 \text{ cm}^{-1}$).

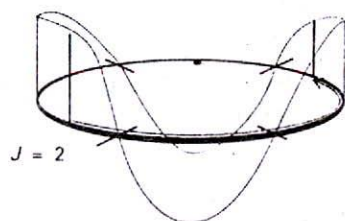
[Stokes lines at $29\,637.3, 29\,597.4, 29\,557.5, 29\,517.6 \text{ cm}^{-1}$,
anti-Stokes lines at $29\,757.1, 29\,797.0 \text{ cm}^{-1}$]

16.8 Nuclear statistics and rotational states

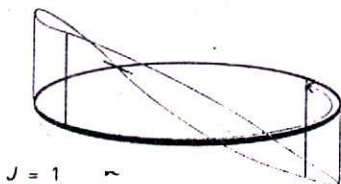
If eqn 48 is used in conjunction with the rotational Raman spectrum of CO_2 , the rotational constant is inconsistent with other measurements of C–O bond lengths. The results are consistent only if it is supposed that the molecule can exist in states with even values of J , so the Stokes lines are $2 \leftarrow 0, 4 \leftarrow 2$, etc. and not $5 \leftarrow 3, 3 \leftarrow 1$, etc.

The explanation of the missing lines is the Pauli principle and the fact that O nuclei are spin-0 bosons: just as the Pauli principle excludes certain electronic states, so too does it exclude certain molecular rotational states. The form of the Pauli principle given in *Justification 13.7* states that, when two identical bosons are exchanged, the overall wavefunction must remain unchanged in every respect, including sign. In particular, when a CO_2 molecule rotates through 180° , two identical O nuclei are interchanged, so the overall wavefunction of the molecule must remain unchanged. However, inspection of the form of the rotational wavefunctions (which have the same form as the s, p , etc. orbitals of atoms) shows that they change sign by $(-1)^J$ under such a rotation (Fig. 16.28). Therefore, only even values of J are permissible for CO_2 , and hence the Raman spectrum shows only alternate lines.

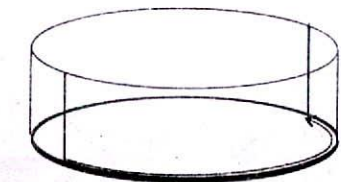
The selective occupation of rotational states that stems from the Pauli principle is termed **nuclear statistics**. Nuclear statistics must be taken into account whenever a rotation interchanges equivalent nuclei. However, the consequences are not always as simple as for CO_2 because there are complicating features when the nuclei have nonzero spin: there may be several different relative nuclear spin orientations consistent with even values of J and a different number of spin orientations consistent with odd values of J . For molecular hydrogen and fluorine, for instance, with their two identical spin- $\frac{1}{2}$ nuclei, we show in the



$J = 2$

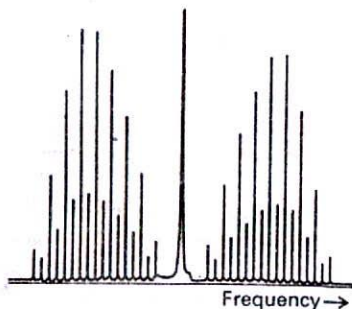


$J = 1$



$J = 0$

16.28 The symmetries of rotational wavefunctions (shown here, for simplicity as a two-dimensional rotor) under a rotation through 180° . Wavefunctions with J even do not change sign; those with J odd do change sign.



16.29 The rotational Raman spectrum of a diatomic molecule with two identical spin- $\frac{1}{2}$ nuclei shows an alternation in intensity as a result of nuclear statistics.

Justification below that there are three times as many ways of achieving a state with odd J than with even J , and there is a corresponding 3 : 1 alternation in intensity in their rotational Raman spectra (Fig. 16.29). In general, for a homonuclear diatomic molecule with nuclei of spin I , the numbers of ways of achieving states of odd and even J are in the ratio

$$\frac{\text{Number of ways of achieving odd } J}{\text{Number of ways of achieving even } J} = \begin{cases} (I+1)/I & \text{for half-integral spin nuclei} \\ I/(I+1) & \text{for integral spin nuclei} \end{cases} \quad (49)$$

For hydrogen, $I = \frac{1}{2}$, and the ratio is 3 : 1. For N_2 , with $I = 1$, the ratio is 1 : 2.

Justification 16.5

Hydrogen nuclei are fermions, so the Pauli principle requires the overall wavefunction to change sign under particle interchange. However, the rotation of an H_2 molecule through 180° has a more complicated effect than merely relabelling the nuclei, because it interchanges their spin states too if the nuclear spins are paired ($\uparrow\downarrow$) but not if they are parallel ($\uparrow\uparrow$).

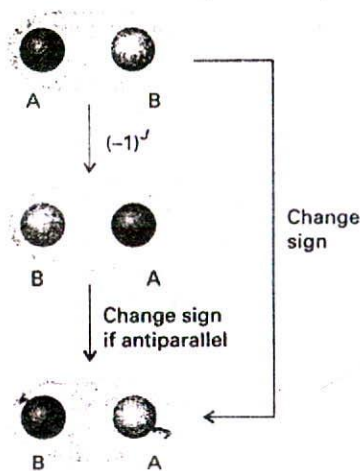
For the overall wavefunction of the molecule to change sign when the spins are parallel, the rotational wavefunction must change sign. Hence, only odd values of J are allowed. In contrast, if the nuclear spins are paired, their wavefunction is $\alpha(A)\beta(B) - \alpha(B)\beta(A)$, which changes sign when α and β are exchanged in order to bring about a simple $A \leftrightarrow B$ interchange overall (Fig. 16.30). Therefore, for the overall wavefunction to change sign in this case requires the rotational wavefunction *not* to change sign. Hence, only even values of J are allowed if the nuclear spins are paired.

As there are three nuclear spin states with parallel spins (just like the triplet state of two parallel electrons, as in Fig. 13.26), but only one state with paired spins (the analogue of the singlet state of two electrons, see Fig. 13.20), it follows that the populations of the odd J and even J states should be in the ratio of 3 : 1, and hence the intensities of transitions originating in these levels will be in the same ratio.

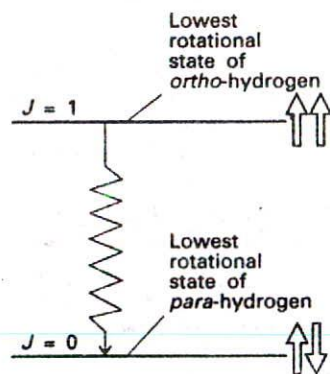
Different relative nuclear spin orientations change into one another only very slowly, so an H_2 molecule with parallel nuclear spins remains distinct from one with paired nuclear spins for long periods. The two forms of hydrogen can be separated by physical techniques, and stored. The form with parallel nuclear spins is called *ortho*-hydrogen and the form with paired nuclear spins is called *para*-hydrogen. Because *ortho*-hydrogen cannot exist in a state with $J = 0$, it continues to rotate at very low temperatures and has an effective rotational zero-point energy (Fig. 16.31). This energy is of some concern to manufacturers of liquid hydrogen, for the slow conversion of *ortho*-hydrogen into *para*-hydrogen (which can exist with $J = 0$) as nuclear spins slowly realign releases rotational energy, which vaporizes the liquid. Techniques are used to accelerate the conversion of *ortho*-hydrogen to *para*-hydrogen to avoid this problem. One such technique is to pass hydrogen over a metal surface: the molecules adsorb on the surface as atoms, which then recombine in the lower energy *para*-hydrogen form.

The vibrations of diatomic molecules

In this section, we adopt the same strategy of finding expressions for the energy levels, establishing the selection rules, and then discussing the form of the spectrum. We shall also see how the simultaneous excitation of rotation modifies the appearance of a vibrational spectrum.



16.30 The interchange of two identical fermion nuclei results in the change in sign of the overall wavefunction. The relabelling can be thought of as occurring in two steps: the first is a rotation of the molecule; the second is the interchange of unlike spins (represented by the different colours of the nuclei). The wavefunction changes sign in the second step if the nuclei have antiparallel spins.



16.31 When hydrogen is cooled, the molecules with parallel nuclear spins accumulate in their lowest available rotational state, the one with $J = 0$. They can enter the lowest rotational state ($J = 0$) only if the spins change their relative orientation and become antiparallel. This is a slow process under normal circumstances, so energy is slowly released.

16.9 Molecular vibrations

We base our discussion on Fig. 16.32, which shows a typical potential energy curve (as in Fig. 14.1) of a diatomic molecule. In regions close to R_e (at the minimum of the curve) the potential energy can be approximated by a parabola, so we can write

$$V = \frac{1}{2}kx^2 \quad x = R - R_e \quad (50)$$

where k is the force constant of the bond. The steeper the walls of the potential (the stiffer the bond), the greater the force constant.

To see the connection between the shape of the molecular potential energy curve and the value of k , note that we can expand the potential energy around its minimum by using a Taylor expansion:

$$V(x) = V(0) + \left(\frac{dV}{dx}\right)_0 x + \frac{1}{2}\left(\frac{d^2V}{dx^2}\right)_0 x^2 + \dots \quad (51)$$

The term $V(0)$ can be set arbitrarily to zero. The first derivative of V is 0 at the minimum. Therefore, the first surviving term is proportional to the square of the displacement. For small displacements we can ignore all the higher terms, and so write

$$V(x) \approx \frac{1}{2}\left(\frac{d^2V}{dx^2}\right)_0 x^2 \quad (52)$$

Therefore, the first approximation to a molecular potential energy curve is a parabolic potential, and we can identify the force constant as

$$k = \left(\frac{d^2V}{dx^2}\right)_0 \quad (53)$$

We see that, if the potential energy curve is sharply curved close to its minimum, then k will be large. Conversely, if the potential energy curve is wide and shallow, then k will be small (Fig. 16.33).

The Schrödinger equation for the relative motion of two atoms of masses m_1 and m_2 with a parabolic potential energy is

$$-\frac{\hbar^2}{2m_{\text{eff}}} \frac{d^2\psi}{dx^2} + \frac{1}{2}kx^2\psi = E\psi \quad (54)$$

where m_{eff} is the effective mass:

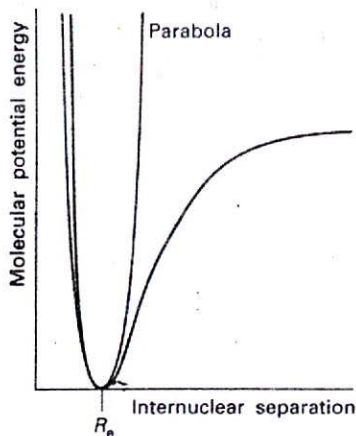
$$m_{\text{eff}} = \frac{m_1 m_2}{m_1 + m_2} \quad (55)$$

These equations are derived in the same way as in *Justification 13.1*, but here the separation of variables procedure is used to separate the relative motion of the atoms from the motion of the molecule as a whole.⁹

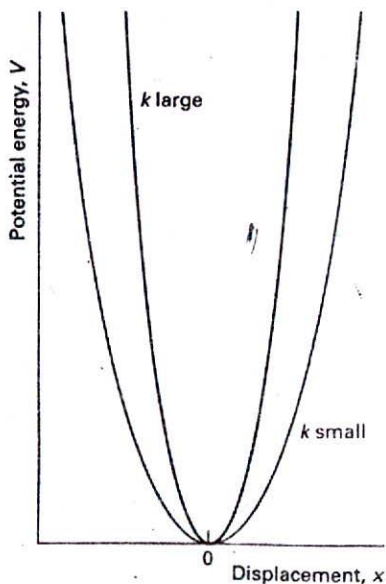
The Schrödinger equation in eqn 54 is the same as eqn 12.30 for a particle of mass m_{eff} undergoing harmonic motion. Therefore, we can use the results of Section 12.4 to write down the permitted vibrational energy levels:

$$E_v = \left(v + \frac{1}{2}\right)\hbar\omega \quad \omega = \left(\frac{k}{m_{\text{eff}}}\right)^{1/2} \quad v = 0, 1, 2, \dots \quad (56)$$

9 In that context, the effective mass is called the 'reduced mass', and the name is widely used in this context too.



16.32 A molecular potential energy curve can be approximated by a parabola near the bottom of the well. The parabolic potential leads to harmonic oscillations. At high excitation energies the parabolic approximation is poor (the true potential is less confining), and is totally wrong near the dissociation limit.



16.33 The force constant is a measure of the curvature of the potential energy close to the equilibrium extension of the bond. A strongly confining well (one with steep sides, a stiff bond) corresponds to high values of k .

The vibrational terms of a molecule, the energies of its vibrational states expressed in wavenumbers, are denoted $G(v)$, with $E_v = hcG(v)$, so

$$G(v) = (v + \frac{1}{2})\tilde{\nu} \quad \tilde{\nu} = \frac{1}{2\pi c} \left(\frac{k}{m_{\text{eff}}} \right)^{1/2} \quad (57)$$

The vibrational wavefunctions are the same as those discussed in Section 12.5.

It is important to note that the vibrational terms depend on the effective mass of the molecule, not directly on its total mass. This dependence is physically reasonable for, if atom 1 were as heavy as a brick wall, then we would find $m_{\text{eff}} \approx m_2$, the mass of the lighter atom. The vibration would then be that of a light atom relative to that of a stationary wall (this is approximately the case in HI, for example, where the I atom barely moves and $m_{\text{eff}} \approx m_{\text{H}}$). For a homonuclear diatomic molecule $m_1 = m_2$, and the effective mass is half the total mass: $m_{\text{eff}} = \frac{1}{2}m$.

Illustration

An HCl molecule has a force constant of 516 N m^{-1} , a reasonably typical value. The effective mass of $^1\text{H}^{35}\text{Cl}$ is $1.63 \times 10^{-27} \text{ kg}$ (note that this mass is very close to the mass of the hydrogen atom, $1.67 \times 10^{-27} \text{ kg}$, so the Cl atom is acting like a brick wall). These values imply $\omega = 5.63 \times 10^{14} \text{ s}^{-1}$, $\nu = 89.5 \text{ THz}$ ($1 \text{ THz} = 10^{12} \text{ Hz}$), $\tilde{\nu} = 2990 \text{ cm}^{-1}$, $\lambda = 3.35 \mu\text{m}$. These characteristics correspond to electromagnetic radiation in the infrared region.

16.10 Selection rules

The gross selection rule for a molecular vibration is that *the electric dipole moment of the molecule must change when the atoms are displaced relative to one another*. Such vibrations are said to be *infrared active*. The classical basis of this rule is that the molecule can shake the electromagnetic field into oscillation if its dipole changes as it vibrates, and vice versa (Fig. 16.34); its formal basis is given in the *Justification* below. Note that the molecule need not have a permanent dipole: the rule requires only a change in dipole moment, possibly from zero. Some vibrations do not affect the molecule's dipole moment (for example, the stretching motion of a homonuclear diatomic molecule), so they neither absorb nor generate radiation: such vibrations are said to be *infrared inactive*. Homonuclear diatomic molecules are infrared inactive because their dipole moments remain zero however long the bond; heteronuclear diatomic molecules are infrared active.

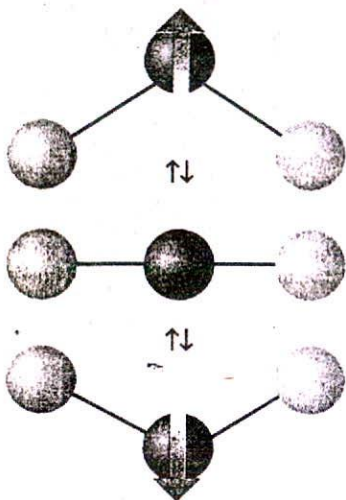
Justification 16.6

The gross selection rule is based on an analysis of the transition dipole moment $\langle v_f | \mu | v_i \rangle$. For simplicity, we shall consider a one-dimensional oscillator (like a diatomic molecule). The electric dipole moment operator depends on the location of all the electrons and all the nuclei in the molecule, so it varies as the internuclear separation changes (Fig. 16.35). If we think of the dipole moment as arising from two partial charges $\pm \delta q$ separated by a distance $R = R_e + x$, we can write its variation with displacement from the equilibrium separation, x , as

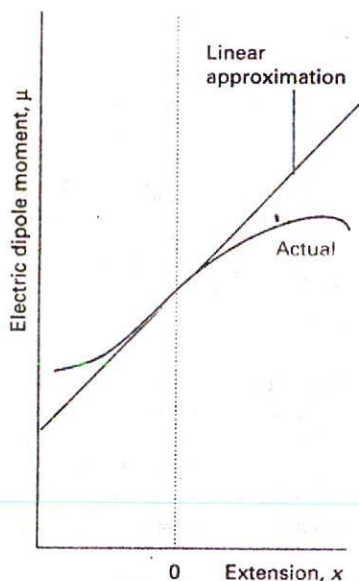
$$\mu = R\delta q = R_e\delta q + x\delta q = \mu_0 + x\delta q$$

where μ_0 is the electric dipole moment operator when the nuclei have their equilibrium separation. It then follows that, with $f \neq i$,

$$\langle v_f | \mu | v_i \rangle = \mu_0 \langle v_f | v_i \rangle + \delta q \langle v_f | x | v_i \rangle$$



16.34 The oscillation of a molecule, even if it is nonpolar, may result in an oscillating dipole that can interact with the electromagnetic field.



16.35 The electric dipole moment of a heteronuclear diatomic molecule varies as shown by the green curve. For small displacements the change in dipole moment is proportional to the displacement.

The term proportional to μ_0 is zero because the states with different values of v are orthogonal. It follows that the transition dipole moment is

$$\langle v_f | \mu | v_i \rangle = \langle v_f | x | v_i \rangle \delta q$$

Because

$$\delta q = \frac{d\mu}{dx}$$

we can write the transition dipole moment more generally as

$$\langle v_f | \mu | v_i \rangle = \langle v_f | x | v_i \rangle \left(\frac{d\mu}{dx} \right) \quad (58)$$

and we see that the right-hand side is zero unless the dipole moment varies with displacement. We consider the matrix element of x in the next *Justification*.

Illustration

Of the molecules N_2 , CO_2 , OCS , H_2O , $CH_2=CH_2$, and C_6H_6 , all except N_2 possess at least one vibrational mode that results in a change of dipole moment, so all except N_2 can show a vibrational absorption spectrum. Not all the modes of complex molecules are vibrationally active. For example, the symmetric stretch of CO_2 , in which the O–C–O bonds stretch and contract symmetrically, is inactive because it leaves the dipole moment unchanged (at zero).

Self-test 16.6 Which of the molecules H_2 , NO , N_2O , and CH_4 have infrared active vibrations?

[NO , N_2O , CH_4]

The specific vibrational selection rule, which is obtained from an analysis of the expression for the transition moment and the properties of integrals over harmonic oscillator wavefunctions (as shown in the *Justification* below), is

$$\Delta v = \pm 1 \quad (59)$$

Transitions for which $\Delta v = +1$ correspond to absorption and those with $\Delta v = -1$ correspond to emission.

Justification 16.7

The specific selection rule is determined by considering the value of the matrix element of x in eqn 58. We need to write out the wavefunctions in terms of the Hermite polynomials given in Section 12.5 and then to use their properties (Example 12.4 should be reviewed, for it gives further details of the calculation). We note that $x = \alpha y$ with $\alpha = (\hbar^2/m_{\text{eff}}k)^{1/4}$ (eqn 12.34), and write

$$\begin{aligned} \langle v_f | x | v_i \rangle &= N_{v_f} N_{v_i} \int_{-\infty}^{\infty} H_{v_f} x H_{v_i} e^{-y^2} dy \\ &= \alpha^2 N_{v_f} N_{v_i} \int_{-\infty}^{\infty} H_{v_f} y H_{v_i} e^{-y^2} dy \end{aligned}$$

To evaluate the integral we use the recursion relation in Table 12.1:

$$yH_v = vH_{v-1} + \frac{1}{2}H_{v+1}$$

This relation turns the matrix element into

$$\begin{aligned} \langle v_f | x | v_i \rangle &= \alpha^2 N_{v_f} N_{v_i} \left\{ v_i \int_{-\infty}^{\infty} H_{v_f} H_{v_i-1} e^{-y^2} dy + \frac{1}{2} \int_{-\infty}^{\infty} H_{v_f} H_{v_i+1} e^{-y^2} dy \right\} \end{aligned}$$

We see from Table 12.1 that the first integral is zero unless $v_f = v_i - 1$ and that the second is zero unless $v_f = v_i + 1$. It follows that the transition dipole moment is zero unless $\Delta v = \pm 1$.

It follows from the specific selection rules that the wavenumbers of allowed vibrational transitions, which are denoted $\Delta G_{v+1/2}$ for the transition $v + 1 \leftarrow v$, are

$$\Delta G_{v+1/2} = G(v+1) - G(v) = \bar{\nu} \quad (60)$$

As we have seen, $\bar{\nu}$ lies in the infrared region of the electromagnetic spectrum, so vibrational transitions absorb and generate infrared radiation.

At room temperature $kT/hc \approx 200 \text{ cm}^{-1}$, and most vibrational wavenumbers are significantly greater than 200 cm^{-1} . It follows from the Boltzmann distribution that almost all the molecules will be in their vibrational ground states initially. Hence, the dominant spectral transition will be the **fundamental transition**, $1 \leftarrow 0$. As a result, the spectrum is expected to consist of a single absorption line. If the molecules are formed in a vibrationally excited state, such as when vibrationally excited HF molecules are formed in the reaction $\text{H}_2 + \text{F}_2 \rightarrow 2\text{HF}^*$, the transitions $5 \rightarrow 4$, $4 \rightarrow 3$, etc. may also appear (in emission). In the harmonic approximation, all these lines lie at the same frequency, and the spectrum is also a single line. However, as we shall now show, the breakdown of the harmonic approximation causes the transitions to lie at slightly different frequencies, so several lines are observed.

16.11 Anharmonicity

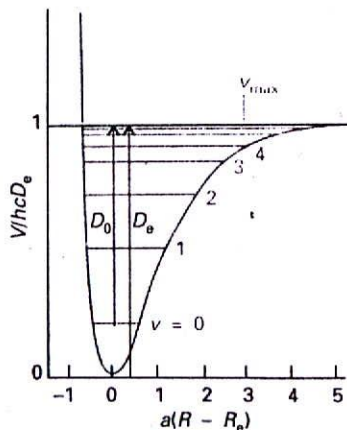
The vibrational terms in eqn 60 are only approximate because they are based on a parabolic approximation to the actual potential energy curve. A parabola cannot be correct at all extensions because it does not allow a bond to dissociate. At high vibrational excitations the swing of the atoms (more precisely, the spread of the vibrational wavefunction) allows the molecule to explore regions of the potential energy curve where the parabolic approximation is poor and additional terms in the Taylor expansion of V (eqn 51) must be retained. The motion then becomes **anharmonic**, in the sense that the restoring force is no longer proportional to the displacement. Because the actual curve is less confining than a parabola, we can anticipate that the energy levels become less widely spaced at high excitations.

(a) The convergence of energy levels

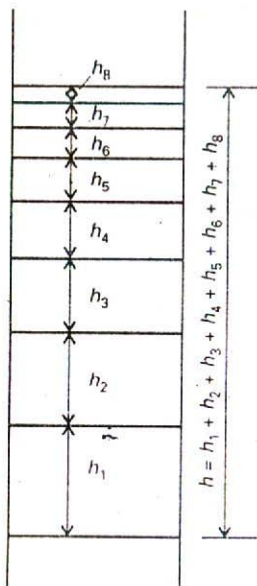
One approach to the calculation of the energy levels in the presence of anharmonicity is to use a function that resembles the true potential energy more closely. The Morse potential energy is

$$V = hcD_e \left\{ 1 - e^{-a(R-R_e)} \right\}^2 \quad a = \left(\frac{m_{\text{eff}} \omega^2}{2hcD_e} \right)^{1/2} \quad (61)$$

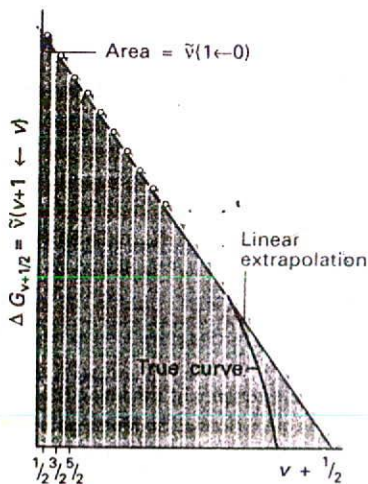
where D_e is the depth of the potential minimum (Fig. 16.36). Near the well minimum the variation of V with displacement resembles a parabola (as can be checked by expanding the exponential as far as the first term) but, unlike a parabola, eqn 61 allows for dissociation at



16.36 The Morse potential energy curve reproduces the general shape of a molecular potential energy curve. The corresponding Schrödinger equation can be solved, and the values of the energies obtained. The number of bound levels is finite. The illustration also shows the relation between the dissociation energy, D_0 , and the minimum energy, D_e , of a molecular potential energy curve.



16.37 The dissociation energy is the sum of the separations of the vibrational energy levels up to the dissociation limit just as the length of a ladder is the sum of the separations of its rungs.



16.38 The area under a plot of transition wavenumber against vibrational quantum number is equal to the dissociation energy of the molecule. The assumption that the differences approach zero linearly is the basis of the Birge-Sponer extrapolation.

large displacements. The Schrödinger equation can be solved for the Morse potential and the permitted energy levels are

$$G(v) = (v + \frac{1}{2})\bar{\nu} - (v + \frac{1}{2})^2 x_e \bar{\nu} \quad x_e = \frac{a^2 \hbar}{2\mu\omega} = \frac{\bar{\nu}}{4D_e} \quad (62)$$

The parameter x_e is called the **anharmonicity constant**. The number of vibrational levels of a Morse oscillator is finite, and $v = 0, 1, 2, \dots, v_{\max}$, as shown in Fig. 16.36. The second term in the expression for G subtracts from the first with increasing effect as v increases, and hence gives rise to the convergence of the levels at high quantum numbers.

Although the Morse oscillator is quite useful theoretically, in practice the more general expression

$$G(v) = (v + \frac{1}{2})\bar{\nu} - (v + \frac{1}{2})^2 x_e \bar{\nu} + (v + \frac{1}{2})^3 y_e \bar{\nu} + \dots \quad (63)$$

where x_e, y_e, \dots are empirical constants characteristic of the molecule, is used to fit the experimental data and to find the dissociation energy of the molecule. When anharmonicities are present, the wavenumbers of transitions with $\Delta v = +1$ are

$$\Delta G_{v+1/2} = \bar{\nu} - 2(v + 1)x_e \bar{\nu} + \dots \quad (64)$$

The latter equation shows that when $x_e \neq 0$ the transitions move to lower wavenumbers as v increases.

Anharmonicity also accounts for the appearance of additional weak absorption lines corresponding to the transitions $2 \leftarrow 0, 3 \leftarrow 0$, etc., even though these first, second, ... overtones are forbidden by the selection rule $\Delta v = \pm 1$. The first overtone, for example, gives rise to an absorption at

$$G(v + 2) - G(\bar{v}) = 2\bar{\nu} - 2(2v + 3)x_e \bar{\nu} + \dots \quad (65)$$

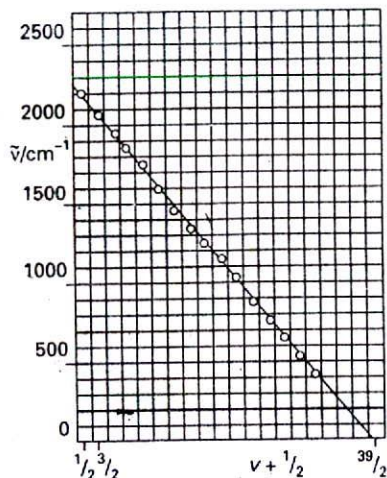
The reason for the appearance of overtones is that the selection rule is derived from the properties of harmonic oscillator wavefunctions, which are only approximately valid when anharmonicity is present. Therefore, the selection rule is also only an approximation. For an anharmonic oscillator, all values of Δv are allowed, but transitions with $\Delta v > 1$ are allowed only weakly if the anharmonicity is slight.

(b) The Birge-Sponer plot

When several vibrational transitions are detectable, a graphical technique called a **Birge-Sponer plot** may be used to determine the dissociation energy, D_0 , of the bond. The basis of the Birge-Sponer plot is that the sum of successive intervals $\Delta G_{v+1/2}$ from the zero-point level to the dissociation limit is the dissociation energy:

$$D_0 = \Delta G_{1/2} + \Delta G_{3/2} + \dots = \sum_v \Delta G_{v+1/2} \quad (66)$$

just as the height of the ladder is the sum of the separations of its rungs (Fig. 16.37). The construction in Fig. 16.38 shows that the area under the plot of $\Delta G_{v+1/2}$ against $v + \frac{1}{2}$ is equal to the sum, and therefore to D_0 . The successive terms decrease linearly when only the x_e anharmonicity constant is taken into account and the inaccessible part of the spectrum can be estimated by linear extrapolation. Most actual plots differ from the linear plot as shown in the illustration, so the value of D_0 obtained in this way is usually an overestimate of the true value.



16.39 The Birge-Sponer plot used in Example 16.5. The area is obtained simply by counting the squares beneath the line or using the formula for the area of a right triangle.

Example 16.5 Using a Birge-Sponer plot

The observed vibrational intervals of H_2^+ lie at the following values for $1 \leftarrow 0, 2 \leftarrow 1, \dots$ respectively (in cm^{-1}): 2191, 2064, 1941, 1821, 1705, 1591, 1479, 1368, 1257, 1145, 1033, 918, 800, 677, 548, 411. Determine the dissociation energy of the molecule.

Method Plot the separations against $v + \frac{1}{2}$, extrapolate linearly to the point cutting the horizontal axis, and then measure the area under the curve.

Answer The points are plotted in Fig. 16.39, and a linear extrapolation is shown as a dotted line. The area under the curve (use the formula for the area of a triangle or count the squares) is 214. Each square corresponds to 100 cm^{-1} (refer to the scale of the vertical axis); hence the dissociation energy is $21\,400 \text{ cm}^{-1}$ (corresponding to 256 kJ mol^{-1}).

Self-test 16.7 The vibrational levels of HgH converge rapidly, and successive intervals are $1203.7, 965.6, 632.4$, and 172 cm^{-1} . Estimate the dissociation energy.

[35.6 kJ mol^{-1}]

16.12 Vibration-rotation spectra

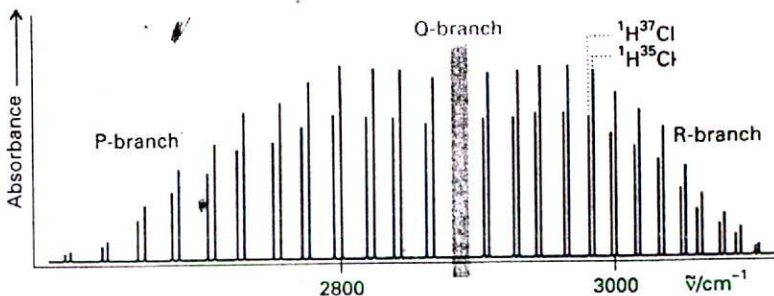
Each line of the high-resolution vibrational spectrum of a gas-phase heteronuclear diatomic molecule is found to consist of a large number of closely spaced components (Fig. 16.40). Hence, molecular spectra are often called **band spectra**. The separation between the components is of the order of 10 cm^{-1} , which suggests that the structure is due to rotational transitions accompanying the vibrational transition. A rotational change should be expected because classically we can think of the transition as leading to a sudden increase or decrease in the instantaneous bond length. Just as ice-skaters rotate more rapidly when they bring their arms in, and more slowly when they throw them out, so the molecular rotation is either accelerated or retarded by a vibrational transition.

(a) Spectral branches

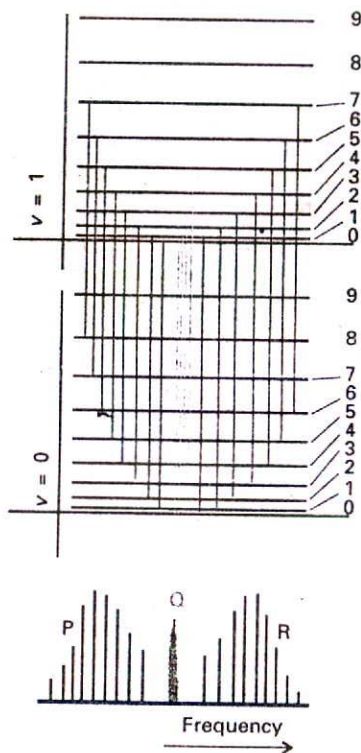
A detailed analysis of the quantum mechanics of simultaneous vibrational and rotational changes shows that the rotational quantum number J changes by ± 1 during the vibrational transition of a diatomic molecule. If the molecule also possesses angular momentum about its axis, as in the case of the electronic orbital angular momentum of the $^2\Pi$ molecule NO , then the selection rules also allow $\Delta J = 0$.

The appearance of the vibration-rotation spectrum of a diatomic molecule can be discussed in terms of the combined vibration-rotation terms, S :

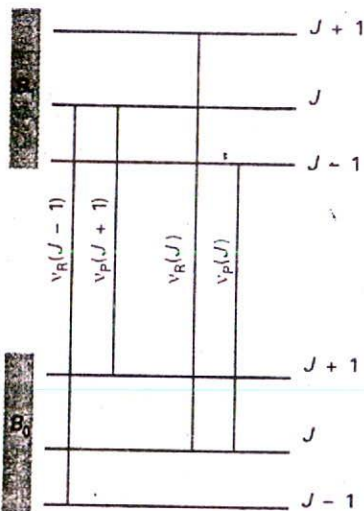
$$S(\nu, J) = G(\nu) + F(J) \quad (67)$$



16.40 A high-resolution vibration-rotation spectrum of HCl . The lines appear in pairs because $^1\text{H}^{35}\text{Cl}$ and $^1\text{H}^{37}\text{Cl}$ both contribute (their abundance ratio is 3 : 1). There is no Q branch, because $\Delta J = 0$ is forbidden for this molecule.



16.41 The formation of P, Q, and R branches in a vibration-rotation spectrum. The intensities reflect the populations of the initial rotational levels.



16.42 The method of combination differences makes use of the fact that some transitions share a common level.

If we ignore anharmonicity and centrifugal distortion,

$$S(v, J) = (v + \frac{1}{2})\bar{\nu} + BJ(J + 1) \quad (68)$$

In a more detailed treatment, B is allowed to depend on the vibrational state because as v increases the molecule swells slightly and the moment of inertia changes. We shall continue with the simple expression initially.

When the vibrational transition $v + 1 \leftarrow v$ occurs, J changes by ± 1 and in some cases by 0 (when $\Delta J = 0$ is allowed). The absorptions then fall into three groups called branches of the spectrum. The **P** branch consists of all transitions with $\Delta J = -1$:

$$\bar{\nu}_P(J) = S(v + 1, J - 1) - S(v, J) = \bar{\nu} - 2BJ \quad (69a)$$

This branch consists of lines at $\bar{\nu} - 2B, \bar{\nu} - 4B, \dots$ with an intensity distribution reflecting both the populations of the rotational levels and the magnitude of the $J - 1 \leftarrow J$ transition moment (Fig. 16.41). The **Q** branch consists of all lines with $\Delta J = 0$, and its wavenumbers are all

$$\bar{\nu}_Q(J) = S(v + 1, J) - S(v, J) = \bar{\nu} \quad (69b)$$

for all values of J . This branch, when it is allowed (as in NO), forms a single line at the vibrational transition wavenumber. In practice, because the rotational constants of the two vibrational levels are slightly different, the Q branch appears as a cluster of closely spaced lines. In Fig. 16.41 there is a gap at the expected location of the Q branch because it is forbidden in HCl. The **R** branch consists of lines with $\Delta J = +1$:

$$\bar{\nu}_R(J) = S(v + 1, J + 1) - S(v, J) = \bar{\nu} + 2B(J + 1) \quad (69c)$$

This branch consists of lines displaced from $\bar{\nu}$ to high wavenumber by $2B, 4B, \dots$

The separation between the lines in the P and R branches of a vibrational transition gives the value of B . Therefore, the bond length can be deduced without needing to take a pure rotational microwave spectrum. However, the latter is more precise.

(b) Combination differences

The rotational constant of the vibrationally excited state, B_1 (in general, B_v), is in fact slightly smaller than that of the ground vibrational state, B_0 , because the anharmonicity of the vibration results in a slightly extended bond in the upper state. As a result, the Q branch (if it exists) consists of a series of closely spaced lines, the lines of the R branch converge slightly as J increases, and those of the P branch diverge:

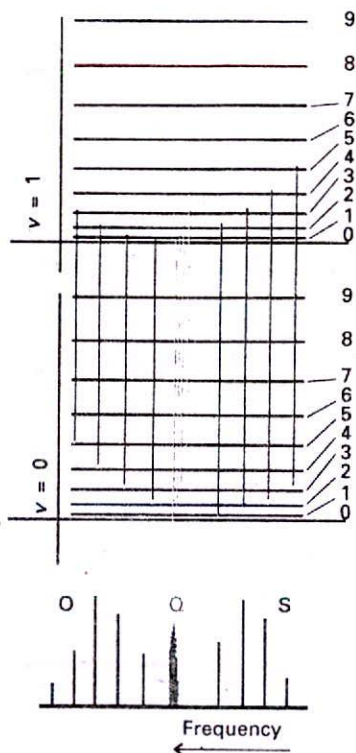
$$\begin{aligned} \bar{\nu}_P(J) &= \bar{\nu} - (B_1 + B_0)J + (B_1 - B_0)J^2 \\ \bar{\nu}_Q(J) &= \bar{\nu} + (B_1 - B_0)J(J + 1) \\ \bar{\nu}_R(J) &= \bar{\nu} + (B_1 + B_0)(J + 1) + (B_1 - B_0)(J + 1)^2 \end{aligned} \quad (70)$$

To determine the two rotational constants individually, we use the method of combination differences. This procedure is used widely in spectroscopy to extract information about a particular state. It involves setting up expressions for the difference in the wavenumbers of transitions to a common state; the resulting expression then depends solely on properties of the other state.

As can be seen from Fig. 16.42, the transitions $\bar{\nu}_R(J - 1)$ and $\bar{\nu}_P(J + 1)$ have a common upper state, and hence can be anticipated to depend on B_1 . Indeed, it is easy to show from eqn 70 that

$$\bar{\nu}_R(J - 1) - \bar{\nu}_P(J + 1) = 4B_0(J + \frac{1}{2}) \quad (71a)$$

Therefore, a plot of the combination difference against $J + \frac{1}{2}$ should be a straight line of slope $4B_0$, so the rotational constant of the molecule in the state $v = 0$ can be determined.



16.43 The formation of O, Q, and S branches in a vibration-rotation Raman spectrum of a linear rotor. Note that the frequency scale runs in the opposite direction to that in Fig. 16.41, because the higher energy transitions (on the right) extract more energy from the incident beam and leave it at lower frequency.

(Any deviation from a straight line is a consequence of centrifugal distortion, so that effect can be investigated too.) Similarly, $\tilde{\nu}_R(J)$ and $\tilde{\nu}_P(J)$ have a common lower state, and hence their combination difference gives information about the upper state:

$$\tilde{\nu}_R(J) - \tilde{\nu}_P(J) = 4B_1(J + \frac{1}{2}) \quad (71b)$$

The two rotational constants of $^1\text{H}^{35}\text{Cl}$ found in this way are $B_0 = 10.440 \text{ cm}^{-1}$ and $B_1 = 10.136 \text{ cm}^{-1}$.

16.13 Vibrational Raman spectra of diatomic molecules

The gross selection rule for vibrational Raman transitions is that *the polarizability should change as the molecule vibrates*. As homonuclear and heteronuclear diatomic molecules swell and contract during a vibration, the control of the nuclei over the electrons varies, and hence the molecular polarizability changes. Both types of diatomic molecule are therefore vibrationally Raman active.

The specific selection rule for vibrational Raman transitions in the harmonic approximation is $\Delta v = \pm 1$. The lines to high frequency of the incident light, the anti-Stokes lines, are those for which $\Delta v = -1$. They are usually weak because very few molecules are in an excited vibrational state initially. The lines to low frequency, the Stokes lines, correspond to $\Delta v = +1$. In gas-phase spectra, these lines have a branch structure arising from the simultaneous rotational transitions that accompany the vibrational excitation (Fig. 16.43). The selection rules are $\Delta J = 0, \pm 2$ (as in pure rotational Raman spectroscopy), and give rise to the O branch ($\Delta J = -2$), the Q branch ($\Delta J = 0$), and the S branch ($\Delta J = +2$):

$$\begin{aligned} \tilde{\nu}_O(J) &= \tilde{\nu}_i - \tilde{\nu} - 2B + 4BJ \\ \tilde{\nu}_Q(J) &= \tilde{\nu}_i - \tilde{\nu} \\ \tilde{\nu}_S(J) &= \tilde{\nu}_i - \tilde{\nu} - 6B + 4BJ \end{aligned} \quad (72)$$

Note that, unlike in infrared spectroscopy, a Q branch is obtained for all linear molecules. The spectrum of CO, for instance, is shown in Fig. 16.44: the structure of the Q branch arises from the differences in rotational constants of the upper and lower vibrational states.

The information available from vibrational Raman spectra adds to that from infrared spectroscopy because homonuclear diatomics can also be studied. The spectra can be interpreted in terms of the force constants, dissociation energies, and bond lengths, and some of the information obtained is included in Table 16.2.

The vibrations of polyatomic molecules

There is only one mode of vibration for a diatomic molecule, the bond stretch. In polyatomic molecules there are several modes of vibration because all the bond lengths and angles may change.

16.14 Normal modes

We begin by calculating the total number of vibrational modes of a polyatomic molecule. We then see that we can choose combinations of these atomic displacements that give the simplest description of the vibrations.

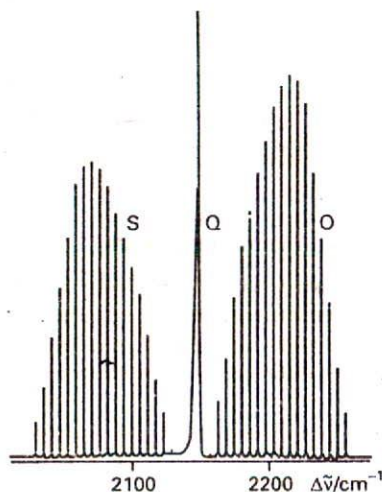
(a) The number of vibrational modes

As shown in the *Justification* below, for a nonlinear molecule that consists of N atoms, there are $3N - 6$ independent modes of vibration. If the molecule is linear, there are $3N - 5$ independent vibrational modes.

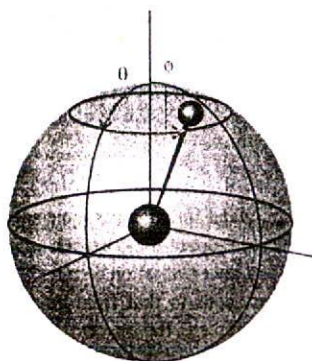
Table 16.2* Properties of diatomic molecules

	$\tilde{\nu}/\text{cm}^{-1}$	B/cm^{-1}	$k/(\text{N m}^{-1})$
$^1\text{H}_2$	4400	60.86	575
$^1\text{H}^{35}\text{Cl}$	2991	10.59	516
$^1\text{H}^{127}\text{I}$	2309	6.61	313
$^{35}\text{Cl}_2$	560	0.244	323

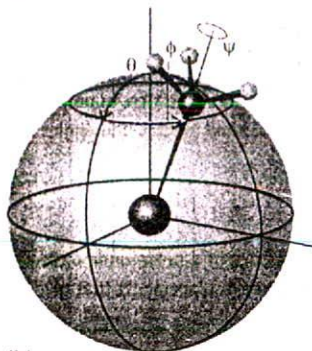
* More values are given in the *Data section* at the end of this volume. See Tables 14.2 and 14.3 for related information (on D_e and R_e).



16.44 The structure of a vibrational line in the vibrational Raman spectrum of carbon monoxide, showing the O, Q, and S branches.



(a)



(b)

16.45 (a) The orientation of a linear molecule requires the specification of two angles. (b) The orientation of a nonlinear molecule requires the specification of three angles.

Justification 16.8

The total number of coordinates needed to specify the locations of N atoms is $3N$. Each atom may change its location by varying one of its three coordinates (x , y , and z), so the total number of displacements available is $3N$. These displacements can be grouped together in a physically sensible way. For example, three coordinates are needed to specify the location of the centre of mass of the molecule, so three of the $3N$ displacements correspond to the translational motion of the molecule as a whole. The remaining $3N - 3$ are non-translational 'internal' modes of the molecule.

Two angles are needed to specify the orientation of a linear molecule in space: in effect, we need to give only the latitude and longitude of the direction in which the molecular axis is pointing (Fig. 16.45a). However, three angles are needed for a nonlinear molecule because we also need to specify the orientation of the molecule around the direction defined by the latitude and longitude (Fig. 16.45b). Therefore, two (linear) or three (nonlinear) of the $3N - 3$ internal displacements are rotational. This leaves $3N - 5$ (linear) or $3N - 6$ (nonlinear) displacements of the atoms relative to one another: these are the vibrational modes. It follows that the number of modes of vibration N_{vib} is $3N - 5$ for linear molecules and $3N - 6$ for nonlinear molecules.

Illustration

Water, H_2O , is a nonlinear triatomic molecule, and has three modes of vibration (and three modes of rotation); CO_2 is a linear triatomic molecule, and has four modes of vibration (and only two modes of rotation). Even a middle-sized molecule such as naphthalene (C_{10}H_8) has 48 distinct modes of vibration.

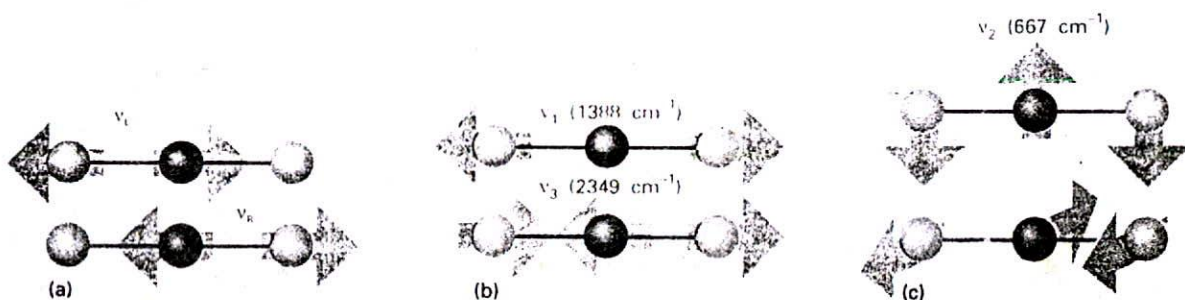
(b) Combinations of displacements

The next step is to find the best description of the modes. One choice for the four modes of CO_2 , for example, might be the ones in Fig. 16.46a. This illustration shows the stretching of one bond (the mode ν_L), the stretching of the other (ν_R), and the two perpendicular bending modes (ν_2). The description, while permissible, has a disadvantage: when one CO bond vibration is excited, the motion of the C atom sets the other CO bond in motion, so energy flows backwards and forwards between ν_L and ν_R . Moreover, the position of the centre of mass of the molecule varies in the course of either vibration.

The description of the vibrational motion is much simpler if linear combinations of ν_L and ν_R are taken. For example, one combination is ν_1 in Fig. 16.46b: this mode is the symmetric stretch. In this mode, the C atom is buffeted simultaneously from each side and the motion continues indefinitely. Another mode is ν_3 , the antisymmetric stretch, in which the two O atoms always move in the same direction and opposite to that of the C atom. Both modes are independent in the sense that, if one is excited, then it does not excite the other. They are two of the 'normal modes' of the molecule, its independent, collective vibrational displacements. The two other normal modes are the bending modes ν_2 . In general, a normal mode is an independent, synchronous motion of atoms or groups of atoms that may be excited without leading to the excitation of any other normal mode.

The four normal modes of CO_2 , and the N_{vib} normal modes of polyatomics in general, are the key to the description of molecular vibrations. Each normal mode, q , behaves like an independent harmonic oscillator (if anharmonicities are neglected), so each has a series of terms

$$G_q(v) = (v + \frac{1}{2})\tilde{\nu}_q \quad \tilde{\nu}_q = \frac{1}{2\pi c} \left(\frac{k_q}{m_q} \right)^{1/2} \quad (73)$$

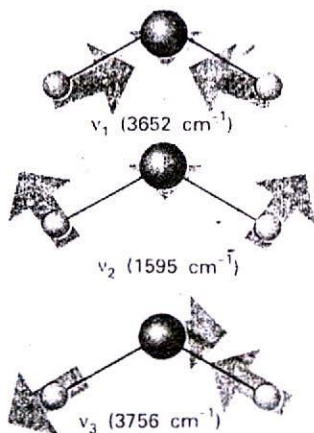


16.46 Alternative descriptions of the vibrations of CO₂. (a) The stretching modes are not independent, and if one CO group is excited the other begins to vibrate. (b) The symmetric and antisymmetric stretches are independent, and one can be excited without affecting the other: they are normal modes. (c) The two perpendicular bending motions are also normal modes.

where $\bar{\nu}_q$ is the wavenumber of mode q and depends on the force constant k_q for the mode and on the effective mass m_q of the mode. The effective mass of the mode is a measure of the mass that is swung about by the vibration and in general is a complicated function of the masses of the atoms. For example, in the symmetric stretch of CO₂, the C atom is stationary, and the effective mass depends on the masses of only the O atoms. In the antisymmetric stretch and in the bends, all three atoms move, so all contribute to the effective mass. The three normal modes of H₂O are shown in Fig. 16.47: note that the predominantly bending mode (ν_2) has a lower frequency than the others, which are predominantly stretching modes. It is generally the case that the frequencies of bending motions are lower than those of stretching modes. One point that must be appreciated is that only in special cases (such as the CO₂ molecule) are the normal modes purely stretches or purely bends. In general, a normal mode is a composite motion of simultaneous stretching and bending of bonds. Another point in this connection is that heavy atoms generally move less than light atoms in normal modes.

(c) The symmetry species of normal modes

One of the most powerful ways of dealing with normal modes, especially of complex molecules, is to classify them according to their symmetries. Each normal mode must belong to one of the symmetry species of the molecular point group, as discussed in Chapter 15.

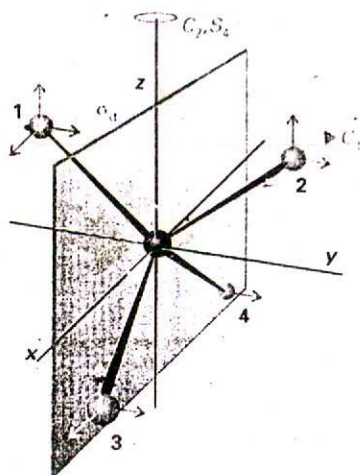


16.47 The three normal modes of H₂O. The mode ν_2 is predominantly bending, and occurs at lower wavenumber than the other two.

Example 16.6 Identifying the symmetry species of a normal mode

Establish the symmetry species of the normal mode vibrations of CH₄, which belongs to the group T_d .

Method The first step in the procedure is to identify the symmetry species of the irreducible representations spanned by all the $3N$ displacements of the atoms, using the characters of the molecular point group. Find these characters by counting 1 if the displacement is unchanged under a symmetry operation, -1 if it changes sign, and 0 if it is changed into some other displacement. Next, subtract the symmetry species of the translations. Translational displacements span the same symmetry species as x , y , and z , so they can be obtained from the right-most column of the character table. Finally, subtract the symmetry species of the rotations, which are also given in the character table (and denoted there by R_x , R_y , or R_z).



16.48 The atomic displacements of CH_4 and the symmetry elements used to calculate the characters.

Answer There are $3 \times 5 = 15$ degrees of freedom, of which $3 \times 5 - 6 = 9$ are vibrations. Refer to Fig. 16.48. Under E , no displacement coordinates are changed, so the character is 15. Under C_3 , no displacements are left unchanged, so the character is 0. Under the C_2 indicated, the z -displacement of the central atom is left unchanged, whereas its x - and y -components both change sign. Therefore $\chi(C_2) = 1 - 1 - 1 + 0 + 0 + \dots = -1$. Under the S_4 indicated, the z -displacement of the central atom is reversed, so $\chi(S_4) = -1$. Under σ_d , the x - and z -displacements of C, H_3 , and H_4 are left unchanged and the y -displacements are reversed; hence $\chi(\sigma_d) = 3 + 3 - 3 = 3$. The characters are therefore 15, 0, -1, -1, 3, corresponding to $A_1 + E + T_1 + 3T_2$. The translations span T_2 ; the rotations span T_1 . Hence, the nine vibrations span $A_1 + E + 2T_2$.

Comment The modes themselves are shown in Fig. 16.49. We shall see that symmetry analysis gives a quick way of deciding which modes are active.

Self-test 16.8 Establish the symmetry species of the normal modes of H_2O .

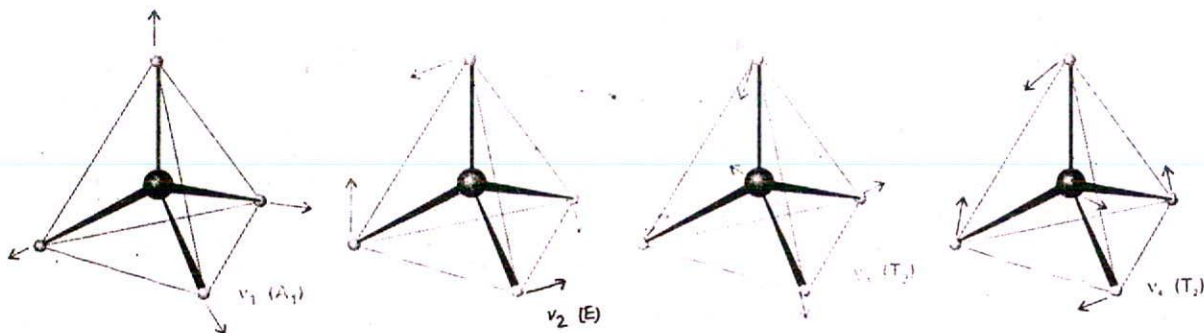
[$2A_1 + B_2$]

16.15 The vibrational spectra of polyatomic molecules

The gross selection rule for infrared activity is that *the motion corresponding to a normal mode should be accompanied by a change of dipole moment*. Deciding whether this is so can sometimes be done by inspection. For example, the symmetric stretch of CO_2 leaves the dipole moment unchanged (at zero, see Fig. 16.46), so this mode is infrared inactive. The antisymmetric stretch, however, changes the dipole moment because the molecule becomes unsymmetrical as it vibrates, so this mode is infrared active. Because the dipole moment change is parallel to the principal axis, the transitions arising from this mode are classified as **parallel bands** in the spectrum. Both bending modes are infrared active: they are accompanied by a changing dipole perpendicular to the principal axis, so transitions involving them lead to a **perpendicular band** in the spectrum. The latter bands eliminate the linearity of the molecule, and as a result a Q branch is observed; a parallel band does not have a Q branch.

(a) Symmetry and normal mode activity

It is best to use group theory to judge the activities of more complex modes of vibration. This is easily done by checking the character table of the molecular point group for the symmetry



16.49 Typical normal modes of vibration of a tetrahedral molecule. There are in fact two modes of symmetry species E and three modes of each T_2 symmetry species.

species of the irreducible representations spanned by x , y , and z , for their species are also the symmetry species of the components of the electric dipole moment. Then apply the following rule:

If the symmetry species of a normal mode is the same as any of the symmetry species of x , y , or z , then the mode is infrared active.

Justification 16.9

The rule hinges on the form of the transition dipole moment between the ground-state vibrational wavefunction, ψ_0 , and that of the first excited state, ψ_1 . The x -component is

$$\mu_{x,10} = \langle 1 | \mu_x | 0 \rangle = -e \int \psi_1^* x \psi_0 d\tau \quad (74)$$

for the x -component, with similar expressions for the two other components of the transition moment. The ground-state vibrational wavefunction is a Gaussian function of the form e^{-x^2} , so it is symmetrical in x . The wavefunction for the first excited state gives a nonvanishing integral only if it is proportional to x , for then the integrand is proportional to x^2 rather than to xy or xz . Consequently, the excited state wavefunction must have the same symmetry as the displacement x .

Example 16.7 Identifying infrared active modes

Which modes of CH_4 are infrared active?

Method Refer to the T_d character table to establish the symmetry species of x , y , and z for this molecule, and then use the rule given above.

Answer The functions x , y , and z span T_2 . We found in Example 16.6 that the symmetry species of the normal modes are $A_1 + E + 2T_2$. Therefore, only the T_2 modes are infrared active.

Comment The distortions accompanying these modes lead to a changing dipole moment. The A_1 mode, which is inactive, is the symmetrical 'breathing' mode of the molecule.

Self-test 16.9 Which of the normal modes of H_2O are infrared active?

[All three]

(b) The appearance of the spectrum

The active modes are subject to the specific selection rule $\Delta v_q = \pm 1$ in the harmonic approximation, so the wavenumber of the fundamental transition (the 'first harmonic') of each active mode is $\tilde{\nu}_q$. From the analysis of the spectrum, a picture may be constructed of the stiffness of various parts of the molecule: that is, we can establish its force field, the set of force constants corresponding to all the displacements of the atoms. Superimposed on this simple scheme are the complications arising from anharmonicities and the effects of molecular rotation. Very often the sample is a liquid or a solid, and the molecules are unable to rotate freely. In a liquid, for example, a molecule may be able to rotate through only a few degrees before it is struck by another, so it changes its rotational state frequently. This random changing of orientation is called **tumbling**.

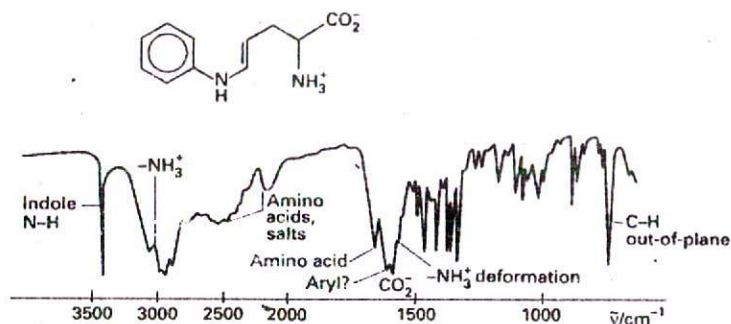
Table 16.3* Typical vibrational wavenumbers, $\bar{\nu}/\text{cm}^{-1}$

C—H stretch	2850–2960
C—H bend	1340–1465
C—C stretch	700–1250
C=C stretch	1620–1680

*More values are given in the Data section.

The lifetimes of rotational states in liquids are very short, so in most cases the rotational energies are ill-defined. Collisions occur at a rate of about 10^{13} s^{-1} and, even allowing for only a 10 per cent success rate in knocking the molecule into another rotational state, a lifetime broadening (eqn 24) of more than 1 cm^{-1} can easily result. The rotational structure of the vibrational spectrum is blurred by this effect, so the infrared spectra of molecules in condensed phases usually consist of broad lines spanning the entire range of the resolved gas-phase spectrum, and showing no branch structure.

One very important application of infrared spectroscopy to condensed phase samples, and for which the blurring of the rotational structure by random collisions is a welcome simplification, is to chemical analysis. The vibrational spectra of different groups in a molecule give rise to absorptions at characteristic frequencies. Their intensities are also transferable between molecules. Consequently, the molecules in a sample can often be identified by examining its infrared spectrum and referring to a table of characteristic frequencies and intensities (Table 16.3 and Fig. 16.50).



16.50 The infrared absorption spectrum of an amino acid, and a partial assignment.

16.16 Vibrational Raman spectra of polyatomic molecules

The normal modes of vibration of molecules are Raman active if they are accompanied by a changing polarizability. It is sometimes quite difficult to judge by inspection when this is so. The symmetric stretch of CO_2 , for example, alternately swells and contracts the molecule: this motion changes the polarizability of the molecule, so the mode is Raman active. The other modes of CO_2 leave the polarizability unchanged, so they are Raman inactive.

(a) Symmetry aspects of Raman transitions

Group theory provides an explicit recipe for judging the Raman activity of a normal mode. In this case, the symmetry species of the quadratic forms (x^2 , xy , etc.) listed in the character table are noted (they transform in the same way as the polarizability), and then we use the following rule:

If the symmetry species of a normal mode is the same as the symmetry species of a quadratic form, then the mode may be Raman active.

Illustration

To decide which of the vibrations of CH_4 are Raman active, refer to the T_d character table. It was established in Example 16.6 that the symmetry species of the normal modes are

$A_1 + E + 2T_2$. Because the quadratic forms span $A_1 + E + T_2$, all the normal modes are Raman active. All totally symmetric vibrations, whatever the point group of the molecule, are Raman active (and polarized; see below).

Self-test 16.10 Which of the vibrational modes of H_2O are Raman active?

[All three]

The exclusion rule also helps us to decide which modes are active:

If the molecule has a centre of symmetry, then no modes can be both infrared and Raman active.

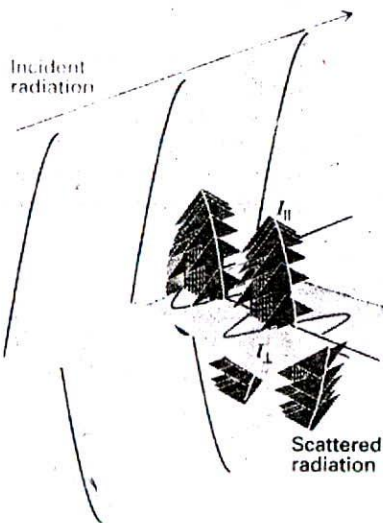
(A mode may be inactive in both.) Because it is often possible to judge intuitively if a mode changes the molecular dipole moment, we can use this rule to identify modes that are not Raman active. The rule applies to CO_2 but to neither H_2O nor CH_4 because they have no centre of symmetry.

(b) Depolarization

The assignment of Raman lines to particular vibrational modes is aided by noting the state of polarization of the scattered light. The depolarization ratio, ρ , of a line is the ratio of the intensities, \mathcal{I} , of the scattered light with polarizations perpendicular and parallel to the plane of polarization of the incident radiation:

$$\rho = \frac{\mathcal{I}_\perp}{\mathcal{I}_\parallel} \quad [75]$$

To measure ρ , the intensity of a Raman line is measured with a polarizing filter (a 'half-wave plate') first parallel and then perpendicular to the polarization of the incident beam. If the emergent light is not polarized, then both intensities are the same and ρ is close to 1; if the light retains its initial polarization, then $\mathcal{I}_\perp = 0$, so $\rho = 0$ (Fig. 16.51). A line is classified as depolarized if it has ρ close to or greater than 0.75 and as polarized if $\rho < 0.75$. Only totally symmetrical vibrations give rise to polarized lines in which the incident polarization is

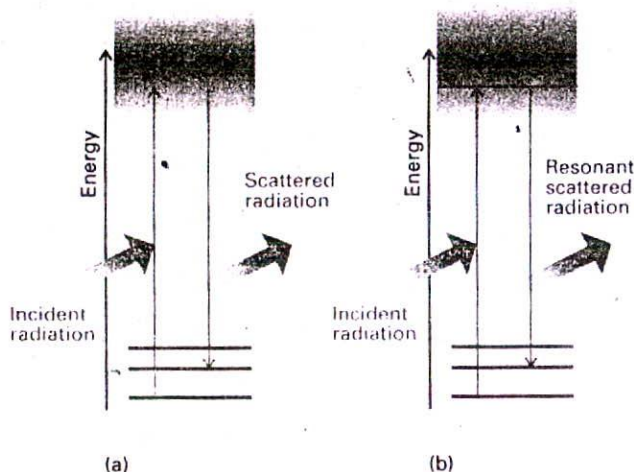


16.51 The definition of the planes used for the specification of the depolarization ratio, ρ , in Raman scattering. The fat arrows represent the electric vector of the incident (green) and scattered (grey) radiation. There is also a perpendicular scattered component, as indicated by the simple wave-like line.

largely preserved. Vibrations that are not totally symmetrical give rise to depolarized lines because the incident radiation can give rise to radiation in the perpendicular direction too.

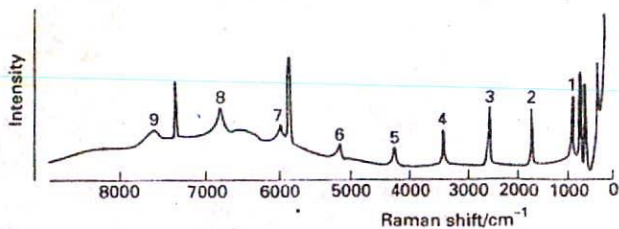
(c) Resonance Raman spectra

A modification of the basic Raman effect involves using incident radiation that nearly coincides with the frequency of an electronic transition of the sample (Fig. 16.52). The technique is then called resonance Raman spectroscopy. It is characterized by a much greater intensity in the scattered radiation. Furthermore, because it is often the case that



16.52 (a) In conventional Raman spectroscopy, the incident radiation does not match an absorption frequency of the molecule, and there is only a 'virtual' transition to an excited state. (b) However, in the resonance Raman effect, the incident radiation has a frequency that coincides with a molecular transition.

only a few vibrational modes contribute to the more intense scattering, the spectrum is greatly simplified. The resonance Raman spectrum shown in Fig. 16.53, for example, is of solid potassium chromate. The nine peaks that are identified are the Stokes lines that correspond to the excitation of the symmetric breathing mode of the tetrahedral CrO_4^{2-} ion and the transfer of up to nine vibrational quanta during the photon-ion collision. The high intensity of the resonance Raman transitions is employed to examine the metal ions in biological macromolecules (such as the iron in haemoglobin and cytochromes or the cobalt in vitamin B₁₂), which are present in such low abundances that conventional Raman spectroscopy cannot detect them. An additional advantage is that resonance picks out the



16.53 The resonance Raman spectrum of solid K_2CrO_4 . The peaks are due to the totally symmetric stretching mode of the CrO_4^{2-} anion. (W. Kiefer and H.J. Bernstein, *Molec. Phys.* 23, 835 (1972).)

fragment of a molecule that in conventional Raman spectroscopy would have a spectrum too complex to interpret.

(d) Coherent anti-Stokes Raman spectroscopy

The intensity of Raman transitions may be enhanced by coherent anti-Stokes Raman spectroscopy (CARS, Fig. 16.54). The technique relies on the fact that, if two laser beams of frequencies ν_1 and ν_2 pass through a sample, then they may mix together and give rise to coherent radiation of several different frequencies, one of which is

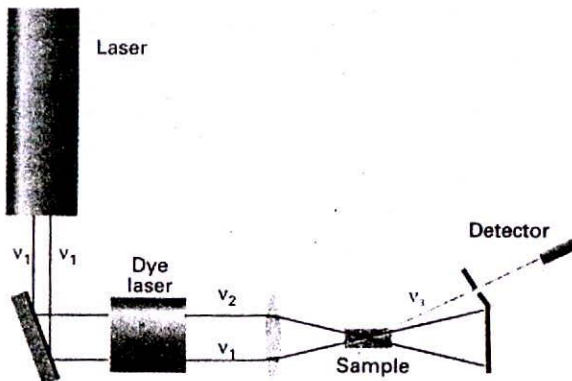
$$\nu' = 2\nu_1 - \nu_2 \quad (76)$$

Suppose that ν_2 is varied until it matches any Stokes line from the sample, such as the one with frequency $\nu_1 - \Delta\nu$; then the coherent emission will have frequency

$$\nu' = 2\nu_1 - (\nu_1 - \Delta\nu) = \nu_1 + \Delta\nu \quad (77)$$

which is the frequency of the corresponding anti-Stokes line. This coherent radiation forms a narrow beam of high intensity.

An advantage of CARS is that it can be used to study Raman transitions in the presence of competing incoherent background radiation, and so can be used to observe the Raman spectra of species in flames. The intensities of the transitions can then be interpreted in terms of the temperatures of different regions of the flame.



16.54 The experimental arrangement for the CARS experiment.

Checklist of key ideas

General features of spectroscopy

16.1 Experimental techniques

- emission spectroscopy
- absorption spectroscopy
- dispersing element
- Fourier transform
- detector
- Raman spectroscopy
- Stokes radiation
- anti-Stokes radiation
- Rayleigh radiation

16.2 The intensities of spectral lines

- transmittance (7)
- Beer-Lambert law (8, 10)
- molar absorption coefficient
- absorbance (9)
- integrated absorption coefficient (11)
- stimulated absorption
- Einstein coefficient of stimulated absorption (12)
- total rate of absorption
- Einstein coefficient of stimulated emission (14)
- spontaneous emission
- Einstein coefficient of spontaneous emission (15)
- gross selection rule
- specific selection rule

16.3 Linewidths

- Doppler effect
- lifetime
- lifetime broadening (24)
- collisional deactivation

- collisional lifetime
- natural linewidth

Pure rotation spectra

16.4 Moments of inertia

- moment of inertia (26)
- rigid rotor
- spherical rotor
- symmetric rotor
- linear rotor
- asymmetric rotor

16.5 The rotational energy levels

- rotational constant (30, 36)
- rotational term (32, 35)
- principal axis
- oblate
- prolate
- Stark effect
- centrifugal distortion constant

16.6 Rotational transitions

- Stark modulation
- energies (43, 44)

16.7 Rotational Raman spectra

- energies (48)

16.8 Nuclear statistics and rotational states

- nuclear statistics

- ortho*-hydrogen
- para*-hydrogen

The vibrations of diatomic molecules**16.9 Molecular vibrations**

- force constant (53)
- effective mass (55)
- vibrational term (57)

16.10 Selection rules

- infrared active
- infrared inactive
- fundamental transition

16.11 Anharmonicity

- anharmonic
- Morse potential energy (61)
- anharmonicity constant (62)
- overtones
- Birge-Sponer plot

16.12 Vibration-rotation spectra

- band spectra
- branches (68)
- P-branch
- Q-branch
- R-branch
- combination difference

16.13 Vibrational Raman spectra of diatomic molecules

- O-branch
- S-branch

The vibrations of polyatomic molecules**16.14 Normal modes**

- symmetric stretch
- antisymmetric stretch
- normal mode

16.15 The vibrational spectra of polyatomic molecules

- parallel band
- perpendicular band
- force field
- tumbling

16.16 Vibrational Raman spectra of polyatomic molecules

- exclusion rule
- depolarization ratio (75)
- polarized
- depolarized
- resonance Raman spectroscopy
- coherent anti-Stokes spectroscopy (CARS)

Further reading

Articles of general interest

- N.C. Thomas, The early history of spectroscopy. *J. Chem. Educ.* **68**, 631 (1991).
- R. Woods and G. Henderson, FTIR rotational spectroscopy. *J. Chem. Educ.* **64**, 921 (1987).
- L. Glasser, Fourier transforms for chemists. Part I. Introduction to the Fourier transform. *J. Chem. Educ.* **64**, A228 (1987); Part II. Fourier transforms in chemistry and spectroscopy. *J. Chem. Educ.* **64**, A260 (1987).
- W.D. Perkins, Fourier transform infrared spectroscopy: Part II. Advantages of FT-IR. *J. Chem. Educ.* **64**, A269 (1987).
- P.L. Goodfriend, Diatomic vibrations revisited. *J. Chem. Educ.* **64**, 753 (1987).
- A.R. Lacey, A student introduction to molecular vibrations. *J. Chem. Educ.* **64**, 756 (1987).
- J.G. Verkade, A novel pictorial approach to teaching molecular motions in polyatomic molecules. *J. Chem. Educ.* **64**, 411 (1987).
- F.A. Miller and G.B. Kauffman, C.V. Raman and the discovery of the Raman effect. *J. Chem. Educ.* **66**, 795 (1989).
- M.-K. Ahn, A comparison of FTNMR and FTIR techniques. *J. Chem. Educ.* **66**, 802 (1989).
- D.P. Strommen, Specific values of the depolarization ratio in Raman spectroscopy: their origins and significance. *J. Chem. Educ.* **69**, 803 (1992).
- B.J. Bozlee, J.H. Luther, and M. Buraczewski, The infrared overtone intensity of a simple diatomic molecule: nitric oxide. *J. Chem. Educ.* **69**, 370 (1992).
- G. Henderson and B. Logsdon, Stark effects on rigid-rotor wavefunctions: a quantum description of dipolar rotors trapped in electric fields. *J. Chem. Educ.* **72**, 1021 (1995).
- E. Grunwald, J. Herzog, and C. Steel, Using Fourier transforms to understand spectral lineshapes. *J. Chem. Educ.* **72**, 210 (1995).
- D.K. Graff, Fourier and Hadamard: transforms in chemistry. *J. Chem. Educ.* **72**, 304 (1995).
- V.B.E. Thomsen, Why do spectral lines have a linewidth? *J. Chem. Educ.* **72**, 616 (1995).
- R.S. Treptow, Bond energies and enthalpies: an often neglected difference. *J. Chem. Educ.* **72**, 497 (1995).
- N.K. Kildahl, Bond energy data summarized. *J. Chem. Educ.* **72**, 423 (1995).
- C.W. David, IR vibration-rotation spectrum of the ammonia molecule. *J. Chem. Educ.* **73**, 46 (1996).
- D.A. Ramsay, Molecular spectroscopy. In *Encyclopedia of applied physics* (ed. G.L. Trigg), **10**, 491. VCH, New York (1994).
- J.R. Lombardi, Radiation interaction with molecules. In *Encyclopedia of applied physics* (ed. G.L. Trigg), **15**, 509. VCH, New York (1996).

I.P. Herman, Raman scattering. In *Encyclopedia of applied physics* (ed. G.L. Trigg), 15, 587. VCH, New York (1996).

H.G.M. Edwards, Raman spectroscopy instrumentation. In *Encyclopedia of applied physics* (ed. G.L. Trigg), 16, 1. VCH, New York (1996).

Texts and sources of data and information

J.M. Hollas, *Modern spectroscopy*. Wiley, New York (1996).

J.M. Hollas, *High resolution spectroscopy*. Butterworth, London (1982).

P.F. Bernath, *Spectra of atoms and molecules*. Oxford University Press, New York (1995).

W. Gordy and R.L. Cook, *Microwave molecular spectra*. Wiley, New York (1974).

S. Wilson (ed.), *Methods in computational chemistry*, Vol. 4. Molecular vibrations. Plenum, New York (1992).

K.P. Huber and G. Herzberg, *Molecular spectra and molecular structure IV. Constants of diatomic molecules*. Van Nostrand-Reinhold, New York (1979).

L. Bellamy, *The infrared spectra of complex molecules*. Chapman & Hall, London (1980).

E.A.V. Ebsworth, D.W.H. Rankin, and S. Cradock, *Structural methods in inorganic chemistry*. Blackwell Scientific, Oxford (1991).

R. Drago, *Physical methods for chemists*. Saunders, Philadelphia (1992).

G. Herzberg, *Infrared and Raman spectra of polyatomic molecules*. Van Nostrand, New York (1945).

E.B. Wilson, J.C. Decius, and P.C. Cross, *Molecular vibrations*. McGraw-Hill, New York (1955).

Exercises

16.1 (a) Calculate the ratio of the Einstein coefficients of spontaneous and stimulated emission, A and B , for transitions with the following characteristics: (a) 70.8 pm X-rays, (b) 500 nm visible light, (c) 3000 cm^{-1} IR radiation.

16.1 (b) Calculate the ratio of the Einstein coefficients of spontaneous and stimulated emission, A and B , for transitions with the following characteristics: (a) 500 MHz radiofrequency radiation, (b) 3.0 cm microwave radiation.

16.2 (a) Calculate the frequency of the $J = 4 \leftarrow 3$ transition in the pure rotational spectrum of $^{14}\text{N}^{16}\text{O}$. The equilibrium bond length is 115 pm.

16.2 (b) Calculate the frequency of the $J = 3 \leftarrow 2$ transition in the pure rotational spectrum of $^{12}\text{C}^{16}\text{O}$. The equilibrium bond length is 112.81 pm.

16.3 (a) If the wavenumber of the $J = 3 \leftarrow 2$ rotational transition of $^1\text{H}^{35}\text{Cl}$ considered as a rigid rotator is 63.56 cm^{-1} , what is (a) the moment of inertia of the molecule, (b) the bond length?

16.3 (b) If the wavenumber of the $J = 1 \leftarrow 0$ rotational transition of $^1\text{H}^{81}\text{Br}$ considered as a rigid rotator is 16.93 cm^{-1} , what is (a) the moment of inertia of the molecule, (b) the bond length?

16.4 (a) Given that the spacing of lines in the microwave spectrum of $^{27}\text{Al}^1\text{H}$ is constant at 12.604 cm^{-1} , calculate the moment of inertia and bond length of the molecule ($m(^{27}\text{Al}) = 26.9815 \text{ u}$).

16.4 (b) Given that the spacing of lines in the microwave spectrum of $^{35}\text{Cl}^{19}\text{F}$ is constant at 1.033 cm^{-1} , calculate the moment of inertia and bond length of the molecule ($m(^{35}\text{Cl}) = 34.9688 \text{ u}$, $m(^{19}\text{F}) = 18.9984 \text{ u}$).

16.5 (a) The rotational constant of $^{127}\text{I}^{35}\text{Cl}$ is 0.1142 cm^{-1} . Calculate the ICl bond length ($m(^{35}\text{Cl}) = 34.9688 \text{ u}$, $m(^{127}\text{I}) = 126.9045 \text{ u}$).

16.5 (b) The rotational constant of $^{12}\text{C}^{16}\text{O}_2$ is 0.39021 cm^{-1} . Calculate the bond length of the molecule ($m(^{12}\text{C}) = 12 \text{ u}$ exactly, $m(^{16}\text{O}) = 15.9949 \text{ u}$).

16.6 (a) Determine the HC and CN bond lengths in HCN from the rotational constants $B(^1\text{H}^{12}\text{C}^{14}\text{N}) = 44.316 \text{ GHz}$, $B(^2\text{H}^{12}\text{C}^{14}\text{N}) = 36.208 \text{ GHz}$.

16.6 (b) Determine the CO and CS bond lengths in OCS from the rotational constants $B(^{16}\text{O}^{12}\text{C}^{32}\text{S}) = 6081.5 \text{ MHz}$, $B(^{16}\text{O}^{12}\text{C}^{34}\text{S}) = 5932.8 \text{ MHz}$.

16.7 (a) The wavenumber of the incident radiation in a Raman spectrometer is 20487 cm^{-1} . What is the wavenumber of the scattered Stokes radiation for the $J = 2 \leftarrow 0$ transition of $^{14}\text{N}_2$?

16.7 (b) The wavenumber of the incident radiation in a Raman spectrometer is 20623 cm^{-1} . What is the wavenumber of the scattered Stokes radiation for the $J = 4 \leftarrow 2$ transition of $^{16}\text{O}_2$?

16.8 (a) Infrared absorption by $^1\text{H}^{81}\text{Br}$ gives rise to an R branch from $v = 0$. What is the wavenumber of the line originating from the rotational state with $J = 2$? Use the information in Table 16.2.

16.8 (b) Infrared absorption by $^1\text{H}^{127}\text{I}$ gives rise to an R branch from $v = 0$. What is the wavenumber of the line originating from the rotational state with $J = 2$? Use the information in Table 16.2.

16.9 (a) An object of mass 1.0 kg suspended from the end of a rubber band has a vibrational frequency of 2.0 Hz. Calculate the force-constant of the rubber band.

- 16.9 (b)** An object of mass 2.0 g suspended from the end of a spring has a vibrational frequency of 3.0 Hz. Calculate the force constant of the spring.
- 16.10 (a)** Calculate the percentage difference in the fundamental vibration wavenumber of $^{23}\text{Na}^{35}\text{Cl}$ and $^{23}\text{Na}^{37}\text{Cl}$ on the assumption that their force constants are the same.
- 16.10 (b)** Calculate the percentage difference in the fundamental vibration wavenumber of $^1\text{H}^{35}\text{Cl}$ and $^2\text{H}^{37}\text{Cl}$ on the assumption that their force constants are the same.
- 16.11 (a)** The wavenumber of the fundamental vibrational transition of $^{35}\text{Cl}_2$ is 564.9 cm^{-1} . Calculate the force constant of the bond ($m(^{35}\text{Cl}) = 34.9688\text{ u}$).
- 16.11 (b)** The wavenumber of the fundamental vibrational transition of $^{79}\text{Br}^{81}\text{Br}$ is 323.2 cm^{-1} . Calculate the force constant of the bond ($m(^{79}\text{Br}) = 78.9183\text{ u}$, $m(^{81}\text{Br}) = 80.9163\text{ u}$).
- 16.12 (a)** The molecule CH_2Cl_2 belongs to the point group C_{2v} . The displacements of the atoms span $5A_1 + 2A_2 + 4B_1 + 4B_2$. What are the symmetries of the normal modes of vibration?
- 16.12 (b)** A carbon disulfide molecule belongs to the point group $D_{\infty h}$. The nine displacements of the three atoms span $A_{1g} + A_{1u} + A_{2g} + 2E_{1u} + E_{1g}$. What are the symmetries of the normal modes of vibration?
- 16.13 (a)** Which of the following molecules may show a pure rotational microwave absorption spectrum: (a) H_2 , (b) HCl , (c) CH_4 , (d) CH_3Cl , (e) CH_2Cl_2 ?
- 16.13 (b)** Which of the following molecules may show a pure rotational microwave absorption spectrum: (a) H_2O , (b) H_2O_2 , (c) NH_3 , (d) N_2O ?
- 16.14 (a)** Which of the following molecules may show infrared absorption spectra: (a) H_2 , (b) HCl , (c) CO_2 , (d) H_2O ?
- 16.14 (b)** Which of the following molecules may show infrared absorption spectra: (a) CH_3CH_3 , (b) CH_4 , (c) CH_3Cl , (d) N_2 ?
- 16.15 (a)** Which of the following molecules may show a pure rotational Raman spectrum: (a) H_2 , (b) HCl , (c) CH_4 , (d) CH_3Cl ?
- 16.15 (b)** Which of the following molecules may show a pure rotational Raman spectrum: (a) CH_2Cl_2 , (b) CH_3CH_3 , (c) SF_6 , (d) N_2O ?
- 16.16 (a)** What is the Doppler-shifted wavelength of a red (660 nm) traffic light approached at 80 km h^{-1} ?
- 16.16 (b)** At what speed of approach would a red (660 nm) traffic light appear green (520 nm)?
- 16.17 (a)** A spectral line of $^{48}\text{Ti}^{8+}$ (of mass 47.95 u) in a distant star was found to be shifted from 654.2 nm to 706.5 nm and to be broadened to 61.8 pm . What is the speed of recession and the surface temperature of the star?
- 16.17 (b)** A spectral line of $^{31}\text{P}^{3+}$ (of mass 30.97 u) in a distant star was found to be shifted from 326 nm to 365 nm and to be broadened to 45.8 pm . What is the speed of recession and the surface temperature of the star?
- 16.18 (a)** Estimate the lifetime of a state that gives rise to a line of width (a) 0.10 cm^{-1} , (b) 1.0 cm^{-1} .
- 16.18 (b)** Estimate the lifetime of a state that gives rise to a line of width (a) 100 MHz, (b) 2.14 cm^{-1} .
- 16.19 (a)** A molecule in a liquid undergoes about 1.0×10^{13} collisions in each second. Suppose that (a) every collision is effective in deactivating the molecule vibrationally and (b) that one collision in 100 is effective. Calculate the width (in cm^{-1}) of vibrational transitions in the molecule.
- 16.19 (b)** A molecule in a gas undergoes about 1.0×10^9 collisions in each second. Suppose that (a) every collision is effective in deactivating the molecule rotationally and (b) that one collision in 10 is effective. Calculate the width (in hertz) of rotational transitions in the molecule.
- 16.20 (a)** Calculate the relative numbers of Cl_2 molecules ($\bar{\nu} = 559.7\text{ cm}^{-1}$) in the ground and first excited vibrational states at (a) 298 K, (b) 500 K.
- 16.20 (b)** Calculate the relative numbers of Br_2 molecules ($\bar{\nu} = 321\text{ cm}^{-1}$) in the second and first excited vibrational states at (a) 298 K, (b) 800 K.
- 16.21 (a)** The hydrogen halides have the following fundamental vibrational wavenumbers: 4141.3 cm^{-1} (HF); 2988.9 cm^{-1} (H^{35}Cl); 2649.7 cm^{-1} (H^{81}Br); 2309.5 cm^{-1} (H^{127}I). Calculate the force constants of the hydrogen-halogen bonds.
- 16.21 (b)** From the data in Exercise 16.21a, predict the fundamental vibrational wavenumbers of the deuterium halides.
- 16.22 (a)** For $^{16}\text{O}_2$, ΔG values for the transitions $v = 1 \leftarrow 0$, $2 \leftarrow 0$, and $3 \leftarrow 0$ are, respectively, 1556.22, 3088.28, and 4596.21 cm^{-1} . Calculate $\bar{\nu}$ and x_e . Assume y_e to be zero.
- 16.22 (b)** For $^{14}\text{N}_2$, ΔG values for the transitions $v = 1 \leftarrow 0$, $2 \leftarrow 0$, and $3 \leftarrow 0$ are, respectively, 2345.15, 4661.40, and 6983.73 cm^{-1} . Calculate $\bar{\nu}$ and x_e . Assume y_e to be zero.
- 16.23 (a)** The first five vibrational energy levels of HCl are at 1481.86, 4367.50, 7149.04, 9826.48, and 12399.8 cm^{-1} . Calculate the dissociation energy of the molecule in reciprocal centimetres and electronvolts.
- 16.23 (b)** The first five vibrational energy levels of HI are at 1144.83, 3374.90, 5525.51, 7596.66, and 9588.35 cm^{-1} . Calculate the dissociation energy of the molecule in reciprocal centimetres and electronvolts.
- 16.24 (a)** The rotational Raman spectrum of $^{35}\text{Cl}_2$ ($m(^{35}\text{Cl}) = 34.9688\text{ u}$) shows a series of Stokes lines separated by 0.9752 cm^{-1} and a similar series of anti-Stokes lines. Calculate the bond length of the molecule.
- 16.24 (b)** The rotational Raman spectrum of $^{19}\text{F}_2$ ($m(^{19}\text{F}) = 18.9984\text{ u}$) shows a series of Stokes lines separated by 3.5312 cm^{-1} and a similar series of anti-Stokes lines. Calculate the bond length of the molecule.
- 16.25 (a)** How many normal modes of vibration are there for the following molecules: (a) H_2O , (b) H_2O_2 , (c) C_2H_4 ?
- 16.25 (b)** How many normal modes of vibration are there for the following molecules: (a) C_6H_6 , (b) $\text{C}_6\text{H}_6\text{CH}_3$, (c) $\text{HC}\equiv\text{C}-\text{C}\equiv\text{CH}$?

16.26 (a) Which of the three vibrations of an AB_2 molecule are infrared or Raman active when it is (a) angular, (b) linear?

16.26 (b) Which of the vibrations of an AB_3 molecule are infrared or Raman active when it is (a) trigonal planar, (b) trigonal pyramidal?

16.27 (a) Consider the vibrational mode that corresponds to the uniform expansion of the benzene ring. Is it (a) Raman, (b) infrared active?

16.27 (b) Consider the vibrational mode that corresponds to the boat-like bending of a benzene ring. Is it (a) Raman, (b) infrared active?

Problems

Numerical problems

16.1 Calculate the Doppler width (as a fraction of the transition wavelength) for any kind of transition in (a) HCl, (b) ICl at 25°C. What would be the widths of the rotational and vibrational transitions in these molecules (in MHz and cm^{-1} , respectively), given $B(\text{ICl}) = 0.1142 \text{ cm}^{-1}$ and $\bar{\nu}(\text{ICl}) = 384 \text{ cm}^{-1}$ and additional information in Table 16.2?

16.2 The collision frequency of a molecule of mass m in a gas of pressure p is $z = 4\sigma(kT/\pi m)^{1/2} p/kT$, where σ is the collision cross-section. Find an expression for the collision-limited lifetime of an excited state assuming that every collision is effective. Estimate the width of rotational transition in HCl ($\sigma = 0.30 \text{ nm}^2$) at 25°C and 1.0 atm. To what value must the pressure of the gas be reduced in order to ensure that collision broadening is less important than Doppler broadening?

16.3 The rotational constant of NH_3 is equivalent to 298 GHz. Compute the separation of the pure rotational spectrum lines in GHz, cm^{-1} , and mm, and show that the value of B is consistent with an N-H bond length of 101.4 pm and a bond angle of 106.78°.

16.4 The rotational constant for CO is 1.9314 cm^{-1} and 1.6116 cm^{-1} in the ground and first excited vibrational states, respectively. By how much does the internuclear distance change as a result of this transition?

16.5 Pure rotational Raman spectra of gaseous C_6H_6 and C_6D_6 yield the following rotational constants: $B(\text{C}_6\text{H}_6) = 0.18960 \text{ cm}^{-1}$, $B(\text{C}_6\text{D}_6) = 0.15681 \text{ cm}^{-1}$. The moments of inertia of the molecules about any axis perpendicular to the C_6 axis were calculated from these data as $I(\text{C}_6\text{H}_6) = 147.59 \times 10^{-47} \text{ kg m}^2$, $I(\text{C}_6\text{D}_6) = 178.45 \times 10^{-47} \text{ kg m}^2$. Calculate the CC, CH, and CD bond lengths.

16.6 The vibrational energy levels of NaI lie at the wavenumbers 142.81, 427.31, 710.31, and 991.81 cm^{-1} . Show that they fit the expression $(v + \frac{1}{2})\bar{\nu} - (v + \frac{1}{2})^2 x_e \bar{\nu}$, and deduce the force constant, zero-point energy, and dissociation energy of the molecule.

16.7 Predict the shape of the nitronium ion, NO_2^+ , from its Lewis structure and the VSEPR model. It has one Raman active vibrational mode at 1400 cm^{-1} , two strong IR active modes at 2360 and 540 cm^{-1} , and one weak IR mode at 3735 cm^{-1} . Are these data consistent with the predicted shape of the molecule? Assign the vibrational wavenumbers to the modes from which they arise.

16.8 Rotational absorption lines from $^1\text{H}^{35}\text{Cl}$ gas were found at the following wavenumbers (R.L. Hausler and R.A. Oetjen, *J. Chem. Phys.* 21, 1340 (1953)): 83.32, 104.13, 124.73, 145.37, 165.89, 186.23, 206.60, 226.86 cm^{-1} . Calculate the moment of inertia and the bond length of the molecule. Predict the positions of the corresponding lines in $^2\text{H}^{35}\text{Cl}$.

16.9 Is the bond length in HCl the same as that in DCl? The wavenumbers of the $J = 1 \leftarrow 0$ rotational transitions for H^{35}Cl and $^2\text{H}^{35}\text{Cl}$ are 20.8784 and 10.7840 cm^{-1} , respectively. Accurate atomic masses are 1.007825 u and 2.0140 u for ^1H and ^2H , respectively. The mass of ^{35}Cl is 34.96885 u. Based on this information alone, can you conclude that the bond lengths are the same or different in the two molecules?

16.10 The microwave spectrum of $^{16}\text{O}^{12}\text{CS}$ (C.H. Townes, A.N. Holden, and F.R. Merritt, *Phys. Rev.* 74, 1113 (1948)) gave absorption lines (in GHz) as follows:

J	1	2	3	4
^{32}S	24.32592	36.48882	48.65164	60.81408
^{34}S	23.73233		47.46240	

Use the expressions for moments of inertia in Table 16.1 and assume that the bond lengths are unchanged by substitution; calculate the CO and CS bond lengths in OCS.

16.11 The HCl molecule is quite well described by the Morse potential with $D_e = 5.33 \text{ eV}$, $\bar{\nu} = 2989.7 \text{ cm}^{-1}$, and $x_e \bar{\nu} = 52.05 \text{ cm}^{-1}$. Assuming that the potential is unchanged on deuteration, predict the dissociation energies (D_0) of (a) HCl, (b) DCl.

16.12 The Morse potential (eqn 61) is very useful as a simple representation of the actual molecular potential energy. When RbH was studied, it was found that $\bar{\nu} = 936.8 \text{ cm}^{-1}$ and $x_e \bar{\nu} = 14.15 \text{ cm}^{-1}$. Plot the potential energy curve from 50 pm to 800 pm around $R_e = 236.7 \text{ pm}$. Then go on to explore how the rotation of a molecule may weaken its bond by allowing for the kinetic energy of rotation of a molecule and plotting $V^* = V + \hbar c B J(J+1)$ with $B = \hbar/4\pi c \mu R^2$. Plot these curves on the same diagram for $J = 40, 80,$ and 100 , and observe how the dissociation energy is affected by the rotation. (Taking $B = 3.020 \text{ cm}^{-1}$ at the equilibrium bond length will greatly simplify the calculation.)

Theoretical problems

16.13 Show that the moment of inertia of a diatomic molecule composed of atoms of masses m_A and m_B and bond length R is equal to $m_{\text{eff}}R^2$, where $m_{\text{eff}} = m_A m_B / (m_A + m_B)$.

16.14 Derive an expression for the value of J corresponding to the most highly populated rotational energy level of a diatomic rotor at a temperature T remembering that the degeneracy of each level is $2J + 1$. Evaluate the expression for ICl (for which $B = 0.1142 \text{ cm}^{-1}$) at 25°C . Repeat the problem for the most highly populated level of a spherical rotor, taking note of the fact that each level is $(2J + 1)^2$ -fold degenerate. Evaluate the expression for CH_4 (for which $B = 5.24 \text{ cm}^{-1}$) at 25°C .

16.15 The moments of inertia of the linear mercury(II) halides are very large, so the O and S branches of their vibrational Raman spectra show little rotational structure. Nevertheless, the peaks of both branches can be identified and have been used to measure the rotational constants of the molecules (R.J.H. Clark and D.M. Rippon, *J. Chem. Soc. Faraday Soc. II* 69, 1496 (1973)). Show, from a knowledge of the value of J corresponding to the intensity maximum, that the separation of the peaks of the O and S branches is given by the Placzek-Teller relation $\delta\tilde{\nu} = (32BkT/hc)^{1/2}$. The following widths were obtained at the temperatures stated:

	HgCl ₂	HgBr ₂	HgI ₂
$\theta/^\circ\text{C}$	282	292	292
$\delta\tilde{\nu}/\text{cm}^{-1}$	23.8	15.2	11.4

Calculate the bond lengths in the three molecules.

Additional problems supplied by Carmen Giunta and Charles Trapp

16.16 The noble gases and their complexes are favourite objects for the study of weak interatomic and intermolecular forces. J.-U. Grabow, A.S. Pine, G.T. Fraser, F.J. Lovas, R.D. Suenram, T. Emilsson, E. Arunan, and H.S. Gutowsky (*J. Chem. Phys.* 102, 1181 (1995)) measured the pure rotational spectrum of $^{20}\text{Ne}^{40}\text{Ar}$ and reported its rotational constant (actually cB) as 2914.9 MHz. What is the internuclear separation of the complex? They also reported the centrifugal distortion constant (actually cD_2) as 231.01 kHz. Estimate the fundamental vibrational wavenumber and the force constant of the weak bond. ($m(^{40}\text{Ar}) = 39.963 \text{ u}$; $m(^{20}\text{Ne}) = 19.992 \text{ u}$.)

16.17 B.D. Shizgal (*J. Molec. Structure (Theochem)* 391, 131 (1997)) reports the wavenumbers of vibrational transitions (based on quantum mechanical computations) for NeAr to be 1909.3, 1060.3, and 386.6 m^{-1} for 1-0, 2-1, and 3-2, respectively. Determine the Morse potential parameters D_e and a for this complex.

16.18 F. Luo, G.C. McBane, G. Kim, C.F. Giese, and W.R. Gentry (*J. Chem. Phys.* 98, 3564 (1993)) reported experimental observation of the He_2 complex, a species which had escaped detection for a long time. The fact that the observation required temperatures in the

neighbourhood of 1 mK is consistent with computational studies which suggest that hcD_e for He_2 is about $1.51 \times 10^{-23} \text{ J}$, hcD_0 about $2 \times 10^{-26} \text{ J}$, and R_e about 297 pm. (a) Estimate the fundamental vibrational wavenumber, force constant, moment of inertia, and rotational constant based on the harmonic-oscillator and rigid-rotor approximations. (b) Such a weakly bound complex is hardly likely to be rigid. Estimate the vibrational wavenumber and anharmonicity constant based on the Morse potential.

16.19 In a study of the rotational spectrum of the linear FeCO radical, K. Tanaka, M. Shirasaka, and T. Tanaka (*J. Chem. Phys.* 106, 6820 (1997)) report the following $J + 1 \leftarrow J$ transitions.

J	24	25	26
$\tilde{\nu}/\text{m}^{-1}$	214 777.7	223 379.0	231 981.2
J	27	28	29
$\tilde{\nu}/\text{m}^{-1}$	240 584.4	249 188.5	257 793.5

Evaluate the rotational constant of the molecule. Also, estimate the value of J for the most highly populated rotational energy level at 298 K and at 100 K.

16.20 In the constellation Ophiuchus, there is a gaseous interstellar cloud illuminated from behind by the star ζ -Ophiuci. Analysis of the Fraunhofer electronic-vibrational-rotational absorption lines obtained by H.S. Uhler and R.A. Patterson (*Astrophys. J.* 42, 434 (1915)) shows the presence of CN molecules in the interstellar medium. A strong absorption line in the ultraviolet region at $\lambda = 387.5 \text{ nm}$ was observed corresponding to the transition $J = 0-1$. Unexpectedly, a second strong absorption line with 25 per cent of the intensity of the first was found at a slightly longer wavelength ($\Delta\lambda = 0.061 \text{ nm}$) corresponding to the transition $J = 1-1$ (here allowed). Calculate the temperature of the CN molecules. Gerhard Herzberg, who was later to receive the Nobel Prize for his contributions to spectroscopy, calculated the temperature as 2.3 K. Although puzzled by this result, he did not realize its full significance. If he had, his prize might have been for the discovery of the cosmic background radiation.

16.21 The rotational energy levels for the H_3^+ molecular ion, an oblate symmetric rotor, are given by eqn 35, with C replacing A , when centrifugal distortion and other complications are ignored. Experimental values of the vibrational-rotational constants are $\tilde{\nu}_2(E') = 2521.6 \text{ cm}^{-1}$, $B = 43.55 \text{ cm}^{-1}$, and $C = 20.71 \text{ cm}^{-1}$. (a) Show that for a nonlinear planar molecule such as H_3^+ that $I_C = 2I_B$. The rather large discrepancy with the experimental values is due to the factors ignored in eqn 35. (b) Calculate an approximate value of the internuclear distance in H_3^+ . (c) The value for R_e obtained from the best quantum mechanical calculations by J.B. Anderson (*J. Chem. Phys.* 96, 3702 (1991)) is 87.32 pm. Use this result to calculate values of the rotational constants B and C . (d) Assuming that the geometry and force constants are the same in D_3^+ and H_3^+ , calculate the spectroscopic constants of D_3^+ . The molecular ion D_3^+ was first produced by J.T. Shy, J.W. Farley, W.E. Lamb, Jr, and W.H. Wing (*Phys. Rev. Lett.* 45, 535 (1980)) who observed the $\nu_2(E')$ band in the infrared.

17

Spectroscopy 2: electronic transitions

The characteristics of electronic transitions

- 17.1 The vibrational structure
- 17.2 Specific types of transitions

The fates of electronically excited states

- 17.3 Fluorescence and phosphorescence
- 17.4 Dissociation and predissociation

Lasers

- 17.5 General principles of laser action
- 17.6 Practical lasers
- 17.7 Applications of lasers in chemistry

Photoelectron spectroscopy

- 17.8 The technique
- 17.9 Ultraviolet photoelectron spectroscopy
- 17.10 X-ray photoelectron spectroscopy

Checklist of key ideas

Further reading

Exercises

Problems

Simple analytical expressions for electronic energy levels cannot be given, so this chapter concentrates on the qualitative features of electronic transitions. A common theme throughout the chapter is that electronic transitions occur within a stationary nuclear framework. We pay particular attention to spontaneous radiative decay processes, which include fluorescence and phosphorescence. A specially important example of stimulated radiative decay is that responsible for the action of lasers, and we see how this stimulated emission may be achieved and employed.

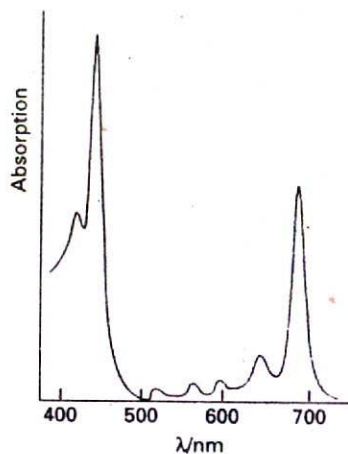
An extreme case of electron excitation is photoionization, in which an electron is expelled completely from a molecule. Photoionization spectroscopy is used to build up detailed pictures of orbital energies and the role of particular electrons in bonding. Hence it is an experimental technique for exploring the concepts encountered in Chapter 14.

The energies needed to change the electron distributions of molecules are of the order of several electronvolts (1 eV is equivalent to about 8000 cm^{-1} or 100 kJ mol^{-1}). Consequently, the photons emitted or absorbed when such changes occur lie in the visible and ultraviolet regions of the spectrum (Table 17.1). In some cases the relocation of electrons may be so extensive that it results in dissociation of the molecule.

Table 17.1* Colour, frequency, and energy of light

Colour	λ/nm	$\nu/(10^{14}\text{ Hz})$	$E/(\text{kJ mol}^{-1})$
Infrared	> 1000	< 3.0	< 120
Red	700	4.3	170
Yellow	580	5.2	210
Blue	470	6.4	250
Ultraviolet	< 300	> 10	> 400

*More values are given in the Data section at the end of this volume.



17.1 The absorption spectrum of chlorophyll in the visible region. Note that it absorbs in the red and blue regions, and that green light is not absorbed.

The characteristics of electronic transitions

The nuclei in a molecule are subjected to different forces after an electronic transition has occurred, and the molecule may respond by starting to vibrate. The resulting vibrational structure of electronic transitions can be resolved for gaseous samples, but in a liquid or solid the lines usually merge together and result in a broad, almost featureless band (Fig. 17.1). Superimposed on these vibrational transitions that accompany the electronic transition of a molecule in the gas phase is an additional branch structure that arises from rotational transitions. The electronic spectra of gaseous samples are therefore very complicated, but rich in information.

17.1 The vibrational structure

The widths of electronic absorption bands in liquid samples can be traced to their vibrational structure, which is usually unresolved in solution. This structure, which can be resolved in gases and weakly interacting solvents, arises from the vibrational transitions that accompany electronic excitation.

(a) The Franck–Condon principle

The vibrational structure of an electronic transition is explained by the Franck–Condon principle:

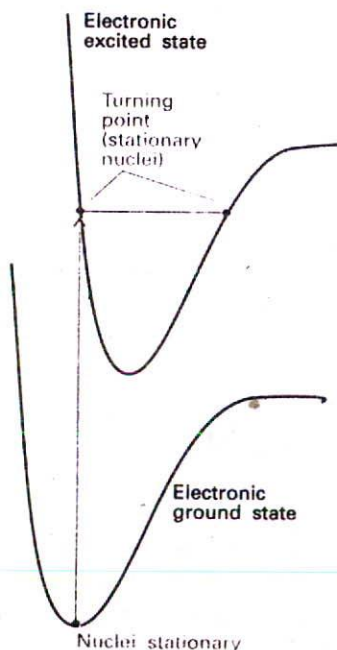
Because the nuclei are so much more massive than the electrons, an electronic transition takes place very much faster than the nuclei can respond.

As a result of the transition, electron density is rapidly built up in new regions of the molecule and removed from others, and the initially stationary nuclei suddenly experience a new force field. They respond to the new force by beginning to vibrate, and (in classical terms) swing backwards and forwards from their original separation, which was maintained during the rapid electronic excitation. The stationary equilibrium separation of the nuclei in the initial electronic state therefore becomes a stationary turning point in the final electronic state (Fig. 17.2).

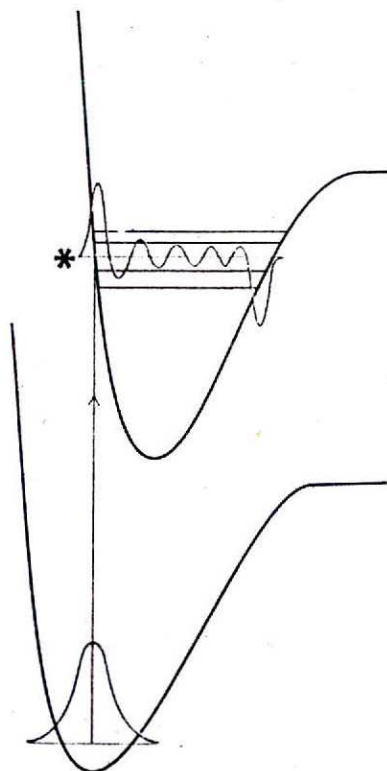
The quantum mechanical version of the Franck–Condon principle refines this picture. Before the absorption, the molecule is in the lowest vibrational state of its lowest electronic state (Fig. 17.3); the most probable location of the nuclei is at their equilibrium separation, R_e . The electronic transition is most likely to take place when the nuclei have this separation. When the transition occurs, the molecule is excited to the state represented by the upper curve. According to the Franck–Condon principle, the nuclear framework remains constant during this excitation, so we may imagine the transition as being up the vertical line in Fig. 17.3. The vertical line is the origin of the expression vertical transition, which is used to denote an electronic transition that occurs without change of nuclear geometry.

The vertical transition cuts through several vibrational levels of the upper electronic state. The level marked * is the one in which the nuclei are most probably at the same initial separation R_e (because the vibrational wavefunction has maximum amplitude there), so this vibrational state is the most probable state for the termination of the transition. However, it is not the only accessible vibrational state because several nearby states have an appreciable probability of the nuclei being at the separation R_e . Therefore, transitions occur to all the vibrational states in this region, but most intensely to the state with a vibrational wavefunction that peaks most strongly near R_e .

The vibrational structure of the spectrum depends on the relative horizontal position of the two potential energy curves, and a long vibrational progression, a lot of vibrational



17.2 According to the Franck–Condon principle, the most intense vibronic transition is from the ground vibrational state to the vibrational state lying vertically above it. Transitions to other vibrational levels also occur, but with lower intensity.



17.3 In the quantum mechanical version of the Franck-Condon principle, the molecule undergoes a transition to the upper vibrational state that most closely resembles the vibrational wavefunction of the vibrational ground state of the lower electronic state. The two wavefunctions shown here have the greatest overlap integral of all the vibrational states of the upper electronic state and hence are most closely similar.

structure, is stimulated if the upper potential energy curve is appreciably displaced horizontally from the lower. The upper curve is usually displaced to greater equilibrium bond lengths because electronically excited states usually have more antibonding character than electronic ground states.

The separation of the vibrational lines of an electronic absorption spectrum depends on the vibrational energies of the *upper* electronic state. Hence, electronic absorption spectra may be used to assess the force fields and dissociation energies of electronically excited molecules (for example, via a Birge-Sponer plot, Section 16.11).

(b) Franck-Condon factors

The quantitative form of the Franck-Condon principle is derived from the expression for the transition dipole moment, $\mu_{fi} = \langle f | \mu | i \rangle$. The dipole moment operator is a sum over all nuclei and electrons in the molecule:

$$\mu = -e \sum_i \mathbf{r}_i + e \sum_j Z_j \mathbf{R}_j \quad (1)$$

where the vectors are the distances from the centre of charge of the molecule. The intensity of the transition is proportional to the square modulus, $|\mu_{fi}|^2$, of the magnitude of the transition dipole moment (eqn 16.20), and we show in the *Justification* below that this intensity is proportional to the square modulus of the overlap integral, $S(v_f, v_i)$, between the vibrational states of the initial and final electronic states. This overlap integral is a measure of the match between the vibrational wavefunctions in the upper and lower electronic states: $S = 1$ for a perfect match and $S = 0$ when there is no similarity.

Justification 17.1

The overall state of the molecule consists of an electronic part, $|\epsilon\rangle$, and a vibrational part, $|v\rangle$. Therefore, within the Born-Oppenheimer approximation, the transition dipole moment factorizes as follows:

$$\begin{aligned} \mu_{fi} &= \langle \epsilon_f v_f | \left\{ -e \sum_i \mathbf{r}_i + e \sum_j Z_j \mathbf{R}_j \right\} | \epsilon_i v_i \rangle \\ &= -e \sum_i \langle \epsilon_f | \mathbf{r}_i | \epsilon_i \rangle \langle v_f | v_i \rangle + e \sum_j Z_j \langle \epsilon_f | \epsilon_i \rangle \langle v_f | \mathbf{R}_j | v_i \rangle \end{aligned}$$

The second term on the right of the last row is zero, because $\langle \epsilon_f | \epsilon_i \rangle = 0$ for two different electronic states (they are orthogonal). Therefore,

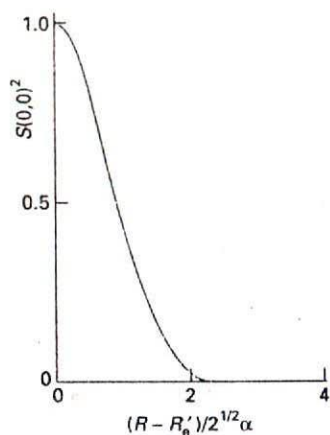
$$\mu_{fi} = -e \sum_i \langle \epsilon_f | \mathbf{r}_i | \epsilon_i \rangle \langle v_f | v_i \rangle = \mu_{\epsilon_f, \epsilon_i} S(v_f, v_i) \quad (2)$$

where

$$\mu_{\epsilon_f, \epsilon_i} = -e \sum_i \langle \epsilon_f | \mathbf{r}_i | \epsilon_i \rangle \quad S(v_f, v_i) = \langle v_f | v_i \rangle \quad (3)$$

The matrix element $\mu_{\epsilon_f, \epsilon_i}$ is the transition dipole moment arising from the redistribution of electrons (and a measure of the 'kick' this redistribution gives to the electromagnetic field, and vice versa for absorption). The factor $S(v_f, v_i)$ is the overlap integral between the vibrational state $|v_i\rangle$ in the initial electronic state of the molecule, and the vibrational state $|v_f\rangle$ in the final electronic state of the molecule.

Because the transition intensity is proportional to the square of the magnitude of the transition dipole moment, the intensity of an absorption is proportional to $|S(v_f, v_i)|^2$, which is known as the Franck-Condon factor for the transition. It follows that, the greater the



17.4 The Franck-Condon factor for the arrangement discussed in Example 17.1.

overlap of the vibrational state wavefunction in the upper electronic state with the vibrational wavefunction in the lower electronic state, the greater the absorption intensity of that particular simultaneous electronic and vibrational transition. This conclusion is the basis of the illustration in Fig. 17.3, where we see that the vibrational wavefunction of the ground state has the greatest overlap with the vibrational states that have peaks at similar bond lengths in the upper electronic state.

Example 17.1 Calculating a Franck-Condon Factor

Consider the transition from one electronic state to another, their bond lengths being R_e and R'_e and their force constants equal. Calculate the Franck-Condon factor for the 0-0 transition and show that the transition is most intense when the bond lengths are equal.

Method We need to calculate $S(0,0)$, the overlap integral of the two ground-state vibrational wavefunctions, and then take its square. The difference between harmonic and anharmonic vibrational wavefunctions is negligible for $v=0$, so harmonic oscillator wavefunctions can be used (Table 12.1).

Answer We use the (real) wavefunctions

$$\psi_0 = \left(\frac{1}{\alpha\pi^{1/2}}\right)^{1/2} e^{-y^2/2} \quad \psi'_0 = \left(\frac{1}{\alpha\pi^{1/2}}\right)^{1/2} e^{-y'^2/2}$$

where $y = (R - R_e)/\alpha$ and $y' = (R - R'_e)/\alpha$, with $\alpha = (\hbar^2/mk)^{1/4}$ (Section 12.5a). The overlap integral is

$$S(0,0) = \langle 0|0 \rangle = \int_{-\infty}^{\infty} \psi'_0 \psi_0 dR = \frac{1}{\pi^{1/2}} \int_{-\infty}^{\infty} e^{-(y^2+y'^2)/2} dy$$

We now write $\alpha z = R - \frac{1}{2}(R_e + R'_e)$, and manipulate this expression into

$$S(0,0) = \frac{1}{\pi^{1/2}} e^{-(R_e - R'_e)^2/4\alpha^2} \int_{-\infty}^{\infty} e^{-z^2} dz$$

The value of the integral is $\pi^{1/2}$. Therefore, the overlap integral is

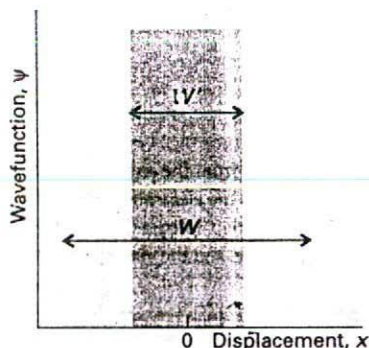
$$S(0,0) = e^{-(R_e - R'_e)^2/4\alpha^2}$$

and the Franck-Condon factor is

$$S(0,0)^2 = e^{-(R_e - R'_e)^2/2\alpha^2}$$

This factor is equal to 1 when $R'_e = R_e$ and decreases as the equilibrium bond lengths diverge from each other (Fig. 17.4).

Comment For Br_2 , $R_e = 228$ pm and there is an upper state with $R'_e = 266$ pm. Taking the vibrational wavenumber as 250 cm^{-1} , gives $S(0,0)^2 = 5.1 \times 10^{-10}$, so the intensity of the 0-0 transition is only 5.1×10^{-10} what it would have been if the potential curves had been directly above each other.



17.5 The model wavefunctions used in Self-test 17.1.

Self-test 17.1 Suppose the vibrational wavefunctions can be approximated by rectangular functions of width W and W' , centred on the equilibrium bond lengths (Fig. 17.5). Find the corresponding Franck-Condon factors when the centres are coincident and $W' < W$.

$$[S^2 = W'/W]$$

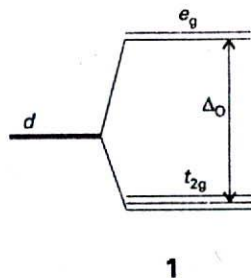
17.2 Specific types of transitions

The absorption of a photon can often be traced to the excitation of specific types of electrons or to electrons that belong to a small group of atoms. For example, when a carbonyl group ($>C=O$) is present, an absorption at about 290 nm is normally observed, although its precise location depends on the nature of the molecule. Groups with characteristic optical absorptions are called **chromophores** (from the Greek for 'colour bringer'), and their presence often accounts for the colours of substances (Table 17.2).

Table 17.2* Absorption characteristics of some groups and molecules

Group	$\tilde{\nu}_{\max}/\text{cm}^{-1}$	λ_{\max}/nm	$\epsilon_{\max}/(\text{L mol}^{-1} \text{cm}^{-1})$
$C=O(\pi^* \leftarrow \pi)$	61 000	163	15 000
	57 300	174	5 500
$C=O(\pi^* \leftarrow n)$	37–35 000	270–290	10–20
$H_2O(\pi^* \leftarrow n)$	60 000	167	7 000

* More values are given in the *Data section*.



(a) *d-d* transitions

All five *d* orbitals of a given shell are degenerate in a free atom. In a *d*-metal complex, where the immediate environment of the atom is no longer spherical, the *d* orbitals are not all degenerate, and electrons can absorb energy by making transitions between them. In an octahedral complex, such as $[\text{Ti}(\text{OH}_2)_6]^{3+}$, the five *d* orbitals of the central atom are split into two sets (1), a triply degenerate set labelled t_{2g} and a doubly degenerate set labelled e_g . The three t_{2g} orbitals lie below the two e_g orbitals; the difference in energy is denoted Δ_O and called the **ligand-field splitting parameter** (the O denoting octahedral symmetry). The *d* orbitals also divide into two sets in a tetrahedral complex, but in this case the e orbitals lie below the t_2 orbitals and their separation is written Δ_T . Neither separation is large, so transitions between the two sets of orbitals typically occur in the visible region of the spectrum even though they are electronic. The transitions are responsible for many of the colours that are so characteristic of *d*-metal complexes. As an example, the spectrum of $[\text{Ti}(\text{OH}_2)_6]^{3+}$ near $20\,000 \text{ cm}^{-1}$ (500 nm) is shown in Fig. 17.6, and can be ascribed to the promotion of its single *d* electron from a t_{2g} orbital to an e_g orbital. The wavenumber of the absorption maximum suggests that $\Delta_O \approx 20\,000 \text{ cm}^{-1}$ for this complex, which corresponds to about 2.5 eV.

(b) Vibronic transitions

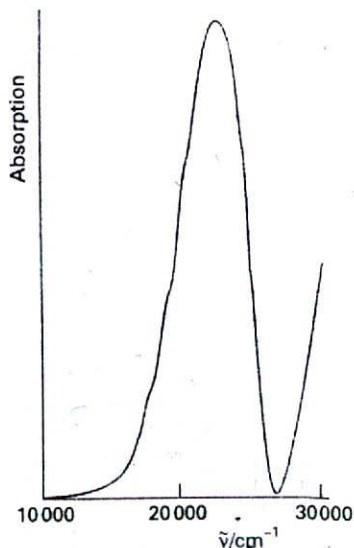
A major problem with the interpretation of visible spectra of octahedral complexes is that their *d-d* transitions are forbidden. The Laporte selection rule for centrosymmetric complexes (those with a centre of inversion) and atoms states that:

The only allowed transitions are transitions that are accompanied by a change of parity.

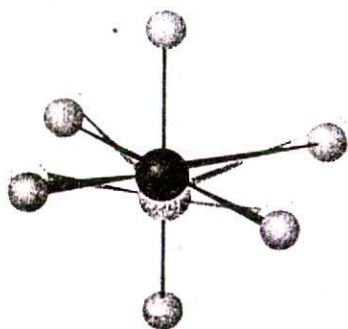
That is, $u \rightarrow g$ and $g \rightarrow u$ transitions are allowed, but $g \rightarrow g$ and $u \rightarrow u$ transitions are forbidden.

Justification 17.2

The transition dipole moment in eqn 16.19 vanishes unless the integrand is invariant under all symmetry operations of the molecule. Hence, in a centrosymmetric complex it must



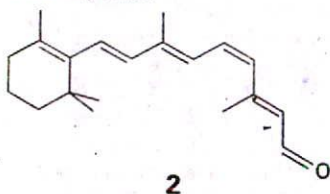
17.6 The electronic absorption spectrum of $[\text{Ti}(\text{OH}_2)_6]^{3+}$ in aqueous solution.



17.7 A $d-d$ transition is parity-forbidden because it corresponds to a $g-g$ transition. However, a vibration of the molecule can destroy the inversion symmetry of the molecule and the g, u classification no longer applies. The removal of the centre of symmetry gives rise to a vibronically allowed transition.



17.8 A $C=C$ double bond acts as a chromophore. One of its important transitions is the $\pi^* \leftarrow \pi$ transition illustrated here, in which an electron is promoted from a π orbital to the corresponding antibonding orbital.



have even (g) parity (in O_h it needs to be A_{1g} , but only the g symmetry is important for this argument). The three components of the dipole moment operator transform like x, y , and z , and are all u . Therefore, for a $d-d$ transition (a $g \rightarrow g$ transition), the overall parity of the transition dipole is $g \times u \times g = u$, so it must be zero. Likewise, for a $u \rightarrow u$ transition, the overall parity is $u \times u \times u = u$, so it must also vanish. Hence, transitions without a change of parity are forbidden.

A forbidden $g \rightarrow g$ transition can become allowed if the centre of symmetry is eliminated by an asymmetrical vibration, such as the one shown in Fig. 17.7. When the centre of symmetry is lost, $d-d$ transitions are no longer parity-forbidden, so the $e_g \leftarrow t_{2g}$ transition becomes weakly allowed. A transition that derives its intensity from an asymmetrical vibration of a molecule is called a **vibronic transition**.

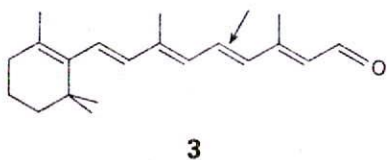
(c) Charge-transfer transitions

A complex may absorb radiation as a result of the transfer of an electron from the ligands into the d orbitals of the central atom, or vice versa. In such **charge-transfer transitions** the electron moves through a considerable distance, which means that the transition dipole moment may be large and the absorption is correspondingly intense. This mode of chromophore activity is shown by the permanganate ion, MnO_4^- , and accounts for its intense violet colour (which arises from strong absorption within the range 420–700 nm). In this oxoanion, the electron migrates from an orbital that is largely confined to the O atom ligands to an orbital that is largely confined to the Mn atom. It is therefore an example of a **ligand-to-metal charge-transfer transition (LMCT)**. The reverse migration, a **metal-to-ligand charge-transfer transition (MLCT)**, can also occur. An example is the transfer of a d electron into the antibonding π orbitals of an aromatic ligand. The resulting excited state may have a very long lifetime if the electron is extensively delocalized over several aromatic rings, and such species can participate in photochemically induced redox reactions.

(d) $\pi^* \leftarrow \pi$ and $\pi^* \leftarrow n$ transitions

Absorption by a $C=C$ double bond excites a π electron into an antibonding π^* orbital (Fig. 17.8). The chromophore activity is therefore due to a $\pi^* \leftarrow \pi$ transition (which is normally read ' π to π -star transition'). Its energy is about 7 eV for an unconjugated double bond, which corresponds to an absorption at 180 nm (in the ultraviolet). When the double bond is part of a conjugated chain, the energies of the molecular orbitals lie closer together and the $\pi^* \leftarrow \pi$ transition moves to longer wavelength; it may even lie in the visible region if the conjugated system is long enough.

An important example of a $\pi^* \leftarrow \pi$ transition is provided by the photochemical mechanism of vision. The retina of the eye contains 'visual purple', which is a protein in combination with 11-*cis*-retinal (2). The 11-*cis*-retinal acts as a chromophore, and is the primary receptor for photons entering the eye. A solution of 11-*cis*-retinal absorbs at about 380 nm, but in combination with the protein (a link which might involve the elimination of the terminal carbonyl) the absorption maximum shifts to about 500 nm and tails into the blue. The conjugated double bonds are responsible for the ability of the molecule to absorb over the entire visible region, but they also play another important role. In its electronically excited state the conjugated chain can isomerize, one half of the chain being able to twist about an excited $C=C$ bond and forming 11-*trans*-retinal (3). The primary step in vision therefore appears to be photon absorption followed by isomerization: the uncoiling of the molecule then triggers a nerve impulse to the brain.



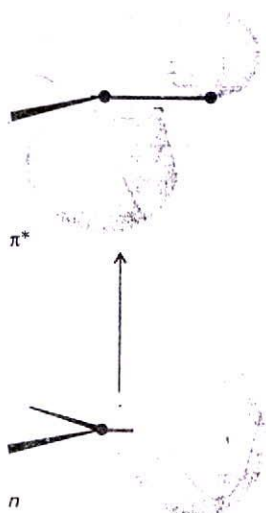
The transition responsible for absorption in carbonyl compounds can be traced to the lone pairs of electrons on the O atom. The Lewis concept of a 'lone pair' of electrons is represented in molecular orbital theory by a pair of electrons in an orbital confined largely to one atom and not appreciably involved in bond formation. One of these electrons may be excited into an empty π^* orbital of the carbonyl group (Fig. 17.9), which gives rise to a $\pi^* \leftarrow n$ transition (an ' n to π -star transition'). Typical absorption energies are about 4 eV (290 nm). Because $\pi^* \leftarrow n$ transitions in carbonyls are symmetry forbidden, the absorptions are weak.

The fates of electronically excited states

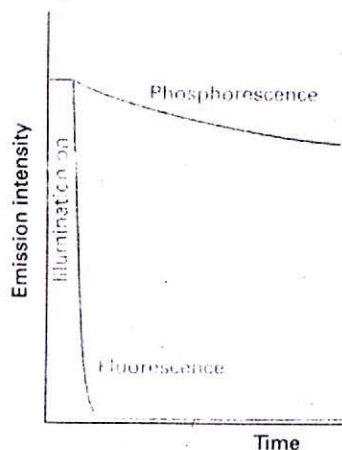
A radiative decay process is a process in which a molecule discards its excitation energy as a photon. A more common fate is **nonradiative decay**, in which the excess energy is transferred into the vibration, rotation, and translation of the surrounding molecules. This thermal degradation converts the excitation energy into thermal motion of the environment (that is, to 'heat'). An excited molecule may also take part in a chemical reaction, as we discuss in Part 3.

17.3 Fluorescence and phosphorescence

In **fluorescence**, the spontaneously emitted radiation ceases immediately after the exciting radiation is extinguished (Fig. 17.10). In **phosphorescence**, the spontaneous emission may persist for long periods (even hours, but characteristically seconds or fractions of seconds). The difference suggests that fluorescence is an immediate conversion of absorbed radiation into re-emitted energy, and that phosphorescence involves the storage of energy in a reservoir from which it slowly leaks.



17.9 A carbonyl (CO) group acts as a chromophore primarily on account of the excitation of a nonbonding O lone-pair electron to an antibonding CO π orbital.

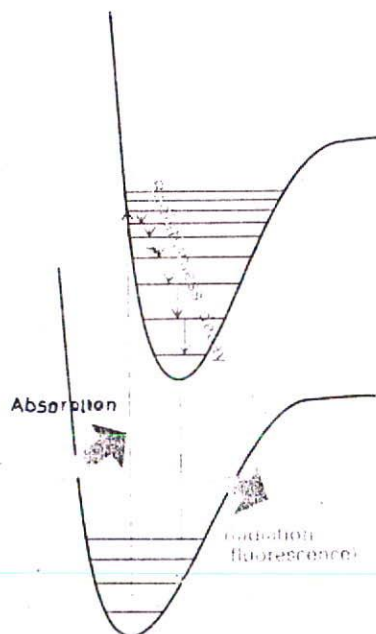


17.10 The empirical (observation-based) distinction between fluorescence and phosphorescence is that the former is extinguished immediately the exciting source is removed, whereas the latter continues with relatively slowly diminishing intensity.

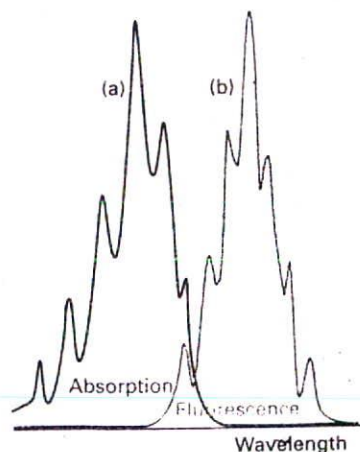
(a) Fluorescence

Figure 17.11 shows the sequence of steps involved in fluorescence. The initial absorption takes the molecule to an excited electronic state, and if the absorption spectrum were monitored it would look like the one shown in Fig. 17.12a. The excited molecule is subjected to collisions with the surrounding molecules, and as it gives up energy nonradiatively it steps down the ladder of vibrational levels to the lowest vibrational level of the electronically excited molecular state. The surrounding molecules, however, might now be unable to accept the larger energy difference needed to lower the molecule to the ground electronic state. It might therefore survive long enough to undergo spontaneous emission, and emit the remaining excess energy as radiation. The downward electronic transition is vertical (in accord with the Franck-Condon principle) and the fluorescence spectrum has a vibrational structure characteristic of the *lower* electronic state (Fig. 17.12b).

Provided they can be seen, the 0-0 absorption and fluorescence transitions can be expected to be coincident. The absorption spectrum arises from 0-0, 1-0, 2-0, etc. transitions and the peaks occur at progressively higher wavenumber and with intensities governed by the Franck-Condon principle. The fluorescence spectrum arises from 0-0, 0-1, 0-2, etc. *downward* transitions, and hence the peaks occur with decreasing wavenumbers. The 0-0 absorption and fluorescence peaks are not always exactly coincident because the solvent may interact differently with the solute in the ground and excited states (for instance, the hydrogen bonding pattern might differ). Because the solvent molecules do not have time to rearrange during the transition, the absorption occurs in an environment characteristic of the solvated ground state; however, the fluorescence occurs in an environment characteristic of the solvated excited state (Fig. 17.13).

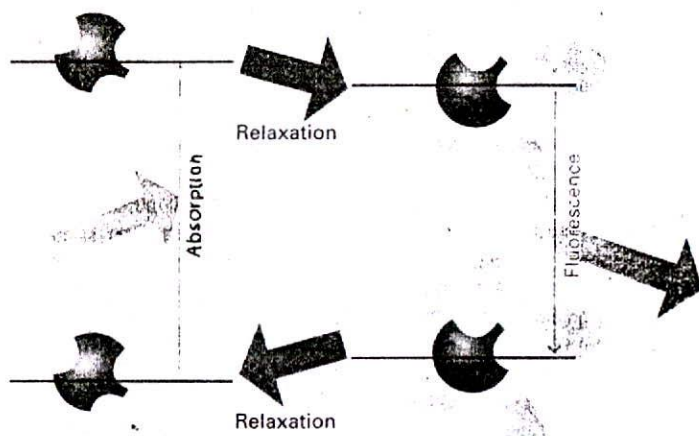


17.11 The sequence of steps leading to fluorescence. After the initial absorption, the upper vibrational states undergo radiationless decay by giving up energy to the surroundings. A radiative transition then occurs from the vibrational ground state of the upper electronic state.

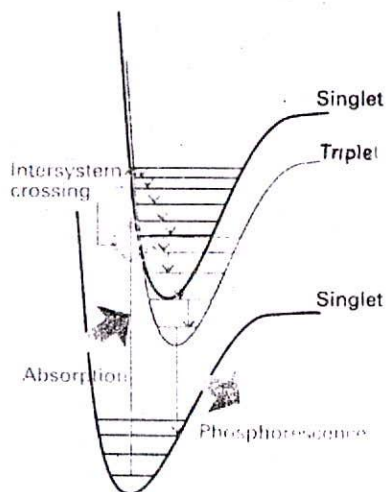


17.12 An absorption spectrum (a) shows a vibrational structure characteristic of the upper state. A fluorescence spectrum (b) shows a structure characteristic of the lower state; it is also displaced to lower frequencies (but the 0-0 transitions are coincident) and resembles a mirror image of the absorption.

17.13 The solvent can shift the fluorescence spectrum relative to the absorption spectrum. On the left we see that the absorption occurs with the solvent (the ellipses) in the arrangement characteristic of the ground electronic state of the molecule (the sphere). However, before fluorescence occurs, the solvent molecules relax into a new arrangement, and that arrangement is preserved during the subsequent radiative transition.



Fluorescence occurs at a lower frequency than the incident radiation because the emissive transition occurs after some vibrational energy has been discarded into the surroundings. The vivid oranges and greens of fluorescent dyes are an everyday manifestation of this effect: they absorb in the ultraviolet and blue, and fluoresce in the visible. The mechanism also suggests that the intensity of the fluorescence ought to depend on the ability of the solvent molecules to accept the electronic and vibrational quanta. It is indeed found that a solvent composed of molecules with widely spaced vibrational levels (such as water) can in some cases accept the large quantum of electronic energy and so extinguish, or 'quench', the fluorescence.



17.14 The sequence of steps leading to phosphorescence. The important step is the intersystem crossing, the switch from a singlet state to a triplet state brought about by spin-orbit coupling. The triplet state acts as a slowly radiating reservoir because the return to the ground state is spin-forbidden.

(b) Phosphorescence

Figure 17.14 shows the sequence of events leading to phosphorescence for a molecule with a singlet ground state. The first steps are the same as in fluorescence, but the presence of a triplet excited state plays a decisive role.¹ The singlet and triplet excited states share a common geometry at the point where their potential energy curves intersect. Hence, if there is a mechanism for unpairing two electron spins (and achieving the conversion of $\uparrow\downarrow$ to $\uparrow\uparrow$), the molecule may undergo intersystem crossing and become a triplet state. We saw in the discussion of atomic spectra (Section 13.9d) that singlet-triplet transitions may occur in the presence of spin-orbit coupling, and the same is true in molecules. We can expect intersystem crossing to be important when a molecule contains a moderately heavy atom (such as S), because then the spin-orbit coupling is large.

If an excited molecule crosses into a triplet state, it continues to deposit energy into the surroundings. However, it is now stepping down the triplet's vibrational ladder, and at the lowest energy level it is trapped because the triplet state is at a lower energy than the corresponding singlet (recall Hund's rule, Section 13.7). The solvent cannot absorb the final, large quantum of electronic excitation energy, and the molecule cannot radiate its energy because return to the ground state is spin-forbidden. The radiative transition, however, is not totally forbidden because the spin-orbit coupling that was responsible for the

1 We first encountered triplet states in Section 13.7: they are states in which two electrons have parallel spins.

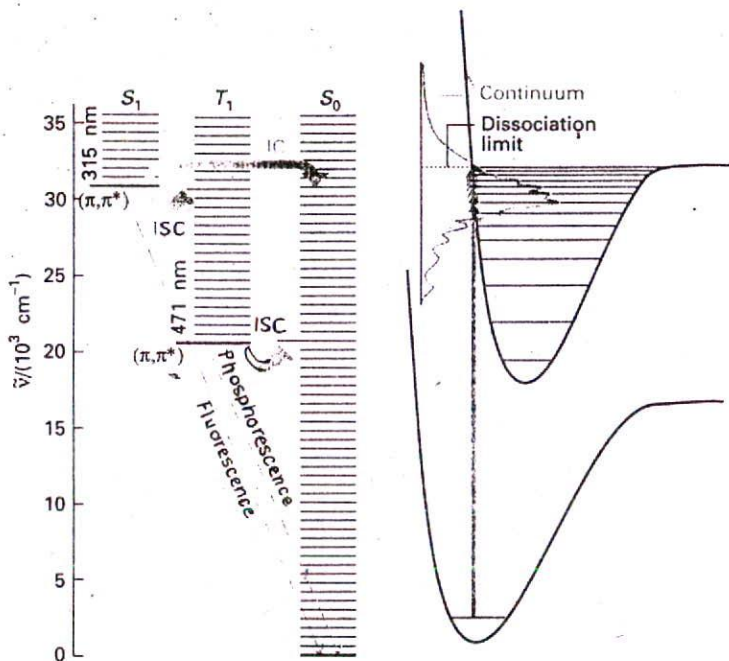
intersystem crossing also breaks the selection rule. The molecules are therefore able to emit weakly, and the emission may continue long after the original excited state was formed.

The mechanism accounts for the observation that the excitation energy seems to get trapped in a slowly leaking reservoir. It also suggests (as is confirmed experimentally) that phosphorescence should be most intense from solid samples: energy transfer is then less efficient and intersystem crossing has time to occur as the singlet excited state steps slowly past the intersection point. The mechanism also suggests that the phosphorescence efficiency should depend on the presence of a moderately heavy atom (with strong spin-orbit coupling), which is in fact the case. The confirmation of the mechanism is the experimental observation (using the sensitive resonance techniques described in Chapter 18) that the sample is paramagnetic while the reservoir state, with its unpaired electron spins, is populated.

The various types of nonradiative and radiative transitions that can occur in molecules are often represented on a schematic Jablonski diagram of the type shown in Fig. 17.15.

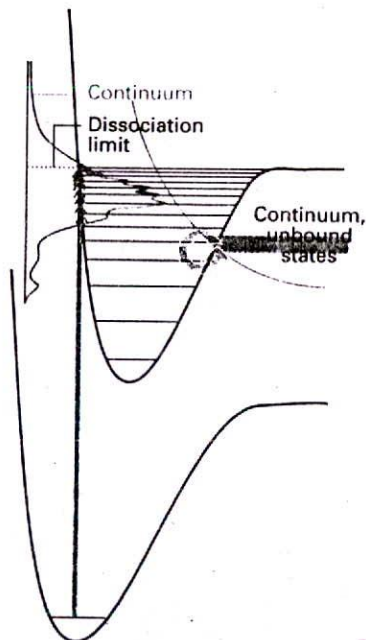
17.4 Dissociation and predissociation

Another fate for an electronically excited molecule is dissociation, the breaking of bonds (Fig. 17.16). The onset of dissociation can be detected in an absorption spectrum by seeing



17.15 A Jablonski diagram (here, for naphthalene) is a simplified portrayal of the relative positions of the electronic energy levels of a molecule. Vibrational levels of states of a given electronic state lie above each other, but the relative horizontal locations of the columns bear no relation to the nuclear separations in the states. The ground vibrational states of each electronic state are correctly located vertically but the other vibrational states are shown only schematically. (IC: internal conversion; ISC: intersystem crossing.)

17.16 When absorption occurs to unbound states of the upper electronic state, the molecule dissociates and the absorption is a continuum. Below the dissociation limit the electronic spectrum shows a normal vibrational structure.



17.17 When a dissociative state crosses a bound state, as in the upper part of the illustration, molecules excited to levels near the crossing may dissociate. This process is called predissociation, and is detected in the spectrum as a loss of vibrational structure that resumes at higher frequencies.

that the vibrational structure of a band terminates at a certain energy. Absorption occurs in a continuous band above this dissociation limit because the final state is an unquantized translational motion of the fragments. Locating the dissociation limit is a valuable way of determining the bond dissociation energy.

In some cases, the vibrational structure disappears but resumes at higher photon energies. This predissociation can be interpreted in terms of the molecular potential energy curves shown in Fig. 17.17. When a molecule is excited to a vibrational level, its electrons may undergo a reorganization that results in it undergoing an internal conversion, a radiationless conversion to another state of the same multiplicity. An internal conversion occurs most readily at the point of intersection of the two molecular potential energy curves, because there the nuclear geometries of the two states are the same. The state into which the molecule converts may be dissociative, so the states near the intersection have a finite lifetime, and hence their energies are imprecisely defined. As a result, the absorption spectrum is blurred in the vicinity of the intersection. When the incoming photon brings enough energy to excite the molecule to a vibrational level high above the intersection, the internal conversion does not occur (the nuclei are unlikely to have the same geometry). Consequently, the levels resume their well-defined, vibrational character with correspondingly well-defined energies, and the line structure resumes on the high-frequency side of the blurred region.

Lasers

Lasers have transformed chemistry as much as they have transformed the everyday world. In this section, we see some of the principles of their operation, and then explore their applications in chemistry. Lasers lie very much on the frontier of physics and chemistry, for their operation depends on details of optics and, in some cases, of solid-state processes. We shall concentrate on the more chemical aspects of their operation, particularly the materials from which they are made and the events taking place within them.

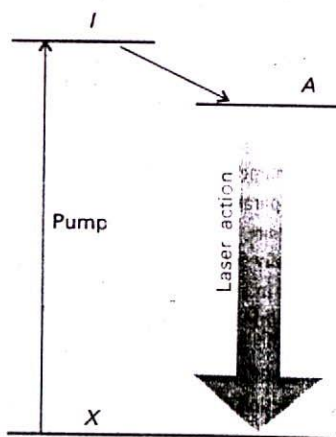
17.5 General principles of laser action

The word laser is an acronym formed from light amplification by stimulated emission of radiation. In stimulated emission, an excited state is stimulated to emit a photon by radiation of the same frequency; the more photons that are present, the greater the probability of the emission. The essential feature of laser action is positive-feedback: the more photons present of the appropriate frequency, the more photons of that frequency that will be stimulated to form.

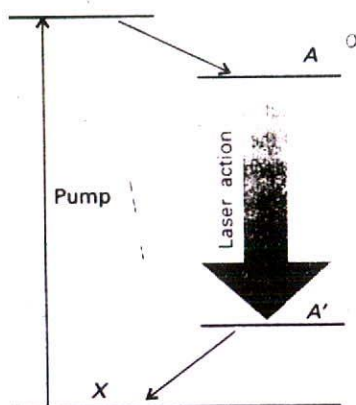
(a) Population inversion

One requirement of laser action is the existence of a metastable excited state, an excited state with a long enough lifetime for it to participate in stimulated emission. Another requirement is the existence of a greater population in the metastable state than in the lower state where the transition terminates, for then there will be a net emission of radiation. Because at thermal equilibrium the opposite is true, it is necessary to achieve a population inversion in which there are more molecules in the upper state than in the lower.

One way of achieving population inversion is illustrated in Fig. 17.18. The molecule is excited to an intermediate state I , which then gives up some of its energy nonradiatively and changes into a lower state A ; the laser transition is the return of A to the ground state X . Because three energy levels are involved overall, this arrangement leads to a three-level laser. In practice, I consists of many states, all of which can convert to the upper of the two

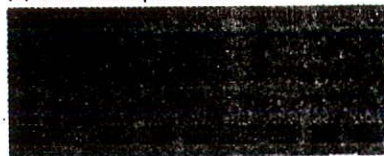


17.18 The transitions involved in one kind of three-level laser. The pumping pulse populates the intermediate state I , which in turn populates the laser state A . The laser transition is the stimulated emission $A \rightarrow X$.



17.19 The transitions involved in a four-level laser. Because the laser transition terminates in an excited state (A'), the population inversion between A and A' is much easier to achieve.

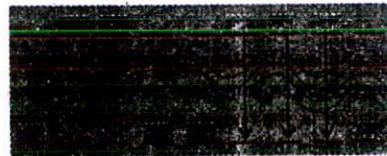
(a) Thermal equilibrium



(b) Population inversion



(c) Laser action



17.20 A schematic illustration of the steps leading to laser action. (a) The Boltzmann population of states, with more atoms in the ground state. (b) When the initial state absorbs, the populations are inverted (the atoms are pumped to the excited state). (c) A cascade of radiation then occurs, as one emitted photon stimulates another atom to emit, and so on. The radiation is coherent (phases in step).

laser states A . The $I \leftarrow X$ transition is stimulated with an intense flash of light in the process called **pumping**. The pumping is often achieved with an electric discharge through xenon or with the light of another laser. The conversion of I to A should be rapid, and the laser transitions from A to X should be relatively slow.

The disadvantage of this three-level arrangement is that it is difficult to achieve population inversion, because so many ground-state molecules must be converted to the excited state by the pumping action. The arrangement adopted in a **four-level laser** simplifies this task by having the laser transition terminate in a state A' other than the ground state (Fig. 17.19). Because A' is unpopulated initially, any population in A corresponds to a population inversion, and we can expect laser action if A is sufficiently metastable. Moreover, this population inversion can be maintained if the $A' \rightarrow X$ transitions are rapid, for these transitions will deplete any population in A' that stems from the laser transition, and keep the state A' relatively empty.

(b) Cavity and mode characteristics

The laser medium is confined to a cavity that ensures that only certain photons of a particular frequency, direction of travel, and state of polarization are generated abundantly. The cavity is essentially a region between two mirrors, which reflect the light back and forth. This arrangement can be regarded as a version of the particle in a box, with the particle now being a photon. As in the treatment of a particle in a box (Section 12.1), the only wavelengths that can be sustained satisfy

$$n \times \frac{1}{2}\lambda = L \quad (4)$$

where n is an integer and L is the length of the cavity. That is, only an integral number of half-wavelengths fit into the cavity; all other waves undergo destructive interference with themselves. In addition, not all wavelengths that can be sustained by the cavity are amplified by the laser medium (many fall outside the range of frequencies of the laser transitions), so only a few contribute to the laser radiation. These wavelengths are the **resonant modes** of the laser.

Photons with the correct wavelength for the resonant modes of the cavity and the correct frequency to stimulate the laser transition are highly amplified. One photon might be generated spontaneously, and travel through the medium. It stimulates the emission of another photon, which in turn stimulates more (Fig. 17.20). The cascade of energy builds up rapidly, and soon the cavity is an intense reservoir of radiation at all the resonant modes it can sustain. Some of this radiation can be withdrawn if one of the mirrors is partially transmitting.

The resonant modes of the cavity have various natural characteristics, and to some extent may be selected. Only photons that are travelling strictly parallel to the axis of the cavity undergo more than a couple of reflections, so only they are amplified, all others simply vanishing into the surroundings. Hence, laser light generally forms a beam with very low divergence. It may also be polarized, with its electric vector in a particular plane (or in some other state of polarization), by including a polarizing filter into the cavity or by making use of polarized transitions in a solid medium.

Laser radiation is **coherent** in the sense that the electromagnetic waves are all in step. In **spatial coherence** the waves are in step across the cross-section of the beam emerging from the cavity. In **temporal coherence** the waves remain in step along the beam. The latter is normally expressed in terms of a coherence length, l_c , and is related to the range of wavelengths, $\Delta\lambda$, present in the beam:

$$l_c = \frac{\lambda^2}{2\Delta\lambda} \quad (5)$$

If the beam were perfectly monochromatic, with strictly one wavelength present, then $\Delta\lambda$ would be zero, and the waves would remain in step for an infinite distance. When many wavelengths are present, the waves get out of step in a short distance and the coherence length is small. A typical light bulb gives out light with a coherence length of only about 400 nm; a He-Ne laser with $\Delta\lambda \approx 2$ pm has a coherence length of about 10 cm.

(c) *Q*-switching

A laser can generate radiation for as long as the population inversion is maintained. A laser can operate continuously when heat is easily dissipated, for then the population of the upper level can be replenished by pumping. Practical considerations govern whether or not continuous pumping is feasible, as we shall see when we consider some particular lasers. When overheating is a problem, the laser can be operated only in pulses, perhaps of microsecond or millisecond duration, so that the medium has a chance to cool or the lower state discard its population. However, it is sometimes desirable to have pulses of radiation rather than a continuous output, with a lot of power concentrated into a brief pulse. One way of achieving pulses is by *Q*-switching, the modification of the resonance characteristics of the laser cavity.²

Example 17.2 Relating the power and energy of a laser

A laser rated at 0.10 J can generate radiation in 3.0 ns pulses. What is the average power output per pulse?

Method The power output, P , is the energy released in an interval divided by the duration of the interval, and is expressed in watts ($1 \text{ W} = 1 \text{ J s}^{-1}$). So, to calculate the power, divide the energy output by the time over which the pulse is generated.

Answer From the data,

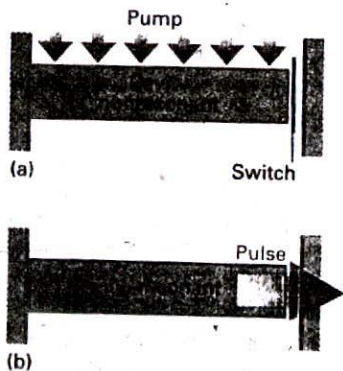
$$P = \frac{0.10 \text{ J}}{3.0 \times 10^{-9} \text{ s}} = 3.3 \times 10^7 \text{ J s}^{-1}$$

That is, the pulses deliver 33 MW of power.

Comment The answer gives the average power; the peak power will be larger if the pulse is not rectangular.

Self-test 17.2 Calculate the average power output of a laser in which a 2.0 J pulse can be delivered in 1.0 ns.

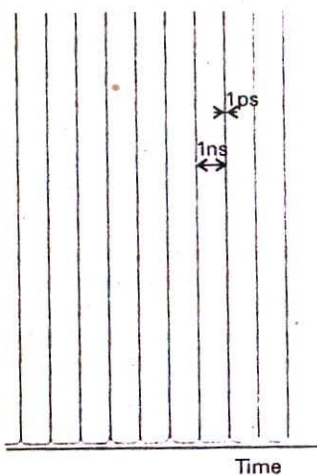
[2.0 GW]



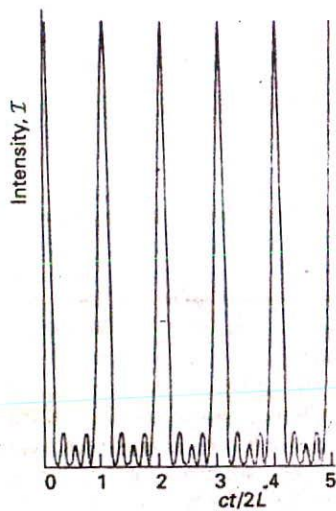
17.21 The principle of *Q*-switching. The excited state is populated while the cavity is nonresonant. Then the resonance characteristics are suddenly restored, and the stimulated emission emerges in a giant pulse.

The aim of *Q*-switching is to achieve a healthy population inversion in the absence of the resonant cavity, then to plunge the population-inverted medium into a cavity, and hence to obtain a sudden pulse of radiation. The switching may be achieved by impairing the resonance characteristics of the cavity in some way while the pumping pulse is active, and then suddenly to improve them (Fig. 17.21). One technique is to use a saturable dye, a dye that loses its power to absorb when many of its molecules have been excited by intense radiation. It then suddenly becomes transparent, and the cavity becomes resonant. In practice, *Q*-switching can give pulses of about 10 ns duration.

² The name comes from the '*Q*-factor' used as a measure of the quality of a resonance cavity in microwave engineering.



17.22 The output of a mode-locked laser consists of a stream of very narrow pulses separated by an interval equal to the time it takes for light to make a round trip inside the cavity.



17.23 The function derived in Justification 17.3 showing in more detail the structure of the pulses generated by a mode-locked laser.

(d) Mode locking

The technique of mode locking can produce pulses of picosecond duration and less. A laser radiates at a number of different frequencies, depending on the precise details of the resonance characteristics of the cavity and in particular on the number of half-wavelengths of radiation that can be trapped between the mirrors (the cavity modes). The resonant modes differ in frequency by multiples of $c/2L$ (as can be inferred from eqn 4 with $\nu = c/\lambda$). Normally, these modes have random phases relative to each other. However, it is possible to lock their phases together. Then interference occurs to give a series of sharp peaks, and the energy of the laser is obtained in picosecond bursts (Fig. 17.22). The sharpness of the peaks depends on the range of modes superimposed and, the wider the range, the narrower the pulses. In a laser with a cavity of length 30 cm, the peaks will be separated by 2 ns. If 1000 modes contribute, the width of the pulses will be 4 ps.

Justification 17.3

The general expression for a (complex) wave of amplitude \mathcal{E}_0 and frequency ω is $\mathcal{E}_0 e^{i\omega t}$. Therefore, each wave that can be supported by a cavity of length L has the form

$$\mathcal{E}_n(t) = \mathcal{E}_0 e^{2\pi i(\nu \frac{c}{2L})t}$$

where ν is the lowest frequency. A wave formed by superimposing N modes with $n = 0, 1, \dots, N-1$ has the form

$$\mathcal{E}(t) = \sum_n \mathcal{E}_n(t) = \mathcal{E}_0 e^{2\pi i \nu t} \sum_{n=0}^{N-1} e^{i n \pi c t / L}$$

The sum is a geometrical progression:

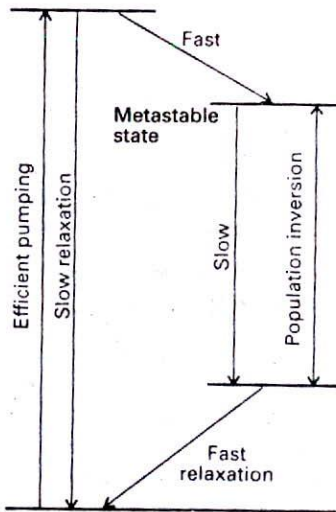
$$\begin{aligned} \sum_{n=0}^{N-1} e^{i n \pi c t / L} &= 1 + e^{i \pi c t / L} + e^{2i \pi c t / L} + \dots \\ &= \frac{\sin(N \pi c t / 2L)}{\sin(\pi c t / 2L)} \times e^{(N-1) i \pi c t / 2L} \end{aligned}$$

The intensity, \mathcal{I} , of the radiation is proportional to the square modulus of the total amplitude, so

$$\mathcal{I} \propto \mathcal{E}^* \mathcal{E} \cong \mathcal{E}_0^2 \frac{\sin^2(N \pi c t / 2L)}{\sin^2(\pi c t / 2L)}$$

This function is shown in Fig. 17.23. We see that it is a series of peaks with maxima separated by $t = 2L/c$, the round-trip transit time of the light in the cavity, and that the peaks become sharper as N is increased.

Mode locking is achieved by varying the Q factor of the cavity periodically at the frequency $c/2L$. The modulation can be pictured as the opening of a shutter in synchrony with the round-trip travel time of the photons in the cavity, so only photons making the journey in that time are amplified. The modulation can be achieved by linking a prism in the cavity to a transducer driven by a radiofrequency source at a frequency $c/2L$. The transducer sets up standing-wave vibrations in the prism and modulates the loss it introduces into the cavity. Mode locking may also be accomplished passively by including a saturable dye. This procedure makes use of the fact that the gain, the growth in intensity of a component, is very sensitive to amplification and, once a particular frequency begins to grow, it can quickly dominate. If a saturable dye is included in the cavity, a spontaneous fluctuation in intensity—a bunching of photons—may result in its becoming transparent, and the bunch can pass through and travel to the far end of the cavity, amplifying as it goes. The dye immediately shuts down again (if it is well chosen), but opens when the intense pulse returns



17.24 A summary of the features needed for efficient laser action.

from the mirror at the far end and saturates it. In this way, that particular bunch of photons may grow to considerable intensity because it alone is stimulating emission in the cavity.

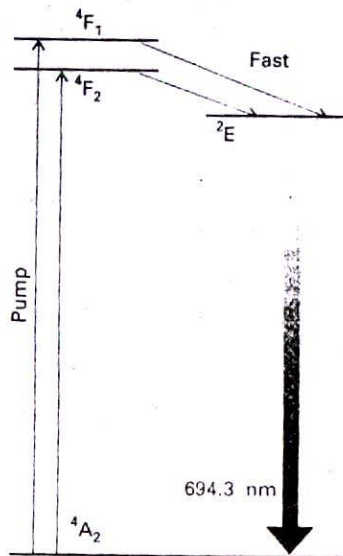
17.6 Practical lasers

Figure 17.24 summarizes the requirements for an efficient laser. In practice, the requirements can be satisfied by using a variety of different systems, and this section reviews some that are commonly available. For completeness, we include some lasers that operate by using other than electronic transitions.

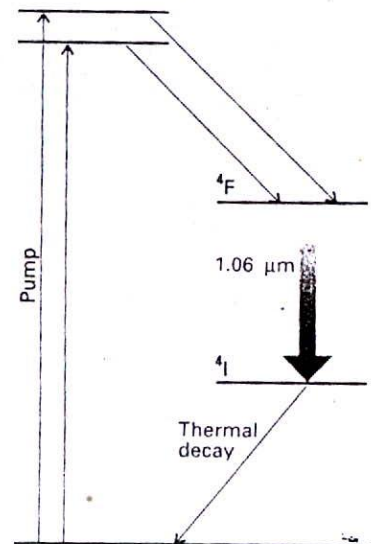
(a) Solid-state lasers

A solid-state laser is one in which the active medium is in the form of a single crystal or a glass. The first successful laser, the ruby laser built by Theodore Maiman in 1960, is an example (Fig. 17.25). Ruby is Al_2O_3 containing a small proportion of Cr^{3+} ions.³ Ruby is a three-level system, and the ground state, which is also the lower level of the laser transition, is $^4\text{A}_2$ with three unpaired spins on each Cr^{3+} ion. The population inversion results from pumping a majority of the Cr^{3+} ions into an excited state by using an intense flash from another source, followed by a radiationless transition to another excited state. The pumping flash need not be monochromatic because the upper level actually consists of several states spanning a band of frequencies. The transition from the lower of the two excited states to the ground state ($^2\text{E} \rightarrow ^4\text{A}_2$) is the laser transition, and gives rise to red 694 nm radiation. The population inversion is very difficult to sustain continuously, and in practice the ruby laser is pulsed. Typical pulses from a Q-switched ruby laser might consist of 2 J pulses persisting for 10 ns, corresponding to an average power of 0.2 GW.

The neodymium laser is an example of a four-level laser (Fig. 17.26). In one form it consists of Nd^{3+} ions at low concentration in yttrium aluminium garnet (YAG, specifically



17.25 The transitions involved in a ruby laser. The laser medium, ruby, consists of Al_2O_3 doped with Cr^{3+} ions.



17.26 The transitions involved in a neodymium laser. The laser action takes place between two excited states, and the population inversion is easier to achieve than in the ruby laser.

³ The normal green of Cr^{3+} is modified to red by the distortion of the local crystal field stemming from the replacement of an Al^{3+} ion by a slightly larger Cr^{3+} ion.

$\text{Y}_3\text{Al}_5\text{O}_{12}$), and is then known as a Nd-YAG laser. A cheaper medium is glass, but glass is a poorer thermal conductor than YAG and the laser must be pulsed. A neodymium laser operates at a number of wavelengths in the infrared, the band at 1064 nm being most common. The transition at 1064 nm is very efficient and the laser is capable of substantial power output. The power is great enough for frequency doubling to be used efficiently. Frequency doubling is a technique in which the laser beam is converted to radiation with twice (and in general a multiple) of its initial frequency as it passes through a suitable transparent material. A frequency-doubled Nd-YAG laser produces green light at 532 nm.

Example 17.3 Accounting for multiphoton phenomena

Show that if a substance responds nonlinearly to incident radiation of frequency ω , then it may act as the source of radiation of twice the incident frequency.

Method Radiation of a particular frequency arises from oscillations of an electric dipole at that frequency. Therefore, express the induced electric dipole moment of the system in terms of powers of the applied electric field, and write the powers of harmonic (cosine) terms as sums and differences of cosine terms. Inspect the sum to see if $\cos 2\omega t$ is present.

Answer The incident electric field \mathcal{E} induces an electric dipole of magnitude μ and, allowing for nonlinear response, we can write

$$\mu = \alpha\mathcal{E} + \beta\mathcal{E}^2 + \dots$$

The nonlinear terms can be expanded as follows if we suppose that the incident electric field is $\mathcal{E}_0 \cos \omega t$:

$$\beta\mathcal{E}^2 = \beta\mathcal{E}_0^2 \cos^2 \omega t = \frac{1}{2}\beta\mathcal{E}_0^2(1 + \cos 2\omega t)$$

Hence, the nonlinear term contributes an induced electric dipole that oscillates at the frequency 2ω and which can act as a source of radiation of that frequency.

Self-test 17.3 Show that, if a substance responds nonlinearly to two sources of radiation, one of frequency ω_1 and the other of frequency ω_2 , then it may give rise to radiation of the sum and difference of the two frequencies.

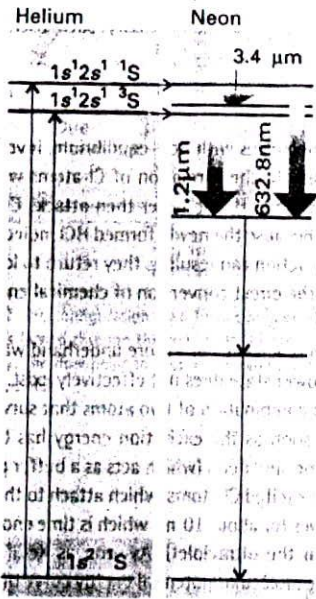
$$[\beta\mathcal{E}^2 \propto \cos(\omega_1 + \omega_2)t + \cos(\omega_1 - \omega_2)t]$$

(b) Gas lasers

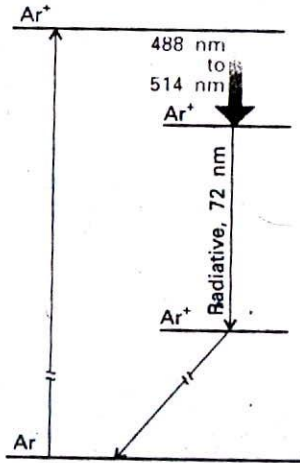
Because gas lasers can be cooled by a rapid flow of the gas through the cavity, they can be used to generate high powers. The pumping is normally achieved using a gas that is different from the gas responsible for the laser emission itself.

In the helium–neon laser the active medium is a mixture of helium and neon in a mole ratio of about 5 : 1 (Fig. 17.27). The initial step is the excitation of an He atom to the metastable $1s^1 2s^1$ configuration by using an electric discharge (the collisions of electrons and ions cause transitions that are not restricted by electric-dipole selection rules). The excitation energy of this transition happens to match an excitation energy of neon, and during an He–Ne collision efficient transfer of energy may occur, leading to the production of highly excited, metastable Ne atoms with unpopulated intermediate states. Laser action generating 633 nm radiation (among about 100 other lines) then occurs.

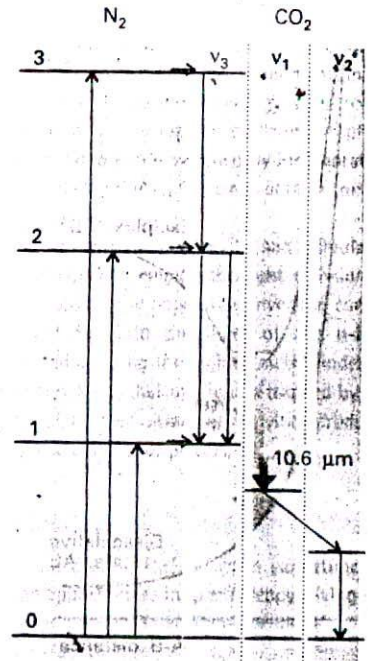
The argon-ion laser (Fig. 17.28), one of a number of 'ion lasers', consists of argon at about 1 Torr, through which is passed an electric discharge. The discharge results in the formation of Ar^+ and Ar^{2+} ions in excited states, which undergo a laser transition to a lower



17.27 The transitions involved in a helium-neon laser. The pumping (of the neon) depends on a coincidental matching of the helium and neon energy separations, so excited He atoms can transfer their excess energy to Ne atoms during a collision.



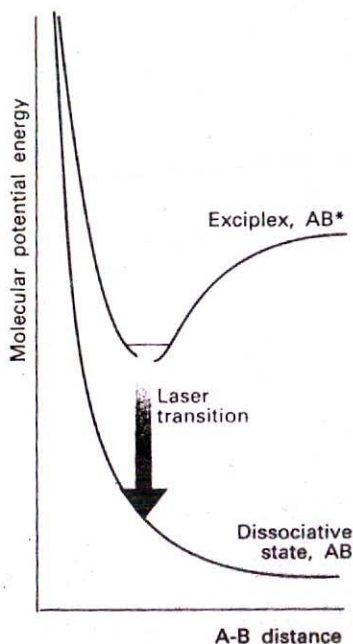
17.28 The transitions involved in an argon-ion laser.



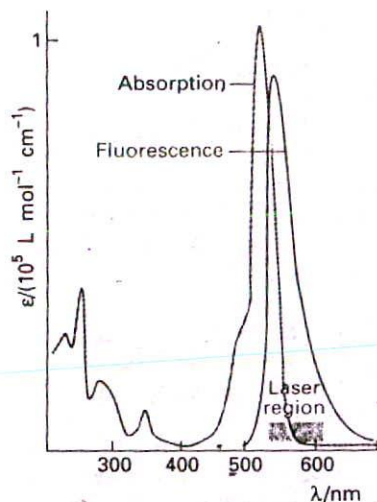
17.29 The transitions involved in a carbon dioxide laser. The pumping also depends on the coincidental matching of energy separations; in this case the vibrationally excited N_2 molecules have excess energies that correspond to a vibrational excitation of the antisymmetric stretch of CO_2 . The laser transition is from $\nu_3 = 1$ to $\nu_1 = 1$.

state. These ions then revert to their ground states by emitting hard ultraviolet radiation (at 72 nm). These ions then revert to their ground states by emitting hard ultraviolet radiation (at 72 nm), and are then neutralized by a series of electrodes in the laser cavity. One of the design problems is to find materials that can withstand this damaging residual radiation. There are many lines in the laser transition because the excited ions may make transitions to many lower states, but two strong emissions from Ar^+ are at 488 nm (blue) and 514 nm (green); other transitions occur elsewhere in the visible region, in the infrared, and in the ultraviolet. The krypton-ion laser works similarly. It is less efficient, but gives a wider range of wavelengths, the most intense being at 647 nm (red), but it can also generate a yellow line. Both lasers are widely used in laser light shows (for this application argon and krypton are often used simultaneously in the same cavity) as well as being used as laboratory sources of high-power radiation.

The carbon dioxide laser works on a slightly different principle (Fig. 17.29), for its radiation (between $9.2 \mu m$ and $10.8 \mu m$, with the strongest emission at $10.6 \mu m$, in the infrared) arises from vibrational transitions. Most of the working gas is nitrogen, which becomes vibrationally excited by electronic and ionic collisions in an electric discharge. The vibrational levels happen to coincide with the ladder of antisymmetric stretch (ν_3 , see Fig. 16.46) energy levels of CO_2 , which pick up the energy during a collision. Laser action then occurs from the lowest excited level of ν_3 to the lowest excited level of the symmetric stretch (ν_1), which has remained unpopulated during the collisions. This transition is allowed by anharmonicities in the molecular potential energy. Some helium is included in the gas to help remove energy from this state and maintain the population inversion.



17.30 The molecular potential energy curves for an exciplex. The species can survive only as an excited state, because on discarding its energy it enters the lower, dissociative state. Because only the upper state can exist, there is never any population in the lower state.



17.31 The optical absorption spectrum of the dye Rhodamine G and the region used for laser action.

In the **nitrogen laser**, the efficiency of the stimulated transition (at 337 nm, in the ultraviolet, the transition $C^3\Pi_u \rightarrow B^3\Pi_g$) is so great that a single passage of a pulse of radiation is enough to generate laser radiation and mirrors are unnecessary—such lasers are said to be **superradiant**.

(c) Chemical and exciplex lasers

Chemical reactions may also be used to generate molecules with non-equilibrium, inverted populations. For example, the photolysis of Cl_2 leads to the formation of Cl atoms which attack H_2 molecules in the mixture and produce HCl and H. The latter then attacks Cl_2 to produce vibrationally excited ('hot') HCl molecules. Because the newly formed HCl molecules have non-equilibrium vibrational populations, laser action can result as they return to lower states. Such processes are remarkable examples of the direct conversion of chemical energy into coherent electromagnetic radiation.

The population inversion needed for laser action is achieved in a more underhand way in **exciplex lasers**,⁴ for in these (as we shall see) the lower state does not effectively exist. This odd situation is achieved by forming an exciplex, a combination of two atoms that survives only in an excited state and which dissociates as soon as the excitation energy has been discarded. An example is a mixture of xenon, chlorine, and neon (which acts as a buffer gas). An electric discharge through the mixture produces excited Cl atoms, which attach to the Xe atoms to give the exciplex $XeCl^*$. The exciplex survives for about 10 ns, which is time enough for it to participate in laser action at 308 nm (in the ultraviolet). As soon as $XeCl^*$ has discarded a photon, the atoms separate because the molecular potential energy curve of the ground state is dissociative, and the ground state of the exciplex cannot become populated (Fig. 17.30). The KrF^* exciplex laser is another example: it produces radiation at 249 nm.

(d) Dye lasers

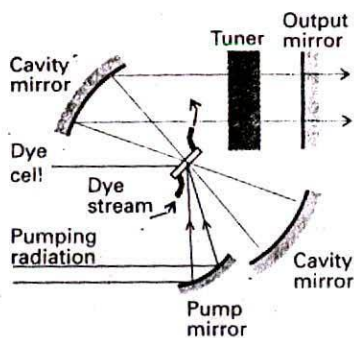
A solid-state laser and a gas laser operate at discrete frequencies and, although the frequency required may be selected by suitable optics, the laser cannot be tuned continuously. The tuning problem is overcome by using a dye laser, which has broad spectral characteristics because the solvent broadens the vibrational structure of the transitions into bands. Hence, it is possible to scan the wavelength continuously (by rotating the diffraction grating in the cavity) and achieve laser action at any chosen wavelength. A commonly used dye is Rhodamine 6G in methanol (Fig. 17.31). As the gain is very high, only a short length of the optical path need be through the dye. The excited states of the active medium, the dye, are sustained by another laser or a flash lamp, and the dye solution is flowed through the laser cavity to avoid thermal degradation (Fig. 17.32).

(e) Light-emitting diodes and semiconductor lasers

We have seen (in Section 14.10d) that a semiconductor is classified as 'n-type' if its conduction band is partly populated and as 'p-type' if its valence band has a small number of holes. In this section we need to consider the properties of a p-n junction, the interface of the two types of semiconductor.

The band structure at the junction is shown in Fig. 17.33. When a 'forward bias' is applied to the junction, in the sense that electrons are supplied through an external circuit to the n side of the junction, the electrons in the conduction band of the n-type semiconductor fall into the holes in the valence band of the p-type semiconductor. As they fall, they emit energy. In silicon semiconductors this energy is largely in the form of heat because the wavefunctions of the relevant states of the bands differ in linear momentum, so the

⁴ The term 'excimer laser' is also widely encountered and used loosely when 'exciplex laser' is more appropriate. An exciplex has the form AB^* whereas an excimer, an excited dimer, is AA^* .



17.32 The configuration used for a dye laser. The dye is flowed through the cell inside the laser cavity. The flow helps to keep it cool and prevents degradation.

transition can occur only if the electron transfers linear momentum to the lattice, and the device becomes warm. However, in some materials, most notably gallium arsenide, GaAs, the wavefunctions of the states involved correspond to the same linear momentum, so transition can occur without the lattice needing to be involved and the energy is emitted as light. Practical light-emitting diodes of this kind are widely used in electronic displays. Gallium arsenide itself emits infrared light, but the band gap is widened by incorporating phosphorus, and a material of composition approximately $\text{GaAs}_{0.6}\text{P}_{0.4}$ emits light in the red region of the spectrum.

A light-emitting diode is not a laser, because no resonance cavity and stimulated emission are involved. However, it is easy (in principle) to employ the light emission of electron-hole recombination as the basis of laser action. The population inversion can be sustained by sweeping away the electrons that fall into the holes of the p-type semiconductor, and a resonant cavity can be formed by using the high refractive index of the semiconducting material and cleaving single crystals so that the light is trapped by the sudden variation of refractive index. One widely used material is $\text{Ga}_{1-x}\text{Al}_x\text{As}$, which produces infrared laser radiation and is widely used in compact-disc (CD) players.

17.7 Applications of lasers in chemistry

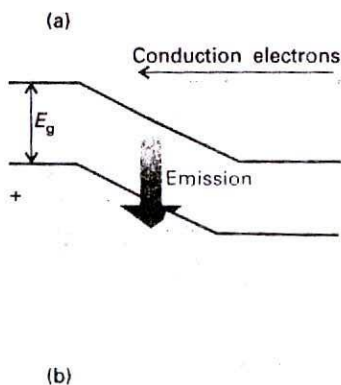
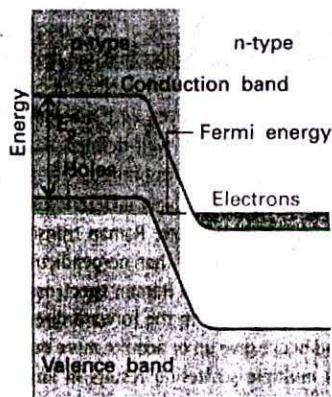
Laser radiation has five striking characteristics (Table 17.3). Each of them (sometimes in combination with the others) opens up interesting opportunities in spectroscopy, giving rise to 'laser spectroscopy' and, in photochemistry, giving rise to 'laser photochemistry'.

(a) Spectroscopy at high photon fluxes

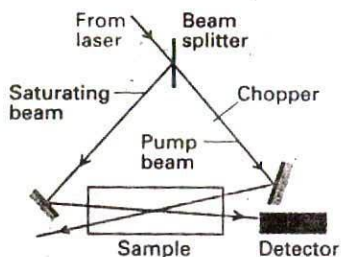
The high spectral power density of a laser—the high intensity of the radiation it produces at well-defined frequencies—is an aid to conventional spectroscopy. Thus, it reduces the problem of detector noise and the interfering effects of background radiation. The high intensity is particularly advantageous in Raman spectroscopy, which until the introduction of lasers was plagued by the low intensity of the scattered radiation (which could be overcome only by using long exposures) and by interference from background scattering (which obscured the signal).

Table 17.3 Characteristics of laser radiation and their chemical applications

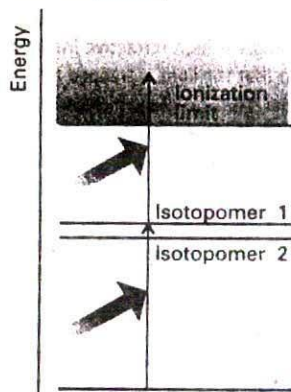
Characteristic	Advantages	Applications
High power	Multiphoton process	Non-linear spectroscopy
	Low detector noise	Saturation spectroscopy
	High scattering intensity	Improved sensitivity Raman spectroscopy
Monochromatic	High resolution	Spectroscopy
	State selection	Isotope separation
		Photochemically precise State-to-state reaction dynamics
Collimated beam	Long path lengths	Sensitivity
	Forward-scattering observable	Non-linear Raman spectroscopy
Coherent	Interference between separate beams	CARS
Pulsed	Precise timing of excitation	Fast reactions
		Relaxation
		Energy transfer



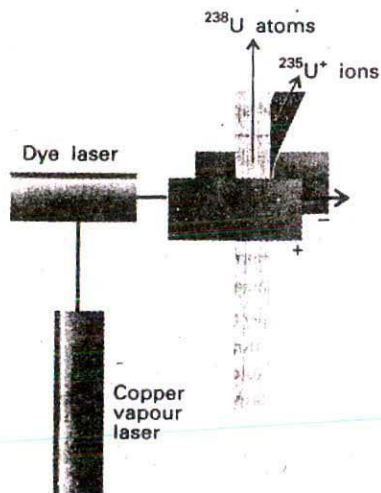
17.33 The structure of a diode junction (a) without bias and (b) with bias.



17.34 The configuration of laser radiation used for saturation spectroscopy.



17.35 In one method of isotope separation, one photon excites an isotopomer to an excited state, and then a second photon achieves photoionization. The success of the first step depends on the nuclear mass.



17.36 An experimental arrangement for isotope separation. The dye laser, which is pumped by a copper-vapour laser, photoionizes the U atoms selectively according to their mass, and the ions are deflected by the electric field applied between the plates.

The large number of photons in an incident beam generated by a laser gives rise to a qualitatively different branch of spectroscopy, for the photon density is so high that more than one photon may be absorbed by a single molecule and give rise to multiphoton processes. One application of multiphoton processes is that states inaccessible by conventional one-photon spectroscopy become observable because the overall transition occurs with no change of parity. For example, in one-photon spectroscopy, only $g \leftrightarrow u$ transitions are observable; in two-photon spectroscopy, however, the overall outcome of absorbing two photons is a $g \rightarrow g$ or a $u \rightarrow u$ transition.

High powers and monochromatic beams make possible the technique of saturation spectroscopy, which permits the very precise location of absorption maxima. As illustrated in Fig. 17.34, the output of a tunable laser is divided into an intense saturating beam and a less intense probe beam that pass through the sample cavity in nearly opposite directions. The chopped saturating beam periodically excites molecules that are Doppler-shifted to its frequency. The probe beam gives a modulated signal at the detector, but only if it is interacting with the same Doppler-shifted molecules despite the fact that it is coming from an opposite direction. Because those molecules must be ones that are not moving parallel to the beams, the technique selects molecules that have essentially zero Doppler shift and hence gives very high resolution.

(b) Collimated beams

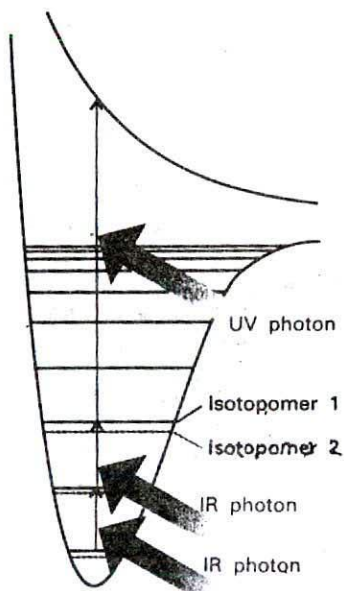
The collimated beams generated by most kinds of lasers permit the use of very long path lengths through spectroscopic samples. A well-defined beam also implies that the detector can be designed to collect only the radiation that has passed through a sample, and can be screened much more effectively against stray scattered light. Moreover, with a collimated beam, the interaction zone in Raman spectroscopy is much more well-defined than in conventional spectroscopy, so the optics of the spectrometer can be optimized.

The availability of nondivergent beams makes possible a qualitatively different kind of spectroscopy. The beam is so well-defined that it is possible to observe Raman transitions very close to the direction of propagation of the incident beam (rather than perpendicular to it). This configuration is employed in the technique called *stimulated Raman spectroscopy*. In this form of spectroscopy, the Stokes and anti-Stokes radiation in the forward direction are powerful enough to undergo more scattering and hence give up or acquire more quanta of energy from the molecules in the sample. This multiple scattering results in lines of frequency $\nu_i \pm 2\nu_M$, $\nu_i \pm 3\nu_M$, and so on, where ν_i is the frequency of the incident radiation and ν_M the frequency of a molecular excitation.

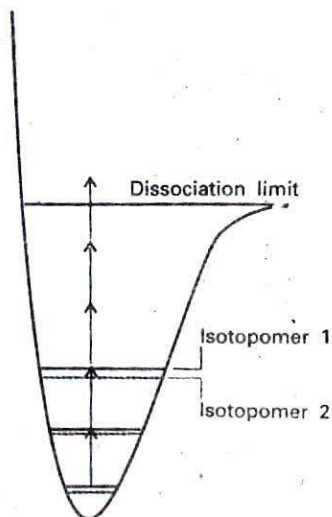
Raman spectroscopy was revitalized by the introduction of lasers. We have already commented on the enhancements of the technique that stem from the high powers and collimation of the incident beam. Its monochromaticity is also a great advantage, for it is now possible to observe scattered light that differs by only fractions of reciprocal centimetres from the incident radiation. Such high resolution is particularly useful for observing the rotational structure of Raman lines because rotational transitions are of the order of a few reciprocal centimetres. Monochromaticity also allows observations to be made very close to absorption frequencies, giving rise to the technique of resonance Raman spectroscopy (Section 16.16c). Modern, small, and efficient semiconductor lasers have also allowed the development of Fourier transform Raman spectrometers.

(c) Precision-specified transitions

The monochromatic character of laser radiation is a very powerful characteristic because it allows us to excite specific states with very high precision. One consequence of state-specificity for photochemistry is that the illumination of a sample may be photochemically

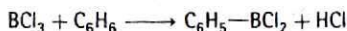


17.37 Isotopomers may be separated by making use of their selective absorption of infrared photons followed by photodissociation with an ultraviolet photon.



17.38 In an alternative scheme for separating isotopomers, multiphoton absorption of infrared photons is used to reach the dissociation limit of a ground electronic state.

precise and hence efficient in stimulating a reaction, because its frequency can be tuned exactly to an absorption. The specific excitation of a particular excited state of a molecule may greatly enhance the rate of a reaction even at low temperatures. The rate of a reaction is generally increased by raising the temperature because the energies of the various modes of motion of the molecule are enhanced. However, this enhancement increases the energy of all the modes, even those that do not contribute appreciably to the reaction rate. With a laser we can excite the kinetically significant mode, so rate enhancement is achieved most efficiently. An example is the reaction



which normally proceeds only above 600°C in the presence of a catalyst; exposure to $10.6\ \mu\text{m}$ CO_2 laser radiation results in the formation of products at room temperature without a catalyst. The commercial potential of this procedure is considerable (provided laser photons can be produced sufficiently cheaply), because heat-sensitive compounds, such as pharmaceuticals, may perhaps be made at lower temperatures than in conventional reactions.

A related application is the study of state-to-state reaction dynamics, in which a specific state of a reactant molecule is excited and we monitor not only the rate at which it forms products but also the states in which they are produced. Studies such as these give highly detailed information about the deployment of energy in chemical reactions (Chapter 27).

(d) Isotope separation

The precision state-selectivity of lasers is also of considerable potential for laser isotope separation. Isotope separation is possible because two isotopomers, or species that differ only in their isotopic composition, have slightly different energy levels and hence slightly different absorption frequencies.

One approach is to use photoionization, the ejection of an electron by the absorption of electromagnetic radiation. Direct photoionization by the absorption of a single photon does not distinguish between isotopomers because the upper level belongs to a continuum; to distinguish isotopomers it is necessary to deal with discrete states. At least two absorption processes are required. In the first step, a photon excites an atom to a higher state; in the second step, a photon achieves photoionization from that state (Fig. 17.35). The energy separation between the two states involved in the first step depends on the nuclear mass. Therefore, if the laser radiation is tuned to the appropriate frequency, only one of the isotopomers will undergo excitation and hence be available for photoionization in the second step. An example of this procedure is the photoionization of uranium vapour, in which the incident laser is tuned to excite ^{235}U but not ^{238}U . The ^{235}U atoms in the atomic beam are ionized in the two-step process; they are then attracted to a negative electrode, and may be collected (Fig. 17.36). This procedure is being used in the latest generation of uranium separation plants.

Molecular isotopomers are used in techniques based on photodissociation, the fragmentation of a molecule following absorption of electromagnetic radiation. The key problem is to achieve both mass selectivity (which requires excitation to take place between discrete states) and dissociation (which requires excitation to continuum states). In one approach, two lasers are used: an infrared photon excites one isotopomer selectively to a higher vibrational level, and then an ultraviolet photon completes the process of photodissociation (Fig. 17.37). An alternative procedure is to make use of multiphoton absorption within the ground electronic state (Fig. 17.38); the efficiency of absorption of the first few photons depends on the match of their frequency to the energy level separations, so it is sensitive to nuclear mass. The absorbed photons open the door to a

subsequent influx of enough photons to complete the dissociation process. The isotopomers $^{32}\text{SF}_6$ and $^{34}\text{SF}_6$ have been separated in this way.

In a third approach, a selectively vibrationally excited species may react with another species and give rise to products that can be separated chemically. This procedure has been employed successfully to separate isotopes of B, N, O, and, most efficiently, H. A variation on this procedure is to achieve selective photoisomerization, the conversion of a species to one of its isomers (particularly a geometrical isomer) on absorption of electromagnetic radiation. Once again, the initial absorption, which is isotope selective, opens the way to subsequent further absorption and the formation of a geometrical isomer that can be separated chemically. The approach has been used with the photoisomerization of CH_3NC to CH_3CN .

A different, more physical approach, that of **photodeflection**, is based on the recoil that occurs when a photon is absorbed by an atom and the linear momentum of the photon (which is equal to h/λ) is transferred to the atom. The atom is deflected from its original path only if the absorption actually occurs, and the incident radiation can be tuned to a particular isotope. The deflection is very small, so an atom must absorb dozens of photons before its path is changed sufficiently to allow collection. For instance, if a Ba atom absorbs about 50 photons of 550 nm light, it will be deflected by only about 1 mm after a flight of 1 m.

(e) Pulse techniques

The ability of lasers to produce pulses of very short duration is particularly useful in chemistry when we want to monitor processes in time. Q-switched lasers produce nanosecond pulses, which are generally fast enough to study reactions with rates controlled by the speed with which reactants can move through a fluid medium. However, when we want to study the rates at which energy is converted from one mode to another within a molecule, we need the shorter timescale of picosecond pulses. These timescales are available from mode-locked lasers, and modern techniques have reduced timescales of pulses to the femtosecond region ($1 \text{ fs} = 10^{-15} \text{ s}$), the shortest pulse currently reported being about 6 fs, corresponding to a packet of electromagnetic radiation of only a few wavelengths long. We shall see some of the information obtained from this femtosecond spectroscopy in Section 27.5f. Pulse techniques are used to study ultrafast dynamical processes such as energy transfer and conversion from one mode of motion to another. They are used to study relaxation of a disturbed set of level populations to thermal equilibrium, and, of particular importance in chemistry, to study the rates of fast reactions.

Photoelectron spectroscopy

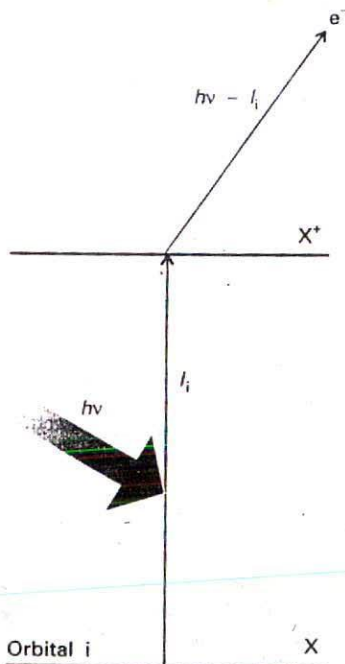
The technique of **photoelectron spectroscopy** (PES) measures the ionization energies of molecules when electrons are ejected from different orbitals, and uses the information to infer the orbital energies. The technique is also used to study solids, and in Chapter 28 we shall see the important information that it gives about species at or on surfaces.

17.8 The technique

Because energy is conserved when a photon ionizes a sample, the energy of the incident photon $h\nu$ must be equal to the sum of the ionization energy, I , of the sample and the kinetic energy of the photoelectron, the ejected electron (Fig. 17.39):

$$h\nu = \frac{1}{2}m_e v^2 + I \quad (6)$$

This equation (which is like the one used for the photoelectric effect, Section 11.2a) can be refined in two ways. First, photoelectrons may originate from one of a number of different



17.39 An incoming photon carries an energy $h\nu$; an energy I_i is needed to remove an electron from an orbital i , and the difference appears as the kinetic energy of the electron.

orbitals, and each one has a different ionization energy. Hence, a series of different kinetic energies of the photoelectrons will be obtained, each one satisfying

$$h\nu = \frac{1}{2}m_e v^2 + I_i \quad (7)$$

where I_i is the ionization energy for ejection of an electron from an orbital i . Therefore, by measuring the kinetic energies of the photoelectrons, and knowing ν , these ionization energies can be determined. Photoelectron spectra are interpreted in terms of an approximation called Koopmans' theorem, which states that the ionization energy I_i is equal to the orbital energy of the ejected electron (formally: $I_i = -\epsilon_i$). That is, we can identify the ionization energy with the energy of the orbital from which it is ejected. The theorem is only an approximation because it ignores the fact that the remaining electrons adjust their distributions when ionization occurs.

The ejection of an electron may leave an ion in a vibrationally excited state. Then not all the excess energy of the photon appears as kinetic energy of the photoelectron, and we should write

$$h\nu = \frac{1}{2}m_e v^2 + I_i + E_{\text{vib}}^+ \quad (8)$$

where E_{vib}^+ is the energy used to excite the ion into vibration. Each vibrational quantum that is excited leads to a different kinetic energy of the photoelectron, and gives rise to the vibrational structure in the photoelectron spectrum.

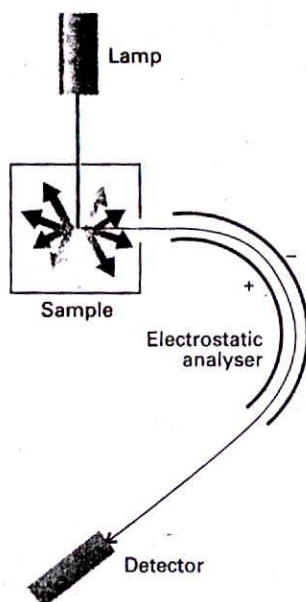
The ionization energies of molecules are several electronvolts even for valence electrons, so it is essential to work in at least the ultraviolet region of the spectrum and with wavelengths of less than about 200 nm. Much work has been done with radiation generated by a discharge through helium: the He(I) line ($1s^1 2p^1 \rightarrow 1s^2$) lies at 58.43 nm, corresponding to a photon energy of 21.22 eV. Its use gives rise to the technique of ultraviolet photoelectron spectroscopy (UPS). When core electrons are being studied, photons of even higher energy are needed to expel them: X-rays are used, and the technique is denoted XPS. A modern version of PES makes use of synchrotron radiation (Section 16.1) which may be continuously tuned between UV and X-ray energies. The additional information that stems from the variation of the photoejection probability with wavelength is a valuable guide to the identity of the molecule and the orbital from which photoionization occurs.

Illustration

Photoelectrons ejected from N_2 with He(I) radiation had kinetic energies of 5.63 eV ($1 \text{ eV} = 8065.5 \text{ cm}^{-1}$). Helium(I) radiation of wavelength 58.43 nm has wavenumber $1.711 \times 10^5 \text{ cm}^{-1}$ and therefore corresponds to an energy of 21.22 eV. Then, from eqn 7, $21.22 \text{ eV} = 5.63 \text{ eV} + I_i$, so $I_i = 15.59 \text{ eV}$. This ionization energy is the energy needed to remove an electron from the HOMO of the N_2 molecule, the $3\sigma_g$ bonding orbital (see Fig. 14.29).

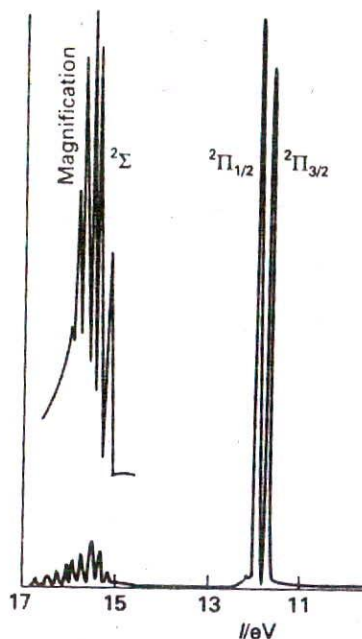
Self-test 17.4 Under the same circumstances, photoelectrons are also detected at 4.53 eV. To what ionization energy does that correspond? Suggest an origin.

[16.7 eV, $1\pi_u$]



17.40 A photoelectron spectrometer consists of a source of ionizing radiation (such as a helium discharge lamp for UPS and an X-ray source for XPS), an electrostatic analyser, and an electron detector. The deflection of the electron path caused by the analyser depends on the speed at which they are ejected from the sample.

The kinetic energies of the photoelectrons are measured using an electrostatic deflector which produces different deflections in the paths of the photoelectrons as they pass between charged plates (Fig. 17.40). As the field strength is increased, electrons of different speeds, and therefore kinetic energies, reach the detector. The electron flux can be recorded and plotted against kinetic energy to obtain the photoelectron spectrum.



17.41 The photoelectron spectrum of HBr. The lowest ionization energy bands (Π) correspond to the ionization of a Br lone-pair electron. The higher ionization energy band (Σ) corresponds to the ionization of a bonding electron. The structure on the latter is due to the vibrational excitation of HBr^+ that results from the ionization.

17.9 Ultraviolet photoelectron spectroscopy

A typical photoelectron spectrum (of HBr) is shown in Fig. 17.41. If we disregard the fine structure, we see that the HBr lines fall into two main groups. The least tightly bound electrons (with the lowest ionization energies and hence highest kinetic energies when ejected) are those in the nonbonding lone pairs of Br (with $I = 11.8$ eV). The next ionization energy lies at 15.2 eV, and corresponds to the removal of an electron from the H–Br σ bond.

The HBr spectrum shows that ejection of a σ electron is accompanied by a long vibrational progression. The Franck–Condon principle would account for this progression if ejection were accompanied by an appreciable change of equilibrium bond length between HBr and HBr^+ because the ion is formed in a bond-compressed state, which is consistent with the important bonding effect of the σ electrons. The lack of much vibrational structure in the two bands labelled ${}^2\Pi$ is consistent with the nonbonding role of the Br $2p\pi$ lone pair of electrons, for the equilibrium bond length is little changed when one is removed.

Example 17.4 Interpreting a UV photoelectron spectrum

The highest kinetic-energy electrons in the spectrum of H_2O using 21.22 eV He radiation are at about 9 eV and show a large vibrational spacing of 0.41 eV. The symmetric stretching mode of the neutral H_2O molecule lies at 3652 cm^{-1} . What conclusions can be drawn from the nature of the orbital from which the electron is ejected?

Method We need to interpret the vibrational fine structure, which indicates the vibrational characteristics of the ion, in relation to the information about the vibrational characteristics of the neutral molecule.

Answer Because 0.41 eV corresponds to 3310 cm^{-1} , which is similar to the 3652 cm^{-1} of the nonionized molecule, we can suspect that the electron is ejected from an orbital that has little influence on the bonding in the molecule. That is, photoejection is from a largely nonbonding orbital.

Self-test 17.5 In the same spectrum of H_2O , the band near 7.0 eV shows a long vibrational series with spacing 0.125 eV. The bending mode of H_2O lies at 1596 cm^{-1} . What conclusions can you draw about the characteristics of the orbital occupied by the photoelectron?

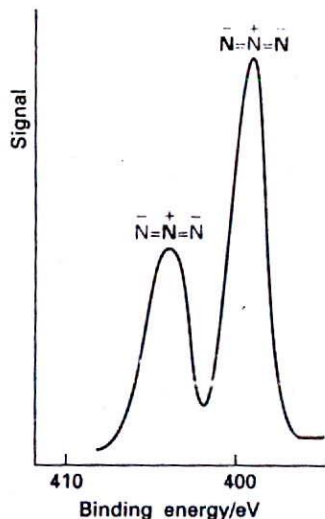
[The electron contributed to non-neighbour H–H bonding]

17.10 X-ray photoelectron spectroscopy

In XPS, the energy of the incident photon is so great that electrons are ejected from inner cores of atoms. As a first approximation, core ionization energies are insensitive to the bonds between atoms because they are too tightly bound to be greatly affected by the changes that accompany bond formation, so core ionization energies are characteristic of the individual atom rather than the overall molecule. Consequently, XPS gives lines characteristic of the elements present in a compound or alloy. For instance, the K -shell ionization energies of the second row elements are

Li	Be	B	C	N	O	F
50	110	190	280	400	530	690 eV

Detection of one of these values (and values corresponding to ejection from other inner shells) indicates the presence of the corresponding element. This application is responsible



17.42 The photoelectron spectrum of solid NaN_3 , excited by Al K -radiation, showing the region of N core ionization and the assignment. (K. Siegbahn, et al., *Science*, 176, 245 (1972).)

for the alternative name electron spectroscopy for chemical analysis (ESCA). The technique is mainly limited to the study of surface layers (as we explore in Chapter 28) because, even though X-rays may penetrate into the bulk sample, the ejected electrons cannot escape except from within a few nanometres of the surface. Despite (or because of) this limitation, the technique is very useful for studying the surface state of heterogeneous catalysts, the differences between surface and bulk structures, and the processes that can cause damage to high-temperature superconductors and semiconductor wafers.

Whereas it is largely true that core ionization energies are unaffected by bond formation, it is not entirely true, and small but detectable shifts can be detected and interpreted in terms of the environments of the atoms. For example, the azide ion, N_3^- , gives the spectrum shown in Fig. 17.42. Although the spectrum lies in the region of 400 eV (and hence is typical of $\text{N}1s$ electrons), it has a doublet structure with splitting 6 eV. This splitting can be understood by noting that the structure of the ion is $\text{N}=\text{N}=\text{N}$, with more negative charge on the outer two N atoms than on the inner (the formal charges are $(-1, +1, -1)$). The presence of the negative charges on the terminal atoms lowers the core ionization energies, whereas the positive charge on the central atom raises it. This inequivalence of the atoms results in two lines in the spectrum with intensities in the ratio 2 : 1. Observations like this can be used to obtain valuable information about the presence of chemically inequivalent atoms of the same element.

Checklist of key ideas

The characteristics of electronic transitions

17.1 The vibrational structure

- Franck–Condon principle
- vertical transition
- vibrational progression
- Franck–Condon factor

17.2 Specific types of transitions

- chromophore
- ligand-field splitting parameter
- Laporte selection rule
- vibronic transition
- charge-transfer transition
- ligand-to-metal charge-transfer transition (LMCT)
- metal-to-ligand charge-transfer transition (MLCT)

The fates of electronically excited states

- radiative decay process
- nonradiative decay

17.3 Fluorescence and phosphorescence

- fluorescence
- phosphorescence
- intersystem crossing
- Jablonski diagram

17.4 Dissociation and predissociation

- dissociation
- dissociation limit
- predissociation
- internal conversion

Lasers

17.5 General principles of laser action

- metastable excited state
- population inversion
- three-level laser
- pumping
- four-level laser
- resonant modes
- coherent radiation
- spatial coherence
- temporal coherence

- coherence length
- Q-switching
- saturable dye
- mode locking
- gain

17.6 Practical lasers

- solid-state laser
- neodymium laser
- frequency doubling
- helium–neon laser
- argon-ion laser
- krypton-ion laser
- carbon dioxide laser
- nitrogen laser
- superradiant
- exciplex laser
- exciplex
- dye laser
- p–n junction
- light-emitting diode

17.7 Applications of lasers in chemistry

- multiphoton processes
- saturation spectroscopy

- stimulated Raman spectroscopy
- state-to-state reaction dynamics
- photoionization
- photodissociation
- photoisomerization
- photodeflection

Photoelectron spectroscopy

- photoelectron spectroscopy (PES)

17.8 The technique

- photoelectron
- Koopmans' theorem
- ultraviolet photoelectron spectroscopy (UPS)

17.9 Ultraviolet photoelectron spectroscopy

17.10 X-ray photoelectron spectroscopy

- electron spectroscopy for chemical analysis (ESCA)

Further reading

Articles of general interest

- R.B. Snadden, The iodine spectrum revisited. *J. Chem. Educ.* **64**, 919 (1987).
- M. Allan, Electron spectroscopic techniques in teaching. *J. Chem. Educ.* **64**, 418 (1987).
- F. Ahmed, A good example of the Franck-Condon principle. *J. Chem. Educ.* **64**, 427 (1987).
- M.G.D. Baumann, J.C. Wright, A.B. Ellis, T. Kuech, and G.C. Lisesnky, Diode lasers. *J. Chem. Educ.* **69**, 89 (1992).
- B.J. Duke and B. O'Leary, Non-Koopmans' molecules. *J. Chem. Educ.* **72**, 501 (1995).
- P. Engelking, Laser photochemistry. In *Encyclopedia of applied physics* (ed. G.L. Trigg), **8**, 283. VCH, New York (1994).
- P.L. Kelley and J.J. Zayhowski, Laser physics. In *Encyclopedia of applied physics* (ed. G.L. Trigg), **8**, 299. VCH, New York (1994).
- H. Takuma, Laser technology. In *Encyclopedia of applied physics* (ed. G.L. Trigg), **8**, 321. VCH, New York (1994).
- D.A. Ramsay, Molecular spectroscopy. In *Encyclopedia of applied physics* (ed. G.L. Trigg), **10**, 491. VCH, New York (1994).
- F.J. Himpell and I. Lindau, Photoemission and photoelectron spectra. In *Encyclopedia of applied physics* (ed. G.L. Trigg), **13**, 477. VCH, New York (1995).
- R. Drago, *Physical methods for chemists*. Saunders, Philadelphia (1992).
- G. Herzberg, *Spectra of diatomic molecules*. Van Nostrand, New York (1950).
- G. Herzberg, *Electronic spectra and electronic structure of polyatomic molecules*. Van Nostrand, New York (1966).
- A.G. Gaydon, *Dissociation energies*. Chapman & Hall, London (1968).
- R.P. Wayne, *Principles and applications of photochemistry*. Oxford University Press (1988).
- D.L. Andrews, *Lasers in chemistry*. Springer-Verlag, Berlin (1990).
- D.L. Andrews, *An introduction to laser spectroscopy*. Plenum, New York (1995).
- A.E. Siegman, *Lasers*. University Science Books, Mill Valley (1988).
- W. Demtröder, *Laser spectroscopy*. Springer, Berlin (1988).
- A.B. Myers and T.R. Rizzo (ed.), *Techniques in chemistry XXIII: laser techniques in chemistry*. Wiley, New York (1995).
- G.R. Fleming, *Chemical applications of ultrafast spectroscopy*. Oxford University Press (1986).
- J.H.D. Eland, *Photoelectron spectra*. Butterworth, London (1984).
- T.L. Barr, *Modern ESCA: the principles and practice of x-ray photoelectron spectroscopy*. CRC Press, Boca Raton (1994).
- C.R. Brundle and A.D. Baker (ed.), *Electron spectroscopy: theory, techniques, and applications*, Vols 1-4. Academic Press, London (1977-81).

Texts and sources of data and information

- J.M. Hollas, *Modern spectroscopy*. Wiley, New York (1996).
- J.M. Hollas, *High resolution spectroscopy*. Butterworth, London (1982).
- E.A.V. Ebsworth, D.W.H. Rankin, and S. Cradock, *Structural methods in inorganic chemistry*. Blackwell Scientific, Oxford (1991).

Exercises

- 17.1 (a)** The molar absorption coefficient of a substance dissolved in hexane is known to be $855 \text{ L mol}^{-1} \text{ cm}^{-1}$ at 270 nm. Calculate the percentage reduction in intensity when light of that wavelength passes through 2.5 mm of a solution of concentration 3.25 mmol L^{-1} .
- 17.1 (b)** The molar absorption coefficient of a substance dissolved in hexane is known to be $327 \text{ L mol}^{-1} \text{ cm}^{-1}$ at 300 nm. Calculate the percentage reduction in intensity when light of that wavelength passes through 1.50 mm of a solution of concentration 2.22 mmol L^{-1} .
- 17.2 (a)** A solution of an unknown component of a biological sample when placed in an absorption cell of path length 1.00 cm transmits 20.1 per cent of light of 340 nm incident upon it. If the concentration of the component is $1.11 \times 10^{-4} \text{ mol L}^{-1}$, what is the molar absorption coefficient?
- 17.2 (b)** When light of wavelength 400 nm passes through 3.5 mm of a solution of an absorbing substance at a concentration $6.67 \times 10^{-4} \text{ mol L}^{-1}$, the transmission is 65.5 per cent. Calculate the molar absorption coefficient of the solute at this wavelength and express the answer in $\text{cm}^2 \text{ mol}^{-1}$.

17.3 (a) The molar absorption coefficient of a solute at 540 nm is $286 \text{ L mol}^{-1} \text{ cm}^{-1}$. When light of that wavelength passes through a 6.5 mm cell containing a solution of the solute, 46.5 per cent of the light was absorbed. What is the concentration of the solution?

17.3 (b) The molar absorption coefficient of a solute at 440 nm is $323 \text{ L mol}^{-1} \text{ cm}^{-1}$. When light of that wavelength passes through a 7.50 mm cell containing a solution of the solute, 52.3 per cent of the light was absorbed. What is the concentration of the solution?

17.4 (a) The absorption associated with a particular transition begins at 230 nm, peaks sharply at 260 nm, and ends at 290 nm. The maximum value of the molar absorption coefficient is $1.21 \times 10^4 \text{ L mol}^{-1} \text{ cm}^{-1}$. Estimate the integrated absorption coefficient of the transition assuming a triangular lineshape (see eqn 16.11).

17.4 (b) The absorption associated with a certain transition begins at 199 nm, peaks sharply at 220 nm, and ends at 275 nm. The maximum value of the molar absorption coefficient is $2.25 \times 10^4 \text{ L mol}^{-1} \text{ cm}^{-1}$. Estimate the integrated absorption coefficient of the transition assuming an inverted parabolic lineshape (Fig. 17.43; use eqn 16.11).

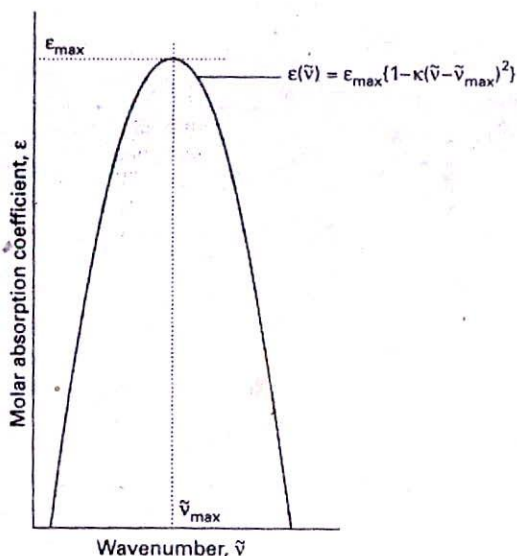


Fig. 17.43

17.5 (a) The two compounds 2,3-dimethyl-2-butene and 2,5-dimethyl-2,4-hexadiene are to be distinguished by their ultraviolet absorption spectra. The maximum absorption in one compound occurs at 192 nm and in the other at 243 nm. Match the maxima to the compounds and justify the assignment.

17.5 (b) 1,3,5-hexatriene (a kind of 'linear' benzene) was converted into benzene itself. On the basis of a free-electron molecular orbital model (in which hexatriene is treated as a linear box and benzene as a

ring), would you expect the lowest energy absorption to rise or fall in energy?

17.6 (a) The following data were obtained for the absorption by Br_2 in carbon tetrachloride using a 2.0 mm cell. Calculate the molar absorption coefficient of bromine at the wavelength employed:

$[\text{Br}_2]/(\text{mol L}^{-1})$	0.0010	0.0050	0.0100	0.0500
$T/(\text{per cent})$	81.4	35.6	12.7	3.0×10^{-3}

17.6 (b) The following data were obtained for the absorption by a dye dissolved in methylbenzene using a 2.50 mm cell. Calculate the molar absorption coefficient of the dye at the wavelength employed:

$[\text{dye}]/(\text{mol L}^{-1})$	0.0010	0.0050	0.0100	0.0500
$T/(\text{per cent})$	73	21	4.2	1.33×10^{-5}

17.7 (a) A 2.0 mm cell was filled with a solution of benzene in a non-absorbing solvent. The concentration of the benzene was 0.010 mol L^{-1} and the wavelength of the radiation was 256 nm (where there is a maximum in the absorption). Calculate the molar absorption coefficient of benzene at this wavelength given that the transmission was 48 per cent. What will the transmittance be in a 4.0 mm cell at the same wavelength?

17.7 (b) A 2.50 mm cell was filled with a solution of a dye. The concentration of the dye was $0.0155 \text{ mol L}^{-1}$. Calculate the molar absorption coefficient of dye at this wavelength given that the transmission was 32 per cent. What will the transmittance be in a 4.50 mm cell at the same wavelength?

17.8 (a) A swimmer enters a gloomier world (in one sense) on diving to greater depths. Given that the mean molar absorption coefficient of sea water in the visible region is $6.2 \times 10^{-5} \text{ L mol}^{-1} \text{ cm}^{-1}$, calculate the depth at which a diver will experience (a) half the surface intensity of light, (b) one-tenth the surface intensity.

17.8 (b) Given that the maximum molar absorption coefficient of a molecule containing a carbonyl group at a concentration of 1.00 mol L^{-1} is $30 \text{ L mol}^{-1} \text{ cm}^{-1}$ near 280 nm, calculate the thickness of a sample that will result in (a) half the initial intensity of radiation, (b) one-tenth the initial intensity.

17.9 (a) The electronic absorption bands of many molecules in solution have half-widths at half-height of about 5000 cm^{-1} . Estimate the integrated absorption coefficients of bands for which (a) $\epsilon_{\text{max}} \approx 1 \times 10^4 \text{ L mol}^{-1} \text{ cm}^{-1}$, (b) $\epsilon_{\text{max}} \approx 5 \times 10^2 \text{ L mol}^{-1} \text{ cm}^{-1}$.

17.9 (b) The electronic absorption band of a compound in solution had a Gaussian lineshape and a half-width at half-height of 4233 cm^{-1} and $\epsilon_{\text{max}} = 1.54 \times 10^4 \text{ L mol}^{-1} \text{ cm}^{-1}$. Estimate the integrated absorption coefficient.

17.10 (a) The photoionization of H_2 by 21 eV photons produces H_2^+ . Explain why the intensity of the $\nu = 2 \leftarrow 0$ transition is stronger than that of the $0 \leftarrow 0$ transition.

17.10 (b) The photoionization of F_2 by 21 eV photons produces F_2^+ . Would you expect the $2 \leftarrow 0$ transition to be weaker or stronger than that of the $0 \leftarrow 0$ transition? Justify your answer.

Problems

Numerical problems

17.1 The vibrational wavenumber of the oxygen molecule in its electronic ground state is 1580 cm^{-1} , whereas that in the first excited state ($B^3\Sigma_u^-$) to which there is an allowed electronic transition is 700 cm^{-1} . If the separation in energy between the minima in their respective potential energy curves of these two electronic states is 6.175 eV , what is the wavenumber of the lowest energy transition in the band of transitions originating from the $v = 0$ vibrational state of the electronic ground state to this excited state? Ignore any rotational structure or anharmonicity.

17.2 A Birge-Sponer extrapolation yields 7760 cm^{-1} as the area under the curve for the B state of the oxygen molecule described in Problem 17.1. Given that the B state dissociates to ground-state atoms (at zero energy, 3P) and $15\,870\text{ cm}^{-1}$ (1D) and the lowest vibrational state of the B state is $49\,363\text{ cm}^{-1}$ above the lowest vibrational state of the ground electronic state, calculate the dissociation energy of the molecular ground state to the ground-state atoms.

17.3 The electronic spectrum of the IBr molecule shows two low-lying, well defined convergence limits at $14\,660$ and $18\,345\text{ cm}^{-1}$. Energy levels for the iodine and bromine atoms occur at $0,7598\text{ cm}^{-1}$; and $0,3685\text{ cm}^{-1}$, respectively. Other atomic levels are at much higher energies. What possibilities exist for the numerical value of the dissociation energy of IBr? Decide which is the correct possibility by calculating this quantity from $\Delta_f H^\ominus(\text{IBr}, g) = +40.79\text{ kJ mol}^{-1}$ and the dissociation energies of $\text{I}_2(g)$ and $\text{Br}_2(g)$ which are 146 and 190 kJ mol^{-1} , respectively.

17.4 In many cases it is possible to assume that an absorption band has a Gaussian lineshape (one proportional to e^{-x^2}) centred on the band maximum. Assume such a lineshape, and show that $A \approx 1.0645 \epsilon_{\text{max}} \Delta \bar{\nu}_{1/2}$, where $\Delta \bar{\nu}_{1/2}$ is the width at half-height. The absorption spectrum of azoethane ($\text{CH}_3\text{CH}_2\text{N}_2$) between $24\,000\text{ cm}^{-1}$ and $34\,000\text{ cm}^{-1}$ is shown in Fig. 17.44. First, estimate A for the band

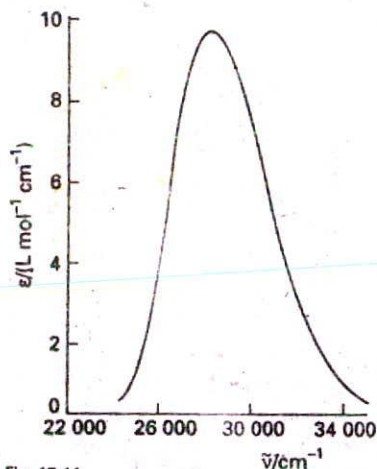


Fig. 17.44

by assuming that it is Gaussian. Then integrate the absorption band graphically. The latter can be done either by ruling and counting squares, or by tracing the lineshape on to paper and weighing. A more sophisticated procedure would be to use mathematical software to fit a polynomial to the absorption band (or a Gaussian), and then to integrate the result analytically.

17.5 A lot of information about the energy levels and wavefunctions of small inorganic molecules can be obtained from their ultraviolet spectra. An example of a spectrum with considerable vibrational structure, that of gaseous SO_2 at 25°C , is shown in Fig. 17.45. Estimate the integrated absorption coefficient for the transition. What electronic states are accessible from the A_1 ground state of this C_{2v} molecule by electric dipole transitions?

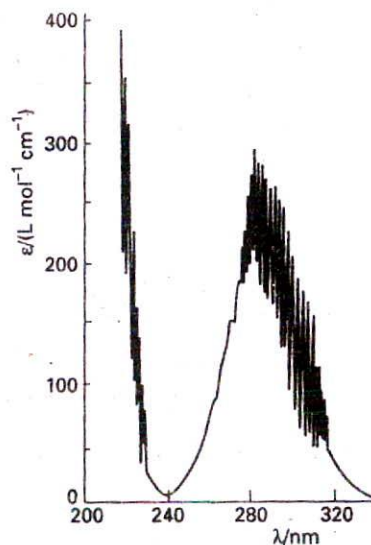


Fig. 17.45

17.6 A certain molecule fluoresces at a wavelength of 400 nm with a half-life of 1.0 ns . It phosphoresces at 500 nm . If the ratio of the transition probabilities for stimulated emission for the $S^* \rightarrow S$ to the $T \rightarrow S$ transitions is 1.0×10^5 , what is the half-life of the phosphorescent state?

17.7 The photoelectron spectra of N_2 and CO are shown in Fig. 17.46. Ascribe the lines to the ionization processes involved and classify the orbitals from which the electrons are ejected as bonding, nonbonding, or antibonding in the light of the extent of vibrational structure in the band. Analyse the bands near 4 eV in terms of the vibrational energy levels of the ions.

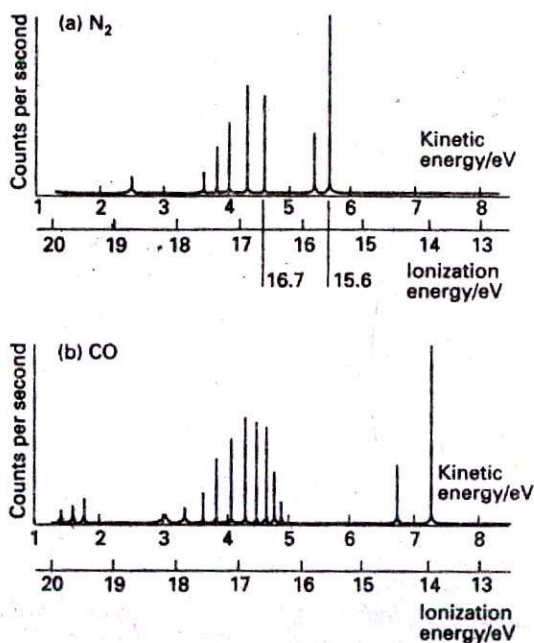


Fig. 17.46

17.8 The photoelectron spectrum of NO can be described as follows (D.W. Turner, in *Physical methods in advanced inorganic chemistry* (ed. H.A.O. Hill and P. Day), Wiley, Chichester (1968)). Using He 58.4 pm (21.21 eV) radiation there is a single strong peak at kinetic energy 4.69 eV and a long series of 24 lines starting at 5.56 eV and ending at 2.2 eV. A shorter series of six lines begins at 12.0 eV and ends at 10.7 eV. Account for this spectrum.

Theoretical problems

17.9 Assume that the electronic states of the π electrons of a conjugated molecule can be approximated by the wavefunctions of a particle in a one-dimensional box, and that the dipole moment can be related to the displacement along this length by $\mu = -ex$. Show that the transition probability connecting states 1 and 2, is nonzero, whereas that connecting states 1 and 3 is zero.

17.10 Use a group theoretical argument to decide which of the following transitions are electric-dipole allowed: (a) the $\pi^* \leftarrow \pi$ transition in ethene, (b) the $\pi^* \leftarrow n$ transition in a carbonyl group in a C_{2v} environment.

17.11 The line marked A in Fig. 17.47 is the fluorescence spectrum of benzophenone in solid solution in ethanol at low temperatures observed when the sample is illuminated with 360 nm light. What can be said about the vibrational energy levels of the carbonyl group in (a) its ground electronic state and (b) its excited electronic state? When naphthalene is illuminated with 360 nm light it does not absorb, but the line marked B in the illustration is the phosphorescence spectrum of a solid solution of a mixture of naphthalene and benzophenone in ethanol. Now a component of fluorescence from naphthalene can be detected. Account for this observation.

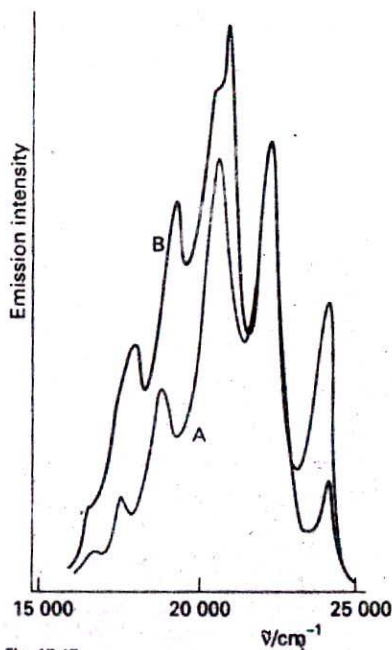


Fig. 17.47

17.12 The fluorescence spectrum of anthracene vapour shows a series of peaks of increasing intensity with individual maxima at 440 nm, 410 nm, 390 nm, and 370 nm followed by a sharp cut-off at shorter wavelengths. The absorption spectrum rises sharply from zero to a maximum at 360 nm with a trail of peaks of lessening intensity at 345 nm, 330 nm, and 305 nm. Account for these observations.

17.13 Suppose that you are a colour chemist and had been asked to intensify the colour of a dye without changing the type of compound, and that the dye in question was a polyene. Would you choose to lengthen or to shorten the chain? Would the modification to the length shift the apparent colour of the dye towards the red or the blue?

17.14 One measure of the intensity of a transition of frequency ν is the oscillator strength, f , which is defined as

$$f = \frac{8\pi^2 m_e \nu |\mu_{12}|^2}{3hc^2}$$

Consider an electron in an atom to be oscillating harmonically in one dimension (the three-dimensional version of this model was used in early attempts to describe atomic structure). The wavefunctions for such an electron are those in Table 12.1. Show that the oscillator strength for the transition of this electron from its ground state is exactly $\frac{1}{3}$.

17.15 Estimate the oscillator strength (see Problem 17.14) of a charge-transfer transition modelled as the migration of an electron from a hydrogen 1s orbital on one atom to another hydrogen 1s orbital on an atom a distance R away. Approximate the transition moment by $-eRS$ where S is the overlap integral of the two orbitals. Sketch the oscillator strength as a function of R using the curve for S given in Fig. 14.31. Why does the intensity fall to zero as R approaches 0 and infinity?

Additional problems supplied by Carmen Giunta and Charles Trapp

17.16 Refer to Fig. 17.25 and estimate the maximum laser power that can be delivered from a ruby crystal of length 5.0 cm and diameter 0.50 cm, in a pulse of duration 100 ns. 'Pink ruby' consists of about 0.050 per cent by mass Cr^{3+} and the mass density of Al_2O_3 is 3.97 g cm^{-3} . Assume that the pumping radiation is of sufficient intensity to pump all the chromium ions out of their ground state at a rate faster than they decay back to the ground state.

17.17 J.G. Dojahn, E.C.M. Chen, and W.E. Wentworth (*J. Phys. Chem.* 100, 9649 (1996)) characterized the potential energy curves of the ground and electronic states of homonuclear diatomic halogen anions. These anions have a $^2\Sigma_u^+$ ground state and $^2\Pi_g$, $^2\Pi_u$, and $^2\Sigma_g^+$ excited states. To which of the excited states are transitions by absorption of photons allowed? Explain.

17.18 M. Schwell, H.-W. Jochims, B. Wassermann, U. Rockland, R. Flesch, and E. Rühl (*J. Phys. Chem.* 100, 10070 (1996)) measured the ionization energies of Cl_2O_2 by photoelectron spectroscopy in which the ionized fragments were detected using a mass spectrometer. From their data, we can infer that the ionization enthalpy of Cl_2O_2 is 11.05 eV and the enthalpy of the dissociative ionization $\text{Cl}_2\text{O}_2 \rightarrow \text{Cl} + \text{OClO}^+ + e^-$ is 10.95 eV. They used this information to make some inferences about the structure of Cl_2O_2 . Computational studies had suggested that the lowest energy isomer is ClOOC , but that ClClO_2 (C_{2v}) and ClOClO are not very much higher in energy. The Cl_2O_2 in the photoionization step is the lowest energy isomer, whatever its structure may be, and its enthalpy of formation had previously been reported as $+133 \text{ kJ mol}^{-1}$. The Cl_2O_2 in the dissociative ionization step is unlikely to be ClOOC , for the product can be derived from it only with substantial rearrangement. Given $\Delta_f H^\ominus(\text{OClO}^+) = +1096 \text{ kJ mol}^{-1}$ and $\Delta_f H^\ominus(e^-) = 0$, determine whether the Cl_2O_2 in the dissociative ionization is the same as that in the photoionization. If different, how much greater is its $\Delta_f H^\ominus$? Are these results consistent with or contradictory to the computational studies?

17.19 G.C.G. Wachewsky, R. Horansky, and V. Vaida (*J. Phys. Chem.* 100, 11559 (1996)) examined the UV absorption spectrum of CH_3I , a species of interest in connection with stratospheric ozone chemistry. They found the integrated absorption coefficient to be dependent on temperature and pressure to an extent inconsistent with internal structural changes in isolated CH_3I molecules; they explained the changes as due to dimerization of a substantial fraction of the CH_3I , a process which would naturally be pressure- and temperature-dependent. (a) Compute the integrated absorption coefficient over a triangular lineshape in the range $31\,250$ to $34\,483 \text{ cm}^{-1}$ and a maximal molar absorption coefficient of $150 \text{ L mol}^{-1} \text{ cm}^{-1}$ at $31\,250 \text{ cm}^{-1}$. (b) Suppose 1 per cent of the CH_3I units in a sample at 2.4 Torr and 373 K exists as dimers. Compute the absorbance expected at $31\,250 \text{ cm}^{-1}$ in a sample cell of length 12.0 cm. (c) Suppose 18 per cent of the CH_3I units in a sample at 100 Torr and

373 K exists as dimers. Compute the absorbance expected at $31\,250 \text{ cm}^{-1}$ in a sample cell of length 12.0 cm; compute the molar absorption coefficient that would be inferred from this absorbance if dimerization were not considered.


17.20 The abundance of ozone is typically inferred from measurements of UV absorption and is often expressed in terms of Dobson units (DU): 1 DU is equivalent to a layer of pure ozone 10^{-3} cm thick at 1 atm and 0°C . Compute the absorbance of UV radiation at 300 nm expected for an ozone abundance of 300 DU (a typical value) and 100 DU (a value reached during seasonal Antarctic ozone depletions) given a molar absorption coefficient of $476 \text{ L mol}^{-1} \text{ cm}^{-1}$.

17.21 Ozone absorbs ultraviolet radiation in a part of the electromagnetic spectrum that is energetic enough to disrupt DNA in biological organisms and that is absorbed by no other abundant atmospheric constituent. This spectral range, denoted UV-B, spans the wavelengths of about 290 nm to 320 nm. The molar extinction coefficient of ozone over this range is given in the table below (W.B. DeMore, S.P. Sander, D.M. Golden, R.F. Hampson, M.J. Kurylo, C.J. Howard, A.R. Ravishankara, C.E. Kolb, and M.J. Molina, *Chemical kinetics and photochemical data for use in stratospheric modeling: Evaluation Number 11*, JPL Publication 94-26 (1994)).

λ/nm	292.0	296.3	300.8	305.4	310.1	315.0	320.0
$\epsilon/(\text{L mol}^{-1} \text{ cm}^{-1})$	1512	865	477	257	135.9	69.5	34.5

Compute the integrated absorption coefficient of ozone over the wavelength range 290–320 nm. (*Hint:* $\epsilon(\tilde{\nu})$ can be fitted to an exponential function quite well.)

17.22 One of the principal methods of obtaining the electronic spectra of unstable radicals is to study the spectra of comets, which consist almost entirely of radical spectra. Many radical spectra have been found in comets including that due to CN. These radicals are produced in comets by the absorption of far ultraviolet solar radiation by their parent compounds. Subsequently, their fluorescence is excited by sunlight of longer wavelength. The spectra of comet Hale-Bopp (C/1995 O1) have been the subject of many recent studies. One such study is that of the fluorescence spectrum of CN in the coma of Hale-Bopp at large heliocentric distances by R.M. Wagner and D.G. Schleicher (*Science* 275, 1918 (1997)), in which the authors determine the spatial distribution and rate of production of CN in the coma. The (0–0) vibrational band is centred on 387.6 nm and the weaker (1–1) band with relative intensity 0.1 is centred on 386.4 nm. The band heads for (0–0) and (0–1) are known to be 388.3 and 421.6 nm, respectively. From these data, calculate the energy of the excited S_1 state relative to the ground S_0 state, the vibrational wavenumbers and the difference in the vibrational wavenumbers of the two states, and the relative populations of the $v = 0$ and $v = 1$ vibrational levels of the S_1 state. Also estimate the effective temperature of the molecule in the excited S_1 state. Only eight rotational levels of the S_1 state are said to be populated. Is that statement consistent with the effective temperature of the S_1 state?



18

Spectroscopy 3: magnetic resonance

Nuclear magnetic resonance



- 18.1 Nuclear magnetic moments
- 18.2 The energies of nuclei in magnetic fields
- 18.3 The chemical shift
- 18.4 The fine structure

Pulse techniques in NMR

- 18.5 The magnetization vector
- 18.6 Linewidths and rate processes
- 18.7 The nuclear Overhauser effect
- 18.8 Two-dimensional NMR
- 18.9 Solid-state NMR

Electron spin resonance

- 18.10 The g -value
- 18.11 Hyperfine structure

Checklist of key ideas

Further reading

Exercises

Problems

One of the most widely used spectroscopic procedures in chemistry makes use of the classical concept of resonance. The chapter begins with an account of conventional nuclear magnetic resonance which shows how the resonance frequency of a magnetic nucleus is affected by its electronic environment and the presence of magnetic nuclei in its vicinity. Then we turn to the modern versions of NMR, which are based on the use of pulses of electromagnetic radiation and the processing of the resulting signal by Fourier transform techniques. The experimental techniques for electron spin resonance resemble those used in the early days of NMR. The information obtained, however, is very useful for the determination of the properties of radicals and d -metal complexes.

When two pendulums share a slightly flexible support and one is set in motion, the other is forced into oscillation by the motion of the common axle. As a result, energy flows between the two pendulums. The energy transfer occurs most efficiently when the frequencies of the two pendulums are identical. The condition of strong effective coupling when the frequencies of two oscillators are identical is called resonance.

Resonance is the basis of a number of everyday phenomena, including the response of radios to the weak oscillations of the electromagnetic field generated by a distant transmitter. In this chapter we explore some spectroscopic applications that, as originally developed (and in some cases still), depend on matching a set of energy levels to a source of monochromatic radiation and observing the strong absorption that occurs at resonance.

Nuclear magnetic resonance

The basic nuclear magnetic resonance (NMR) experiment is the resonant absorption of radiofrequency radiation by nuclei exposed to a magnetic field. Although simple in concept, NMR spectra can be highly complex; yet they have proved invaluable in chemistry, for they reveal so much structural information. A magnetic nucleus is a very sensitive, noninvasive probe of the surrounding electronic structure.

18.1 Nuclear magnetic moments

Many nuclei possess spin angular momentum. A nucleus with spin quantum number I (which is a fixed characteristic property of a nucleus and may be an integer or a half-integer but is never negative) has the following properties:

1. An angular momentum of magnitude $\{I(I+1)\}^{1/2}\hbar$.
2. A component of angular momentum $m_I\hbar$ on an arbitrary axis, where $m_I = I, I-1, \dots, -I$.
3. If $I > 0$, a magnetic moment with a constant magnitude and an orientation that is determined by the value of m_I .

To say that a nucleus has a magnetic moment means that, to some extent, it behaves like a small bar magnet.

According to the second property, the spin, and hence the magnetic moment, of the nucleus may lie in $2I+1$ different orientations relative to an axis. A proton has $I = \frac{1}{2}$ and its spin may adopt either of two orientations; a ^{14}N nucleus has $I = 1$ and its spin may adopt any of three orientations. For much of this chapter we shall consider spin- $\frac{1}{2}$ nuclei, which are nuclei with $I = \frac{1}{2}$, but NMR is applicable to nuclei with any nonzero spin. As well as protons, which are the most common nuclei studied by NMR, spin- $\frac{1}{2}$ nuclei include ^{13}C , ^{19}F , and ^{31}P nuclei. The state with $m_I = +\frac{1}{2}$ (\uparrow) is denoted α and the state with $m_I = -\frac{1}{2}$ (\downarrow) is denoted β . It is worth bearing in mind that two very common nuclei, ^{12}C and ^{16}O , have zero spin, and hence zero magnetic moment, and so are invisible in magnetic resonance.

18.2 The energies of nuclei in magnetic fields

The nuclear magnetic moment of a nucleus is denoted μ . The component of the nuclear magnetic moment on the z -axis, μ_z , is proportional to the component of spin angular momentum on that axis, $m_I\hbar$, and we write

$$\mu_z = \gamma\hbar m_I \quad (1)$$

The coefficient of proportionality γ is called the magnetogyric ratio of the nucleus, and is an experimentally determined quantity (Table 18.1). The magnetic moment is sometimes expressed in terms of the nuclear g -factor, g_I , and the nuclear magneton, μ_N , by using

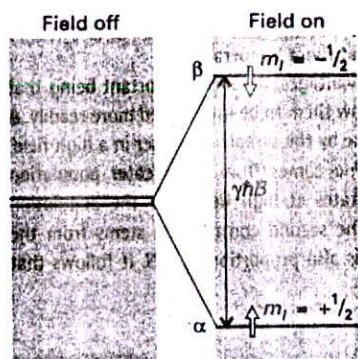
$$\gamma\hbar = g_I\mu_N \quad \mu_N = \frac{e\hbar}{2m_p} = 5.051 \times 10^{-27} \text{ J T}^{-1} \quad (2)$$

where m_p is the mass of the proton. Nuclear g -factors are numbers of the order of 1 (Table 18.1): positive values of g_I and γ denote a magnetic moment that is parallel to the spin; negative values indicate that the magnetic moment and spin are antiparallel. The nuclear magneton is about 2000 times smaller than the Bohr magneton, so nuclear magnetic moments are about 2000 times weaker than the electron spin magnetic moment.

Table 18.1* Nuclear spin properties

Nuclide	Natural abundance/%	Spin I	g -value, g_I	$\gamma/(10^7 \text{ T}^{-1} \text{ s}^{-1})$
^1n		$\frac{1}{2}$	-3.826	-18.32
^1H	99.98	$\frac{1}{2}$	5.586	26.75
^2H	0.02	1	0.857	4.10
^{13}C	1.11	$\frac{1}{2}$	1.405	6.73
^{14}N	99.64	1	0.404	1.93

*More values are given in the Data section at the end of this volume. Note that $\gamma = g_I\mu_N/\hbar$.



18.1 The nuclear spin energy levels of a spin- $\frac{1}{2}$ nucleus (for example, ^1H or ^{13}C) in a magnetic field. Resonance occurs when the energy separation of the levels matches the energy of the photons in the electromagnetic field.

(a) The basic resonance experiment

Each value of m_l corresponds to a different orientation of the nuclear spin and therefore of the nuclear magnetic moment too. In a magnetic field B in the z -direction, the $2I + 1$ orientations of the nucleus have different energies, which are given by

$$E_{m_l} = -\mu_z B = -\gamma \hbar B m_l \quad (3)$$

These energies are often expressed in terms of the Larmor frequency, ν_L :

$$E_{m_l} = -m_l h \nu_L \quad \nu_L = \frac{\gamma B}{2\pi} \quad (4)$$

The stronger the magnetic field, the higher the Larmor frequency. A field of 12 T corresponds to a Larmor frequency of about 500 MHz for protons.

The energy separation of the two states of spin- $\frac{1}{2}$ nuclei is

$$\Delta E = E_\beta - E_\alpha = \frac{1}{2}\gamma \hbar B - (-\frac{1}{2}\gamma \hbar B) = \gamma \hbar B = h \nu_L \quad (5)$$

For most nuclei γ is positive. In such cases, the β state lies above the α state, and there are slightly more α spins than β spins. When the sample is exposed to radiation of frequency ν , the energy separations come into resonance with the radiation when the frequency satisfies the resonance condition (Fig. 18.1):

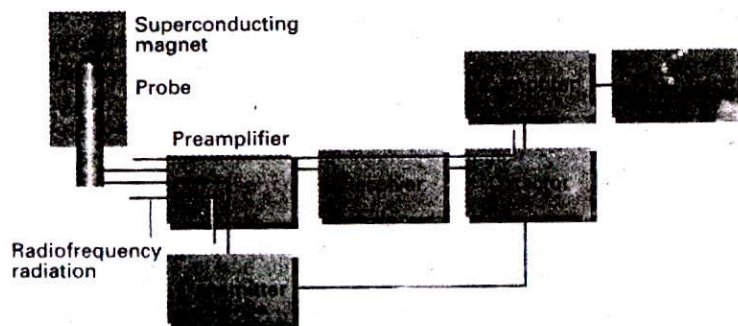
$$h\nu = \gamma \hbar B = h \nu_L \quad (6)$$

That is, there is resonance when $\nu = \nu_L$. At resonance there is strong coupling between the nuclear spins and the radiation, and strong absorption occurs as the spins make the transition $\alpha \rightarrow \beta$. At 12 T, protons come into resonance at about 500 MHz (the Larmor frequency at that magnetic field).

(b) The technique

In its simplest form, nuclear magnetic resonance (NMR) is the study of the properties of molecules containing magnetic nuclei by applying a magnetic field and observing the frequency of the resonant electromagnetic field. Larmor frequencies of nuclei at the fields normally employed typically lie in the radiofrequency region of the electromagnetic spectrum, so NMR is a radiofrequency technique.

An NMR spectrometer consists of a magnet that can produce a uniform, intense field and the appropriate sources of radiofrequency electromagnetic radiation. In simple instruments, the magnetic field is provided by a permanent magnet. For serious work, a superconducting magnet capable of producing fields of the order of 2 T and more is used (Fig. 18.2). The sample is placed in the cylindrically wound magnet. In some cases the sample is rotated rapidly to remove magnetic inhomogeneities. However, sample spinning is a source of noise,



18.2 The layout of a typical NMR spectrometer. The link from the transmitter to the detector indicates that the high frequency of the transmitter is subtracted from the high-frequency received signal to give a low-frequency signal for processing.

and is often avoided. Although a superconducting magnet operates at the temperature of liquid helium (4 K), the sample itself is normally at room temperature.

The use of high magnetic fields has several advantages, the most important being that they simplify the appearance of spectra and so allow them to be interpreted more readily. A further advantage is that the rate of energy uptake by the sample is greater in a high field. There are two contributions to this increase. One comes from the greater population difference between the upper and lower spin states at high fields, for the population difference is approximately proportional to B . The second contribution stems from the greater energy of each absorbed photon, which is also proportional to B . It follows that overall the signal is proportional to B^2 .

Justification 18.1

According to the Boltzmann distribution, the ratio of populations is

$$\frac{N_\beta}{N_\alpha} = e^{-\Delta E/kT} \approx 1 - \frac{\Delta E}{kT}$$

It follows that

$$\frac{N_\alpha - N_\beta}{N_\alpha + N_\beta} \approx \frac{\Delta E}{2kT} = \frac{\gamma\hbar B}{2kT}$$

and the population difference is proportional to B . The energy of the photon absorbed when a nucleus makes a transition from its lower state to its higher state is $h\nu$; at resonance ν is equal to ν_L , and ν_L is proportional to B . Hence, at resonance, each photon has an energy that is proportional to B . The net rate of energy absorption is proportional to the population difference multiplied by the energy of each absorption event (the photon energy), so overall the net rate is proportional to B^2 .

18.3 The chemical shift

Nuclear magnetic moments interact with the *local* magnetic field. The local field may differ from the applied field because the latter induces electronic orbital angular momentum (that is, the circulation of electronic currents) which gives rise to a small additional magnetic field δB at the nuclei. This additional field is proportional to the applied field, and it is conventional to write

$$\delta B = -\sigma B \quad (7)$$

where the dimensionless quantity σ is called the *shielding constant* of the nucleus (σ is usually positive but may be negative). The ability of the applied field to induce an electronic current in the molecule, and the strength of the resulting local magnetic field experienced by the nucleus, depend on the details of the electronic structure near the magnetic nucleus of interest, so nuclei in different chemical groups have different shielding constants. The calculation of reliable values of the shielding constant is very difficult, but trends in it are quite well understood, and we concentrate on them.

(a) The δ scale of chemical shifts

Because the total local field is

$$B_{\text{loc}} = B + \delta B = (1 - \sigma)B \quad (8)$$

the Larmor frequency is

$$\nu_L = \frac{\gamma B_{\text{loc}}}{2\pi} = (1 - \sigma) \frac{\gamma B}{2\pi} \quad (9)$$

This frequency is different for nuclei in different environments. Hence, different nuclei, even of the same element, come into resonance at different frequencies.

It is conventional to express the resonance frequencies in terms of an empirical quantity called the **chemical shift**, which is related to the difference between the resonance frequency, ν , of the nucleus in question and that of a reference standard, ν° :

$$\delta = \frac{\nu - \nu^\circ}{\nu^\circ} \times 10^6 \quad (10)$$

The standard for protons is the proton resonance in tetramethylsilane ($\text{Si}(\text{CH}_3)_4$, commonly referred to as TMS), which bristles with protons and dissolves without reaction in many liquids. Other references are used for other nuclei. For ^{13}C , the reference frequency is the ^{13}C resonance in TMS; for ^{31}P it is the ^{31}P resonance in 85 per cent $\text{H}_3\text{PO}_4(\text{aq})$. The advantage of the δ -scale is that shifts reported on it are independent of the applied field (because both numerator and denominator are proportional to the applied field).

Illustration

A nucleus with $\delta = 1.00$ (which is often, but unnecessarily, expressed as 1.00 ppm on account of the 10^6 in the definition of δ) in a spectrometer operating at 500 MHz will have a shift relative to the reference equal to

$$\nu - \nu^\circ = (500 \text{ MHz}) \times (1.00) \times 10^{-6} = 500 \text{ Hz}$$

In a spectrometer operating at 100 MHz, the shift relative to the reference would be only 100 Hz.

The relation between δ and σ is obtained by substituting eqn 8 into eqn 10:

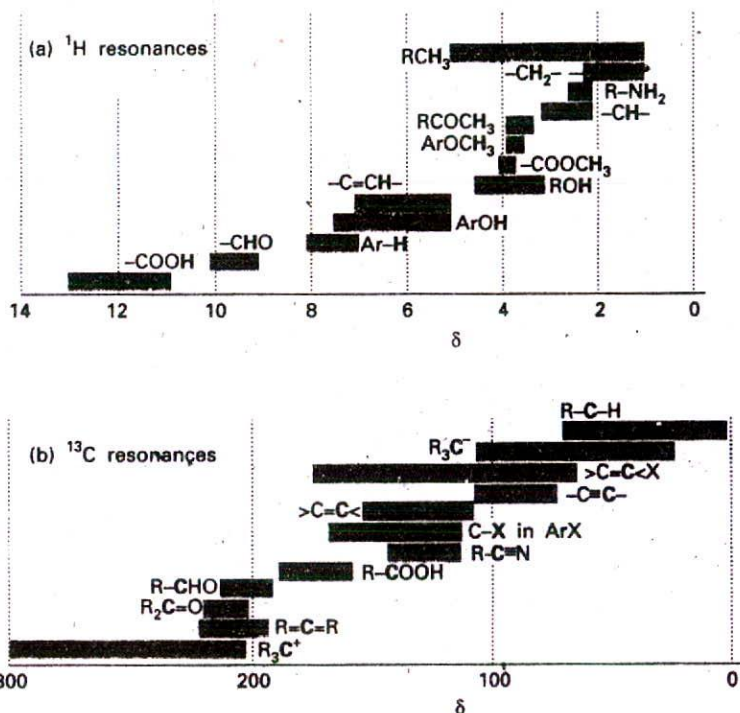
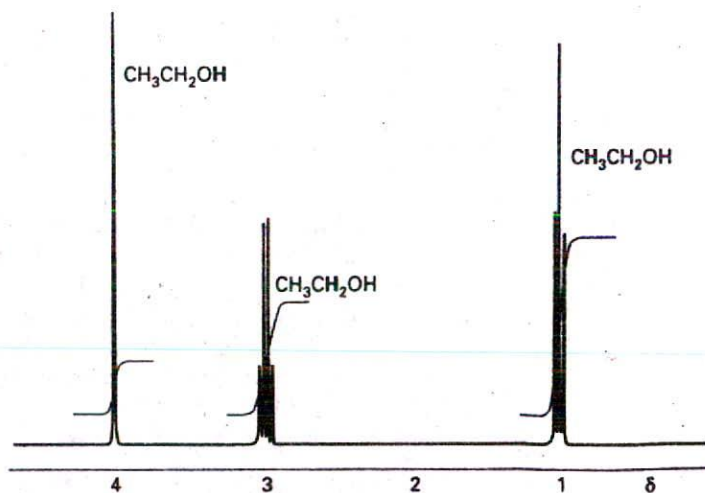
$$\begin{aligned} \delta &= \frac{(1 - \sigma)B - (1 - \sigma^\circ)B}{(1 - \sigma^\circ)B} \times 10^6 = \frac{\sigma^\circ - \sigma}{1 - \sigma^\circ} \times 10^6 \\ &\approx (\sigma^\circ - \sigma) \times 10^6 \end{aligned} \quad (11)$$

As the shielding, σ , gets smaller, δ increases. Therefore, we speak of nuclei with large chemical shift as being strongly deshielded. Some typical chemical shifts are given in Fig. 18.3. As can be seen from the illustration, the nuclei of different elements have very different ranges of chemical shifts. The ranges exhibit the variety of electronic environments of the nuclei in molecules.

By convention, NMR spectra are plotted with δ increasing from right to left. Consequently, in a given applied magnetic field the Larmor frequency also increases from right to left. In a continuous wave (CW) spectrometer, in which the radiofrequency is held constant and the magnetic field is varied (a 'field sweep experiment'), the spectrum is displayed with the applied magnetic field increasing from left to right: a nucleus with a small chemical shift experiences a relatively low local magnetic field, so it needs a higher applied magnetic field to bring it into resonance with the radiofrequency field. Consequently, the right-hand end (low chemical shift) end of the spectrum is commonly referred to as the 'high field end' of the spectrum.

(b) Resonance of different groups of nuclei

The existence of a chemical shift explains the general features of the spectrum of ethanol shown in Fig. 18.4. The CH_3 protons form one group of nuclei with $\delta \approx 1$. The two CH_2

18.3 The range of typical chemical shifts for (a) ^1H resonances and (b) ^{13}C resonances.18.4 The ^1H -NMR spectrum of ethanol. The bold letters denote the protons giving rise to the resonance peak, and the step-like curve is the integrated signal.

protons are in a different part of the molecule, experience a different local magnetic field, and resonate at $\delta \approx 3$. Finally, the OH proton is in another environment, and has a chemical shift of $\delta \approx 4$. The increasing value of δ (that is, the increase in deshielding) is consistent with the electron-withdrawing power of the O atom: it reduces the electron density of the OH proton most, and that proton is strongly deshielded. It reduces the electron density of the distant methyl protons least, and those nuclei are least deshielded.

The relative intensities of the signal (the areas under the absorption lines) can be used to help distinguish which group of lines corresponds to which chemical group. The determination of the area under an absorption line is referred to as the integration of the signal (just as any area under a curve may be determined by mathematical integration). Spectrometers can integrate the absorption automatically (as indicated in Fig. 18.4). In ethanol the group intensities are in the ratio 3 : 2 : 1 because there are three CH_3 protons, two CH_2 protons, and one OH proton in each molecule. Counting the number of magnetic nuclei as well as noting their chemical shifts helps to identify a compound present in a sample.

(c) The origin of shielding constants

The calculation of shielding constants is very difficult, even for small molecules, for it requires detailed information about the distribution of electron density in the ground and excited states and the excitation energies of the molecule. Some success has been achieved with the calculation for diatomic molecules and small polyatomic molecules such as H_2O and CH_4 , but large molecules are much more difficult. Nevertheless, a considerable body of useful empirical information about a variety of contributions to chemical shifts in large molecules has been compiled, and has been used to understand and interpret observations reasonably systematically.

The empirical approach supposes that the observed shielding constant is the sum of three contributions:

$$\sigma = \sigma(\text{local}) + \sigma(\text{neighbour}) + \sigma(\text{solvent}) \quad (12)$$

The local contribution, $\sigma(\text{local})$, is essentially the contribution of the electrons of the atom that contains the nucleus in question. The neighbouring group contribution, $\sigma(\text{neighbour})$, is the contribution from the groups of atoms that form the rest of the molecule. The solvent contribution, $\sigma(\text{solvent})$, is the contribution from the solvent molecules.

(d) The local contribution

It is convenient to regard the local contribution to the shielding constant as the sum of a positive diamagnetic contribution, σ_d , and a negative paramagnetic contribution, σ_p :

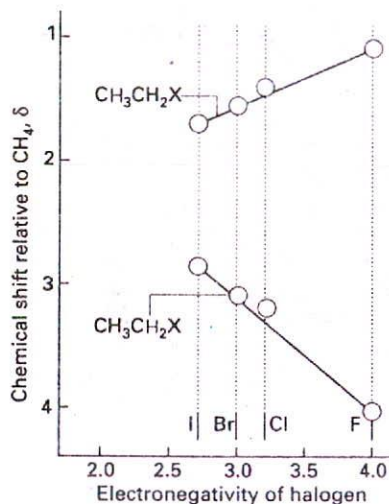
$$\sigma(\text{local}) = \sigma_d + \sigma_p \quad (13)$$

The total local contribution is positive if the diamagnetic contribution dominates, and is negative if the paramagnetic contribution dominates.

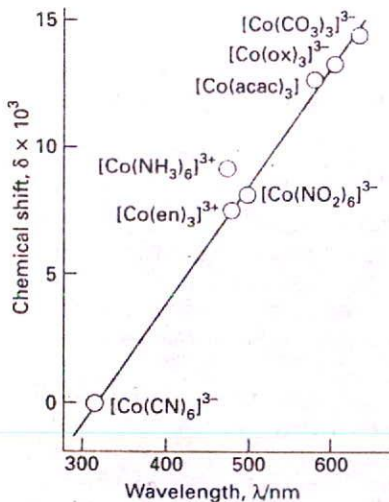
The diamagnetic contribution arises from the ability of the applied field to generate a circulation of charge in the ground-state electron distribution of the atom. The circulation generates a magnetic field that opposes the applied field and hence shields the nucleus. The magnitude of σ_d depends on the electron density close to the nucleus and can be calculated from the Lamb formula:

$$\sigma_d = \frac{e^2 \mu_0}{12\pi m_e} \left\langle \frac{1}{r} \right\rangle \quad (14)$$

where μ_0 is the vacuum permeability (a fundamental constant, see inside the front cover) and r is the electron-nucleus distance.



18.5 The variation of chemical shielding with electronegativity. The shifts for the methylene protons agree with the trend expected with increasing electronegativity. However, to emphasize that chemical shifts are subtle phenomena, notice that the trend for the methyl protons is opposite to that expected. For these protons another contribution (the magnetic anisotropy of C-H and C-X bonds) is dominant.



18.6 The correlation of chemical shifts relative to $[\text{Co}(\text{CN})_6]^{3-}$ and the ligand field parameter for complexes of cobalt. The wavelength is that of the lowest energy transition (and $\Delta \propto 1/\lambda$, approximately). Data from R. Freeman, G.R. Murray, and R.E. Richards, *Proc. Roy. Soc. A242*, 455 (1957).

Example 18.1 Using the Lamb formula

Calculate the shielding constant for the proton in a free H atom.

Method To use the Lamb formula, we need to calculate the expectation value of $1/r$ for a hydrogen 1s orbital. Wavefunctions are given in Table 13.1, and a useful integral is given in Example 11.6.

Answer Because $d\tau = r^2 dr \sin \theta d\theta d\phi$, we can write

$$\begin{aligned} \left\langle \frac{1}{r} \right\rangle &= \int \frac{\psi^* \psi}{r} d\tau = \frac{1}{\pi a_0^3} \int_0^{2\pi} d\phi \int_0^\pi \sin \theta d\theta \int_0^\infty r e^{-2r/a_0} dr \\ &= \frac{4}{a_0^3} \int_0^\infty r e^{-2r/a_0} dr = \frac{1}{a_0} \end{aligned}$$

Therefore,

$$\sigma_d = \frac{e^2 \mu_0}{12\pi m_e a_0}$$

With the values of the fundamental constants inside the front cover, this expression evaluates to 1.78×10^{-5} .

Comment The shielding constant is inversely proportional to the Bohr radius. This distance dependence can be understood as arising from the classical result that the magnetic moment of a current loop is proportional to its area (which for a hydrogen atom is of the order of a_0^2) and the magnetic field that it generates at the nucleus is inversely proportional to the cube of the latter's distance (a_0^3). Hence, the local field is proportional to $a_0^2 \times 1/a_0^3 = 1/a_0$.

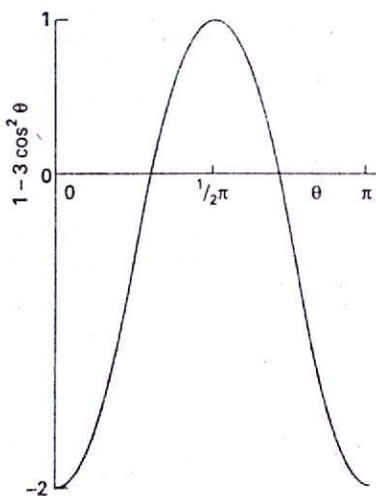
Self-test 18.1 Calculate σ_d for a hydrogenic atom with atomic number Z .

$$[\sigma_d = Z\sigma_d(\text{H})]$$

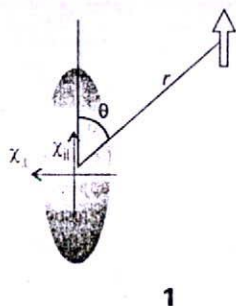
The diamagnetic contribution is the only contribution in closed-shell free atoms. It is also the only contribution to the local shielding for distributions of charge that have spherical or cylindrical symmetry. Thus, it is the only contribution to the local shielding from inner cores of atoms, for cores remain spherical even though the atom may be a component of a molecule and its valence electron distribution highly distorted. The diamagnetic contribution is broadly proportional to the electron density of the atom containing the nucleus of interest. It follows that the shielding is decreased if the electron density on the atom is reduced by the influence of an electronegative atom nearby. That reduction in shielding translates into an increase in deshielding, and hence to an increase in the chemical shift δ as the electronegativity of a neighbouring atom increases (Fig. 18.5). That is, as the electronegativity increases, δ decreases.

The local paramagnetic contribution, σ_p , arises from the ability of the applied field to force the electrons to circulate through the molecule by making use of orbitals that are unoccupied in the ground state. It is zero in free atoms and around the axes of linear molecules (such as ethyne, $\text{HC}\equiv\text{CH}$) where the electrons can circulate freely and a field applied along the internuclear axis is unable to force them into other orbitals.

The magnitude of the paramagnetic contribution depends on the ease with which the applied field can promote electrons into unoccupied orbitals. Hence, it is inversely proportional to the energy separation of the highest filled (HOMO) and lowest unfilled (LUMO) orbitals of the molecule, Δ . The strength of the magnetic field generated by the magnetic moment of the resulting circulation of charge is inversely proportional to the cube



18.7 The variation of the function $1 - 3 \cos^2 \theta$ with the angle θ .



1

18.8 The neighbouring group effect in NMR. (a) The protons in $\text{HC}\equiv\text{CH}$ are shielded by the currents induced in the triple bond, but a proton perpendicular to the bond is deshielded. (b) The opposite is true for protons near a $\text{C}=\text{C}$ double bond because the applied field can induce a paramagnetic current parallel to the axis of a double bond.

of the distance of the nucleus from the circulating current, so the field at the nucleus is proportional to $\langle r^{-3} \rangle$. Overall, therefore,

$$\sigma_p \propto -\frac{\langle r^{-3} \rangle}{\Delta} \quad (15)$$

We can therefore expect large paramagnetic contributions from small atoms in molecules with low-lying excited states. In fact, the paramagnetic contribution is the dominant local contribution for atoms other than hydrogen. The shielding constants of the nuclei of d -metal ions in complexes correlate quite well with spectroscopic data if Δ is identified with the ligand-field splitting parameter (Fig. 18.6).

(e) Neighbouring group contributions

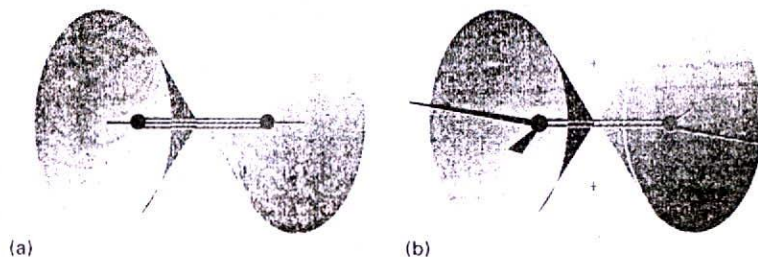
The neighbouring group contribution arises from the currents induced in nearby groups of atoms. The effect of either kind of current (diamagnetic or paramagnetic) is to shield or deshield the nucleus depending on the relative location of the nucleus to the neighbouring group.

The applied field generates currents in the electron distribution of the neighbouring group and gives rise to a magnetic moment proportional to the applied field; the constant of proportionality is the magnetic susceptibility, χ , of the group.¹ This induced magnetic moment gives rise to a magnetic field at the nucleus with a strength that is inversely proportional to the cube of the distance of the nucleus from the group of atoms. The field varies with the orientation of the molecule, but it does not average to zero because the magnetic susceptibility also changes as the molecule presents different orientations to the applied field. The result is that the shielding constant depends on three quantities: the difference in the magnetic susceptibilities parallel and perpendicular to the group (we are assuming that the group has cylindrical symmetry), the angle θ that the vector to the magnetic nucleus makes to the axis of symmetry of the group, and the distance r of the nucleus from the group (1):

$$\sigma(\text{neighbour}) \propto (\chi_{\parallel} - \chi_{\perp}) \left(\frac{1 - 3 \cos^2 \theta}{r^3} \right) \quad (16)$$

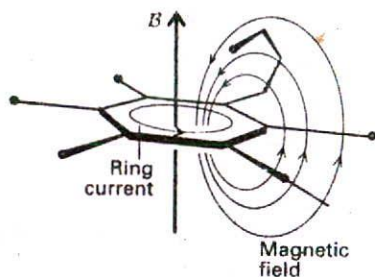
This expression shows that the neighbouring group contribution may be positive or negative according to the relative magnitudes of the two magnetic susceptibilities and the relative orientation of the nucleus. The latter effect is easy to anticipate: if $54.7^\circ < \theta < 125.3^\circ$, then $1 - 3 \cos^2 \theta$ is positive, but it is negative otherwise (Fig. 18.7).

A $\text{C}\equiv\text{C}$ group is linear, and an applied field cannot induce a paramagnetic current when it is parallel to the group's axis.² The pattern of shielding and deshielding resulting from the diamagnetic current is shown in Fig. 18.8. Protons lying on the axis of the group (as



1 Magnetic susceptibilities are discussed in Section 22.6.

2 The electrons are in orbitals that are eigenfunctions of the angular momentum operator, L_z , for circulation about the axis of the molecule. When the field is applied along that axis, it gives rise to a perturbation proportional to $B_z L_z$, which cannot mix excited states into its own eigenfunctions.



18.9 The shielding and deshielding effects of the ring current induced in the benzene ring by the applied field. Protons attached to the ring are deshielded but a proton attached to a substituent that projects above the ring is shielded.

in ethyne itself) are shielded, but a proton that lies perpendicular to the bond (as part of a larger molecule) is deshielded. The opposite is true for protons near a C=C double bond because in this nonlinear group the applied field can induce a paramagnetic current when it lies parallel to the axis.

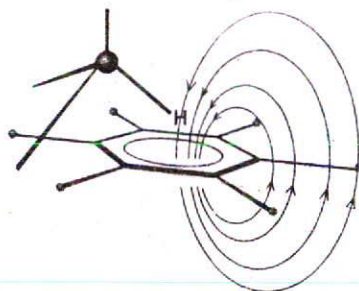
A special case of a neighbouring group effect is found in aromatic compounds. The strong anisotropy of the magnetic susceptibility of the benzene ring is ascribed to the ability of the field to induce a ring current, a circulation of electrons around the ring, when it is applied perpendicular to the molecular plane. Protons in the plane are deshielded (Fig. 18.9), but any that happen to lie above or below the plane (as members of substituents of the ring) are shielded.

(f) The solvent contribution

A solvent can influence the local magnetic field experienced by a nucleus in a variety of ways. Some of these effects arise from specific interactions between the solute and the solvent (such as hydrogen-bond formation and other forms of Lewis acid-base complex formation). The magnetic susceptibility of the solvent molecules, especially if they are aromatic, can also be the source of a local magnetic field. Moreover, if there are steric interactions that result in a loose but specific interaction between a solute molecule and a solvent molecule, then protons in the solute molecule may experience shielding or deshielding effects according to their location relative to the solvent molecule (Fig. 18.10). We shall see that the NMR spectra of species that contain protons with widely different chemical shifts are easier to interpret than those in which the shifts are similar, so the appropriate choice of solvent may help to simplify the appearance and interpretation of a spectrum.

18.4 The fine structure

The splitting of resonances into individual lines in Fig. 18.4 is called the fine structure of the spectrum. It arises because each magnetic nucleus may contribute to the local field experienced by the other nuclei and so modify their resonance frequencies. The strength of the interaction is expressed in terms of the scalar coupling constant, J , and reported in hertz (Hz).³ Spin coupling constants are independent of the strength of the applied field because they do not depend on the latter's ability to generate local fields. If the resonance line of a particular nucleus is split by a certain amount by a second nucleus, then the resonance line of the second nucleus is split by the first to the same extent.



18.10 An aromatic solvent (benzene here) can give rise to local currents that shield or deshield a proton in a solvent molecule. In this relative orientation of the solvent and solute, the proton on the solute molecule is shielded.



18.11 The effect of spin-spin coupling on an AX spectrum. Each resonance is split into two lines separated by J . The pairs of resonances are centred on the chemical shifts of the protons in the absence of spin-spin coupling.

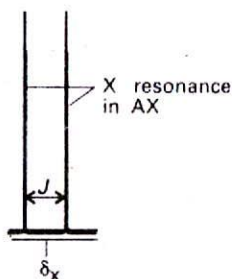
³ The scalar coupling constant is so called because the interaction it describes is proportional to the scalar product of the two interacting spins: $E \propto I_1 \cdot I_2$. The constant of proportionality in this expression is J . (More precisely, it is hJ/h^2 , because each angular momentum is proportional to h .)

(a) Patterns of coupling

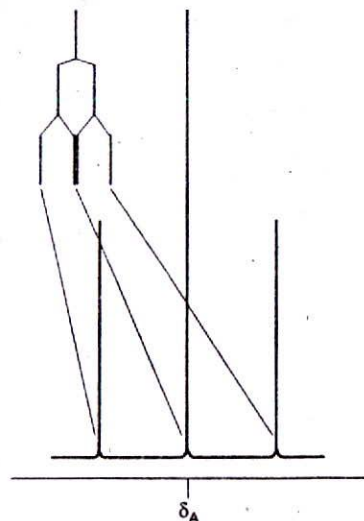
In NMR, letters far apart in the alphabet (typically A and X) are used to indicate nuclei with very different chemical shifts; letters close together (such as A and B) are used for nuclei with similar chemical shifts. We shall consider first an AX system, a molecule that contains two spin- $\frac{1}{2}$ nuclei A and X with very different chemical shifts in the sense that the difference in chemical shifts is large compared with their spin-spin coupling.

Suppose the spin of X is α ; then the spin of A will have a Larmor frequency as a result of the combined effect of the external field, the shielding constant, and the spin-spin interaction of A with X. The spin-spin coupling will result in one line in the spectrum of A being shifted by $-\frac{1}{2}J$ from the frequency it would have in the absence of coupling. If the spin of X is β , the spin of A will have a Larmor frequency shifted by $+\frac{1}{2}J$. Therefore, instead of a single line from A, we get a doublet of lines separated by J and centred on the chemical shift characteristic of A (Fig. 18.11). The same splitting occurs in the X resonance: instead of a single line, the resonance is a doublet with splitting J (the same value as for the splitting of A) centred on the chemical shift characteristic of X.

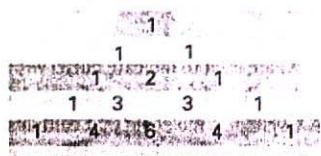
A subtle point is that the X resonance in an AX_n species (such as an AX_2 or AX_3 species) is also a doublet with splitting J . As we shall explain below, a group of equivalent nuclei resonates like a single nucleus. The only difference for the X resonance of an AX_n species is that the intensity is n times as great as that of an AX species (Fig. 18.12). The A resonance in an AX_n species, though, is quite different from the A resonance in an AX species. For example, consider an AX_2 species with two equivalent X nuclei. The resonance of A is split into a doublet of separation J by one X, and each line of that doublet is split again by the same amount by the second X (Fig. 18.13). This splitting results in three lines in the intensity ratio 1 : 2 : 1 (because the central frequency can be obtained in two ways). The A resonance



18.12 The X resonance of an AX_2 species is also a doublet; because the two equivalent X nuclei behave like a single nucleus; however, the overall absorption is twice as intense as that of an AX species.



18.13 The origin of the 1 : 2 : 1 triplet in the A resonance of an AX_2 species. The resonance of A is split into two by coupling with one X nucleus (as shown in the inset), and then each of those two lines is split into two by coupling to the second X nucleus. Because each X nucleus causes the same splitting, the two central transitions are coincident and give rise to an absorption line of double the intensity of the outer lines.



2

of an A_nX_2 species would also be a 1 : 2 : 1 triplet of splitting J , the only difference being that the intensity of the A resonance would be n times as great as that of AX_2 .

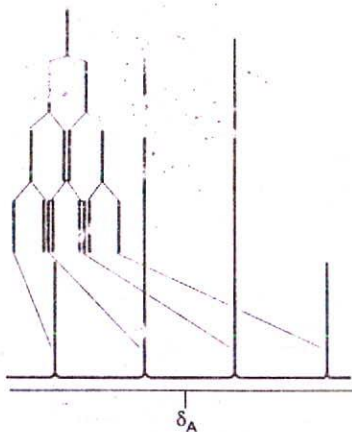
Three equivalent X nuclei (an AX_3 species) split the resonance of A into four lines of intensity ratio 1 : 3 : 3 : 1 and separation J (Fig. 18.14). The X resonance, though, is still a doublet of separation J . In general, n equivalent spin- $\frac{1}{2}$ nuclei split the resonance of a nearby spin or group of equivalent spins into $n + 1$ lines with an intensity distribution given by Pascal's triangle (2). The easiest way of constructing the pattern of fine structure is to draw a diagram in which successive rows show the splitting of a subsequent proton. The procedure is illustrated in Fig. 18.15 and was used in Figs. 18.13 and 18.14. It is easily extended to molecules containing nuclei with $I > \frac{1}{2}$ (Fig. 18.16).

Example 18.2 Accounting for the fine structure in a spectrum

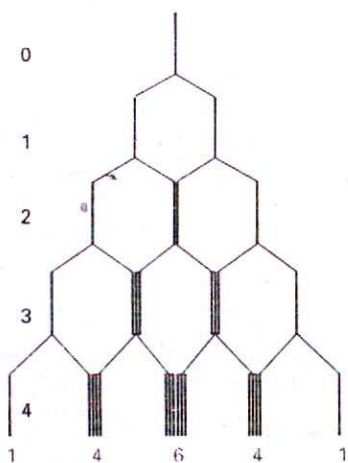
Account for the fine structure in the NMR spectrum of the C-H protons of ethanol.

Method Consider how each group of equivalent protons (for example, three methyl protons) split the resonance of the other groups of protons. There is no splitting within groups of equivalent protons. Each splitting pattern can be decided by referring to Pascal's triangle.

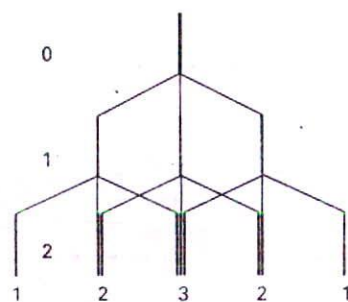
Answer The three protons of the CH_3 group split the resonance of the CH_2 protons into a 1 : 3 : 3 : 1 quartet with a splitting J . Likewise, the two protons of the CH_2 group split the resonance of the CH_3 protons into a 1 : 2 : 1 triplet with the same splitting J . All the lines mentioned so far are split into doublets by the OH proton, but the splitting cannot be detected because the OH protons migrate rapidly from molecule to molecule and their effect averages to zero.



18.14 The origin of the 1 : 3 : 3 : 1 quartet in the A resonance of an AX_3 species. The third X nucleus splits each of the lines shown in Fig. 18.13 for an AX_2 species into a doublet, and the intensity distribution reflects the number of transitions that have the same energy.



18.15 The intensity distribution of the A resonance of an AX_n resonance can be constructed by considering the splitting caused by 1, 2, ..., n protons, as in Figs. 18.13 and 18.14. The resulting intensity distribution has a binomial distribution and is given by the integers in the corresponding row of Pascal's triangle. Note that, although the lines have been drawn side-by-side for clarity, the members of each group are coincident. Four protons, in AX_4 , split the A resonance into a 1 : 4 : 6 : 4 : 1 quintet.



18.16 The intensity distribution arising from spin-spin interaction with nuclei with $I = 1$ can be constructed similarly, but each successive nucleus splits the lines into three equal intensity components. Two equivalent spin-1 nuclei give rise to a 1 : 2 : 3 : 2 : 1 quintet.

Self-test 18.2 What fine structure can be expected for the protons in $^{14}\text{NH}_4^+$? The spin quantum number of nitrogen is 1.

[1 : 1 : 1 triplet from N]

(b) The energy levels of coupled systems

It will be useful for later discussions to consider an NMR spectrum in terms of the energy levels of the nuclei and the transitions between them. The energy level diagram for a single spin- $\frac{1}{2}$ nucleus and its single transition were shown in Fig. 18.1, and nothing more needs to be said. For a spin- $\frac{1}{2}$ AX system there are four spin states:

$$\alpha_A\alpha_X \quad \alpha_A\beta_X \quad \beta_A\alpha_X \quad \beta_A\beta_X$$

The energy depends on the orientation of the spins in the external magnetic field, and, if spin-spin coupling is neglected,

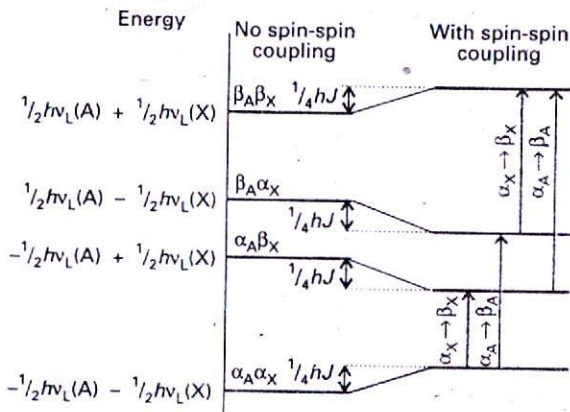
$$E = -\gamma\hbar(1 - \sigma_A)Bm_A - \gamma\hbar(1 - \sigma_X)Bm_X = -h\nu_A m_A - h\nu_X m_X \quad (17)$$

where ν_A and ν_X are the Larmor frequencies of A and X and m_A and m_X are their quantum numbers. This expression gives the four lines on the left of Fig. 18.17. The spin-spin coupling depends on the relative orientation of the two nuclear spins, so it is proportional to the product $m_A m_X$; the constant of proportionality is hJ . Therefore, the energy including spin-spin coupling is

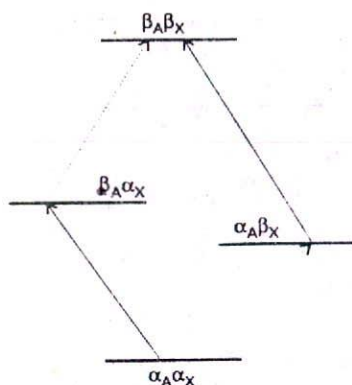
$$E = -h\nu_A m_A - h\nu_X m_X + hJ m_A m_X \quad (18)$$

If $J > 0$, a lower energy is obtained when $m_A m_X < 0$, which is the case if one spin is α and the other is β . A higher energy is obtained if both spins are α or both spins are β . The opposite is true if $J < 0$. The resulting energy level diagram (for $J > 0$) is shown on the right of Fig. 18.17. We see that the $\alpha\alpha$ and $\beta\beta$ states are both raised by $\frac{1}{4}hJ$ and that the $\alpha\beta$ and $\beta\alpha$ states are both lowered by $\frac{1}{4}hJ$.

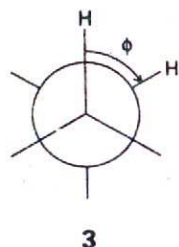
When a transition of nucleus A occurs, nucleus X remains unchanged. Therefore, the A resonance is a transition for which $\Delta m_A = +1$ and $\Delta m_X = 0$. There are two such transitions, one in which $\beta_A \leftarrow \alpha_A$ occurs when the X nucleus is α_X , and the other in which $\beta_A \leftarrow \alpha_A$ occurs when the X nucleus is β_X . They are shown in Fig. 18.17 and in a slightly different



18.17 The energy levels of an AX system. The four levels on the left are those of the two spins in the absence of spin-spin coupling. The four levels on the right show how a positive spin-spin coupling constant affects the energies. The transitions shown are for $\beta \leftarrow \alpha$ of A or X, the other nucleus (X or A, respectively) remaining unchanged.



18.18 An alternative depiction of the energy levels and transitions shown in Fig. 18.17.



form in Fig. 18.18. The energies of the transitions are

$$\Delta E = h\nu_A \pm \frac{1}{2}hJ \quad (19)$$

Therefore, the A resonance consists of a doublet of separation J centred on the chemical shift of A (as in Fig. 18.11).

Similar remarks apply to the X resonance, which consists of two transitions according to whether the A nucleus is α or β (Fig. 18.18). The transition energies are

$$\Delta E = h\nu_X \pm \frac{1}{2}hJ \quad (20)$$

It follows that the X resonance also consists of two lines of separation J , but they are centred on the chemical shift of X (as shown in Fig. 18.11).

(c) The magnitudes of coupling constants

The scalar coupling constant of two nuclei separated by N bonds is denoted ${}^N J$, with subscripts for the types of nuclei involved. Thus, ${}^1 J_{\text{CH}}$ is the coupling constant for a proton joined directly to a ${}^{13}\text{C}$ atom, and ${}^2 J_{\text{CH}}$ is the coupling constant when the same two nuclei are separated by two bonds (as in ${}^{13}\text{C}-\text{C}-\text{H}$). A typical value of ${}^1 J_{\text{CH}}$ is in the range 120 to 250 Hz; ${}^2 J_{\text{CH}}$ is between 0 and 10 Hz. Both ${}^3 J$ and ${}^4 J$ give detectable effects in a spectrum, but couplings over larger numbers of bonds can generally be ignored. One of the longest couplings that has been detected is ${}^9 J_{\text{HH}} = 0.4$ Hz for CH_3 and CH_2 protons in $\text{CH}_3\text{C}\equiv\text{CC}\equiv\text{CC}\equiv\text{CCH}_2\text{OH}$.

The sign of J_{XY} indicates whether the energy of two spins is lower when they are parallel ($J < 0$) or when they are antiparallel ($J > 0$). It is found that ${}^1 J_{\text{CH}}$ is often positive, ${}^2 J_{\text{HH}}$ is often negative, ${}^3 J_{\text{HH}}$ is often positive, and so on. An additional point is that J varies with the angle between the bonds (Fig. 18.19). Thus, a ${}^3 J_{\text{HH}}$ coupling constant is often found to depend on the angle ϕ (3) according to the Karplus equation:

$$J = A + B \cos \phi + C \cos 2\phi \quad (21)$$

with A , B , and C empirical constants with values close to +7 Hz, -1 Hz, and +5 Hz, respectively. It follows that the measurement of ${}^3 J_{\text{HH}}$ in a series of related compounds can be used to determine their conformations. The coupling constant ${}^1 J_{\text{CH}}$ also depends on the hybridization of the C atom, as the following values indicate:

${}^1 J_{\text{CH}}/\text{Hz}$:	sp	sp^2	sp^3
	250	160	125

(d) The origin of spin-spin coupling

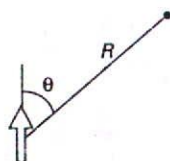
Spin-spin coupling is a very subtle phenomenon, and it is better to treat J as an empirical parameter than to use calculated values. However, we can get some insight into its origins, if not its precise magnitude—or always reliably its sign—by considering the magnetic interactions within molecules.

A nucleus with spin projection m_l gives rise to a magnetic field with z component B_{nuc} at a distance R , where

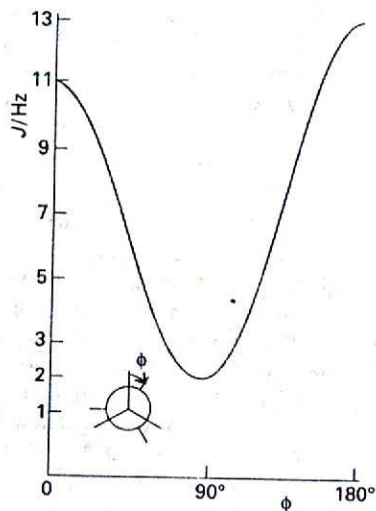
$$B_{\text{nuc}} = -\frac{\gamma h \mu_0}{4\pi R^3} (1 - 3 \cos^2 \theta) m_l \quad (22)$$

The angle θ is defined in (4). The magnitude of this field is about 0.1 mT when $R = 0.3$ nm, corresponding to a splitting of resonance signal of about 10^4 Hz, and is of the order of magnitude of the splitting observed in solid samples (see Section 18.9a).

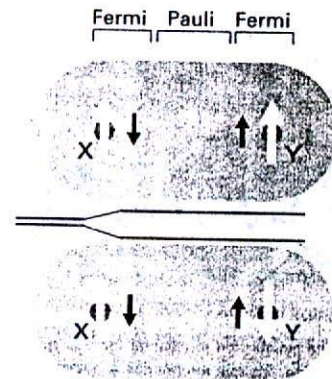
In a liquid, the angle θ sweeps over all values as the molecule tumbles, and $1 - 3 \cos^2 \theta$



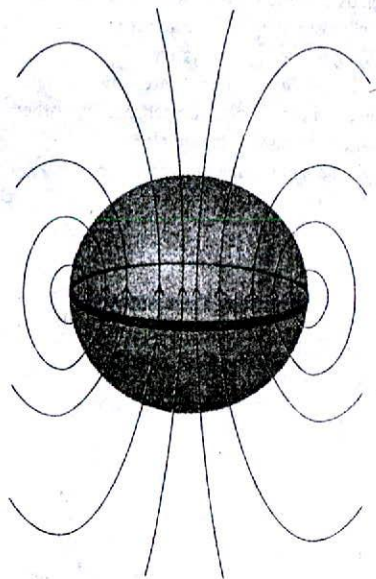
4



18.19 The variation of the spin-spin coupling constant with angle predicted by the Karplus equation.



18.20 The polarization mechanism for spin-spin coupling ($^1J_{\text{HH}}$). The two arrangements have slightly different energies. In this case, J is positive, corresponding to a lower energy when the nuclear spins are antiparallel.



18.21 The origin of the Fermi contact interaction. From far away, the magnetic field pattern arising from a ring of current (representing the rotating charge of the nucleus, the pale grey sphere) is that of a point dipole. However, if an electron can sample the field close to the region indicated by the sphere, the field distribution differs significantly from that of a point dipole. For example, if the electron can penetrate the sphere, then the spherical average of the field it experiences is not zero.

averages to zero.⁴ Hence the direct dipolar interaction between spins cannot account for the fine structure of the spectra of rapidly tumbling molecules. The direct interaction does make an important contribution to the spectra of solid samples and to the spectra of molecules that tumble only slowly in solution, such as biological and synthetic macromolecules.

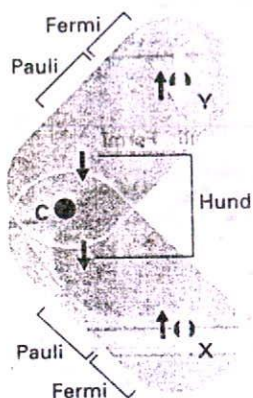
Spin-spin coupling in molecules in solution can be explained in terms of the **polarization mechanism**, in which the interaction is transmitted through the bonds. The simplest case to consider is that of $^1J_{\text{XY}}$ where X and Y are spin- $\frac{1}{2}$ nuclei joined by an electron-pair bond (Fig. 18.20). The coupling mechanism depends on the fact that in some atoms it is favourable for the nucleus and a nearby electron spin to be parallel (both α or both β), but in others it is favourable for them to be antiparallel (one α and the other β). The electron-nucleus coupling is magnetic in origin, and may be either a dipolar interaction between the magnetic moments of the electron and nuclear spins or a Fermi contact interaction. As shown in the *Justification* below, the latter depends on the very close approach of an electron to the nucleus and hence can occur only if the electron occupies an s orbital. We shall suppose that it is energetically favourable for an electron spin and a nuclear spin to be antiparallel (as is the case for a proton and an electron in a hydrogen atom).

Justification 18.2

A pictorial description of the Fermi contact interaction is as follows. First, we regard the magnetic moment of the nucleus as arising from the circulation of a current in a tiny loop with a radius similar to that of the nucleus (Fig. 18.21). Far from the nucleus the field generated by this loop is indistinguishable from the field generated by a point magnetic dipole. Close to the loop, however, the field differs from that of a point dipole. The

⁴ The volume element in polar coordinates is proportional to $\sin \theta d\theta$, and θ ranges from 0 to π . Therefore the average value of B_{int} for a tumbling molecule is proportional to

$$\int_0^\pi (1 - 3 \cos^2 \theta) \sin \theta d\theta = 0$$



18.22 The polarization mechanism for ${}^2J_{\text{HH}}$ spin-spin coupling. The spin information is transmitted from one bond to the next by a version of the mechanism that accounts for the lower energy of electrons with parallel spins in different atomic orbitals (Hund's rule of maximum multiplicity). In this case, J is negative, corresponding to a lower energy when the nuclear spins are parallel.

magnetic interaction between this non-dipolar field and the electron's magnetic moment is the contact interaction. The lines of force depicted in Fig. 18.21 correspond to those for a proton with α spin. The lower energy state of an electron spin in such a field is the β state.

If the X nucleus is α , a β electron of the bonding pair will tend to be found nearby (since that is energetically favourable for it). The second electron in the bond, which must have α spin if the other is β , will be found mainly at the far end of the bond (because electrons tend to stay apart to reduce their mutual repulsion). Because it is energetically favourable for the spin of Y to be antiparallel to an electron spin, a Y nucleus with β spin has a lower energy, and hence a lower Larmor frequency, than a Y nucleus with α spin. The opposite is true when X is β , for now the α spin of Y has the lower energy. In other words, the antiparallel arrangement of nuclear spins lies lower in energy than the parallel arrangement as a result of their magnetic coupling with the bond electrons. That is, ${}^1J_{\text{HH}}$ is positive.

To account for the value of ${}^2J_{\text{XY}}$, as in H-C-H, we need a mechanism that can transmit the spin alignments through the central C atom (which may be ${}^{12}\text{C}$, with no nuclear spin of its own). In this case (Fig. 18.22), an X nucleus with α spin polarizes the electrons in its bond, and the α electron is likely to be found closer to the C nucleus. The more favourable arrangement of two electrons on the same atom is with their spins parallel (Hund's rule, Section 13.4d), so the more favourable arrangement is for the α electron of the neighbouring bond to be close to the C nucleus. Consequently, the β electron of that bond is more likely to be found close to the Y nucleus, and therefore that nucleus will have a lower energy if it is α . Hence, according to this mechanism, the lower Larmor frequency of Y will be obtained if its spin is parallel to that of X. That is, ${}^2J_{\text{HH}}$ is negative.

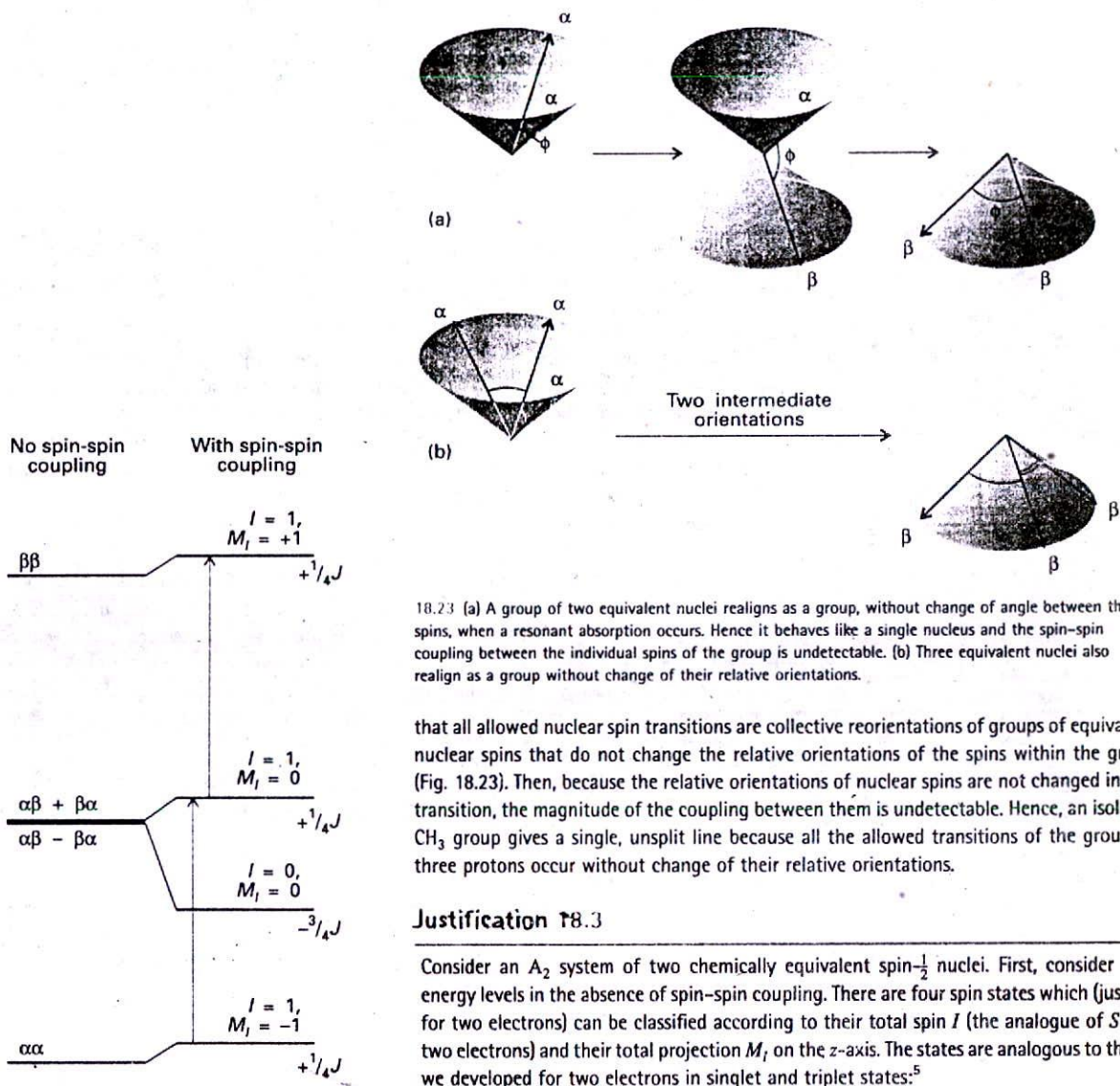
The coupling of nuclear spin to electron spin by the Fermi contact interaction is most important for proton spins, but it is not necessarily the most important mechanism for other nuclei. These nuclei may also interact by a dipolar mechanism with the electrons and with their orbital motion, and there is no simple way of specifying which will be positive or negative.

(e) Equivalent nuclei

A group of nuclei are chemically equivalent if they are related by a symmetry operation of the molecule and have the same chemical shifts. Chemically equivalent nuclei are nuclei that would be regarded as 'equivalent' according to ordinary chemical criteria. Nuclei are magnetically equivalent if, as well as being chemically equivalent, they also have identical spin-spin interactions with any other magnetic nuclei in the molecule.

The difference between chemical and magnetic equivalence is illustrated by CH_2F_2 and $\text{H}_2\text{C}=\text{CF}_2$, in both of which the protons are chemically equivalent: they are related by symmetry and undergo the same chemical reactions. However, although the protons in CH_2F_2 are magnetically equivalent, those in $\text{CH}_2=\text{CF}_2$ are not. One proton in the latter has spin-coupling interactions with a *cis* F nucleus which might be α whereas the other proton has a *trans* interaction with it. In CH_2F_2 both protons are equally distant from the two F nuclei, so there is no distinction between them. Strictly speaking, the CH_3 protons in ethanol (and other compounds) are magnetically inequivalent on account of their different interactions with the CH_2 protons in the next group. However, they are in practice made magnetically equivalent by the rapid rotation of the CH_3 group, which averages out any differences. Magnetically inequivalent species can give very complicated spectra (for instance, the spectrum of $\text{H}_2\text{C}=\text{CF}_2$ consists of ten lines), and we shall not consider them further.

An important feature of chemically equivalent magnetic nuclei is that, although they do couple together, the coupling has no effect on the appearance of the spectrum. The reason for the invisibility of the coupling is set out in the *Justification* below, but qualitatively it is



18.24 The energy levels of an A_2 system in the absence of spin-spin coupling are shown on the left. When spin-spin coupling is taken into account, the energy levels on the right are obtained. Note that the three states with total nuclear spin $I = 1$ correspond to parallel spins and give rise to the same increase in energy (J is positive); the one state with $I = 0$ (antiparallel nuclear spins) has a lower energy in the presence of spin-spin coupling. The only allowed transitions are those that preserve the angle between the spins, and so take place between the three states with $I = 1$. They occur at the same resonance frequency as they would have in the absence of spin-spin coupling.

18.23 (a) A group of two equivalent nuclei realigns as a group, without change of angle between the spins, when a resonant absorption occurs. Hence it behaves like a single nucleus and the spin-spin coupling between the individual spins of the group is undetectable. (b) Three equivalent nuclei also realign as a group without change of their relative orientations.

that all allowed nuclear spin transitions are collective reorientations of groups of equivalent nuclear spins that do not change the relative orientations of the spins within the group (Fig. 18.23). Then, because the relative orientations of nuclear spins are not changed in any transition, the magnitude of the coupling between them is undetectable. Hence, an isolated CH_3 group gives a single, unsplit line because all the allowed transitions of the group of three protons occur without change of their relative orientations.

Justification 18.3

Consider an A_2 system of two chemically equivalent spin- $\frac{1}{2}$ nuclei. First, consider the energy levels in the absence of spin-spin coupling. There are four spin states which (just as for two electrons) can be classified according to their total spin I (the analogue of S for two electrons) and their total projection M_I on the z -axis. The states are analogous to those we developed for two electrons in singlet and triplet states:⁵

$$\begin{aligned} \text{Spins parallel, } I = 1: & \quad M_I = +1 \quad \alpha\alpha \\ & \quad M_I = 0 \quad (1/2^{1/2})\{\alpha\beta + \beta\alpha\} \\ & \quad M_I = -1 \quad \beta\beta \\ \text{Spins paired, } I = 0: & \quad M_I = 0 \quad (1/2^{1/2})\{\alpha\beta - \beta\alpha\} \end{aligned}$$

The effect of a magnetic field on these four states is shown on the left in Fig. 18.24: the energies of the two states with $M_I = 0$ are unchanged by the field because they are composed of equal proportions of α and β spins.

5 As in Section 13.7, the states we have selected are those with a definite resultant, and hence a well defined value of I . The + sign in $\alpha\beta + \beta\alpha$ signifies an in-phase alignment of spins and $I = 1$; the - sign in $\alpha\beta - \beta\alpha$ signifies an alignment out of phase by π , and hence $I = 0$. See Fig. 13.26.

The spin-spin coupling energy is proportional to the scalar product of the vectors representing the spins, and we write $E = (hJ/\hbar^2) \mathbf{I}_1 \cdot \mathbf{I}_2$. The scalar product can be expressed in terms of the total nuclear spin by noting that

$$I^2 = (\mathbf{I}_1 + \mathbf{I}_2) \cdot (\mathbf{I}_1 + \mathbf{I}_2) = I_1^2 + I_2^2 + 2\mathbf{I}_1 \cdot \mathbf{I}_2$$

and replacing the magnitudes by their quantum mechanical values:

$$\mathbf{I}_1 \cdot \mathbf{I}_2 = \frac{1}{2} \{ I(I+1) - I_1(I_1+1) - I_2(I_2+1) \} \hbar^2 \quad (23)$$

Then, because $I_1 = I_2 = \frac{1}{2}$, it follows that

$$E = \frac{1}{2} hJ \{ I(I+1) - \frac{3}{2} \} \quad (24)$$

For parallel spins, $I = 1$ and $E = +\frac{1}{4} hJ$; for antiparallel spins $I = 0$ and $E = -\frac{3}{4} hJ$, as in the illustration. We see that three of the states move in energy in one direction and the fourth (the one with antiparallel spins) moves three times as much in the opposite direction. The resulting energy levels are shown in Fig. 18.24.

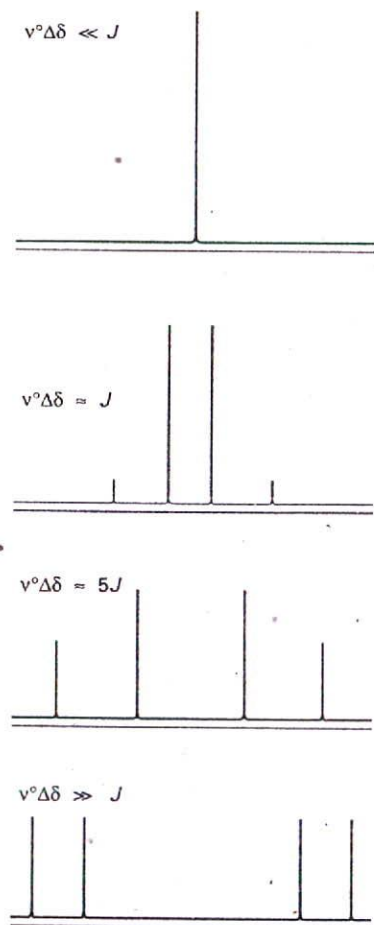
The NMR spectrum of the A_2 species arises from transitions between the levels. However, the radiofrequency field affects the two equivalent protons equally, so it cannot change the orientation of one proton relative to the other; therefore, the transitions take place within the set of states that correspond to parallel spin (those labelled $I = 1$), and no spin-parallel state can change to a spin-antiparallel state (the state with $I = 0$). Put another way, the allowed transitions are subject to the selection rule $\Delta I = 0$. This selection rule is in addition to the rule $\Delta M_I = \pm 1$ that arises from the conservation of angular momentum and the unit spin of the photon. The allowed transitions are shown in Fig. 18.24: we see that there are only two transitions, and that they occur at the same resonance frequency that the nuclei would have in the absence of spin-spin coupling. Hence, the spin-spin coupling interaction does not affect the appearance of the spectrum.

(f) Strongly coupled nuclei

NMR spectra are usually much more complex than the foregoing simple analysis suggests. We have described the extreme case in which the differences in chemical shifts are much greater than the spin-spin coupling constants. In such cases it is simple to identify groups of magnetically equivalent nuclei and to think of the groups of nuclear spins as reorientating relative to each other. The spectra that result are called first-order spectra.

Transitions cannot be allocated to definite groups when the differences in their chemical shifts are comparable to their spin-spin coupling interactions. The complicated spectra that are then obtained are called **strongly coupled** (or 'second-order spectra') and are much more difficult to analyse (Fig. 18.25). Because the difference in resonance frequencies increases with field, but spin-spin coupling constants are independent of it, a second-order spectrum may become simpler (and first-order) at high fields because individual groups of nuclei become identifiable again.

A clue to the type of analysis that is appropriate is given by the notation for the types of spins involved. Thus, an AX spin system (which consists of two nuclei with a large chemical shift difference) has a first-order spectrum. An AB system, on the other hand (with two nuclei of similar chemical shifts), gives a spectrum typical of a strongly coupled system. An AX system may have widely different chemical shifts because A and X are nuclei of different elements (such as ^{13}C and ^1H), in which case they form a heteronuclear spin system. AX may also denote a homonuclear spin system in which the nuclei are of the same element but in markedly different environments.



18.25 The NMR spectrum of an A_2 system (top) and an AX system (bottom) are simple, and give rise to 'first-order spectra'. At intermediate relative values of the chemical shift difference and the spin-spin coupling, complex 'strongly coupled' spectra are obtained. Note how the inner two lines of the bottom spectrum move together, grow in intensity, and form the single central line of the top spectrum. The two outer lines diminish in intensity and are absent in the top spectrum.

(g) Dilute and abundant spins: spin decoupling

Carbon-13 is a dilute-spin species in the sense that it is unlikely that more than one ^{13}C nucleus will be found in any given small molecule (provided the sample has not been enriched with that isotope; the natural abundance of ^{13}C is only 1.1 per cent). Even in large molecules, although more than one ^{13}C nucleus may be present, it is unlikely that they will be close enough to give an observable splitting. Hence, it is not normally necessary to take into account ^{13}C — ^{13}C spin-spin coupling within a molecule.

Protons are abundant-spin species in the sense that a molecule is likely to contain many of them. If we were observing a ^{13}C -NMR spectrum, we would obtain a very complex spectrum on account of the coupling of the one ^{13}C nucleus with all the protons that are present. To avoid this difficulty, ^{13}C -NMR spectra are normally observed using the technique of proton decoupling. Thus, if the CH_3 protons of ethanol are irradiated with a second, strong, resonant radiofrequency source, they undergo rapid spin reorientations and the ^{13}C nucleus senses an average orientation. As a result, its resonance is a single line and not a 1 : 3 : 3 : 1 quartet. Proton decoupling has the additional advantage of enhancing sensitivity, because the intensity is concentrated into a single transition frequency instead of being spread over several transition frequencies. If care is taken to ensure that the other parameters on which the strength of the signal depends are kept constant, the intensities of proton-decoupled spectra are proportional to the number of ^{13}C nuclei present. The technique is widely used to characterize synthetic polymers.

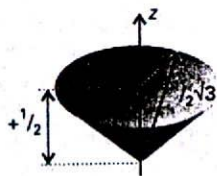
Pulse techniques in NMR

Modern methods of detecting the energy separation between nuclear spin states are more sophisticated than simply looking for the frequency at which resonance occurs. One of the best analogies that has been suggested to illustrate the difference between the old and new ways of observing an NMR spectrum is that of detecting the spectrum of vibrations of a bell. We could stimulate the bell with a gentle vibration at a gradually increasing frequency, and note the frequencies at which it resonated with the stimulation. A lot of time would be spent getting zero response when the stimulating frequency was between the bell's vibrational modes. However, if we were simply to hit the bell with a hammer, we would immediately obtain a clang composed of all the frequencies that the bell can produce. The equivalent in NMR is to monitor the radiation nuclear spins emit as they return to equilibrium after the appropriate stimulation. The resulting Fourier-transform NMR gives greatly increased sensitivity, so opening up the entire periodic table to the technique. Moreover, multiple-pulse FT-NMR gives chemists unparalleled control over the information content and display of spectra. We need to understand how the equivalent of the hammer blow is delivered and how the signal is monitored and interpreted. These features are generally expressed in terms of the vector model of angular momentum introduced in Section 12.7d.

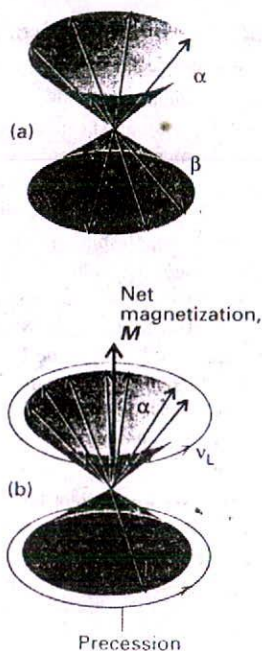
18.5 The magnetization vector

Consider a sample composed of many identical spin- $\frac{1}{2}$ nuclei. As we saw in Section 12.7d, an angular momentum can be represented by a vector of length $\{I(I+1)\}^{1/2}$ units with a component of length m_l units along the z -axis. As the uncertainty principle does not allow us to specify the x - and y -components of the angular momentum, all we know is that the vector lies somewhere on a cone around the z -axis. For $I = \frac{1}{2}$, the length of the vector is $\frac{1}{2}\sqrt{3}$ and it makes an angle of 55° to the z -axis (Fig. 18.26).

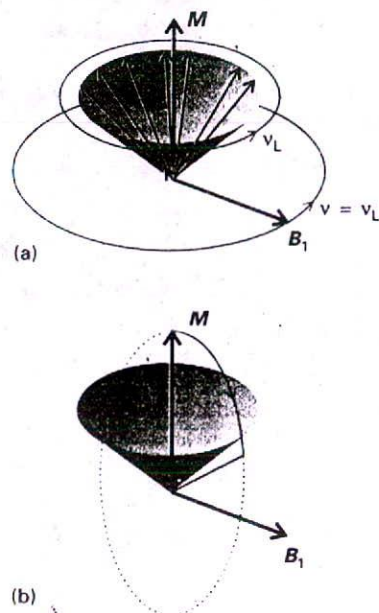
In the absence of a magnetic field, the sample consists of equal numbers of α and β nuclear spins with their vectors lying at random angles on the cones. These angles are



18.26 The vector model of angular momentum for a single spin- $\frac{1}{2}$ nucleus. The angle around the z -axis is indeterminate.



18.27 The magnetization of a sample of spin- $\frac{1}{2}$ nuclei is the resultant of all their magnetic moments. (a) In the absence of an externally applied field, there are equal numbers of α and β spins at random angles around the z-axis (the field direction) and the magnetization is zero. (b) In the presence of a field, the spins precess around their cones (that is, there is an energy difference between the α and β states) and there are slightly more α spins than β spins. As a result, there is a net magnetization along the z-axis.



18.28 (a) In a resonance experiment, a circularly polarized radiofrequency magnetic field B_1 is applied in the xy -plane (the magnetization vector lies along the z -axis). (b) If we step into a frame rotating at the Larmor frequency, the radiofrequency field appears to be stationary if its frequency is the same as the Larmor frequency. When the two frequencies coincide, the magnetization vector of the sample begins to rotate around the direction of the B_1 field.

unpredictable, and at this stage we picture the spin vectors as stationary. The magnetization, M , of the sample, its net nuclear magnetic moment, is zero (Fig. 18.27a).

(a) The effect of the static field

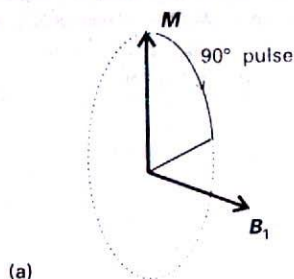
Two changes occur in the magnetization when a magnetic field is present. First, the energies of the two orientations change, the α spins moving to low energy and the β spins to high energy (provided $\gamma > 0$). At 10 T, the Larmor frequency for protons is 427 MHz, and in the vector model the individual vectors are pictured as **precessing**, or sweeping round their cones, at this rate. This motion is a pictorial representation of the change in energy of the spin states (it is not an actual representation of reality). As the field is increased, the Larmor frequency increases and the precession becomes faster. Secondly, the populations of the two spin states (the numbers of α and β spins) change, and there will be more α spins than β spins. Because $h\nu_L/kT \approx 7 \times 10^{-5}$ for protons at 300 K and 10 T, there is only a tiny imbalance of populations, and it is even smaller for other nuclei with their smaller magnetogyric ratios. However, despite its smallness, the imbalance means that there is a net magnetization that we can represent by a vector M pointing in the z -direction and with a length proportional to the population difference (Fig. 18.27b).

(b) The effect of the radiofrequency field

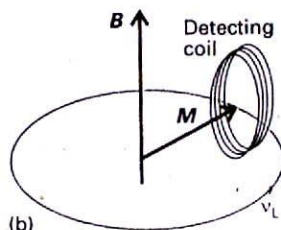
We now consider the effect of a circularly polarized radiofrequency field in the xy -plane. We have considered the electric component of this field in the other forms of spectroscopy that we have treated. However, in this chapter we consider only the magnetic component, for it is this component that interacts with the nuclear magnetic moment. The strength of the oscillating magnetic field is B_1 .

Suppose we choose the frequency of the oscillating field to be equal to the Larmor frequency of the spins. This choice is equivalent to selecting the resonance condition in the conventional experiment. The nuclei now experience a steady B_1 field because the rotating magnetic field is in step with the precessing spins (Fig. 18.28). Under the influence of this effectively steady field, the magnetization vector begins to precess around the direction of B_1 at a rate that is proportional to B_1 . If we apply the B_1 field in a pulse of a certain duration, the magnetization precesses into the xy -plane, and we say that we have applied a 90° pulse (or a ' $\pi/2$ pulse'). The duration of the pulse depends on the strength of the B_1 field, but is typically of the order of microseconds. To a stationary external observer (a radiofrequency coil, Fig. 18.29), the magnetization vector is now rotating in the xy -plane at the Larmor frequency (at about 430 MHz). The rotating magnetization induces a 430 MHz signal in the coil, which can be amplified and processed. In practice, the processing takes place after subtraction of a constant high-frequency component, so that all the signal manipulation takes place at frequencies of a few kilohertz.

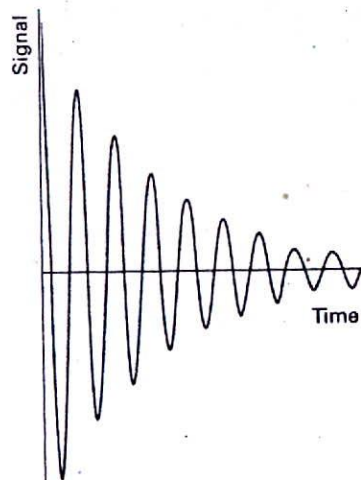
As time passes, the individual spins move out of step (partly because they are precessing at slightly different rates, as we shall explain later), so the magnetization vector shrinks exponentially with a time constant T_2 and induces an ever weaker signal in the detector coil. The form of the signal that we can expect is therefore the oscillating-decaying free-induction decay (FID) shown in Fig. 18.30, and the y -component of the magnetization



(a)

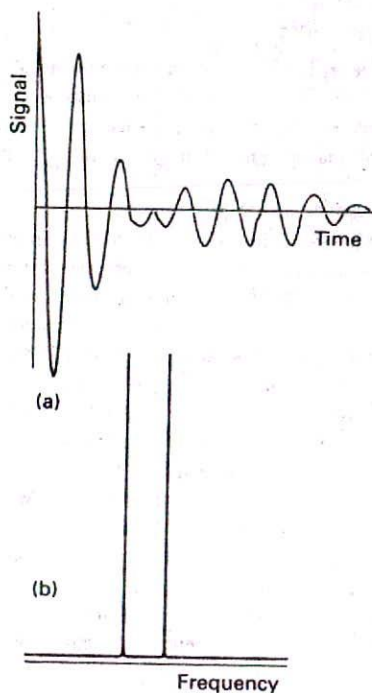


(b)



18.29 (a) If the radiofrequency field is applied for a certain time, the magnetization vector is rotated into the xy -plane. (b) To an external stationary observer (the coil), the magnetization vector is rotating at the Larmor frequency, and can induce a signal in the coil.

18.30 A simple free induction decay of a sample of spins with a single resonance frequency.



18.31 (a) A free induction decay signal of a sample of AX species and (b) its analysis into its frequency components.

varies as

$$M_y(t) = M_0 \cos(2\pi\nu_L t) e^{-t/T_2} \quad (25)$$

We have considered the effect of a pulse applied at exactly the Larmor frequency. However, virtually the same effect is obtained off resonance, provided that the pulse is applied close to ν_L . If the difference in frequency is small compared to the inverse of the duration of the 90° pulse, the magnetization will end up in the xy -plane. Note that we do not need to know the Larmor frequency beforehand: the short pulse is the analogue of the hammer blow on the bell, exciting a range of frequencies. The detected signal shows that a particular resonant frequency is present.

(c) Time- and frequency-domain spectra

We can think of the magnetization vector of a homonuclear AX spin system with $J = 0$ as consisting of two parts, one formed by the A spins and the other by the X spins. When the 90° pulse is applied, both magnetization vectors are rotated into the xy -plane. However, because the A and X nuclei precess at different frequencies, they induce two signals in the detector coils, and the overall FID curve may resemble that in Fig. 18.31a. The composite FID curve is the analogue of the struck bell emitting a rich tone composed of all the frequencies at which it can vibrate.

The problem we must address is how to recover the resonance frequencies present in a free-induction decay. We encountered a similar problem when discussing Fourier-transform infrared spectra in Section 16.1c, where all the vibrational frequencies were detected at once. The same technique is used here. We know that the FID curve is a sum of oscillating functions, so the problem is to analyse it into its harmonic components.

The analysis of the FID curve is achieved by the standard mathematical technique of Fourier transformation. We start by noting that the signal $S(t)$ in the time domain, the total FID curve, is the sum (more precisely, the integral) over all the contributing frequencies⁶

$$S(t) = \int_{-\infty}^{\infty} I(\nu) e^{-2\pi i \nu t} d\nu \quad (26)$$

We need $I(\nu)$, the spectrum in the frequency domain; it is obtained by evaluating the integral

$$I(\nu) = 2\text{Re} \int_0^{\infty} S(t) e^{2i\pi\nu t} dt \quad (27)$$

where Re means take the real part of the following expression. This integral is very much like an overlap integral: it gives a nonzero value if $S(t)$ contains a component that matches the oscillating function $e^{2i\pi\nu t}$. The integration is carried out at a series of frequencies ν on a computer that is built into the spectrometer. When the signal in Fig. 18.31a is transformed in this way, we get the frequency-domain spectrum shown in Fig. 18.31b. One line represents the Larmor frequency of the A nuclei and the other that of the X nuclei.

The FID curve in Fig. 18.32 is obtained from a sample of ethanol. The frequency-domain spectrum obtained from it by Fourier transformation is the one that we have already discussed (Fig. 18.4). We can now see why the FID curve in Fig. 18.32 is so complex: it arises from the precession of a magnetization vector that is composed of eight components, each with a characteristic frequency.

⁶ Because $e^{2\pi i \nu t} = \cos(2\pi\nu t) + i \sin(2\pi\nu t)$, this expression is a sum over harmonically oscillating functions, with each one weighted by the intensity $I(\nu)$.



18.32 A free induction decay signal of a sample of ethanol. Its Fourier transform is the frequency-domain spectrum shown in Fig. 18.4.

18.6 Linewidths and rate processes

The linewidths of NMR spectra, in common with other spectroscopic techniques, provide information about the rates of processes relating to the molecules in the sample. We have seen that the FID signal decreases with time, which implies that the component of the magnetization vector in the xy -plane must be shrinking. In this section we see some of the processes involved.

(a) Spin relaxation

There are two reasons why the component of the magnetization vector in the xy -plane shrinks. Both reflect the fact that the nuclear spins are not in thermal equilibrium with their surroundings (for then M lies parallel to z). The return to equilibrium is the process called **spin relaxation**.

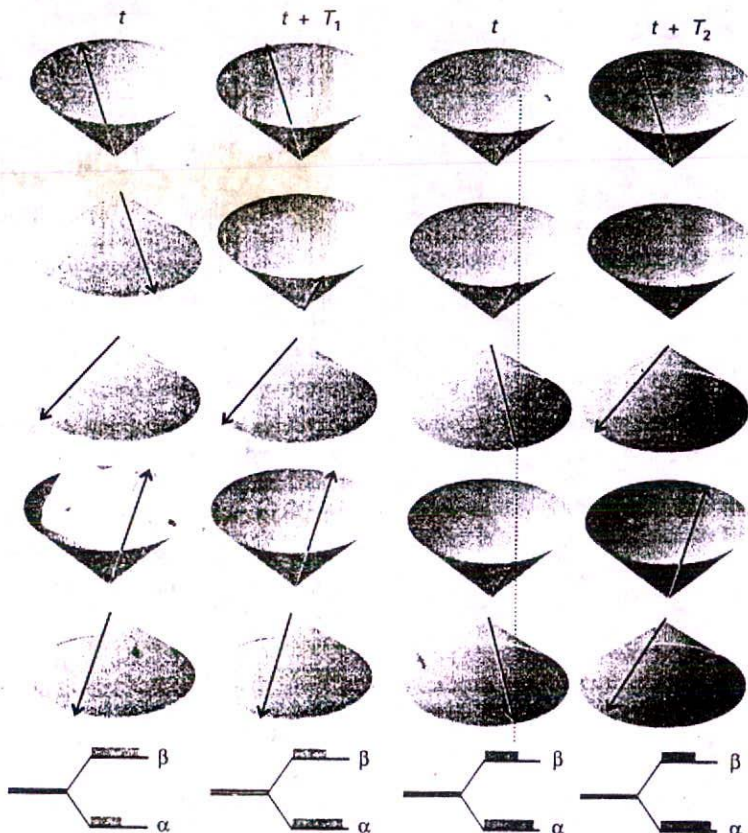
At thermal equilibrium the spins have a Boltzmann distribution, with more α spins than β spins; however, a magnetization vector in the xy -plane immediately after a 90° pulse has equal numbers of α and β spins. The populations revert to their thermal equilibrium values exponentially. As they do so, the z -component of magnetization reverts to its equilibrium value M_0 with a time constant called the **longitudinal relaxation time**, T_1 (Fig. 18.33):

$$M_z(t) - M_0 \propto e^{-t/T_1} \quad (28)$$

Because this relaxation process involves giving up energy to the surroundings (the 'lattice') as β spins revert to α spins, the time constant T_1 is also called the **spin-lattice relaxation time**. Spin-lattice relaxation is caused by fluctuating local magnetic fields arising from the motion of the molecules. These fluctuations can stimulate the spins to change from β to α , and vice versa, and hence to relax towards the thermal equilibrium population.

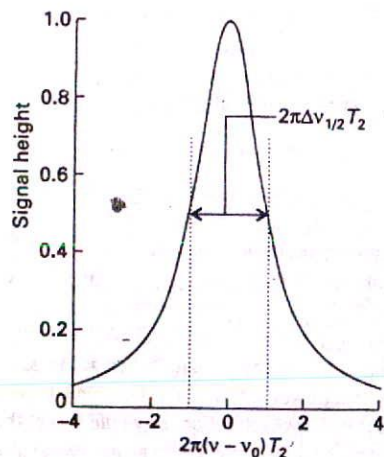
A second aspect of spin relaxation is the fanning-out of the spins in the xy -plane if they precess at different rates (Fig. 18.34). The magnetization vector is large when all the spins are bunched together immediately after a 90° pulse. However, this orderly bunching of spins is not at equilibrium and, even if there were no spin-lattice relaxation, we would expect the individual spins to spread out until they were uniformly distributed with all possible angles around the z -axis. At that stage, the component of magnetization vector in the plane would be zero. The randomization of the spin directions occurs exponentially with a time constant called the **transverse relaxation time**, T_2 :

$$M_y(t) \propto e^{-t/T_2} \quad (29)$$



18.33 In longitudinal relaxation the spins relax back towards their thermal equilibrium populations. On the left we see the precessional cones representing spin- $\frac{1}{2}$ angular momenta, and they do not have their thermal equilibrium populations (there are more β -spins than α -spins). On the right, which represents the sample after a time T_1 , the populations are those characteristic of a Boltzmann distribution.

18.34 The transverse relaxation time, T_2 , is the time it takes for the phases of the spins to become randomized (another condition for equilibrium) and to change from the orderly arrangement shown on the left to the disorderly arrangement on the right. Note that the populations of the states remain the same; only the relative phase of the spins relaxes.



18.35 A Lorentzian absorption line. The width at half-height is inversely proportional to the parameter T_2 (so $\Delta\nu_{1/2}T_2$ is a constant) and, the longer the transverse relaxation time, the narrower the line.

Because the relaxation involves the relative orientation of the spins, T_2 is also known as the spin-spin relaxation time.

If the y-component of magnetization decays with a time constant T_2 , the spectral line is broadened (Fig. 18.35), and its width at half-height becomes

$$\Delta\nu_{1/2} = \frac{1}{\pi T_2} \quad (30)$$

Typical values of T_2 in proton NMR are of the order of seconds, so linewidths of around 0.1 Hz can be anticipated, in broad agreement with observation. In mobile liquids, $T_2 \approx T_1$.

So far, we have assumed that the equipment, and in particular the magnet, are perfect, and that the differences in Larmor frequencies arise solely from interactions within the sample. In practice, the magnet is not perfect, and the field is different at different locations in the sample. The inhomogeneity broadens the resonance, and in most cases this

inhomogeneous broadening dominates the broadening we have discussed so far. It is common to express the extent of inhomogeneous broadening in terms of an effective transverse relaxation time, T_2^* , by using a relation like eqn 30, but writing

$$T_2^* = \frac{1}{\pi \Delta\nu_{1/2}} \quad (31)$$

where $\Delta\nu_{1/2}$ is the observed width at half-height.⁷

Illustration

If a line in a spectrum has a width of 10 Hz, the effective transverse relaxation time is

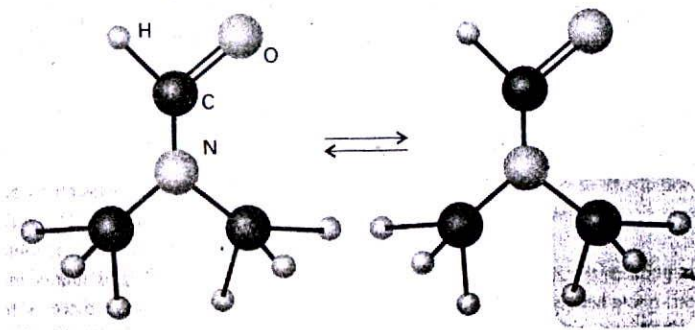
$$T_2^* = \frac{1}{\pi \times (10 \text{ s}^{-1})} = 32 \text{ ms}$$

(b) Conformational conversion and exchange processes

The appearance of an NMR spectrum is changed if magnetic nuclei can jump rapidly between different environments. Consider a fluxional molecule, such as *N,N*-dimethylformamide, that can jump between conformations; in its case, the methyl shifts depend on whether they are *cis* or *trans* to the carbonyl group. (Fig. 18.36). When the jumping rate is low, the spectrum shows two sets of lines, one each from molecules in each conformation. When the inversion is fast, the spectrum shows a single line at the mean of the two chemical shifts. At intermediate inversion rates, the line is very broad. This maximum broadening occurs when the lifetime, τ , of a conformation gives rise to a linewidth that is comparable to the difference of resonance frequencies, $\delta\nu$, and both broadened lines blend together into a very broad line. Coalescence of the two lines occurs when

$$\tau = \frac{\sqrt{2}}{\pi \delta\nu} \quad (32)$$

For example, if the chemical shifts differ by 100 Hz, the spectrum collapses into a single line when the conformation lifetime is less than about 5 ms.



18.36 When a molecule changes from one conformation to another, the positions of its protons are interchanged and jump between magnetically distinct environments.

⁷ This formula assumes that the lineshape is Lorentzian; that is, of the form $y = 1/(1 + x^2)$.

Example 18.3 Interpreting line broadening

The NO group in *N,N*-dimethylnitrosamine, $(\text{CH}_3)_2\text{N}-\text{NO}$, rotates and, as a result, the magnetic environments of the two CH_3 groups are interchanged. In a 600 MHz spectrometer the two CH_3 resonances are separated by 390 Hz. At what rate of interconversion will the resonance collapse to a single line?

Method Use eqn 32 for the average lifetimes of the conformations. The rate of interconversion is the inverse of their lifetime.

Answer With $\delta\nu = 390$ Hz,

$$\tau = \frac{\sqrt{2}}{\pi \times (390 \text{ s}^{-1})} = 1.2 \text{ ms}$$

It follows that the signal will collapse to a single line when the interconversion rate exceeds about 830 s^{-1} .

Comment The dependence of the rate of collapse on the temperature is used to determine the energy barrier to interconversion.

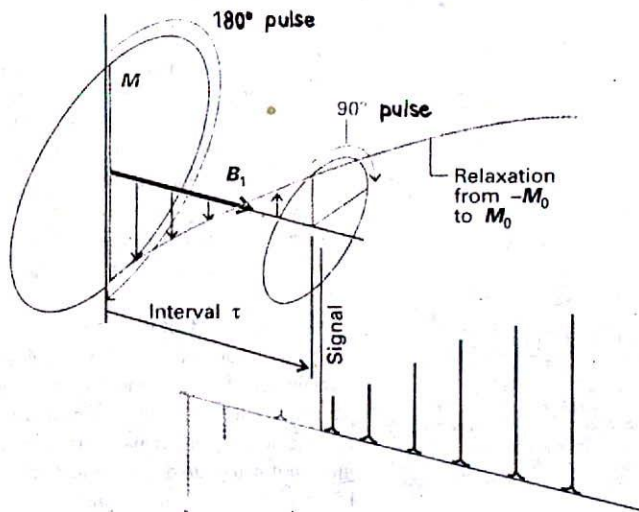
Self-test 18.3 What would you deduce from the observation of a single line from the same molecule in a 300 MHz spectrometer?

[Conformation lifetime less than 2.3 ms]

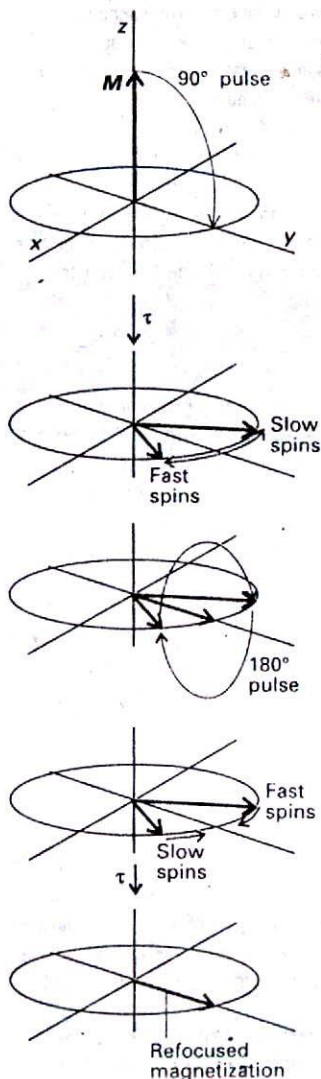
A similar explanation accounts for the loss of structure in solvents able to exchange protons with the sample. For example, hydroxyl protons are able to exchange with water protons. When this chemical exchange occurs, a molecule ROH with an α -spin proton (we write this ROH_α) rapidly converts to ROH_β and then perhaps to ROH_α again because the protons provided by the solvent molecules in successive exchanges have random spin orientations. Therefore, instead of seeing a spectrum composed of contributions from both ROH_α and ROH_β molecules (that is, a spectrum showing a doublet structure due to the OH proton), we see a single, unsplit line at the mean position (as in Fig. 18.4). The effect is observed when the lifetime of a molecule due to this chemical exchange is so short that the lifetime broadening is greater than the doublet splitting. Because this splitting is often very small (about 1 Hz), a proton must remain attached to the same molecule for longer than about 0.1 s for the splitting to be observable. In water, the exchange rate is much faster than that, so alcohols show no splitting from the OH protons. In dry dimethylsulfoxide (DMSO), the exchange rate may be slow enough for the splitting to be detected.

(c) The measurement of T_1

The longitudinal relaxation time can be measured by the inversion recovery technique. The first step is to apply a 180° pulse to the sample. A 180° pulse is achieved by applying the B_1 field for twice as long as for a 90° pulse, so the magnetization vector precesses through 180° and points in the $-z$ direction (Fig. 18.37). No signal can be seen at this stage because there is no component of magnetization in the xy -plane (where the detection coils are sensitive). The β spins begin to relax back into α spins, and the magnetization vector shrinks exponentially back towards its thermal equilibrium value, M_z . After an interval τ , a 90° pulse is applied that rotates the magnetization into the xy -plane, where it starts to generate an FID signal. The frequency-domain spectrum is then obtained by Fourier transformation.



18.37 The result of applying a 180° pulse to the magnetization in the rotating frame and the effect of a subsequent 90° pulse. The amplitude of the frequency-domain spectrum varies with the interval between the two pulses because spin-lattice relaxation has time to occur.



18.38 The sequence of pulses leading to the observation of a spin echo (see text).

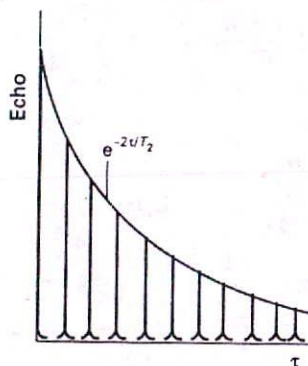
The intensity of the spectrum obtained in this way depends on the length of the magnetization vector that is rotated into the xy -plane. The length of that vector returns exponentially to its thermal equilibrium value as the interval between the two pulses is increased, so the intensity of the spectrum also returns exponentially to its equilibrium intensity with increasing τ . We can therefore measure T_1 by fitting an exponential curve to the series of spectra obtained after different values of τ .

(d) Spin echoes

The measurement of T_2 (as distinct from T_2^*) depends on being able to eliminate the effects of inhomogeneous broadening. The cunning required is at the root of some of the most important advances that have been made in NMR since its introduction.

A spin echo is the magnetic analogue of an audible echo: transverse magnetization is created by a radiofrequency pulse, decays away, is reflected by a second pulse, and grows back to form an echo. The sequence of events is illustrated in Fig. 18.38. We can consider the overall magnetization as being made up of a number of different magnetizations, each of which arises from a spin packet of nuclei with very similar precession frequencies. The spread in these frequencies arises because the applied field B_0 is inhomogeneous, so different parts of the sample experience different fields. The precession frequencies also differ if there is more than one chemical shift present. As will be seen, the importance of a spin echo is that it can suppress the effects of both field inhomogeneities and chemical shifts.

First, a 90° pulse is applied to the sample. The frame of reference is rotating at the same rate as the radiofrequency magnetic field of the pulse, with B_1 applied along the x -axis, so the magnetization is rotated down into the xy -plane. The spin packets now begin to fan out because they have different Larmor frequencies, with some above the radiofrequency and some below. The detected signal depends on the resultant of the spin-packet magnetization vectors, and decays with a time constant T_2^* because of the combined effects of field inhomogeneity and spin-spin relaxation.



18.39 The exponential decay of the spin echoes can be used to determine the transverse relaxation time.

After an interval τ , a 180° pulse is applied to the sample; this time, about the y -axis of the rotating frame.⁸ The pulse rotates the magnetization vectors of the faster spin packets into the positions previously occupied by the slower spin packets, and vice versa. Thus, as the vectors continue to precess, the fast vectors are now behind the slow; the fan begins to close up again, and the resultant signal begins to grow back into an echo. At time 2τ , all the vectors will once more be aligned along the y -axis, and the fanning out caused by the field inhomogeneity is said to have been refocused; the spin echo has reached its maximum. Because the effects of field inhomogeneities have been suppressed by the refocusing, the echo signal will have been attenuated by the factor $e^{-2\tau/T_2}$ caused by spin-spin relaxation alone. After the time 2τ , the magnetization will continue to precess, fanning out once again, giving a resultant that decays with time constant T_2^* .

The important feature of the technique is that the size of the echo is independent of any local fields that remain constant during the two τ intervals. If a spin packet is 'fast' because it happens to be composed of spins in a region of the sample that experiences higher than average fields, then it remains fast throughout both intervals, and what it gains on the first interval it makes up on the second interval. Hence, the size of the echo is independent of inhomogeneities in the magnetic field, for these remain constant. The true transverse relaxation arises from fields that fluctuate on a molecular timescale, and there is no guarantee that an individual 'fast' spin will remain 'fast' in the refocusing phase: the spins within the packets therefore spread with a time constant T_2 . Hence, the effects of the true relaxation are not refocused, and the size of the echo decays with the time constant T_2 (Fig. 18.39).

18.7 The nuclear Overhauser effect

Spin relaxation can be used constructively to enhance the intensities of resonance lines. The enhancement is brought about by the nuclear Overhauser effect (NOE) which we shall explain by considering a simple AX system in which A is a ^{13}C nucleus and X is a proton.

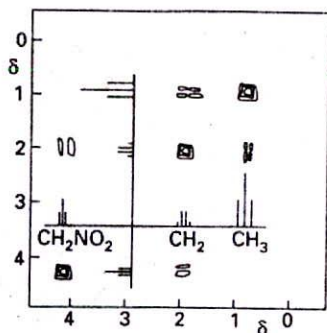
We have seen already that one advantage of protons in NMR is their high magnetogyric ratio, which results in relatively large Boltzmann population differences and hence appreciable resonance intensities. In the nuclear Overhauser effect, relaxation processes involving internuclear dipole-dipole interactions are used to transfer this population advantage to another nucleus (to ^{13}C in the case we are considering), so that the latter's resonances are enhanced. A detailed calculation (which we do not reproduce here) shows that, if the relaxation of a nucleus A is dominated by its dipolar interaction with a nucleus X, and X is saturated by strong irradiation at its resonance frequency, then the signal enhancement is

$$\frac{\mathcal{I}_A}{\mathcal{I}_A^0} = 1 + \frac{\gamma_X}{2\gamma_A} \quad (33)$$

where \mathcal{I}_J is the signal intensity of nucleus J. For ^{13}C coupled to a saturated proton, the ratio evaluates to 2.99, which shows that an enhancement of about a factor of 3 can be achieved.

The NOE is also used to determine interproton distances. The Overhauser enhancement of a proton A generated by saturating a spin X depends on the fraction of A's spin-lattice relaxation that is caused by its dipolar interaction with X. Because the dipolar field is proportional to r^{-3} , where r is the internuclear distance, and the relaxation effect is proportional to the square of the field, and therefore to r^{-6} , the NOE may be used to determine the geometries of molecules in solution. The determination of the structure of a small protein in solution involves the use of several hundred NOE measurements, effectively casting a net over the protons present.

⁸ The axis of the pulse is changed from x to y by a 90° phase shift of the radiofrequency radiation.



18.40 A typical two-dimensional ^{13}C -NMR spectrum obtained by correlation spectroscopy. The sample is l-nitropropane. Diagonal peaks show the normal one-dimensional spectrum, and cross-peaks at (δ_A, δ_X) appear where A and X are coupled. (Spectrum provided by Dr G. Morris.)

18.8 Two-dimensional NMR

An NMR spectrum contains a great deal of information and, if many protons are present, is very complex. Even a first-order spectrum is complex, for the fine structure of different groups of lines can overlap. The complexity would be reduced if we could use two axes to display the data, with resonances belonging to different groups lying at different locations on the second axis. This separation is essentially what is achieved in two-dimensional NMR.

We have seen that a spin-echo experiment refocuses spins that are in a constant environment. Hence, if two spins are in environments with different chemical shifts, they will be refocused and a single line will be obtained. That is, we can eliminate chemical shifts from a spectrum. Since we saw earlier that we can also remove the effects of spin-spin coupling by decoupling techniques, we can separate the two contributions to the spectrum. In practice, a clever choice of pulses and Fourier transformation techniques makes it possible to display spin coupling in one dimension and the chemical shifts in another, and so greatly simplify the appearance of a spectrum.

Much modern NMR work makes use of correlation spectroscopy (COSY) in which the basic pulse sequence is $90_x^\circ - t_1 - 90_x^\circ - \text{acquire } (t_2)$. A series of acquisitions is taken with a variable delay t_1 , much as in a spin-echo experiment. The double Fourier transform is then performed on the real time-domain variable t_2 and then on the interferograms arising from the time delay t_1 . A typical outcome for an AX system is shown in Fig. 18.40: the diagram shows contours of equal signal intensity.

The detailed analysis of the appearance of the contour plot is quite difficult, and a simple vector diagram of the processes involved cannot be given. However, the general rules of interpretation are quite straightforward (in simple cases, at least). The peaks across the diagonal constitute the normal four peaks of a one-dimensional NMR spectrum of an AX system, so they add nothing new. The interesting information is in the off-diagonal peaks, for they indicate that the protons to which they correlate by vertical and horizontal lines are spin-spin coupled. Although this information is trivial in this AX system, it can be of enormous help in the interpretation of more complex spectra. A complex spectrum that would be impossible to interpret in one-dimensional NMR can be interpreted reasonably rapidly by two-dimensional NMR. The techniques themselves are described in the books listed in *Further reading* at the end of the chapter.

18.9 Solid-state NMR

The principal difficulty with the application of NMR to solids is the low resolution that is characteristic of solid samples. Nevertheless, there are good reasons for seeking to overcome these difficulties. They include the possibility that a compound of interest is unstable in solution or that it is insoluble, so conventional solution NMR cannot be employed. Moreover, many species are intrinsically interesting as solids, and it is important to determine their structures and dynamics. Synthetic polymers are particularly interesting in this regard, and information can be obtained about the arrangement of molecules, their conformations, and the motion of different parts of the chain. This kind of information is crucial to an interpretation of the bulk properties of the polymer in terms of its molecular characteristics. Similarly, inorganic substances, such as the zeolites that are used as molecular sieves and shape-selective catalysts, can be studied using solid-state NMR, and structural problems can be resolved that cannot be tackled by X-ray diffraction.

Problems of resolution and linewidth are not the only features that plague NMR studies of solids. Because molecular rotation has almost ceased (except in special cases, including 'plastic crystals' in which the molecules continue to tumble), spin-lattice relaxation times are very long but spin-spin relaxation times are very short. Hence, in a pulse experiment,

there need to be lengthy delays—of several seconds—between successive pulses so that the spin system has time to revert to equilibrium. Even gathering the murky information may therefore be a lengthy process. Moreover, because lines are so broad, very high powers of radiofrequency radiation may be required to achieve saturation. Whereas solution pulse NMR uses transmitters of a few tens of watts, solid-state NMR may require transmitters rated at several hundreds of watts.

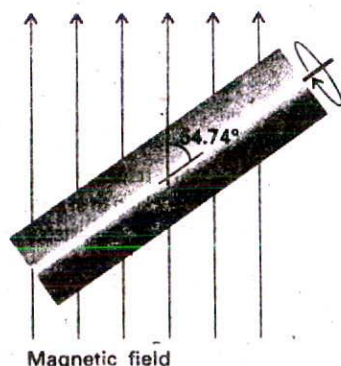
(a) The origins of linewidths in solids

There are two principal contributions to the linewidths of solids. One is the direct magnetic dipolar interaction between nuclear spins. As we saw in the discussion of spin-spin coupling, a nuclear magnetic moment will give rise to a local magnetic field

$$B_{\text{loc}} = -\frac{\gamma\hbar\mu_0 m_I}{4\pi R^3} (1 - 3\cos^2\theta) \quad (34)$$

Unlike in solution, this field is not motionally averaged to zero. Many nuclei may contribute to the total local field experienced by a nucleus of interest, and different nuclei in a sample may experience a wide range of fields. Typical dipole-dipole fields are of the order of 10^{-3} T, which corresponds to splittings and linewidths of the order of 10^6 Hz.

A second source of linewidth is the anisotropy of the chemical shift. We have seen that chemical shifts arise from the ability of the applied field to generate electron currents in molecules. In general, this ability depends on the orientation of the molecule relative to the applied field. In solution, when the molecule is tumbling rapidly, only the average value of the chemical shift is relevant. However, the anisotropy is not averaged to zero for stationary molecules in a solid, and molecules in different orientations have resonances at different frequencies. The chemical shift anisotropy also varies with the angle between the applied field and the principal axis of the molecule as $1 - 3\cos^2\theta$.

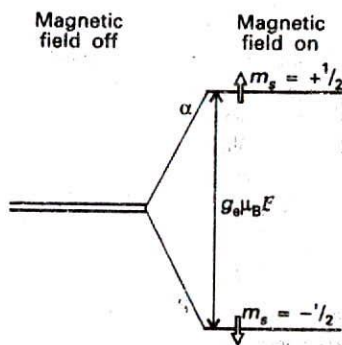


18.41 In magic angle spinning, the sample spins at 54.74° (that is, $\arccos 1/3^{1/2}$) to the applied magnetic field. Rapid motion at this angle averages dipole-dipole interactions and chemical shift anisotropies to zero.

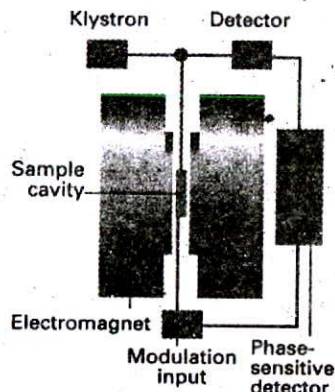
(b) The reduction of linewidths

Fortunately, there are techniques available for reducing the linewidths of solid samples. One technique, magic-angle spinning (MAS), takes note of the $1 - 3\cos^2\theta$ dependence of both the dipole-dipole interaction and the chemical shift anisotropy. The 'magic angle' is the angle at which $1 - 3\cos^2\theta = 0$, and corresponds to 54.74° . In the technique, the sample is spun at high speed at the magic angle to the applied field (Fig. 18.41). All the dipolar interactions and the anisotropies average to the value they would have at the magic angle, but at that angle they are zero. The difficulty with MAS is that the spinning frequency must not be less than the width of the spectrum, which is of the order of kilohertz. However, gas-driven sample spinners that can be rotated at up to 25 kHz are now routinely available, and a considerable body of work has been done.

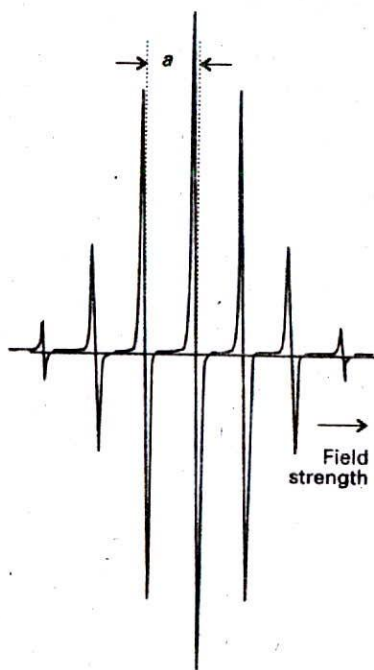
The saturation and pulse techniques that we have described earlier in this section may also be used to reduce linewidths. The dipolar field of protons, for instance, may be reduced by a decoupling procedure. However, because the range of coupling strengths is so large, radiofrequency power of the order of 1 kW is required. Elaborate pulse sequences have also been devised that reduce linewidths by averaging procedures that make use of twisting the magnetization vector through an elaborate series of angles.



18.42 Electron spin levels in a magnetic field. Note that the β state is lower in energy than the α state (because the magnetogyric ratio of an electron is negative). Resonance is achieved when the frequency of the incident radiation matches the frequency corresponding to the energy separation.



18.43 The layout of an ESR spectrometer. A typical magnetic field is 0.3 T, which requires 9 GHz (3 cm) microwaves for resonance.



18.44 The ESR spectrum of the benzene radical anion, $C_6H_6^-$, in fluid solution. a is the hyperfine splitting of the spectrum; the centre of the spectrum is determined by the g -value of the radical.

Electron spin resonance

The energy levels of an electron spin in a magnetic field B (Fig. 18.42) are

$$E_{m_s} = g_e \mu_B B m_s \quad m_s = \pm \frac{1}{2} \quad (35)$$

where μ_B is the Bohr magneton and $g_e = 2.0023$ (Section 13.10a). This equation shows that the energy of an α electron ($m_s = +\frac{1}{2}$) increases and the energy of a β electron ($m_s = -\frac{1}{2}$) decreases as the field is increased, and that the separation of the levels is

$$\Delta E = E_\beta - E_\alpha = g_e \mu_B B \quad (36)$$

When the sample is exposed to electromagnetic radiation of frequency ν , resonant absorption occurs when the resonance condition

$$h\nu = g_e \mu_B B \quad (37)$$

is fulfilled. Electron spin resonance (ESR), or electron paramagnetic resonance (EPR), is the study of molecules and ions containing unpaired electrons by observing the magnetic fields at which they come into resonance with monochromatic radiation. Magnetic fields of about 0.3 T (the value used in most commercial ESR spectrometers) correspond to resonance with an electromagnetic field of frequency 10 GHz (10^{10} Hz) and wavelength 3 cm. Because 3 cm radiation falls in the X-band of the microwave region of the electromagnetic spectrum, ESR is a microwave technique.

The layout of an ESR spectrometer is shown in Fig. 18.43. It consists of a microwave source (a klystron), a cavity in which the sample is inserted in a glass or quartz container, a microwave detector, and an electromagnet with a field that can be varied in the region of 0.3 T. The ESR spectrum is obtained by monitoring the microwave absorption as the field is changed, and a typical spectrum (of the benzene radical anion, $C_6H_6^-$) is shown in Fig. 18.44. The peculiar appearance of the spectrum, which is in fact the first derivative of the

absorption, arises from the detection technique, which is sensitive to the slope of the absorption curve (Fig. 18.45).

The sample must possess unpaired electron spins, so ESR is less widely applicable than NMR. It is used to study radicals formed during chemical reactions or by radiation, many *d*-metal complexes, and molecules in triplet states (such as those involved in phosphorescence, Section 17.3b). It is insensitive to normal, spin-paired molecules. The sample may be a gas, a liquid, or a solid, but the free rotation of molecules in the gas phase gives rise to complications.

18.10 The *g*-value

As in NMR, the spin magnetic moment interacts with the local magnetic field, and the resonance condition is normally written

$$h\nu = g\mu_B B \quad (38)$$

where *g* is the *g*-value of the radical or complex.

Illustration

The centre of the ESR spectrum of the methyl radical occurred at 329.40 mT in a spectrometer operating at 9.2330 GHz. Its *g*-value is therefore

$$g = \frac{h\nu}{\mu_B B} = \frac{(6.626\ 08 \times 10^{-34}\ \text{J s}) \times (9.2330 \times 10^9\ \text{s}^{-1})}{(9.2740 \times 10^{-24}\ \text{J T}^{-1}) \times (0.32940\ \text{T})} = 2.0027$$

Comment Many organic radicals have *g*-values close to 2.0027; inorganic radicals have *g*-values typically in the range 1.9 to 2.1; *d*-metal complexes have *g*-values in a wider range (for example, 0 to 4).

Self-test 18.4 At what magnetic field would the methyl radical come into resonance in a spectrometer operating at 9.468 GHz?

[337.8 mT]

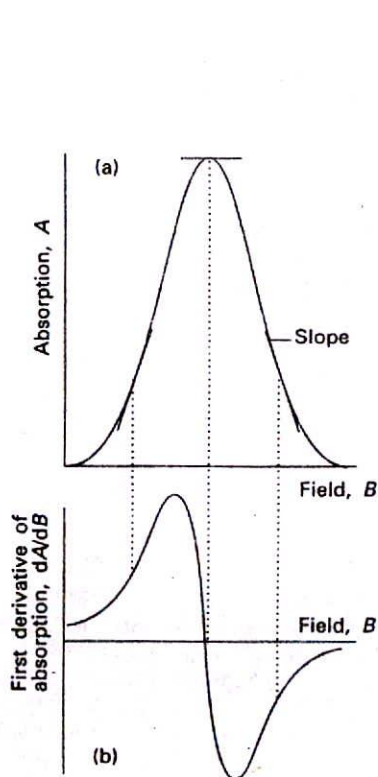
The deviation of *g* from $g_e = 2.0023$ depends on the ability of the applied field to induce local electron currents in the radical, and therefore its value gives some information about electronic structure. However, because *g*-values differ very little from g_e in many radicals (for example, 2.003 for H, 1.999 for NO₂, 2.01 for ClO₂), its main use in chemical applications is to aid the identification of the species present in a sample.

18.11 Hyperfine structure

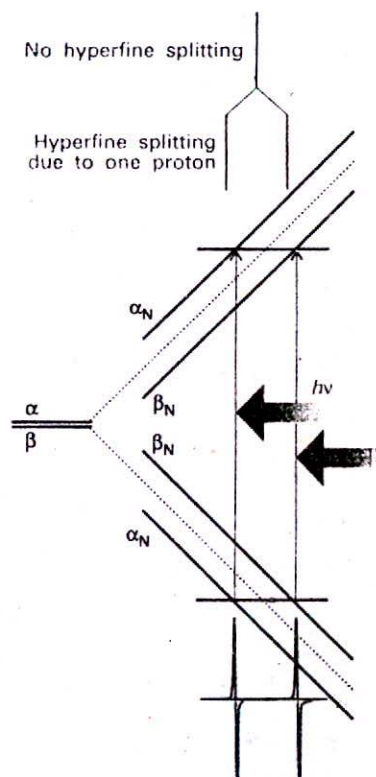
The most important feature of ESR spectra is their hyperfine structure, the splitting of individual resonance lines into components. In general in spectroscopy, the term 'hyperfine structure' means the structure of a spectrum that can be traced to interactions of the electrons with nuclei other than as a result of the latter's point electric charge. The source of the hyperfine structure in ESR is the magnetic interaction between the electron spin and the magnetic dipole moments of the nuclei present in the radical.

(a) The effects of nuclear spin

Consider the effect on the ESR spectrum of a single H nucleus located somewhere in a radical. The proton spin is a source of magnetic field and, depending on the orientation of



18.45 When phase-sensitive detection is used, the signal is the first derivative of the absorption intensity. (a) The absorption; (b) the signal, the slope of the absorption signal at each point. Note that the peak of the absorption corresponds to the point where the derivative passes through zero.



18.46 The hyperfine interaction between an electron and a spin- $\frac{1}{2}$ nucleus results in four energy levels in place of the original two. As a result, the spectrum consists of two lines (of equal intensity) instead of one. The intensity distribution can be summarized by a simple stick diagram. The diagonal lines show the energies of the states as the applied field is increased, and resonance occurs when the separation of states matches the fixed energy of the microwave photon.

the nuclear spin, the field it generates adds to or subtracts from the applied field. The total local field is therefore

$$B_{\text{loc}} = B + am_I \quad m_I = \pm \frac{1}{2} \quad (39)$$

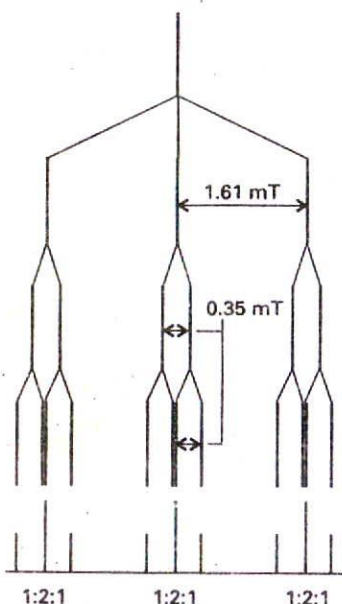
where a is the hyperfine coupling constant. Half the radicals in a sample have $m_I = +\frac{1}{2}$, so half resonate when the applied field satisfies the condition

$$h\nu = g\mu_B(B + \frac{1}{2}a), \quad \text{or } B = \frac{h\nu}{g\mu_B} - \frac{1}{2}a \quad (40a)$$

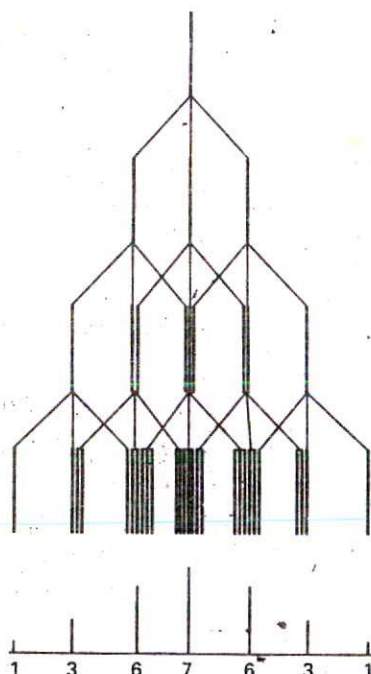
The other half (which have $m_I = -\frac{1}{2}$) resonate when

$$h\nu = g\mu_B(B - \frac{1}{2}a), \quad \text{or } B = \frac{h\nu}{g\mu_B} + \frac{1}{2}a \quad (40b)$$

Therefore, instead of a single line, the spectrum shows two lines of half the original intensity separated by a and centred on the field determined by g (Fig. 18.46).



18.47 The analysis of the hyperfine structure of radicals containing one ^{14}N nucleus ($I = 1$) and two equivalent protons.



18.48 The analysis of the hyperfine structure of radicals containing three equivalent ^{14}N nuclei.

If the radical contains an ^{14}N atom ($I = 1$), its ESR spectrum consists of three lines of equal intensity, because the ^{14}N nucleus has three possible spin orientations, and each spin orientation is possessed by one-third of all the radicals in the sample. In general, a spin- I nucleus splits the spectrum into $2I + 1$ hyperfine lines of equal intensity.

When there are several magnetic nuclei present in the radical, each one contributes to the hyperfine structure. In the case of equivalent protons (for example, the two CH_2 protons in the radical CH_2CH_2) some of the hyperfine lines are coincident. It is not hard to show that, if the radical contains N equivalent protons, then there are $N + 1$ hyperfine lines with a binomial intensity distribution (that is, the intensity distribution given by Pascal's triangle). The spectrum of the benzene radical anion in Fig. 18.44, which has seven lines with intensity ratio 1 : 6 : 15 : 20 : 15 : 6 : 1, is consistent with a radical containing six equivalent protons.

Example 18.4 Predicting the hyperfine structure of an ESR spectrum

A radical contains one ^{14}N nucleus ($I = 1$) with hyperfine constant 1.61 mT and two equivalent protons ($I = \frac{1}{2}$) with hyperfine constant 0.35 mT. Predict the form of the ESR spectrum.

Method We should consider the hyperfine structure that arises from each type of nucleus or group of equivalent nuclei in succession. So, split a line with one nucleus; then each of those lines is split by a second nucleus (or group of nuclei), and so on. It is best to start with the nucleus with the largest hyperfine splitting; however, any choice could be made, and the order in which nuclei are considered does not affect the conclusion.

Answer The ^{14}N nucleus gives three hyperfine lines of equal intensity separated by 1.61 mT. Each line is split into doublets of spacing 0.35 mT by the first proton, and each line of these doublets is split into doublets with the same 0.35 mT splitting (Fig. 18.47). The central lines of each split doublet coincide, so the proton splitting gives 1 : 2 : 1 triplets of internal splitting 0.35 mT. Therefore, the spectrum consists of three equivalent 1 : 2 : 1 triplets.

Comment Often it is quicker to realize that a group of equivalent protons gives a characteristic hyperfine pattern (two giving a 1 : 2 : 1 triplet, in this case), and to superimpose the patterns directly.

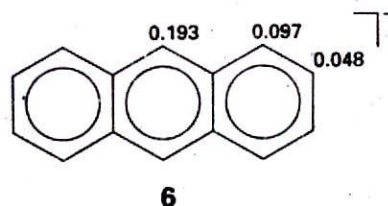
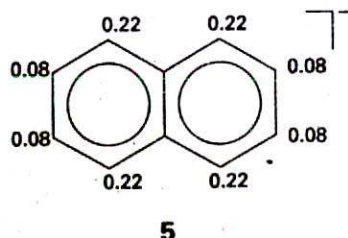
Self-test 18.5 Predict the form of the ESR spectrum of a radical containing three equivalent ^{14}N nuclei.

[Fig. 18.48]

The hyperfine structure of an ESR spectrum is a kind of fingerprint that helps to identify the radicals present in a sample. Moreover, because the magnitude of the splitting depends on the distribution of the unpaired electron near the magnetic nuclei present, the spectrum can be used to map the molecular orbital occupied by the unpaired electron. For example, because the hyperfine splitting in C_6H_6^- is 0.375 mT, and one proton is close to a C atom with one-sixth the unpaired electron spin density (because the electron is spread uniformly around the ring), the hyperfine splitting caused by a proton in the electron sp^2 entirely confined to a single adjacent C atom should be $6 \times 0.375 \text{ mT} = 2.25 \text{ mT}$. If in another aromatic radical we find a hyperfine splitting constant a , then the spin density, ρ , the probability that an unpaired electron is on the atom, can be calculated from the McConnell equation:

$$a = Q\rho$$

(41)



with $Q = 2.25$ mT. In this equation, ρ is the spin density on a C atom and a is the hyperfine splitting observed for the H atom to which it is attached.

Illustration

The hyperfine structure of the ESR spectrum of the radical anion (naphthalene)⁻ can be interpreted as arising from two groups of four equivalent protons. Those at the 1, 4, 5, and 8 positions in the ring have $a = 0.490$ mT and those in the 2, 3, 6, and 7 positions have $a = 0.183$ mT. The densities obtained by using the McConnell equation are 0.22 and 0.08, respectively (5).

Self-test 18.6 The spin density in (anthracene)⁻ is shown in (6). Predict the form of its ESR spectrum.

[A 1 : 2 : 1 triplet of splitting 0.43 mT split into a 1 : 4 : 6 : 4 : 1 quintet of splitting 0.22 mT, split into a 1 : 4 : 6 : 4 : 1 quintet of splitting 0.11 mT, $3 \times 5 \times 5 = 75$ lines in all]

(b) The origin of the hyperfine interaction

The hyperfine interaction is an interaction between the magnetic moments of the unpaired electron and the nuclei. There are two contributions to the interaction.

An electron in a p orbital does not approach the nucleus very closely, so it experiences a field that appears to arise from a point magnetic dipole. The resulting interaction is called the dipole-dipole interaction. The contribution of a magnetic nucleus to the local field experienced by the unpaired electron is given by an expression like that in eqn 34. A characteristic of this type of interaction is that it is anisotropic: that is, its magnitude (and sign) depends on the orientation of the radical with respect to the applied field. Furthermore, just as in the case of NMR, the dipole-dipole interaction averages to zero when the radical is free to tumble. Therefore, hyperfine structure due to the dipole-dipole interaction is observed only for radicals trapped in solids.

An s electron is spherically distributed around a nucleus and so has zero average dipole-dipole interaction with the nucleus even in a solid sample. However, because an s electron has a nonzero probability of being at the nucleus, it is incorrect to treat the interaction as one between two point dipoles. An s electron has a Fermi contact interaction with the nucleus, which as we saw in Section 18.4d is a magnetic interaction that occurs when the point dipole approximation fails. The contact interaction is isotropic (that is, independent of the radical's orientation), and consequently is shown even by rapidly tumbling molecules in fluids (provided the spin density has some s -character).

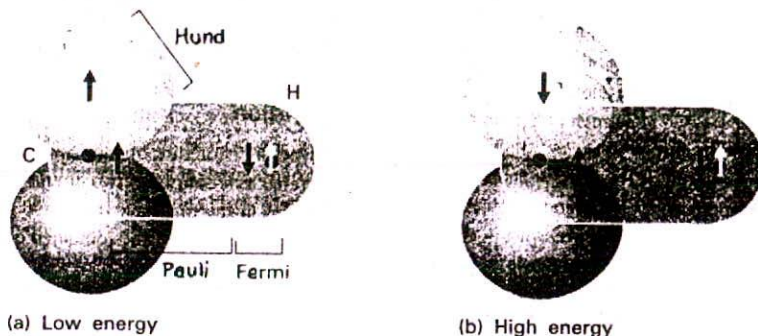
The dipole-dipole interactions of p electrons and the Fermi contact interaction of s electrons can be quite large. For example, a $2p$ electron in a nitrogen atom experiences an average field of about 3.4 mT from the ¹⁴N nucleus. A $1s$ electron in a hydrogen atom experiences a field of about 50 mT as a result of its Fermi contact interaction with the central proton. More values are listed in Table 18.2. The magnitudes of the contact interactions in radicals can be interpreted in terms of the s orbital character of the molecular orbital occupied by the unpaired electron, and the dipole-dipole interaction can be interpreted in terms of the p character. The analysis of hyperfine structure therefore gives information about the composition of the orbital, and especially the hybridization of the atomic orbitals (see Problem 18.6).

We still have the source of the hyperfine structure of the C₆H₆⁻ anion and other aromatic radical anions to explain. The sample is fluid, and as the radicals are tumbling the hyperfine structure cannot be due to the dipole-dipole interaction. Moreover, the protons lie in the

Table 18.2* Hyperfine coupling constants for atoms, a /mT

Nuclide	Isotropic coupling	Anisotropic coupling
¹ H	50.8(1s)	
² H	7.8(1s)	
¹⁴ N	55.2(2s)	3.4(2p)
¹⁹ F	1720(2s)	108.4(2p)

*More values are given in the Data section.



18.49 The polarization mechanism for the hyperfine interaction in π -electron radicals. The arrangement in (a) is lower in energy than that in (b), so there is an effective coupling between the unpaired electron and the proton.

nodal plane of the π orbital occupied by the unpaired electron, so the structure cannot be due to a Fermi contact interaction. The explanation lies in a **polarization mechanism** similar to the one responsible for spin-spin coupling in NMR. There is a magnetic interaction between a proton and the σ electrons which results in one of the electrons tending to be found with a greater probability nearby (Fig. 18.49). The electron with opposite spin is therefore more likely to be close to the C atom at the other end of the bond. The unpaired electron on the C atom has a lower energy if it is parallel to that electron (Hund's rule favours parallel electrons on atoms), so the unpaired electron can detect the spin of the proton indirectly. Calculation using this model leads to a hyperfine interaction in agreement with the observed value of 2.25 mT.

Checklist of key ideas

Nuclear magnetic resonance

18.1 Nuclear magnetic moments

- spin- $\frac{1}{2}$ nuclei

18.2 The energies of nuclei in magnetic fields

- magnetogyric ratio
- nuclear g -factor
- nuclear magneton
- Larmor frequency
- resonance condition (6)
- nuclear magnetic resonance (NMR)

18.3 The chemical shift

- shielding constant
- chemical shift (10)
- deshielded nuclei
- integration
- local contribution
- neighbouring group contribution
- solvent contribution

- diamagnetic contribution
- paramagnetic contribution
- Lamb formula (14)
- ring current

18.4 The fine structure

- fine structure
- scalar coupling constant
- Karplus equation (21)
- polarization mechanism
- Fermi contact interaction
- chemically equivalent nuclei
- magnetically equivalent nuclei
- first-order spectra
- strongly coupled spectra
- heteronuclear spin system
- homonuclear spin system
- dilute-spin species
- abundant-spin species
- proton decoupling

Pulse techniques in NMR

- Fourier-transform NMR

18.5 The magnetization vector

- magnetization
- precessing
- 90° pulse
- free-induction decay (FID)

18.6 Linewidths and rate processes

- spin relaxation
- longitudinal relaxation time
- spin-lattice relaxation time
- transverse relaxation time
- spin-spin relaxation time
- inhomogeneous broadening
- effective transverse relaxation time (31)
- chemical exchange
- inversion recovery technique
- spin echo
- spin packet
- refocused

18.7 The nuclear Overhauser effect

- nuclear Overhauser effect (NOE)

18.8 Two-dimensional NMR

- two-dimensional NMR
- correlation spectroscopy (COSY)

18.9 Solid-state NMR

- magic-angle spinning (MAS)

Electron spin resonance

- electron spin resonance (ESR)
- electron paramagnetic resonance (EPR)
- resonance condition (38)

18.10 The g -value

- g -value

18.11 Hyperfine structure

- hyperfine structure
- hyperfine coupling constant
- spin density
- McConnell equation (41)
- dipole-dipole interaction
- polarization mechanism

Further reading

Articles of general interest

- R.H. Orcutt, A straightforward way to determine relative intensities of spin-spin splitting lines of equivalent nuclei in NMR spectra. *J. Chem. Educ.* **64**, 763 (1987).
- T.D. Lash and S.S. Lash, The use of Pascal-like triangles in describing first-order coupling patterns. *J. Chem. Educ.* **64**, 315 (1987).
- T.A. Shaler, Generalization of Pascal's triangle to nuclei of any spin. *J. Chem. Educ.* **68**, 853 (1991).
- L.J. Schwartz, A step-by-step picture of pulsed (time-domain) NMR. *J. Chem. Educ.* **65**, 959 (1988); *idem*, 752.
- M.-K. Ahn, A comparison of FTNMR and FTIR techniques. *J. Chem. Educ.* **66**, 802 (1989).
- D.J. Wink, Spin-lattice relaxation times in ^1H NMR spectroscopy. *J. Chem. Educ.* **66**, 810 (1989).
- R.W. King and K.R. Williams, The Fourier transform in chemistry. Part 1. Nuclear magnetic resonance: introduction. *J. Chem. Educ.* **66**, A213 (1989); Part 2. Nuclear magnetic resonance: the single pulse experiment. *Ibid.* A243; Part 3. Multiple-pulse experiments. *J. Chem. Educ.* **67**, A9 (1990); Part 4. NMR: two-dimensional methods. *Ibid.* A125; A glossary of NMR terms. *Ibid.* A100.
- R. Freeman, Selective excitation in high-resolution NMR. *Chem. Rev.* **91**, 1397 (1991).
- D.H. Grant, Paramagnetic susceptibility by NMR: the "solvent correction" reexamined. *J. Chem. Educ.* **72**, 39 (1995).
- B.E. Mann, The analysis of first-order coupling patterns in NMR. *J. Chem. Educ.* **72**, 614 (1995).
- J.C. Paniagua and A. Moyano, On the way of introducing some basic NMR aspects: from the classical and naive quantum models to the density-operator approach. *J. Chem. Educ.* **73**, 310 (1996).
- L.R. Dalton, A. Bain, and C.K. Westbrook, Recent advances in electron paramagnetic resonance. *Ann. Rev. Phys. Chem.* **41**, 389 (1990).
- B.H. Suits, Magnetic resonance spectrometers. In *Encyclopedia of applied physics* (ed. G.L. Trigg), **9**, 71. VCH, New York (1994).
- R.G. Barnes, Electron paramagnetic resonance. In *Encyclopedia of applied physics* (ed. G.L. Trigg), **5**, 475. VCH, New York (1993).

Texts and sources of data and information

- P.J. Hore, *Nuclear magnetic resonance*, Oxford Chemistry Primers. Oxford University Press (1995).
- R.J. Abraham, J. Fisher, and P. Lofthus, *Introduction to NMR spectroscopy*. Wiley, New York (1991).
- R.K. Harris, *Nuclear magnetic resonance spectroscopy*. Longman, London (1986).
- A.E. Derome, *Modern NMR techniques for chemistry research*. Pergamon, Oxford (1987).
- J.K.M. Sanders and B.K. Hunter, *Modern NMR spectroscopy*. Oxford University Press (1993).
- J.K.M. Sanders, E.C. Constable, and B.K. Hunter, *Modern NMR spectroscopy: a workbook of chemical problems*. Oxford University Press (1993).
- R. Freeman, *A handbook of nuclear magnetic resonance spectroscopy*. Longman, London (1997).
- R. Freeman, *Spin choreography: basic steps in high resolution NMR*. Spektrum, Oxford (1997).
- H. Günther, *NMR spectroscopy: basic principles, concepts, and applications in chemistry*. Wiley, New York (1995).
- D. Canet, *Nuclear magnetic resonance: concepts and methods*. Wiley, New York (1996).
- J.N.S. Evans, *Biomolecular NMR spectroscopy*. Oxford University Press (1995).
- E.A.V. Ebsworth, D.W.H. Rankin, and S. Craddock, *Structural methods in inorganic chemistry*. Blackwell Scientific, Oxford (1991).
- R. Drago, *Physical methods for chemists*. Saunders, Philadelphia (1992).
- D.M. Grant and R.K. Harris (ed.), *Encyclopedia of nuclear magnetic resonance*, Vols 1-8. Wiley, New York (1996).
- N.M. Atherton, *Principles of electron spin resonance*. Ellis Horwood/Prentice-Hall, Hemel Hempstead (1993).

Exercises

- 18.1 (a)** What is the resonance frequency of a proton in a magnetic field of 14.1 T?
- 18.1 (b)** What is the resonance frequency of a ^{19}F nucleus in a magnetic field of 16.2 T?
- 18.2 (a)** ^{32}S has a nuclear spin of $\frac{3}{2}$ and a nuclear g factor of 0.4289. Calculate the energies of the nuclear spin states in a magnetic field of 7.500 T.
- 18.2 (b)** ^{14}N has a nuclear spin of 1 and a nuclear g factor of 0.404. Calculate the energies of the nuclear spin states in a magnetic field of 11.50 T.
- 18.3 (a)** Calculate the frequency separation of the nuclear spin levels of a ^{13}C nucleus in a magnetic field of 14.4 T given that the magnetogyric ratio is $6.73 \times 10^7 \text{ T}^{-1} \text{ s}^{-1}$.
- 18.3 (b)** Calculate the frequency separation of the nuclear spin levels of a ^{14}N nucleus in a magnetic field of 15.4 T given that the magnetogyric ratio is $1.93 \times 10^7 \text{ T}^{-1} \text{ s}^{-1}$.
- 18.4 (a)** In which of the following systems is the energy level separation the largest: (a) a proton in a 600 MHz NMR spectrometer, (b) a deuteron in the same spectrometer?
- 18.4 (b)** In which of the following systems is the energy level separation the largest: (a) a ^{14}N nucleus in a 600 MHz NMR spectrometer, (b) an electron in a radical in a field of 0.300 T?
- 18.5 (a)** Calculate the energy difference between the lowest and highest nuclear spin states of a ^{14}N nucleus in a 15.00 T magnetic field.
- 18.5 (b)** Calculate the magnetic field needed to satisfy the resonance condition for unshielded protons in a 150.0 MHz radiofrequency field.
- 18.6 (a)** Use Table 18.1 to predict the magnetic fields at which (a) ^1H , (b) ^2H , (c) ^{13}C come into resonance at (i) 250 MHz, (ii) 500 MHz.
- 18.6 (b)** Use Table 18.1 to predict the magnetic fields at which (a) ^{14}N , (b) ^{19}F , and (c) ^{31}P come into resonance at (i) 300 MHz, (ii) 750 MHz.
- 18.7 (a)** Calculate the relative population differences ($\delta N/N$) for protons in fields of (a) 0.30 T, (b) 1.5 T, and (c) 10 T at 25°C.
- 18.7 (b)** Calculate the relative population differences ($\delta N/N$) for ^{13}C nuclei in fields of (a) 0.50 T, (b) 2.5 T, and (c) 15.5 T at 25°C.
- 18.8 (a)** The first generally available NMR spectrometers operated at a frequency of 60 MHz; today it is not uncommon to use a spectrometer that operates at 600 MHz. What are the relative population differences of ^{13}C spin states in these two spectrometers at 25°C?
- 18.8 (b)** What are the relative values of the chemical shifts observed for nuclei in the spectrometers mentioned in Exercise 18.8a in terms of (a) δ values, (b) frequencies?
- 18.9 (a)** The chemical shift of the CH_3 protons in acetaldehyde (ethanal) is $\delta = 2.20$ and that of the CHO proton is 9.80. What is the difference in local magnetic field between the two regions of the molecule when the applied field is (a) 1.5 T, (b) 15 T?
- 18.9 (b)** The chemical shift of the CH_3 protons in diethyl ether is $\delta = 1.16$ and that of the CH_2 protons is $\delta = 3.36$. What is the difference in local magnetic field between the two regions of the molecule when the applied field is (a) 1.9 T, (b) 16.5 T?
- 18.10 (a)** Sketch the appearance of the ^1H -NMR spectrum of acetaldehyde (ethanal) using $J = 2.90$ and the data in Exercise 18.9a in a spectrometer operating at (a) 250 MHz, (b) 500 MHz.
- 18.10 (b)** Sketch the appearance of the ^1H -NMR spectrum of diethyl ether using $J = 6.97 \text{ Hz}$ and the data in Exercise 18.9b in a spectrometer operating at (a) 350 MHz, (b) 650 MHz.
- 18.11 (a)** Two groups of protons are made equivalent by the isomerization of a fluxional molecule. At low temperatures, where the interconversion is slow, one group has $\delta = 4.0$ and the other has $\delta = 5.2$. At what rate of interconversion will the two signals merge in a spectrometer operating at 250 MHz?
- 18.11 (b)** Two groups of protons are made equivalent by the isomerization of a fluxional molecule. At low temperatures, where the interconversion is slow, one group has $\delta = 5.5$ and the other has $\delta = 6.8$. At what rate of interconversion will the two signals merge in a spectrometer operating at 350 MHz?
- 18.12 (a)** Sketch the form of the ^{19}F -NMR spectra of a natural sample of tetrafluoroborate ions, BF_4^- , allowing for the relative abundances of $^{10}\text{BF}_4^-$ and $^{11}\text{BF}_4^-$.
- 18.12 (b)** From the data in Table 18.1, predict the frequency needed for ^{31}P -NMR in an NMR spectrometer designed to observe proton resonance at 500 MHz. Sketch the proton and ^{31}P resonances in the NMR spectrum of PH_4^+ .
- 18.13 (a)** Sketch the form of an $\text{A}_3\text{M}_2\text{X}_4$ spectrum, where A, M, and X are protons with distinctly different chemical shifts and $J_{\text{AM}} > J_{\text{AX}} > J_{\text{MX}}$.
- 18.13 (b)** Sketch the form of an $\text{A}_2\text{M}_2\text{X}_2$ spectrum, where A, M, and X are protons with distinctly different chemical shifts and $J_{\text{AM}} > J_{\text{AX}} > J_{\text{MX}}$.
- 18.14 (a)** Which of the following molecules have sets of nuclei that are chemically but not magnetically equivalent: (a) CH_3CH_2 , (b) $\text{CH}_2=\text{CH}_2$?
- 18.14 (b)** Which of the following molecules have sets of nuclei that are chemically but not magnetically equivalent: (a) $\text{CH}_2=\text{C}=\text{CF}_2$, (b) *cis*- and *trans*- $[\text{Mo}(\text{CO})_4(\text{PH}_3)_2]$?
- 18.15 (a)** The duration of a 90° or 180° pulse depends on the strength of the B_1 field. If a 90° pulse requires 10 μs , what is the strength of the B_1 field? How long would the corresponding 180° pulse require?
- 18.15 (b)** The duration of a 90° or 180° pulse depends on the strength of the B_1 field. If a 180° pulse requires 12.5 μs , what is the strength of the B_1 field? How long would the corresponding 90° pulse require?

18.16 (a) What magnetic field would be required in order to use an ESR X-band spectrometer (9 GHz) to observe ^1H -NMR and a 300 MHz spectrometer to observe ESR?

18.16 (b) Some commercial ESR spectrometers use 8 mm microwave radiation (the Q band). What magnetic field is needed to satisfy the resonance condition?

18.17 (a) The centre of the ESR spectrum of atomic hydrogen lies at 329.12 mT in a spectrometer operating at 9.2231 GHz. What is the g -value of the atom?

18.17 (b) The centre of the ESR spectrum of atomic deuterium lies at 330.02 mT in a spectrometer operating at 9.2482 GHz. What is the g -value of the atom?

18.18 (a) A radical containing two equivalent protons shows a three-line spectrum with an intensity distribution 1 : 2 : 1. The lines occur at 330.2 mT, 332.5 mT, and 334.8 mT. What is the hyperfine coupling constant for each proton? What is the g -value of the radical given that the spectrometer is operating at 9.319 GHz?

18.18 (b) A radical containing three equivalent protons shows a four-line spectrum with an intensity distribution 1 : 3 : 3 : 1. The lines occur at 331.4 mT, 333.6 mT, 335.8 mT, and 338.0 mT. What is the hyperfine coupling constant for each proton? What is the g -value of the radical given that the spectrometer is operating at 9.332 GHz?

18.19 (a) A radical containing two inequivalent protons with hyperfine constants 2.0 mT and 2.6 mT gives a spectrum centred on 332.5 mT. At what fields do the hyperfine lines occur and what are their relative intensities?

18.19 (b) A radical containing three inequivalent protons with hyperfine constants 2.11 mT, 2.87 mT, and 2.89 mT gives a spectrum centred on 332.8 mT. At what fields do the hyperfine lines occur and what are their relative intensities?

18.20 (a) Predict the intensity distribution in the hyperfine lines of the ESR spectra of (a) $\cdot\text{CH}_3$, (b) $\cdot\text{CD}_3$.

18.20 (b) Predict the intensity distribution in the hyperfine lines of the ESR spectra of (a) $\cdot\text{CH}_2\text{CH}_3$, (b) $\cdot\text{CD}_2\text{CD}_3$.

18.21 (a) The benzene radical anion has $g = 2.0025$. At what field should you search for resonance in a spectrometer operating at (a) 9.302 GHz, (b) 33.67 GHz?

18.21 (b) The naphthalene radical anion has $g = 2.0024$. At what field should you search for resonance in a spectrometer operating at (a) 9.312 GHz, (b) 33.88 GHz?

18.22 (a) The ESR spectrum of a radical with a single magnetic nucleus is split into four lines of equal intensity. What is the nuclear spin of the nucleus?

18.22 (b) The ESR spectrum of a radical with two equivalent nuclei of a particular kind is split into five lines of intensity ratio 1 : 2 : 3 : 2 : 1. What is the spin of the nuclei?

18.23 (a) Sketch the form of the hyperfine structures of radicals XH_2 and XD_2 , where the nucleus X has $I = \frac{3}{2}$.

18.23 (b) Sketch the form of the hyperfine structures of radicals XH_3 and XD_3 , where the nucleus X has $I = \frac{3}{2}$.

Problems

Numerical problems

18.1 A scientist investigates the possibility of neutron spin resonance, and has available a commercial NMR spectrometer operating at 300 MHz. What field is required for resonance? What is the relative population difference at room temperature? Which is the lower energy spin state of the neutron?

18.2 Two groups of protons have $\delta = 4.0$ and $\delta = 5.2$ and are interconverted by a conformational change of a fluxional molecule. In a 60 MHz spectrometer the spectrum collapsed into a single line at 280 K but at 300 MHz the collapse did not occur until the temperature had been raised to 300 K. What is the activation energy of the interconversion?

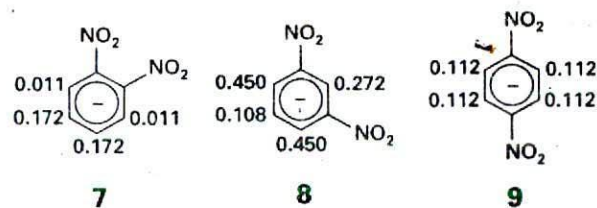
18.3 The angular NO_2 molecule has a single unpaired electron and can be trapped in a solid matrix or prepared inside a nitrite crystal by radiation damage of NO_2^- ions. When the applied field is parallel to the OO direction the centre of the spectrum lies at 333.64 mT in a spectrometer operating at 9.302 GHz. When the field lies along the bisector of the ONO angle, the resonance lies at 331.94 mT. What are the g -values in the two orientations?

18.4 The hyperfine coupling constant in $\cdot\text{CH}_3$ is 2.3 mT. Use the information in Table 18.1 to predict the splitting between the

hyperfine lines of the spectrum of $\cdot\text{CD}_3$. What are the overall widths of the hyperfine spectra in each case?

18.5 The p -dinitrobenzene radical anion can be prepared by reduction of p -dinitrobenzene. The radical anion has two equivalent N nuclei ($I = 1$) and four equivalent protons. Predict the form of the ESR spectrum using $a(\text{N}) = 0.148$ mT and $a(\text{H}) = 0.112$ mT.

18.6 The hyperfine coupling constants observed in the radical anions (7), (8), and (9) are shown (in mT). Use the value for the benzene radical anion to map the probability of finding the unpaired electron in the π orbital on each C atom.



Theoretical problems

18.7 The z -component of the magnetic field at a distance R from a magnetic moment parallel to the z -axis is given by eqn 22. In a solid, a proton at a distance R from another can experience such a field and the measurement of the splitting it causes in the spectrum can be used to calculate R . In gypsum, for instance, the splitting in the H_2O resonance can be interpreted in terms of a magnetic field of 0.715 mT generated by one proton and experienced by the other. What is the separation of the protons in the H_2O molecule?

18.8 In a liquid crystal, a molecule might not rotate freely in all directions and the dipolar interaction might not average to zero. Suppose a molecule is trapped so that, although the vector separating two protons may rotate freely around the z -axis, the colatitude may vary only between 0 and θ' . Average the dipolar field over this restricted range of orientations and confirm that the average vanishes when $\theta' = \pi$ (corresponding to rotation over an entire sphere). What is the average value of the local dipolar field for the H_2O molecule in Problem 18.7 if it is dissolved in a liquid crystal that enables it to rotate up to $\theta' = 30^\circ$?

18.9 The shape of a spectral line, $I(\omega)$, is related to the free induction decay signal $G(t)$ by

$$I(\omega) = a \operatorname{Re} \int_0^\infty G(t) e^{i\omega t} dt$$

where a is a constant and 'Re' means take the real part of what follows. Calculate the lineshape corresponding to an oscillating, decaying function $G(t) = \cos \omega_0 t e^{-t/\tau}$.

18.10 In the language of Problem 18.9, show that, if $G(t) = (a \cos \omega_1 t + b \cos \omega_2 t) e^{-t/\tau}$, then the spectrum consists of two lines with intensities proportional to a and b and located at $\omega = \omega_1$ and ω_2 , respectively.

Additional problems supplied by Carmen Giunta and Charles Trapp

18.11 Suppose that the FID in Fig. 18.30 was recorded in a 300 MHz spectrometer, and that the interval between maxima in the oscillations in the FID is 0.10 s. What is the Larmor frequency of the nuclei and the spin-spin relaxation time?

18.12 In a classical study of the application of NMR to the measurement of rotational barriers in molecules, P.M. Nair and J.D. Roberts (*J. Am. Chem. Soc.* 79, 4565 (1957)) obtained the 40 MHz ^{19}F -NMR spectrum of $\text{F}_2\text{BrCCBrCl}_2$. Their spectra are reproduced in Fig. 18.50. At 193 K, the spectrum shows five resonance peaks. Peaks I and III are separated by 160 Hz, as are IV and V. The ratio of the integrated intensities of peak II to peaks I, III, IV,

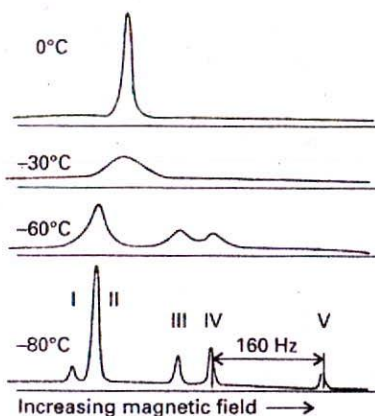


Fig. 18.50

and V is approximately 10 to 1. At 273 K, the five peaks have collapsed into one. Explain the spectrum and its change with temperature. At what rate of interconversion will the spectrum collapse to a single line? Calculate the rotational energy barrier between the rotational isomers on the assumption that it is related to the rate of interconversion between the isomers.

18.13 Various versions of the Karplus equation (eqn 21) have been used to correlate data on vicinal proton coupling constants in systems of the type $\text{R}_1\text{R}_2\text{CHCHR}_3\text{R}_4$. The original version, (M. Karplus, *J. Am. Chem. Soc.* 85, 2870 (1963)), is $^3J_{\text{HH}} = A \cos^2 \phi_{\text{HH}} + B$. When $\text{R}_3 = \text{R}_4 = \text{H}$, $^3J_{\text{HH}} = 7.3$ Hz; when $\text{R}_3 = \text{CH}_3$ and $\text{R}_4 = \text{H}$, $^3J_{\text{HH}} = 8.0$ Hz; when $\text{R}_3 = \text{R}_4 = \text{CH}_3$, $^3J_{\text{HH}} = 11.2$ Hz. Assume that only staggered conformations are important and determine which version of the Karplus equation fits the data better.


18.14 It might be unexpected that the Karplus equation, which was first derived for $^3J_{\text{HH}}$ coupling constants, should also apply to vicinal coupling between the nuclei of metals such as tin. T.N. Mitchell and B. Kowall (*Magn. Reson. Chem.* 33, 325 (1995)) have studied the relation between $^3J_{\text{HH}}$ and $^3J_{\text{SnSn}}$ in compounds of the type $\text{Me}_3\text{SnCH}_2\text{CHR}_3\text{SnMe}_3$ and find that $^3J_{\text{SnSn}} = 78.86 ^3J_{\text{HH}} + 27.84$ Hz. (a) Does this result support a Karplus type equation for tin? Explain your reasoning. (b) Obtain the Karplus equation for $^3J_{\text{SnSn}}$ and plot it as a function of the dihedral angle. (c) Draw the preferred conformation.

18.15 The relative sensitivity of NMR lines for equal numbers of different nuclei at constant temperature for a given frequency is $R_{\nu} \propto (I+1)\mu\omega_0^2$ whereas for a given field it is $R_{\text{B}} \propto \{(I+1)/I^2\} \mu^3$. (a) From the data in Table 18.1, calculate these sensitivities for the deuteron, ^{13}C , ^{14}N , ^{19}F , and ^{31}P relative to the proton. (b) Derive the equation for R_{B} from the equation for R_{ν} .



19

Statistical thermodynamics: the concepts



The distribution of molecular states

- 19.1 Configurations and weights
- 19.2 The molecular partition function

The internal energy and the

- 19.3 The internal energy
- 19.4 The statistical entropy

The canonical partition function

- 19.5 The canonical ensemble
- 19.6 The thermodynamic information in the partition function
- 19.7 Independent molecules

Checklist of key ideas

Further reading

Exercises

Problems

Statistical thermodynamics provides the link between the microscopic properties of matter and its bulk properties. Two key ideas are introduced in this chapter. The first is the Boltzmann distribution. This enormously important result was described in the Introduction, where we saw that it can be used to predict the populations of states. In this chapter we see its derivation in terms of the distribution of particles over available states. The derivation leads naturally to the introduction of the partition function, which is the central mathematical concept of these two chapters. We see how to interpret the partition function and how to calculate it in a number of simple cases. The next part of the chapter shows how to extract thermodynamic information from the partition function.

In the final part of the chapter, we generalize the discussion to include systems that are composed of assemblies of interacting particles. Very similar equations are developed to those in the first part of the chapter, but they are much more widely applicable.

The preceding chapters of this part of the text have shown how the energy levels of molecules can be calculated, determined spectroscopically, and related to their structures. The next major step is to see how a knowledge of these energy levels can be used to account for the properties of matter in bulk. To do so, we now introduce the concepts of statistical thermodynamics, the link between molecular properties and bulk thermodynamic properties.

The crucial step in going from the quantum mechanics of individual molecules to the thermodynamics of bulk samples is to recognize that the latter deals with the average behaviour of large numbers of molecules. For example, the pressure of a gas depends on the average force exerted by its molecules, and there is no need to specify which molecules happen to be striking the wall at any instant. Nor is it necessary to consider the fluctuations in the pressure as different numbers of molecules collide with the wall at different moments. The fluctuations in pressure are very small compared with the steady pressure: it is highly improbable that there will be a sudden lull in the number of collisions, or a sudden surge.

This chapter introduces statistical thermodynamics in two stages. The first, the derivation of the Boltzmann distribution for individual particles, is of restricted applicability, but it has the advantage of taking us directly to a result of central importance in a straightforward and elementary way. We can use statistical thermodynamics once we have deduced the Boltzmann distribution. Then (in Section 19.5) we extend the arguments to systems composed of interacting particles.

The distribution of molecular states

We consider a closed system composed of N molecules. Although the total energy is constant at E , it is not possible to be definite about how that energy is shared between the molecules. Collisions result in the ceaseless redistribution of energy, not only between the molecules but also among their different modes. The closest we can come to a description of the distribution of energy is to report the population of a state, the average number of molecules that occupy it, and to say that on average there are n_i molecules in a state of energy ϵ_i . The populations of the states remain almost constant, but the precise identities of the molecules in each state may change at every collision.

The problem we address in this section is the calculation of the populations of states for any type of molecule in any mode of motion at any temperature. The only restriction is that the molecules should be independent, in the sense that the total energy of the system is a sum of their individual energies. We are discounting (at this stage) the possibility that in a real system a contribution to the total energy may arise from interactions between molecules. We also adopt the principle of equal *a priori* probabilities,¹ the assumption that all possibilities for the distribution of energy are equally probable. That is, we assume that vibrational states of a certain energy, for instance, are as likely to be populated as rotational states of the same energy.

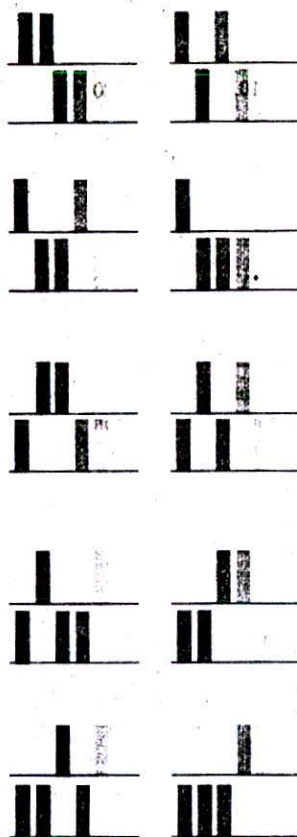
19.1 Configurations and weights

Any individual molecule may exist in states with energies $\epsilon_0, \epsilon_1, \dots$. We shall always take ϵ_0 , the lowest state, as the zero of energy ($\epsilon_0 = 0$), and measure all other energies relative to that state. To obtain the actual internal energy, U , we may have to add a constant to the calculated energy of the system. For example, if we are considering the vibrational contribution to the internal energy, we must add the total zero-point energy of any oscillators in the sample.

(a) Instantaneous configurations

At any instant there will be n_0 molecules in the state with energy ϵ_0 , n_1 with ϵ_1 , and so on. The specification of the set of populations n_0, n_1, \dots in the form $\{n_0, n_1, \dots\}$ is a statement of the instantaneous configuration of the system. The instantaneous configuration fluctuates with time because the populations change. We can picture a large number of different instantaneous configurations. One, for example, might be $\{N, 0, 0, \dots\}$, corresponding to every molecule being in its ground state. Another might be $\{N-2, 2, 0, 0, \dots\}$, in which two molecules are in the first excited state. The latter configuration is intrinsically more likely to be found than the former because it can be

¹ *A priori* means in this context loosely 'as far as one knows'. We have no reason to presume otherwise than that all states are equally likely to be occupied whatever their nature.



19.1 Whereas a configuration $\{5, 0, 0, \dots\}$ can be achieved in only one way, a configuration $\{3, 2, 0, \dots\}$ can be achieved in the ten different ways shown here, where the tinted blocks represent different molecules.

19.2 The 18 molecules shown here can be distributed into four receptacles (distinguished by the three vertical lines) in $18!$ different ways. However, $3!$ of the selections that put three molecules in the first receptacle are equivalent, $6!$ that put six molecules into the second receptacle are equivalent, and so on. Hence the number of distinguishable arrangements is $18!/3!6!5!4!$.

achieved in more ways: $\{N, 0, 0, \dots\}$ can be achieved in only one way, but $\{N - 2, 2, 0, \dots\}$ can be achieved in $\frac{1}{2}N(N - 1)$ different ways (Fig. 19.1).²

Justification 19.1

One candidate for promotion to an upper state can be selected in N ways. There are $N - 1$ candidates for the second choice, so the total number of choices is $N(N - 1)$. However, we should not distinguish the choice (Jack, Jill) from the choice (Jill, Jack) because they lead to the same configurations. Therefore, only half the choices lead to distinguishable configurations, and the total number of distinguishable choices is $\frac{1}{2}N(N - 1)$.

If, as a result of collisions, the system were to fluctuate between the configurations $\{N, 0, 0, \dots\}$ and $\{N - 2, 2, 0, \dots\}$, it would almost always be found in the second, more likely state (especially if N were large). In other words, a system free to switch between the two configurations would show properties characteristic almost exclusively of the second configuration.

A general configuration $\{n_0, n_1, \dots\}$ can be achieved in W different ways, where W is called the weight of the configuration. The weight of the configuration $\{n_0, n_1, \dots\}$ is given by the expression

$$W = \frac{N!}{n_0!n_1!n_2!\dots} \quad (1)$$

where $x!$, x factorial, denotes $x(x - 1)(x - 2) \dots 1$, and by definition $0! = 1$. This expression is a generalization of the formula $W = \frac{1}{2}N(N - 1)$, and reduces to it for the configuration $\{N - 2, 2, 0, \dots\}$.

Justification 19.2

Consider the number of ways of distributing N balls into bins. The first ball can be selected in N different ways, the next ball in $N - 1$ different ways for the balls remaining, and so on. Therefore, there are $N(N - 1) \dots 1 = N!$ ways of selecting the balls for distribution over the bins. However, if there are n_0 balls in the bin labelled e_0 , there would be $n_0!$ different ways in which the same balls could have been chosen (Fig. 19.2). Similarly, there are $n_1!$ ways in which the n_1 balls in the bin labelled e_1 can be chosen, and so on. Therefore, the total number of distinguishable ways of distributing the balls so that there are n_0 in bin e_0 , n_1 in bin e_1 , etc. regardless of the order in which the balls were chosen is $N!/n_0!n_1! \dots$, which is the content of eqn 1.



² At this stage in the argument, we are ignoring the requirement that the total energy of the system should be constant (the second configuration has a higher energy than the first). The constraint of total energy is imposed later in this section.

Illustration

To calculate the number of ways of distributing 20 identical objects with the arrangement 1, 0, 3, 5, 10, 1, we note that the configuration is $\{1, 0, 3, 5, 10, 1\}$ with $N = 20$; therefore the weight is

$$W = \frac{20!}{1!0!3!5!10!1!} = 9.31 \times 10^8$$

Self-test 19.1 Calculate the weight of the configuration in which 20 objects are distributed in the arrangement 0, 1, 5, 0, 8, 0, 3, 2, 0, 1.

[4.19×10^{10}]

It will turn out to be more convenient to deal with the natural logarithm of the weight, $\ln W$, rather than with the weight itself. We shall therefore need the expression

$$\begin{aligned} \ln W &= \ln \left(\frac{N!}{n_0!n_1!n_2!\dots} \right) = \ln N! - \ln(n_0!n_1!n_2!\dots) \\ &= \ln N! - (\ln n_0! + \ln n_1! + \ln n_2! + \dots) \\ &= \ln N! - \sum_i \ln n_i! \end{aligned}$$

where in the first line we have used $\ln(x/y) = \ln x - \ln y$ and in the second $\ln xy = \ln x + \ln y$. One reason for introducing $\ln W$ is that it is easier to make approximations. In particular, we can simplify the factorials by using Stirling's approximation in the form³

$$\ln x! \approx x \ln x - x \quad (2)$$

Then the approximate expression for the weight is

$$\begin{aligned} \ln W &= (N \ln N - N) - \sum_i (n_i \ln n_i - n_i) \\ &= N \ln N - \sum_i n_i \ln n_i \end{aligned} \quad (3)$$

The second line is derived by noting that the sum of n_i is equal to N , so the second and fourth terms on the right in the first line of eqn 3 cancel.

(b) The dominating configuration

We have seen that the configuration $\{N - 2, 2, 0, \dots\}$ dominates $\{N, 0, 0, \dots\}$, and it should be easy to believe that there may be other configurations that greatly dominate both. We shall see, in fact, that there is a configuration with so great a weight that it overwhelms all the rest in importance to such an extent that the system will almost always be found in it. The properties of the system will therefore be characteristic of that particular dominating configuration. This dominating configuration can be found by looking for the values of n_i that lead to a maximum value of W . Because W is a function of all the n_i , we can do this search by varying the n_i and looking for the values that correspond to $dW = 0$ (just as in the

³ The precise form of Stirling's approximation is

$$x! \approx (2\pi)^{1/2} x^{x+1/2} e^{-x}$$

and it is reliable when x is greater than about 10. We deal with far larger values of x , and the simplified version in eqn 2 is adequate.

search for the maximum of any function), or equivalently a maximum value of $\ln W$. However, there are two difficulties with this procedure.

The first difficulty is that the only permitted configurations are those corresponding to the specified, constant, total energy of the system. This requirement rules out many configurations; $\{N, 0, 0, \dots\}$ and $\{N - 2, 2, 0, \dots\}$, for instance, have different energies, so both cannot occur in the same isolated system. It follows that, in looking for the configuration with the greatest weight, we must ensure that the configuration also satisfies the condition

$$\text{Constant total energy: } \sum_i n_i \varepsilon_i = E \quad (4)$$

where E is the total energy of the system.

The second constraint is that, because the total number of molecules present is also fixed ($\text{at } N$), we cannot arbitrarily vary all the populations simultaneously. Thus, increasing the population of one state by 1 demands that the population of another state must be reduced by 1. Therefore, the search for the maximum value of W is also subject to the condition

$$\text{Constant total number of molecules: } \sum_i n_i = N \quad (5)$$

(c) The Boltzmann distribution

We are looking for the set of numbers n_0, n_1, \dots for which W has its maximum value. We show in the following *Justification* that the populations in the configuration of greatest weight depend on the energy of the state according to the **Boltzmann distribution**:

$$\frac{n_i}{N} = \frac{e^{-\beta \varepsilon_i}}{\sum_j e^{-\beta \varepsilon_j}} \quad \beta = \frac{1}{kT} \quad (6)$$

where T is the thermodynamic temperature and k is the Boltzmann constant.

Justification 19.3

We have already remarked that it turns out to be simpler to find the condition for $\ln W$ being a maximum rather than dealing directly with W . Because $\ln W$ depends on all the n_i , when a configuration changes and the n_i change to $n_i + dn_i$, the function $\ln W$ changes to $\ln W + d \ln W$, where

$$d \ln W = \sum_i \left(\frac{\partial \ln W}{\partial n_i} \right) dn_i$$

At a maximum, $d \ln W = 0$. However, when the n_i change, they do so subject to the two constraints

$$\sum_i \varepsilon_i dn_i = 0 \quad \sum_i dn_i = 0 \quad (7)$$

The first constraint recognizes that the total energy must not change, and the second recognizes that the total number of molecules must not change. These two constraints prevent us from solving $d \ln W = 0$ simply by setting all $(\partial \ln W / \partial n_i) = 0$ because the dn_i are not all independent.

The way to take constraints into account was devised by the French mathematician Lagrange, and is called the **method of undetermined multipliers**. The technique is described in *Further information 3*. All we need here is the rule that *a constraint should be multiplied by a constant and then added to the main variation equation*. The variables

are then treated as though they were all independent, and the constants are evaluated at the end of the calculation.

We employ the technique as follows. The two constraints are multiplied by the constants $-\beta$ and α , respectively (the minus sign in $-\beta$ has been included for future convenience), and then added to the expression for $d \ln W$:

$$\begin{aligned} d \ln W &= \sum_i \left(\frac{\partial \ln W}{\partial n_i} \right) dn_i + \alpha \sum_i dn_i - \beta \sum_i \epsilon_i dn_i \\ &= \sum_i \left\{ \left(\frac{\partial \ln W}{\partial n_i} \right) + \alpha - \beta \epsilon_i \right\} dn_i \end{aligned}$$

All the dn_i are now treated as independent. Hence the only way of satisfying $d \ln W = 0$ is to require that, for each i ,

$$\left(\frac{\partial \ln W}{\partial n_i} \right) + \alpha - \beta \epsilon_i = 0 \quad (8)$$

when the n_i have their most probable values.

The expression for $\ln W$ is given in eqn 3. Differentiation of it with respect to n_i gives

$$\left(\frac{\partial \ln W}{\partial n_i} \right) = \frac{\partial(N \ln N)}{\partial n_i} - \sum_j \frac{\partial(n_j \ln n_j)}{\partial n_i}$$

The derivative of the first term is obtained as follows:

$$\frac{\partial(N \ln N)}{\partial n_i} = \left(\frac{\partial N}{\partial n_i} \right) \ln N + \frac{\partial N}{\partial n_i} = \ln N + 1$$

because $N = n_1 + n_2 + \dots$ and its derivative with respect to any of the n s is 1. The derivative of the second term is⁴

$$\begin{aligned} \sum_j \frac{\partial(n_j \ln n_j)}{\partial n_i} &= \sum_j \left\{ \left(\frac{\partial n_j}{\partial n_i} \right) \ln n_j + n_j \left(\frac{\partial \ln n_j}{\partial n_i} \right) \right\} \\ &= \sum_j \left(\frac{\partial n_j}{\partial n_i} \right) (\ln n_j + 1) = \ln n_i + 1 \end{aligned}$$

and therefore

$$\frac{\partial \ln W}{\partial n_i} = -(\ln n_i + 1) + (\ln N + 1) = -\ln \left(\frac{n_i}{N} \right)$$

It follows from eqn 8 that

$$-\ln \left(\frac{n_i}{N} \right) + \alpha - \beta \epsilon_i = 0$$

and therefore that

$$\frac{n_i}{N} = e^{\alpha - \beta \epsilon_i}$$

⁴ We use

$$\frac{\partial \ln n_j}{\partial n_i} = \frac{1}{n_j} \left(\frac{\partial n_j}{\partial n_i} \right)$$

Then, if $i \neq j$, n_j is independent of n_i , so $\partial n_j / \partial n_i = 0$. However, if $i = j$,

$$\frac{\partial n_j}{\partial n_i} = \frac{\partial n_j}{\partial n_j} = 1$$

At this stage we note that

$$N = \sum_j n_j = N e^{\alpha} \sum_j e^{-\beta \epsilon_j}$$

(We are free to label the states with j instead of i .) Because the N cancels on each side of this equality, it follows that

$$e^{\alpha} = \frac{1}{\sum_j e^{-\beta \epsilon_j}} \quad (9)$$

and the Boltzmann distribution in eqn 6 follows immediately. We justify the relation $\beta = 1/kT$ shortly (Section 19.3b).

19.2 The molecular partition function

From now on we write the Boltzmann distribution as

$$p_i = \frac{e^{-\beta \epsilon_i}}{q} \quad (10)$$

where p_i is the fraction of molecules in the state i , $p_i = n_i/N$, and q is the molecular partition function:

$$q = \sum_j e^{-\beta \epsilon_j} \quad (11)$$

The sum in q is sometimes expressed slightly differently. It may happen that several states have the same energy, and so give the same contribution to the sum. If, for example, g_j states have the same energy ϵ_j (so the level is g_j -fold degenerate), we could write

$$q = \sum_{\text{levels } j} g_j e^{-\beta \epsilon_j} \quad (12)$$

where the sum is now over energy levels (sets of states with the same energy), not individual states.

Example 19.1 Writing a partition function

Write an expression for the partition function of a linear molecule (such as HCl) treated as a rigid rotor.

Method To use eqn 12 we need to know (a) the energies of the levels, (b) the degeneracies, the number of states that belong to each level. Whenever calculating a partition function, the energies of the levels are expressed relative to 0 for the state of lowest energy. The energy levels of a rigid linear rotor were derived in Section 16.5c.

Answer From eqn 16.37, the energy levels of a linear rotor are $hcBJ(J+1)$, with $J = 0, 1, 2, \dots$. The state of lowest energy has zero energy, so no adjustment need be made to the energies given by this expression. Each level consists of $2J+1$ degenerate states. Therefore,

$$q = \sum_{J=0}^{\infty} (2J+1) e^{-\beta hcBJ(J+1)}$$

Comment The sum can be evaluated numerically by supplying the value of B (from spectroscopy or calculation) and the temperature. For reasons explained in Section 20.2b,

this expression applies only to unsymmetrical linear rotors (for example, HCl, not CO₂; in general, to C_{∞v} and not D_{∞h} species).

Self-test 19.2 Write the partition function for a two-level system, the lower state (at energy 0) being non-degenerate, and the upper state (at an energy ϵ) doubly degenerate.

$$[q = 1 + 2e^{-\beta\epsilon}]$$

(a) An interpretation of the partition function

Some insight into the significance of a partition function can be obtained by considering how q depends on the temperature. When T is close to zero, the parameter $\beta = 1/kT$ is close to infinity. Then every term except one in the sum defining q is zero because each one has the form e^{-x} with $x \rightarrow \infty$. The exception is the term with $\epsilon_0 \equiv 0$ (or the g_0 terms at zero energy if the ground state is g_0 -fold degenerate), because then $\epsilon_0/kT \equiv 0$ whatever the temperature, including zero. As there is only one surviving term when $T = 0$, and its value is g_0 , it follows that

$$\lim_{T \rightarrow 0} q = g_0 \quad (13)$$

That is, at $T = 0$, the partition function is equal to the degeneracy of the ground state.

Now consider the case when T is so high that for each term in the sum $\epsilon_i/kT \approx 0$. Because $e^{-x} = 1$ when $x = 0$, each term in the sum now contributes 1. It follows that the sum is equal to the number of molecular states, which in general is infinite:

$$\lim_{T \rightarrow \infty} q \rightarrow \infty \quad (14)$$

In some idealized cases, the molecule may have only a finite number of states; then the upper limit of q is equal to the number of states. For example, if we were considering only the spin energy levels of a radical in a magnetic field, then there would be only two states ($m_s = \pm \frac{1}{2}$). The partition function for such a system can therefore be expected to rise towards 2 as T is increased towards infinity.

We see that the molecular partition function gives an indication of the average number of states that are thermally accessible to a molecule at the temperature of the system. At $T = 0$, only the ground level is accessible and $q = g_0$. At very high temperatures, virtually all states are accessible, and q is correspondingly large.

Example 19.2 Evaluating the partition function for a uniform ladder of energy levels

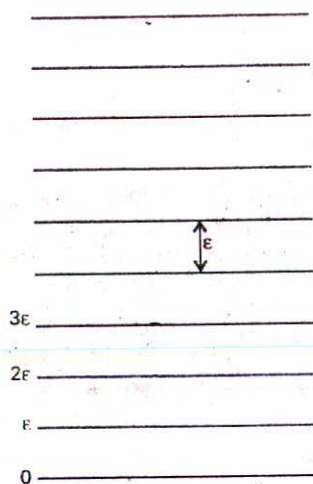
Evaluate the partition function for a molecule with an infinite number of equally spaced non-degenerate energy levels (Fig. 19.3). These levels can be thought of as the vibrational energy levels of a diatomic molecule in the harmonic approximation.

Method We expect the partition function to increase from 1 at $T = 0$ and approach infinity as $T \rightarrow \infty$. To evaluate eqn 11 explicitly, note that⁵

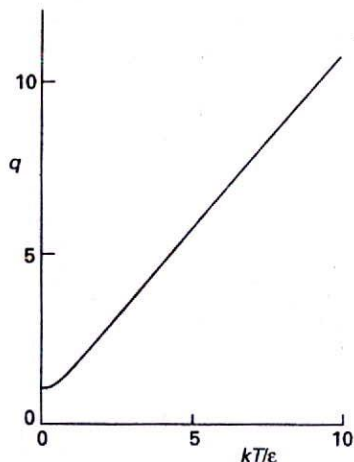
$$1 + x + x^2 + \dots = \frac{1}{1-x}$$

⁵ The sum of the infinite series $S = 1 + x + x^2 + \dots$ is obtained by multiplying both sides by x , which gives $xS = x + x^2 + x^3 + \dots = S - 1$. This relation reorganizes into

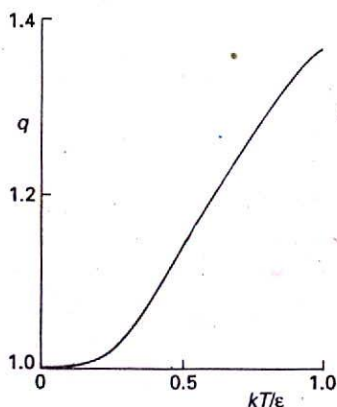
$$S = \frac{1}{1-x}$$



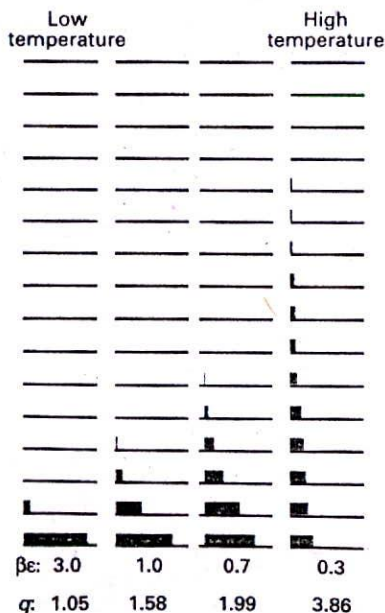
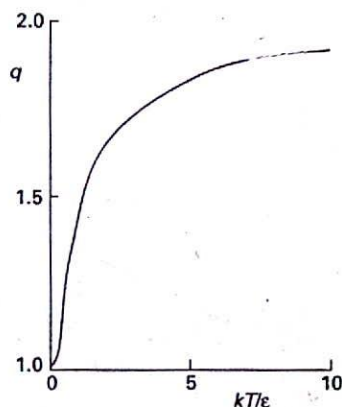
19.3 The equally spaced infinite array of energy levels used in the calculation of the partition function. A harmonic oscillator has the same spectrum of levels.



19.4 The partition function for the system shown in Fig. 19.3 (a harmonic oscillator) as a function of temperature.



19.5 The partition function for a two-level system as a function of temperature. The two graphs differ in the scale of the temperature axis to show the approach to 1 as $T \rightarrow 0$ and the slow approach to 2 as $T \rightarrow \infty$.



19.6 The populations of the energy levels of the system shown in Fig. 19.3 at different temperatures, and the corresponding values of the partition function calculated in Self-test 19.3. Note that $\beta = 1/kT$.

Answer If the separation of neighbouring levels is ϵ , the partition function is

$$q = 1 + e^{-\beta\epsilon} + e^{-2\beta\epsilon} + \dots = 1 + e^{-\beta\epsilon} + (e^{-\beta\epsilon})^2 + \dots$$

$$= \frac{1}{1 - e^{-\beta\epsilon}}$$

This expression is plotted in Fig. 19.4: notice that it rises from 1 to infinity as the temperature is raised, as anticipated.

Self-test 19.3 Find and plot an expression for the partition function of a system with one state at zero energy and another state at the energy ϵ .

$$[q = 1 + e^{-\beta\epsilon}, \text{ Fig. 19.5}]$$

It follows from eqn 10 and the expression for q derived in Example 19.2 for a uniform ladder of states of spacing ϵ ,

$$q = \frac{1}{1 - e^{-\beta\epsilon}} \quad (15)$$

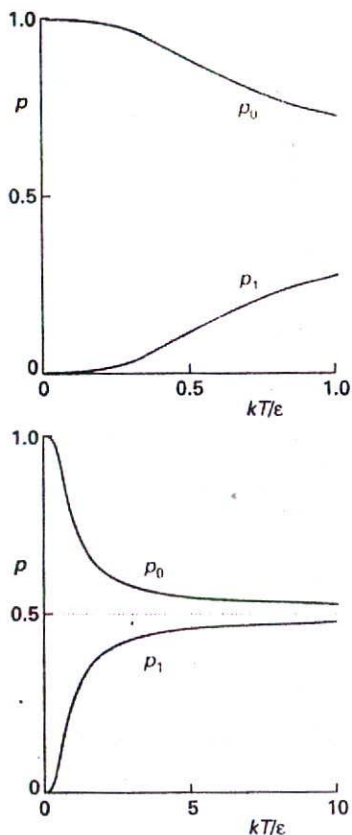
that the fraction of molecules in the state with energy ϵ_i is

$$p_i = (1 - e^{-\beta\epsilon})e^{-\beta\epsilon_i} \quad (16)$$

The variation of p_i with temperature is illustrated in Fig. 19.6. We see that at very low temperatures, where q is close to 1, only the lowest state is significantly populated. As the temperature is raised, the population breaks out of the lowest state, and the upper states become progressively more highly populated. At the same time the partition function rises from 1, and its value gives an indication of the range of states populated. The name 'partition function' reflects the sense in which q measures how the total number of molecules is distributed—partitioned—over the available states.

The corresponding expressions for a two-level system derived in Self-test 19.3 are

$$p_0 = \frac{1}{1 + e^{-\beta\epsilon}} \quad p_1 = \frac{e^{-\beta\epsilon}}{1 + e^{-\beta\epsilon}} \quad (17)$$



19.7 The fraction of populations of the two states of a two-level system as a function of temperature (eqn 17). Note that, as the temperature approaches infinity, the populations of the two states become equal (and the fractions both approach 0.5).

These functions are plotted in Fig. 19.7. Notice how the populations tend towards equality ($p_0 = 0.5, p_1 = 0.5$) as $T \rightarrow \infty$. A common error is to suppose that all the molecules in the system will be found in the upper energy state when $T = \infty$; however, we see from eqn 17 that, as $T \rightarrow \infty$, the populations of states become equal. The same conclusion is true of multi-level systems too: as $T \rightarrow \infty$, all states become equally populated.

Example 19.3 Using the partition function to calculate a population

Calculate the proportion of I_2 molecules in their ground, first excited, and second excited vibrational states at 25°C. The vibrational wavenumber is 214.6 cm^{-1} .

Method Vibrational energy levels have a constant separation (in the harmonic approximation, Section 16.9), so the partition function is given by eqn 15 and the populations by eqn 16. To use the latter equation, we identify the index i with the quantum number v , and calculate p_v for $v = 0, 1$, and 2. At 298.15 K, $kT/hc = 207.226 \text{ cm}^{-1}$.

Answer First, we note that

$$\beta\epsilon = \frac{hc\tilde{\nu}}{kT} = \frac{214.6 \text{ cm}^{-1}}{207.226 \text{ cm}^{-1}} = 1.036$$

Then it follows from eqn 16 that the populations are

$$p_v = (1 - e^{-\beta\epsilon})e^{-v\beta\epsilon} = 0.645 e^{-1.036v}$$

Therefore, $p_0 = 0.645, p_1 = 0.229, p_2 = 0.081$.

Comment The I-I bond is not stiff and the atoms are heavy: as a result, the vibrational energy separations are small and at room temperature several vibrational levels are significantly populated. The value of the partition function, $q = 1.55$, reflects this small but significant spread of populations.

Self-test 19.4 At what temperature would the $v = 1$ level of I_2 have (a) half the population of the ground state, (b) the same population as the ground state?

[(a) 445 K, (b) infinite]

(b) Approximations and factorizations

In general, exact analytical expressions for partition functions cannot be obtained. However, closed approximate expressions can often be found and prove to be very important in a number of chemical applications. For instance, the expression for the partition function for a particle of mass m free to move in a one-dimensional container of length X can be evaluated by making use of the fact that the separation of energy levels is very small and that large numbers of states are accessible at normal temperatures. As shown in the *Justification* below, in this case

$$q_x = \left(\frac{2\pi m}{h^2\beta} \right)^{1/2} X \quad (18)$$

Justification 19.4

The energy levels of a molecule of mass m in a container of length X are given by eqn 12.7 with $L = X$:

$$E_n = \frac{n^2 h^2}{8mX^2} \quad n = 1, 2, \dots$$

The lowest level ($n = 1$) has energy $h^2/8mX^2$, so the energies relative to that level are

$$\epsilon_n = (n^2 - 1)\epsilon \quad \epsilon = \frac{h^2}{8mX^2}$$

The sum to evaluate is therefore

$$q_X = \sum_{n=1}^{\infty} e^{-(n^2-1)\beta\epsilon}$$

The translational energy levels are very close together in a container the size of a typical laboratory vessel; therefore, the sum can be approximated by an integral:

$$q_X = \int_1^{\infty} e^{-(n^2-1)\beta\epsilon} dn$$

The extension of the lower limit to $n = 0$ and the replacement of $n^2 - 1$ by n^2 introduces negligible error but turns the integral into standard form. We make the substitution $x^2 = n^2\beta\epsilon$, implying $dn = dx/(\beta\epsilon)^{1/2}$, and therefore that

$$q_X = \left(\frac{1}{\beta\epsilon}\right)^{1/2} \int_0^{\infty} e^{-x^2} dx = \left(\frac{1}{\beta\epsilon}\right)^{1/2} \left(\frac{\pi^{1/2}}{2}\right) = \left(\frac{2\pi m}{h^2\beta}\right)^{1/2} X$$

Another useful feature of partition functions is used to derive expressions when the energy of a molecule arises from several different, independent sources: *if the energy is a sum of independent contributions, the partition function is a product of partition functions for each mode of motion*. For instance, suppose the molecule we are considering is free to move in three dimensions. We take the length of the container in the y -direction to be Y and that in the z -direction to be Z . The total energy of a molecule ϵ is the sum of its translational energies in all three directions:

$$\epsilon_{n_1, n_2, n_3} = \epsilon_{n_1}^{(X)} + \epsilon_{n_2}^{(Y)} + \epsilon_{n_3}^{(Z)} \quad (19)$$

where n_1 , n_2 , and n_3 are the quantum numbers for motion in the x -, y -, and z -directions, respectively. Therefore, because $e^{a+b+c} = e^a e^b e^c$, the partition function factorizes as follows:

$$\begin{aligned} q &= \sum_{\text{all } n} e^{-\beta\epsilon_{n_1}^{(X)} - \beta\epsilon_{n_2}^{(Y)} - \beta\epsilon_{n_3}^{(Z)}} = \sum_{\text{all } n} e^{-\beta\epsilon_{n_1}^{(X)}} e^{-\beta\epsilon_{n_2}^{(Y)}} e^{-\beta\epsilon_{n_3}^{(Z)}} \\ &= \left(\sum_{n_1} e^{-\beta\epsilon_{n_1}^{(X)}}\right) \left(\sum_{n_2} e^{-\beta\epsilon_{n_2}^{(Y)}}\right) \left(\sum_{n_3} e^{-\beta\epsilon_{n_3}^{(Z)}}\right) = q_X q_Y q_Z \end{aligned} \quad (20)$$

It is generally true that, *if the energy of a molecule can be written as the sum of independent terms, the partition function is the corresponding product of individual contributions*.

Equation 18 gives the partition function for translational motion in the x -direction. The only change for the other two directions is to replace the length X by the lengths Y or Z . Hence the partition function for motion in three dimensions is

$$q = \left(\frac{2\pi m}{h^2\beta}\right)^{3/2} XYZ \quad (21)$$

The product of lengths XYZ is the volume, V , of the container, so we can write

$$q = \frac{V}{\Lambda^3} \quad \Lambda = h \left(\frac{\beta}{2\pi m} \right)^{1/2} = \frac{h}{(2\pi mkT)^{1/2}} \quad (22)$$

The quantity Λ has the dimensions of length and is called the **thermal wavelength** of the molecule.

Illustration

To calculate the translational partition function of an H_2 molecule confined to a 100 cm^3 vessel at 25°C we use $m = 2.016 \text{ u}$; then

$$\begin{aligned} \Lambda &= \frac{6.626 \times 10^{-34} \text{ J}}{\{2\pi \times (2.016 \times 1.6605 \times 10^{-27} \text{ kg}) \times (1.38 \times 10^{-23} \text{ JK}^{-1}) \times (298 \text{ K})\}^{1/2}} \\ &= 7.12 \times 10^{-11} \text{ m} \end{aligned}$$

Therefore,

$$q = \frac{1.00 \times 10^{-4} \text{ m}^3}{(7.12 \times 10^{-11} \text{ m})^3} = 2.77 \times 10^{26}$$

About 10^{26} quantum states are thermally accessible, even at room temperature and for this light molecule. Many states are occupied if the thermal wavelength (which in this case is 71.2 pm) is small compared with the linear dimensions of the container.

Self-test 19.5 Calculate the translational partition function for a D_2 molecule under the same conditions.

$$[q = 7.8 \times 10^{26}, 2^{3/2} \text{ times larger}]$$

The internal energy and the entropy

The importance of the molecular partition function is that it contains all the information needed to calculate the thermodynamic properties of a system of independent particles. In this respect, q plays a role in statistical thermodynamics very similar to that played by the wavefunction in quantum mechanics: q is a kind of thermal wavefunction.

19.3 The internal energy

We shall begin to unfold the importance of q by showing how to derive an expression for the internal energy of the system.

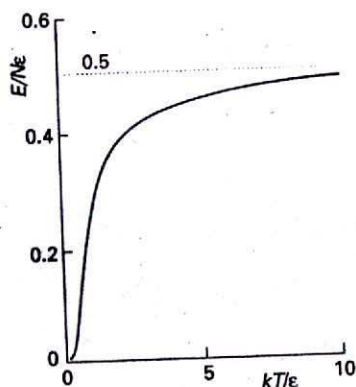
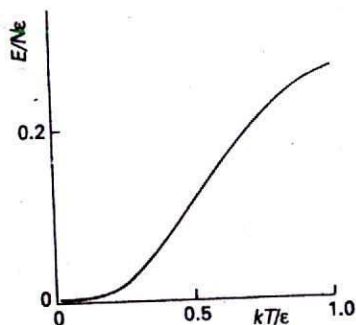
(a) The relation between U and q

The total energy of the system is

$$E = \sum_i n_i \epsilon_i \quad (23)$$

Because the most probable configuration is so strongly dominating, we can use the Boltzmann distribution for the populations and write

$$E = \frac{N}{q} \sum_i \epsilon_i e^{-\beta \epsilon_i} \quad (24)$$



19.8 The total energy of a two-level system (expressed as a multiple of $N\epsilon$) as a function of temperature, on two temperature scales. The graph at the top shows the slow rise away from zero energy at low temperatures; the slope of the graph at $T = 0$ is 0 (that is, the heat capacity is zero at $T = 0$). The graph below shows the slow rise to 0.5 as $T \rightarrow \infty$ as both states become equally populated (see Fig. 19.7).

To manipulate this expression into a form involving only q we note that

$$\frac{d}{d\beta} e^{-\beta\epsilon_i} = -\epsilon_i e^{-\beta\epsilon_i}$$

It follows that

$$E = -\frac{N}{q} \sum_i \frac{d}{d\beta} e^{-\beta\epsilon_i} = -\frac{N}{q} \frac{d}{d\beta} \sum_i e^{-\beta\epsilon_i} = -\frac{N}{q} \frac{dq}{d\beta} \quad (25)$$

Illustration

From the two-level partition function $q = 1 + e^{-\beta\epsilon}$, we can deduce that the total energy of N two-level systems is

$$\begin{aligned} E &= -\left(\frac{N}{1 + e^{-\beta\epsilon}}\right) \frac{d}{d\beta} (1 + e^{-\beta\epsilon}) = \frac{N\epsilon e^{-\beta\epsilon}}{1 + e^{-\beta\epsilon}} \\ &= \frac{N\epsilon}{1 + e^{\beta\epsilon}} \end{aligned}$$

This function is plotted in Fig. 19.8. Notice how the energy is zero at $T = 0$, when only the lower state (at the zero of energy) is occupied, and rises to $\frac{1}{2}N\epsilon$ as $T \rightarrow \infty$, when the two levels become equally populated.

There are several points in relation to eqn 25 that need to be made. Because $\epsilon_0 = 0$, (remember that we measure all energies from the lowest available level), E should be interpreted as the value of the internal energy U , we must add the internal energy at $T = 0$:

$$U = U(0) + E \quad (26)$$

Secondly, because the partition function may depend on variables other than the temperature (for example, the volume), the derivative with respect to β in eqn 25 is actually a *partial* derivative with these other variables held constant. The complete expression relating the molecular partition function to the thermodynamic internal energy of a system of independent molecules is therefore

$$U = U(0) - \frac{N}{q} \left(\frac{\partial q}{\partial \beta}\right)_V \quad (27a)$$

An equivalent form is obtained by noting that $dx/x = d \ln x$:

$$U = U(0) - N \left(\frac{\partial \ln q}{\partial \beta}\right)_V \quad (27b)$$

These two equations confirm that we need know only the partition function (as a function of temperature) to calculate the internal energy relative to its value at $T = 0$.

(b) The value of β

We now confirm that the parameter β , which we have anticipated is equal to $1/kT$, does indeed have that value. To do so, we shall compare the equipartition expression for the internal energy of a monatomic perfect gas, which from *Molecular interpretation 2.2* we know to be

$$U = U(0) + \frac{3}{2}nRT \quad (28a)$$

with the value calculated from the translational partition function (see the following *Justification*), which is

$$U = U(0) + \frac{3N}{2\beta} \quad (28b)$$

It follows by comparing these two expressions that

$$\beta = \frac{N}{nRT} = \frac{nN_A}{nN_A kT} = \frac{1}{kT} \quad (29)$$

as was to be proved. (We have used $N = nN_A$, where n is the amount of gas molecules, N_A is the Avogadro constant, and $R = N_A k$.)

Justification 19.5

To use eqn 27, we introduce the translational partition function from eqn 22:

$$\left(\frac{\partial q}{\partial \beta}\right)_V = \left(\frac{\partial V}{\partial \beta} \frac{1}{\Lambda^3}\right)_V = V \frac{d}{d\beta} \frac{1}{\Lambda^3} = -3 \frac{V}{\Lambda^4} \frac{d\Lambda}{d\beta}$$

Then we note from the formula for Λ in eqn 22 that

$$\frac{d\Lambda}{d\beta} = \frac{d}{d\beta} \left\{ \frac{h\beta^{1/2}}{(2\pi m)^{1/2}} \right\} = \frac{1}{2\beta^{1/2}} \times \frac{h}{(2\pi m)^{1/2}} = \frac{\Lambda}{2\beta}$$

and so obtain

$$\left(\frac{\partial q}{\partial \beta}\right)_V = -\frac{3V}{2\beta\Lambda^3}$$

Then, by eqn 27a,

$$U = U(0) - N \left(\frac{\Lambda^3}{V}\right) \left(-\frac{3V}{2\beta\Lambda^3}\right) = U(0) + \frac{3N}{2\beta}$$

19.4 The statistical entropy

If it is true that the partition function contains all thermodynamic information, then it must be possible to use it to calculate the entropy as well as the internal energy. Because we know (from Section 4.2) that entropy is related to the dispersal of energy and that the partition function is a measure of the number of states that are thermally accessible, we can be confident that the two are indeed related.

We shall develop the relation between the entropy and the partition function in two stages. In the first stage, we justify one of the most celebrated equations in statistical thermodynamics, the Boltzmann formula for the entropy:

$$S = k \ln W \quad [30]$$

In this expression, W is the weight of the most probable configuration of the system. In the second stage, we express W in terms of the partition function.

Justification 19.6

A change in the internal energy

$$U = U(0) + \sum_i n_i \epsilon_i \quad (31)$$

may arise from either a modification of the energy levels of a system (when ϵ_i changes to $\epsilon_i + d\epsilon_i$) or from a modification of the populations (when n_i changes to $n_i + dn_i$). The most general change is therefore

$$dU = dU(0) + \sum_i n_i d\epsilon_i + \sum_i \epsilon_i dn_i \quad (32)$$

Because the energy levels do not change when a system is heated at constant volume (Fig. 19.9), in the absence of all changes other than heating

$$dU = \sum_i \epsilon_i dn_i$$

We know from thermodynamics (and specifically from eqn 5.2) that under the same conditions

$$dU = dq_{\text{rev}} = TdS$$

Therefore,

$$dS = \frac{dU}{T} = k\beta \sum_i \epsilon_i dn_i \quad (33)$$

We also know that for changes in the most probable configuration (the only one we need consider)

$$\left(\frac{\partial \ln W}{\partial n_i} \right) + \alpha - \beta \epsilon_i = 0$$

(this is eqn 8). After rearranging this expression to

$$\beta \epsilon_i = \left(\frac{\partial \ln W}{\partial n_i} \right) + \alpha$$

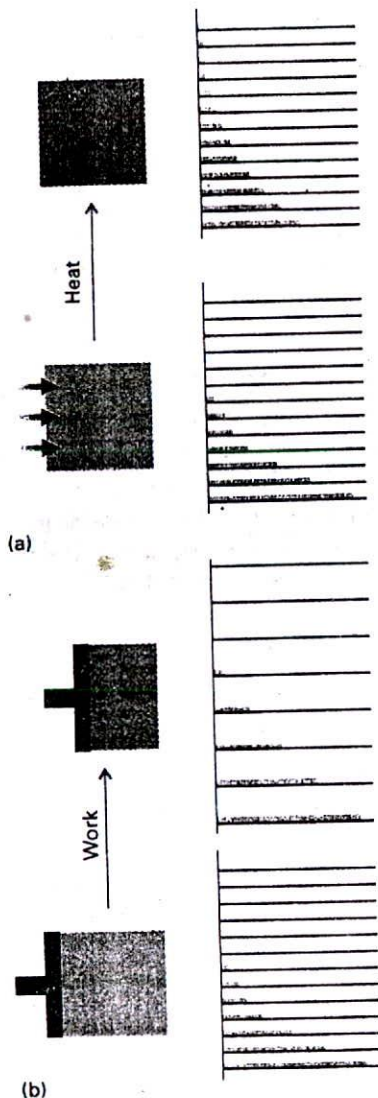
we find that

$$dS = k \sum_i \left(\frac{\partial \ln W}{\partial n_i} \right) dn_i + k\alpha \sum_i dn_i$$

But the sum over the dn_i is zero, because the number of molecules is constant. Hence

$$dS = k \sum_i \left(\frac{\partial \ln W}{\partial n_i} \right) dn_i = k(d \ln W) \quad (34)$$

This relation strongly suggests the definition $S = k \ln W$, as in eqn 30.

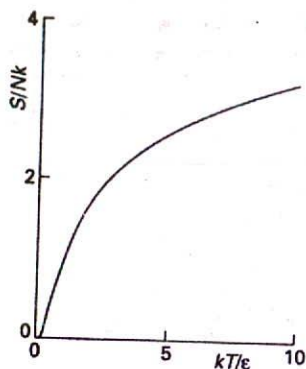


19.9 (a) When a system is heated, the energy levels are unchanged but their populations are changed. (b) When work is done on a system, the energy levels themselves are changed. The levels in this case are the one-dimensional particle-in-a-box energy levels of Chapter 12: they depend on the size of the container and move apart as its length is decreased. For simplicity in making the essential point, we have shown the energy levels as equally spaced; in fact, their separation increases with energy.

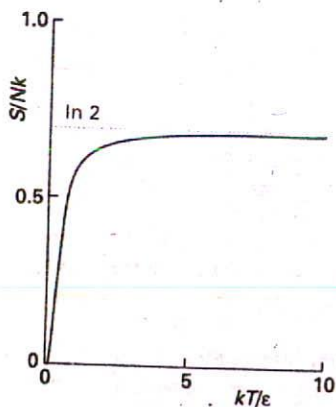
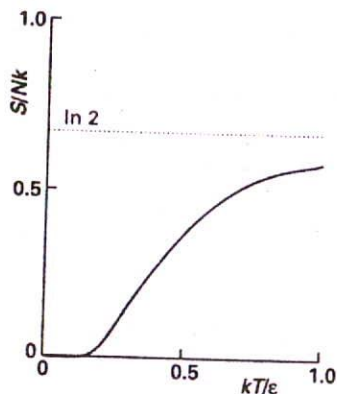
The statistical entropy behaves in exactly the same way as the thermodynamic entropy. Thus, as the temperature is lowered, the value of W , and hence of S , decreases because fewer configurations are compatible with the total energy. In the limit $T \rightarrow 0$, $W = 1$, so $\ln W = 0$, because only one configuration (every molecule in the lowest level) is compatible with $E = 0$. It follows that $S \rightarrow 0$ as $T \rightarrow 0$, which is compatible with the Third Law of thermodynamics, that the entropies of all perfect crystals approach the same value as $T \rightarrow 0$ (Section 4.4a).

Now we relate the Boltzmann formula for the entropy to the partition function. To do so, we substitute the expression for $\ln W$ given in eqn 3 into eqn 30 and, as shown in the *Justification* below, obtain

$$S = \frac{U - U(0)}{T} + Nk \ln q \quad (35)$$



19.10 The temperature variation of the entropy of the system shown in Fig. 19.3 (expressed here as a multiple of Nk). The entropy approaches zero as $T \rightarrow 0$, and increases without limit as $T \rightarrow \infty$.



19.11 The temperature variation of the entropy of a two-level system (expressed as a multiple of Nk). As $T \rightarrow \infty$, the two states become equally populated and S approaches $Nk \ln 2$.

Justification 19.7

The first stage is to write

$$S = k \sum_i (n_i \ln N - n_i \ln n_i) = -k \sum_i n_i \ln \left(\frac{n_i}{N} \right) = -Nk \sum_i p_i \ln p_i \quad (36)$$

where $p_i = n_i/N$, the fraction of molecules in state i . It follows from eqn 10 that

$$\ln p_i = -\beta \epsilon_i - \ln q$$

and therefore that

$$S = -Nk \left(-\beta \sum_i p_i \epsilon_i - \sum_i p_i \ln q \right) = k\beta \{U - U(0)\} + Nk \ln q$$

We have used the fact that the sum over the p_i is equal to 1 and the sum over $Np_i \epsilon_i$ is equal to $U - U(0)$ (see eqn 31). We have already established that $\beta = 1/kT$, so eqn 35 immediately follows.

Example 19.4 Calculating the entropy of a collection of oscillators

Calculate the entropy of a collection of N independent harmonic oscillators, and evaluate it using vibrational data for I_2 at 25°C (Example 19.3).

Method To use eqn 31, we use the partition function for a molecule with evenly spaced vibrational energy levels, eqn 15. With the partition function available, the internal energy can be found by differentiation (as in eqn 27a), and the two expressions then combined to give S .

Answer The molecular partition function as given in eqn 15 is

$$q = \frac{1}{1 - e^{-\beta \epsilon}}$$

The internal energy is obtained by using eqn 27a:

$$U - U(0) = -\frac{N}{q} \left(\frac{\partial q}{\partial \beta} \right)_V = \frac{N \epsilon e^{-\beta \epsilon}}{1 - e^{-\beta \epsilon}} = \frac{N \epsilon}{e^{\beta \epsilon} - 1}$$

The entropy is therefore

$$S = Nk \left\{ \frac{\beta \epsilon}{e^{\beta \epsilon} - 1} - \ln(1 - e^{-\beta \epsilon}) \right\}$$

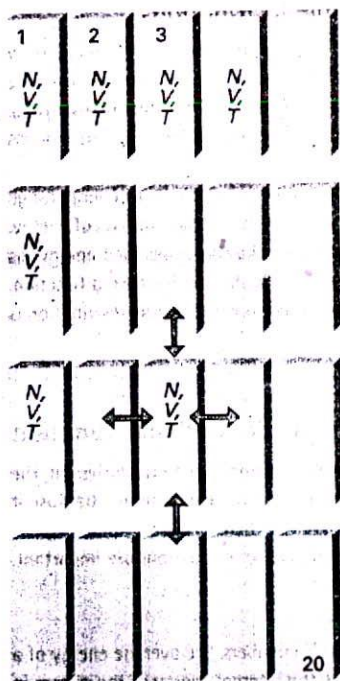
This function is plotted in Fig. 19.10. For I_2 at 25°C, $\beta \epsilon = 1.036$ (Example 19.3), so $S_m = 8.38 \text{ J K}^{-1} \text{ mol}^{-1}$.

Self-test 19.6 Evaluate the molar entropy of N two-level systems and plot the resulting expression. What is the entropy when the two states are equally thermally accessible?

$$[S/Nk = \beta \epsilon / (1 + e^{\beta \epsilon}) + \ln(1 + e^{-\beta \epsilon}); \text{ see Fig. 19.11}; S = Nk \ln 2]$$

The canonical partition function

In this section we see how to generalize our conclusions to include systems composed of interacting molecules. We shall also see how to obtain the molecular partition function from the more general form of the partition function developed here.



19.12 A representation of the canonical ensemble, in this case for $\tilde{N} = 20$. The individual replications of the actual system all have the same composition and volume. They are all in mutual thermal contact, and so all have the same temperature. Energy may be transferred between them as heat, and so they do not all have the same energy. The total energy (\bar{E}) of all 20 replications is a constant because the ensemble is isolated overall.

19.5 The canonical ensemble

The crucial new concept we need when treating systems of interacting particles is the ensemble. Like so many scientific terms, the term has basically its normal meaning of 'collection', but it has been sharpened and refined into a precise significance.

(a) The concept of ensemble

To set up an ensemble, we take a closed system of specified volume, composition, and temperature, and think of it as replicated \tilde{N} times (Fig. 19.12). All the identical closed systems are regarded as being in thermal contact with one another, so they can exchange energy. The total energy of all the systems is \bar{E} and, because they are in thermal equilibrium with one another, they all have the same temperature, T . This imaginary collection of replications of the actual system with a common temperature is called the **canonical ensemble**.⁶

The important point about an ensemble is that it is a collection of *imaginary* replications of the system, so we are free to let the number of members be as large as we like; when appropriate, we can let \tilde{N} become infinite.⁷ The number of members of the ensemble in a state with energy E_i is denoted \tilde{n}_i , and we can speak of the configuration of the ensemble (by analogy with the configuration of the system used in Section 19.1) and its weight, \bar{W} .

(b) Dominating configurations

Just as in Section 19.1, some of the configurations of the ensemble will be very much more probable than others. For instance, it is very unlikely that the whole of the total energy, \bar{E} , will accumulate in one system. By analogy with the earlier discussion, we can anticipate that there will be a dominating configuration, and that we can evaluate the thermodynamic properties by taking the average over the ensemble using that single, most probable, configuration. In the thermodynamic limit of $\tilde{N} \rightarrow \infty$, this dominating configuration is overwhelmingly the most probable, and it dominates the properties of the system virtually completely.

The quantitative discussion follows the argument in Section 19.1 with the modification that N and n_i are replaced by \tilde{N} and \tilde{n}_i . The weight of a configuration $\{\tilde{n}_0, \tilde{n}_1, \dots\}$ is

$$\bar{W} = \frac{\tilde{N}!}{\tilde{n}_0! \tilde{n}_1! \dots} \quad (37)$$

The configuration of greatest weight, subject to the constraints that the total energy of the ensemble is constant at \bar{E} and that the total number of members is fixed at \tilde{N} , is given by the **canonical distribution**:

$$\frac{\tilde{n}_i}{\tilde{N}} = \frac{e^{-\beta E_i}}{Q} \quad Q = \sum_i e^{-\beta E_i} \quad (38)$$

The quantity Q , which is a function of the temperature, is called the **canonical partition function**.

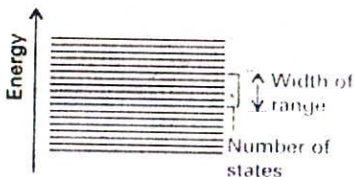
6 The word 'canon' means 'according to a rule'. There are two other important ensembles. In the *microcanonical ensemble* the condition of constant temperature is replaced by the requirement that all the systems should have exactly the same energy: each system is individually isolated. In the *grand canonical ensemble* the volume and temperature of each system are the same, but they are open, which means that matter can be imagined as able to pass between the systems; the composition of each one may fluctuate, but now the chemical potential is the same in each system:

Microcanonical ensemble: N, V, E common

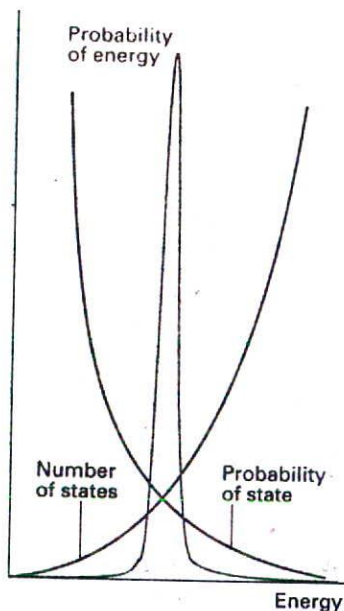
Canonical ensemble: N, V, T common

Grand canonical ensemble: μ, V, T common

7 Note that \tilde{N} is unrelated to N , the number of molecules in the actual system; \tilde{N} is the number of imaginary replications of that system.



19.13 The energy density of states is the number of states in an energy range divided by the width of the range.



19.14 To construct the form of the distribution of members of the canonical ensemble in terms of their energies, we multiply the probability that any one is in a state of given energy, eqn 38, by the number of states corresponding to that energy (a steeply rising function). The product is a sharply peaked function at the mean energy, which shows that almost all the members of the ensemble have that energy.

(c) Fluctuations from the most probable distribution

The shape of the canonical distribution in eqn 38 is only *apparently* an exponentially decreasing function of the energy of the system. We must appreciate that eqn 38 gives the probability of occurrence of members in a single state i of the entire system of energy E_i . There may in fact be numerous states with almost identical energies. For example, in a gas the identities of the molecules moving slowly or quickly can change without necessarily affecting the total energy. The density of states, the number of states in an energy range divided by the width of the range (Fig. 19.13), is a very sharply increasing function of energy. It follows that the probability of a member of an ensemble having a specified energy (as distinct from being in a specified state) is given by eqn 38, a sharply decreasing function, multiplied by a sharply increasing function (Fig. 19.14). Therefore, the overall distribution is a sharply peaked function. We conclude that most members of the ensemble have an energy very close to the mean value.

19.6 The thermodynamic information in the partition function

Like the molecular partition function, the canonical partition function carries all the thermodynamic information about a system. However, Q is more general than q because it does not assume that the molecules are independent. We can therefore use Q to discuss the properties of condensed phases and real gases where molecular interactions are important.

(a) The internal energy

If the total energy of the ensemble is \bar{E} , and there are \bar{N} members, the average energy of a member is $E = \bar{E}/\bar{N}$. We use this quantity to calculate the internal energy of the system in the limit of \bar{N} (and \bar{E}) approaching infinity:

$$U = U(0) + E = U(0) + \frac{\bar{E}}{\bar{N}} \quad \text{as } \bar{N} \rightarrow \infty \quad (39)$$

The fraction, \bar{p}_i , of members of the ensemble in a state i with energy E_i is given by the analogue of eqn 10 as

$$\bar{p}_i = \frac{e^{-\beta E_i}}{Q} \quad (40)$$

It follows that the internal energy is given by

$$U = U(0) + \sum_i \bar{p}_i E_i = U(0) + \frac{1}{Q} \sum_i E_i e^{-\beta E_i} \quad (41)$$

By the same argument that led to eqn 27,

$$U = U(0) - \frac{1}{Q} \left(\frac{\partial Q}{\partial \beta} \right)_V = U(0) - \left(\frac{\partial \ln Q}{\partial \beta} \right)_V \quad (42)$$

(b) The entropy

The total weight, \bar{W} , of a configuration of the ensemble is the product of the average weight W of each member of the ensemble; $\bar{W} = W^{\bar{N}}$. Hence, we can calculate S from

$$S = k \ln \bar{W} = k \ln W^{\bar{N}} = \frac{k}{\bar{N}} \ln \bar{W} \quad (43)$$

It follows, by the same argument used in Section 19.4, that

$$S = \frac{U - U(0)}{T} + k \ln Q \quad (44)$$

19.7 Independent molecules

We shall now see how to recover the molecular partition function from the more general canonical partition function when the molecules are independent. When the molecules are independent and distinguishable (in the sense to be described), the relation between Q and q is

$$Q = q^N \quad (45)$$

Justification 19.8

The total energy of a collection of N independent molecules is the sum of the energies of the molecules. Therefore, we can write the total energy of a state i of the system as

$$E_i = \varepsilon_i(1) + \varepsilon_i(2) + \cdots + \varepsilon_i(N)$$

In this expression, $\varepsilon_i(1)$ is the energy of molecule 1 when the system is in the state i , $\varepsilon_i(2)$ the energy of molecule 2 when the system is in the same state i , and so on. The canonical partition function is then

$$Q = \sum_i e^{-\beta\varepsilon_i(1) - \beta\varepsilon_i(2) - \cdots - \beta\varepsilon_i(N)}$$

The sum over the states of the system can be reproduced by letting each molecule enter all its own individual states (although we meet an important proviso shortly). Therefore, instead of summing over the states i of the system, we can sum over all the individual states i of molecule 1, all the states i of molecule 2, and so on. This rewriting of the original expression leads to

$$Q = \left(\sum_i e^{-\beta\varepsilon_i} \right) \left(\sum_i e^{-\beta\varepsilon_i} \right) \cdots \left(\sum_i e^{-\beta\varepsilon_i} \right) = \left(\sum_i e^{-\beta\varepsilon_i} \right)^N = q^N$$

(a) Distinguishable and indistinguishable molecules

If all the molecules are identical and free to move through space, we cannot distinguish them and the relation $Q = q^N$ is not valid. Suppose that molecule 1 is in some state a , molecule 2 is in b , and molecule 3 is in c , then one member of the ensemble has an energy $E = \varepsilon_a + \varepsilon_b + \varepsilon_c$. This member, however, is indistinguishable from one formed by putting molecule 1 in state b , molecule 2 in state c , and molecule 3 in state a , or some other permutation. There are six such permutations in all, and $N!$ in general. In the case of indistinguishable molecules, it follows that we have counted too many states in going from the sum over system states to the sum over molecular states, so writing $Q = q^N$ overestimates the value of Q . The detailed argument is quite involved, but at all except very low temperatures it turns out that the correction factor is $1/N!$. Therefore:

$$\begin{aligned} \text{(a) For distinguishable independent molecules: } Q &= q^N \\ \text{(b) For indistinguishable independent molecules: } Q &= \frac{q^N}{N!} \end{aligned} \quad (46)$$

For molecules to be indistinguishable, they must be of the same kind: an Ar atom is never indistinguishable from a Ne atom. Their identity, however, is not the only criterion. Each identical molecule in a crystal lattice, for instance, can be 'named' with a set of coordinates. Identical molecules in a lattice are therefore distinguishable because their sites are distinguishable, and we use eqn 46a for any of their modes that may be considered independent of their neighbours. Equation 46a is also applicable to a collection of N molecules, each one of which is in its own box. On the other hand, identical molecules in a gas are free to move to different locations, and there is no way of keeping track of the identity of a given molecule; we therefore use eqn 46b.

(b) The entropy of a monatomic gas

An important application of the previous material is the derivation (as shown in the *Justification* below) of the Sackur-Tetrode equation for the entropy of a monatomic gas:

$$S = nR \ln \left(\frac{e^{5/2} V}{n N_A \Lambda^3} \right) \quad \Lambda = \frac{h}{(2\pi m k T)^{1/2}} \quad (47a)$$

Because the gas is perfect, we can use the relation $V = nRT/p$ to express the entropy in terms of the pressure as

$$S = nR \ln \left(\frac{e^{5/2} k T}{p \Lambda^3} \right) \quad (47b)$$

Justification 19.9

For a gas of independent molecules, Q may be replaced by $q^N/N!$, with the result that eqn 44 becomes

$$S = \frac{U - U(0)}{T} + Nk \ln q - k \ln N!$$

Because the number of molecules ($N = nN_A$) in a typical sample is large, we can use Stirling's approximation (eqn 2) to write

$$S = \frac{U - U(0)}{T} + Nk \ln q - k(N \ln N - N)$$

The only mode of motion for a gas of atoms is translation, and the partition function is $q = V/\Lambda^3$ (eqn 22), where Λ is the thermal wavelength. The internal energy is given by eqn 28, so the entropy is

$$\begin{aligned} S &= \frac{3}{2}nR + nR \left(\ln \frac{V}{\Lambda^3} - \ln nN_A + 1 \right) \\ &= nR \left(\ln e^{3/2} + \ln \frac{V}{\Lambda^3} - \ln nN_A + \ln e \right) \end{aligned}$$

which rearranges into eqn 47.

Example 19.5 Using the Sackur-Tetrode equation

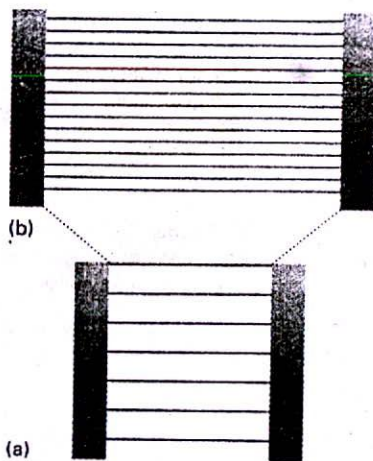
Calculate the standard molar entropy of gaseous argon at 25°C.

Method To calculate the *molar* entropy, S_m , from eqn 47b, divide both sides by n . To calculate the *standard* molar entropy, S_m^\ominus , set $p = p^\ominus$ in the expression for S_m :

$$S_m^\ominus = R \ln \left(\frac{e^{5/2} k T}{p^\ominus \Lambda^3} \right)$$

Answer The mass of an Ar atom is $m = 39.95$ u. At 25°C, its thermal wavelength is 16.0 pm (by the same kind of calculation as in the *Illustration* following eqn 22). Therefore,

$$\begin{aligned} S_m^\ominus &= R \ln \left\{ \frac{e^{5/2} \times (4.12 \times 10^{-21} \text{ J})}{(10^5 \text{ N m}^{-2}) \times (1.60 \times 10^{-11} \text{ m})^3} \right\} \\ &= 18.6R = 155 \text{ J K}^{-1} \text{ mol}^{-1} \end{aligned}$$



19.15 As the width of a container is increased (going from (a) to (b)), the energy levels become closer together (as $1/L^2$), and as a result more are thermally accessible at a given temperature. Consequently, the entropy of the system rises as the container expands. As before, this diagram is schematic: the separation of levels increases with energy.

Comment We can anticipate, on the basis of the number of accessible states for a lighter molecule, that the standard molar entropy of Ne is likely to be smaller than for Ar; its actual value is $17.60R$ at 298 K.

Self-test 19.7 Calculate the translational contribution to the standard molar entropy of H_2 at 25°C.

[14.2R]

The Sackur-Tetrode equation implies that, when a monatomic perfect gas expands isothermally from V_i to V_f , its entropy changes by

$$\Delta S = nR \ln(aV_f) - nR \ln(aV_i) = nR \ln\left(\frac{V_f}{V_i}\right) \quad (48)$$

where aV is the collection of quantities inside the logarithm of eqn 47a. This is exactly the expression we obtained by using classical thermodynamics (Example 4.1). Now, though, we see that that classical expression is in fact a consequence of the increase in the number of accessible translational states when the volume of the container is increased (Fig. 19.15).

Table 19.1 Key equations, with $\beta = 1/kT$

Definition of molecular partition function:

$$q = \sum_i e^{-\beta \epsilon_i} \quad q = \sum_{\text{levels, } i} g_i e^{-\beta \epsilon_i}$$

Definition of canonical partition function:

$$Q = \sum_i e^{-\beta \epsilon_i} = \begin{cases} q^N & \text{distinguishable independent particles} \\ q^N/N! & \text{indistinguishable independent particles} \end{cases}$$

Two-level system, energies 0, ϵ :

$$q = 1 + e^{-\beta \epsilon}$$

Evenly spaced, infinite level system, energies 0, $\epsilon, 2\epsilon, \dots$:

$$q = (1 - e^{-\beta \epsilon})^{-1}$$

Translational motion of particle of mass m in volume V :

$$q = \frac{V}{\Lambda^3} \quad \Lambda = \left(\frac{h^2 \beta}{2\pi m}\right)^{1/2} = \frac{h}{(2\pi m k T)^{1/2}}$$

Boltzmann distribution:

$$p_i = \frac{e^{-\beta \epsilon_i}}{q} \quad p_i = \frac{n_i}{N}$$

Boltzmann formula:

$$S = k \ln W$$

Internal energy (independent particles):

$$U = U(0) - \frac{N}{q} \left(\frac{\partial q}{\partial \beta}\right)_V = U(0) - N \left(\frac{\partial \ln q}{\partial \beta}\right)_V$$

Internal energy (general):

$$U = U(0) - \frac{1}{Q} \left(\frac{\partial Q}{\partial \beta}\right)_V = U(0) - \left(\frac{\partial \ln Q}{\partial \beta}\right)_V$$

Entropy (independent particles):

$$S = \frac{U - U(0)}{T} + Nk \ln q$$

Entropy (general):

$$S = \frac{U - U(0)}{T} + k \ln Q$$

Checklist of key ideas

statistical thermodynamics

The distribution of molecular states

- population
 principle of equal *a priori* probabilities

19.1 Configurations and weights

- configuration
 weight (1)
 Stirling's approximation (2)
 Boltzmann distribution (6)
 method of undetermined multipliers

19.2 The molecular partition function

- molecular partition function (11, 12)
 thermal wavelength

The internal energy and the entropy

- q for uniform array (15)
 q for translation (18, 22)

19.3 The internal energy

- U in terms of q (27)

19.4 The statistical entropy

- Boltzmann formula (30)
 S in terms of q (35)

The canonical partition function

19.5 The canonical ensemble

- ensemble
 canonical ensemble
 thermodynamic limit
 canonical distribution (38)
 canonical partition function
 density of states

19.6 The thermodynamic information in the partition function

- U in terms of Q (41)
 S in terms of Q (44)

19.7 Independent molecules

- distinguishable and indistinguishable molecules (46)
 Sackur-Tetrode equation (47)

Further reading

Articles of general interest

C.W. David, On the Legendre transformation and the Sackur-Tetrode equation. *J. Chem. Educ.* **65**, 876 (1988).

P.G. Nelson, Statistical mechanical interpretation of entropy. *J. Chem. Educ.* **71**, 103 (1994).

Texts and sources of data and information

P.W. Atkins, *The second law*. Scientific American Books, New York (1984, revised 1994).

R.P.H. Gasser and W.G. Richards, *Introduction to statistical thermodynamics*. World Scientific, Singapore (1995).

T.L. Hill, *An introduction to statistical mechanics*. Dover, New York (1986).

D. Chandler, *Introduction to statistical mechanics*. Oxford University Press (1987).

C.E. Hecht, *Statistical mechanics and kinetic theory*. W.H. Freeman & Co, New York (1990).

Exercises

19.1 (a) What are the relative populations of the states of a two-level system when the temperature is infinite?

19.1 (b) What is the temperature of a two-level system of energy separation equivalent to 300 cm^{-1} when the population of the upper state is one-half that of the lower state?

19.2 (a) Calculate the translational partition function at (a) 300 K and (b) 600 K of a molecule of molar mass 120 g mol^{-1} in a container of volume 2.00 cm^3 .

19.2 (b) Calculate (a) the thermal wavelength, (b) the translational partition function of an Ar atom in a cubic box of side 1.00 cm at (i) 300 K and (ii) 3000 K.

19.3 (a) Calculate the ratio of the translational partition functions of D_2 and H_2 at the same temperature and volume.

19.3 (b) Calculate the ratio of the translational partition functions of xenon and helium at the same temperature and volume.

19.4 (a) A certain atom has a threefold degenerate ground level, a non-degenerate electronically excited level at 3500 cm^{-1} , and a threefold degenerate level at 4700 cm^{-1} . Calculate the partition function of these electronic states at 1900 K.

19.4 (b) A certain atom has a doubly degenerate ground level, a triply degenerate electronically excited level at 1250 cm^{-1} , and a doubly degenerate level at 1300 cm^{-1} . Calculate the partition function of these electronic states at 2000 K.

19.5 (a) Calculate the electronic contribution to the molar internal energy at 1900 K for a sample composed of the atoms specified in Exercise 19.4a.

19.5 (b) Calculate the electronic contribution to the molar internal energy at 2000 K for a sample composed of the atoms specified in Exercise 19.4b.

- 19.6 (a)** A certain molecule has a non-degenerate excited state lying at 540 cm^{-1} above the non-degenerate ground state. At what temperature will 10 per cent of the molecules be in the upper state?
- 19.6 (b)** A certain molecule has a doubly degenerate excited state lying at 360 cm^{-1} above the non-degenerate ground state. At what temperature will 15 per cent of the molecules be in the upper state?
- 19.7 (a)** An electron spin can adopt either of two orientations in a magnetic field, and its energies are $\pm\mu_B B$, where μ_B is the Bohr magneton. Deduce an expression for the partition function and mean energy of the electron and sketch the variation of the functions with B . Calculate the relative populations of the spin states at (a) 4.0 K, (b) 298 K when $B = 1.0\text{ T}$.
- 19.7 (b)** The spin of a nitrogen nucleus can adopt any of three orientations in a magnetic field, and its energies are $0, \pm\gamma_N \hbar B$, where γ_N is the magnetogyric ratio of the nucleus. Deduce an expression for the partition function and mean energy of the nucleus and sketch the variation of the functions with B . Calculate the relative populations of the spin states at (a) 1.0 K, (b) 298 K when $B = 20.0\text{ T}$.
- 19.8 (a)** Consider a system of distinguishable particles having only two non-degenerate energy levels separated by an energy which is equal to the value of kT at 10 K. Calculate (a) the ratio of populations in the two states at (1) 1.0 K, (2) 10 K, and (3) 100 K, (b) the molecular partition function at 10 K, (c) the molar energy at 10 K, (d) the molar heat capacity at 10 K, (e) the molar entropy at 10 K.
- 19.8 (b)** Consider a system of distinguishable particles having only three non-degenerate energy levels separated by an energy which is equal to the value of kT at 25.0 K. Calculate (a) the ratio of populations in the states at (1) 1.00 K, (2) 25.0 K, and (3) 100 K, (b) the molecular partition function at 25.0 K, (c) the molar energy at 25.0 K, (d) the molar heat capacity at 25.0 K, (e) the molar entropy at 25.0 K.
- 19.9 (a)** At what temperature would the population of the first excited vibrational state of HCl be $1/e$ times its population of the ground state?
- 19.9 (b)** At what temperature would the population of the first rotational level of HCl be $1/e$ times the population of the ground state?
- 19.10 (a)** Calculate the standard molar entropy of neon gas at (a) 200 K, (b) 298.15 K.
- 19.10 (b)** Calculate the standard molar entropy of xenon gas at (a) 100 K, (b) 298.15 K.
- 19.11 (a)** Calculate the vibrational contribution to the entropy of Cl_2 at 500 K given that the wavenumber of the vibration is 560 cm^{-1} .
- 19.11 (b)** Calculate the vibrational contribution to the entropy of Br_2 at 600 K given that the wavenumber of the vibration is 321 cm^{-1} .
- 19.12 (a)** Identify the systems for which it is essential to include a factor of $1/N!$ on going from Q to q : (a) a sample of helium gas, (b) a sample of carbon monoxide gas, (c) a solid sample of carbon monoxide, (d) water vapour.
- 19.12 (b)** Identify the systems for which it is essential to include a factor of $1/N!$ on going from Q to q : (a) a sample of carbon dioxide gas, (b) a sample of graphite, (c) a sample of diamond, (d) ice.

Problems

Numerical problems

- 19.1** A certain atom has a doubly degenerate ground level pair and an upper level of four degenerate states at 450 cm^{-1} above the ground level. In an atomic beam study of the atoms it was observed that 30 per cent of the atoms were in the upper level, and the translational temperature of the beam was 300 K. Are the electronic states of the atoms in thermal equilibrium with the translational states?
- 19.2** Explore the conditions under which the 'integral' approximation for the translational partition function is not valid by considering the translational partition function of an Ar atom in a cubic box of side 1.00 cm. Estimate the temperature at which, according to the integral approximation, $q = 10$ and evaluate the exact partition function at that temperature.
- 19.3 (a)** Calculate the electronic partition function of a tellurium atom at (i) 298 K, (ii) 5000 K by direct summation using the following data:
- | Term | Degeneracy | Wavenumber/ cm^{-1} |
|--------|------------|------------------------------|
| Ground | 5 | 0 |
| 1 | 1 | 4707 |
| 2 | 3 | 4751 |
| 3 | 5 | 10559 |
- (b) What proportion of the Te atoms are in the ground term and in the term labelled 2 at the two temperatures? (c) Calculate the electronic contribution to the standard molar entropy of gaseous Te atoms.
- 19.4** The four lowest electronic levels of a Ti atom are: 3F_2 , 3F_3 , 3F_4 , and 5F_1 , at 0, 170, 387, and 6557 cm^{-1} , respectively. There are many other electronic states at higher energies. The boiling point of titanium is 3287°C . What are the relative populations of these levels at the boiling point? (*Hint*: The degeneracies of the levels are $2J + 1$.)
- 19.5** The NO molecule has a doubly degenerate excited level 121.1 cm^{-1} above the doubly degenerate ground term. Calculate

and plot the electronic partition function of NO from $T = 0$ to 1000 K. Evaluate (a) the term populations and (b) the electronic contribution to the molar internal energy at 300 K. Calculate the electronic contribution to the molar entropy of the NO molecule at 300 K and 500 K.

19.6 Calculate, by explicit summation, the vibrational partition function and the vibrational contribution to the molar internal energy of I_2 molecules at (a) 100 K, (b) 298 K given that its vibrational energy levels lie at the following wavenumbers above the zero-point energy level: 0, 213.30, 425.39, 636.27, 845.93 cm^{-1} . What proportion of I_2 molecules are in the ground and first two excited levels at the two temperatures? Calculate the vibrational contribution to the molar entropy of I_2 at the two temperatures.

Theoretical problems

19.7 A sample consisting of five molecules has a total energy 5ϵ . Each molecule is able to occupy states of energy $j\epsilon$, with $j = 0, 1, 2, \dots$ (a) Calculate the weight of the configuration in which the molecules are distributed evenly over the available states. (b) Draw up a table with columns headed by the energy of the states and write beneath them all configurations that are consistent with the total energy. Calculate the weights of each configuration and identify the most probable configurations.

19.8 A sample of nine molecules is numerically tractable but on the verge of being thermodynamically significant. Draw up a table of configurations for $N = 9$, total energy 9ϵ in a system with energy levels $j\epsilon$ (as in Problem 19.7). Before evaluating the weights of the configurations, guess (by looking for the most 'exponential' distribution of populations) which of the configurations will turn out to be the most probable. Go on to calculate the weights and identify the most probable configuration.

19.9 The most probable configuration is characterized by a parameter we know as the 'temperature'. The temperatures of the system specified in Problems 19.7 and 19.8 must be such as to give a mean value of ϵ for the energy of each molecule and a total energy $N\epsilon$ for the system. (a) Show that the temperature can be obtained by plotting p_j against j , where p_j is the (most probable) fraction of molecules in the state with energy $j\epsilon$. Apply the procedure to the system in Problem 19.8. What is the temperature of the system when ϵ corresponds to 50 cm^{-1} ? (b) Choose configurations other than the most probable, and show that the same procedure gives a worse straight line, indicating that a temperature is not well-defined for them.

19.10 A certain molecule can exist in either a non-degenerate singlet state or a triplet state (with degeneracy 3). The energy of the triplet exceeds that of the singlet by ϵ . Assuming that the molecules are distinguishable (localized) and independent, (a) obtain the expression for the molecular partition function, (b) find expressions in terms of ϵ for the molar energy, molar heat capacity, and molar entropy of such molecules and calculate their values at $T = \epsilon/k$.

19.11 Consider a system with energy levels $\epsilon_j = j\epsilon$ and N molecules. (a) Show that, if the mean energy per molecule is $a\epsilon$, then the

temperature is given by

$$\beta = \frac{1}{\epsilon} \ln \left(1 + \frac{1}{a} \right)$$

Evaluate the temperature for a system in which the mean energy is ϵ , taking ϵ equivalent to 50 cm^{-1} . (b) Calculate the molecular partition function q for the system when its mean energy is $a\epsilon$. (c) Show that the entropy of the system is

$$S/k = (1+a) \ln(1+a) - a \ln a$$

and evaluate this expression for a mean energy ϵ .

19.12 Suppose that by some means we contrive to invert the population of a two-level system, in the sense that the upper and lower levels have the populations of the lower and upper levels, respectively, in the system in thermal equilibrium at a temperature T . Show that the relative populations are still given by a Boltzmann-like expression but with a temperature $-T$. Under what circumstances is it possible to speak of negative temperatures of an evenly spaced three-level system?

19.13 Consider Stirling's approximation for $\ln N!$ in the derivation of the Boltzmann distribution. What difference would it make if (a) a cruder approximation, $N! = N^N$, (b) the better approximation in footnote 3 of Section 19.1a were used instead?

Additional problems supplied by Carmen Giunta and Charles Trapp

19.14 Consider a system A consisting of subsystems A_1 and A_2 , for which $W_1 = 1 \times 10^{20}$ and $W_2 = 2 \times 10^{20}$. What is the number of configurations available to the combined system? Also, compute the entropies S , S_1 , and S_2 . What is the significance of this result?

19.15 Consider 1.00×10^{22} ^4He atoms in a box of dimensions 1.0 cm \times 1.0 cm \times 1.0 cm. Calculate the occupancy of the first excited level at 1.0 mK, 2.0 K, and 4.0 K. Do the same for ^3He . What conclusions might you draw from the results of your calculations?

19.16 Given that for gases the canonical partition function, Q , is related to the molecular partition function q by $Q = q^N/N!$, prove, using the expression for q and general thermodynamic relations, the perfect gas law $pV = nRT$.

19.17 By what factor does the number of available configurations increase when 100 J of energy is added to a system containing 1.00 mol of particles at constant volume at 298 K?

19.18 By what factor does the number of available configurations increase when 20 m^3 of air at 1.00 atm and 300 K is allowed to expand by 0.0010 per cent at constant temperature?

19.19 (a) The standard molar entropy of graphite at 298, 410, and 498 K is 5.69, 9.03, and 11.63 $\text{JK}^{-1} \text{mol}^{-1}$, respectively. If 1.00 mol C(graphite) at 298 K is surrounded by thermal insulation and placed next to 1.00 mol C(graphite) at 498 K, also insulated, how many configurations are there altogether for the combined but independent systems? (b) If the same two samples are now placed in thermal contact and brought to thermal equilibrium, the final temperature will be 410 K. (Why might the final temperature not be

the average? It isn't.) How many configurations are there now in the combined system? Neglect any volume changes. (c) Demonstrate that this process is spontaneous.

19.20 Obtain the barometric formula (Problem 1.35) from the Boltzmann distribution. Recall that the potential energy of a particle at height h above the surface of the Earth is mgh . Convert the barometric formula from pressure to number density, \mathcal{N} . Compare the relative number densities, $\mathcal{N}(h)/\mathcal{N}(0)$, for O_2 and H_2O at $h = 8.0$ km, a typical cruising altitude for commercial aircraft.

19.21 Over time planets lose their atmospheres unless they are replenished. A complete analysis of the overall process is very complicated and depends upon the radius of the planet, temperature, atmospheric composition, and other factors. Prove that the atmosphere of planets cannot be in an equilibrium state by demonstrating that the Boltzmann distribution leads to a uniform finite number density as $r \rightarrow \infty$. *Hint.* Recall that in a gravitational field the potential energy is $V(r) = -GMm/r$, where G is the gravitational constant, M is the planet's mass, and m the mass of the particle.

19.22 Consider the distribution of particles in a fluid (liquid) as a function of height in the fluid. Assume the particles have a slightly greater density than the fluid. (a) Show that the potential energy of such a particle is given by $V(h) = v(\rho - \rho_0)gh$, where ρ is the mass density of the particle, and ρ_0 is the mass density of the fluid. (b) Derive a formula for the number density of particles, \mathcal{N} , in the fluid as a function of height. (c) Perrin (1906) found for gamboge gum grains in water with density $1.21 \times 10^3 \text{ kg m}^{-3}$ and volume $1.03 \times 10^{-19} \text{ m}^3$ at 4°C that the number density decreased to half its value at $h = 1.23 \times 10^{-5} \text{ m}$. From this result determine the Boltzmann constant and the Avogadro constant.

19.23 J. Sugar and A. Musgrove (*J. Phys. Chem. Ref. Data* **22**, 1213 (1993)) have published tables of energy levels for germanium atoms and cations from Ge^{+1} to Ge^{+31} . The lowest-lying energy levels in neutral Ge are as follows.


	3P_0	3P_1	3P_2	1D_2	1S_0
E/cm^{-1}	0.0	557.1	1410.0	7125.3	16367.3

Calculate the electronic partition function at 298 K and 1000 K by direct summation. *Hint.* The degeneracy of a level is $2J + 1$.



20

Statistical thermodynamics: the machinery



Fundamental relations

- 20.1 The thermodynamic functions
- 20.2 The molecular partition function

Using statistical thermodynamics

- 20.3 Mean energies
- 20.4 Heat capacities
- 20.5 Equations of state
- 20.6 Residual entropies
- 20.7 Equilibrium constants

Checklist of key ideas

Further reading

Exercises

Problems

In this chapter we apply the concepts of statistical thermodynamics to the calculation of chemically significant quantities. First, we establish the relations between thermodynamic functions and partition functions. Next, we show that the molecular partition function can be factorized into contributions from each mode of motion, and establish the formulas for the partition functions for translational, rotational, vibrational, and electronic modes of motion. These contributions can be calculated from spectroscopic data. Finally, we turn to specific calculations. These applications include the mean energies of modes of motion, the heat capacities of substances, and residual entropies. In the final section, we see how to calculate the equilibrium constant of a reaction and through that calculation understand some of the molecular features that determine the magnitudes of equilibrium constants and their temperature dependence.

A partition function is the bridge between thermodynamics, spectroscopy, and quantum mechanics. Once it is known, it can be used to calculate thermodynamic functions, heat capacities, entropies, and equilibrium constants. It also sheds light on the significance of these properties.

Fundamental relations

In this section we see how all the thermodynamic functions can be obtained once we know the partition function. Then we see how to calculate the molecular partition function, and through that the thermodynamic functions, from spectroscopic data.

19.1 The thermodynamic functions

We have already derived (in Chapter 19) the two expressions for calculating the internal energy and the entropy of a system from its canonical partition function, Q :

$$U - U(0) = - \left(\frac{\partial \ln Q}{\partial \beta} \right)_V \quad S = \frac{U - U(0)}{T} + k \ln Q \quad (1)$$

Table 20.1 Statistical thermodynamic relations

In terms of the canonical partition function Q

$$U - U(0) = - \left(\frac{\partial \ln Q}{\partial \beta} \right)_V$$

$$S = \frac{U - U(0)}{T} + k \ln Q$$

$$A - A(0) = -kT \ln Q$$

$$p = kT \left(\frac{\partial \ln Q}{\partial V} \right)_T$$

$$H - H(0) = - \left(\frac{\partial \ln Q}{\partial \beta} \right)_V + kTV \left(\frac{\partial \ln Q}{\partial V} \right)_T$$

$$G - G(0) = -kT \ln Q + kTV \left(\frac{\partial \ln Q}{\partial V} \right)_T$$

For indistinguishable, independent particles

$$Q = q^N / N!$$

$$U - U(0) = -N \left(\frac{\partial \ln q}{\partial \beta} \right)_V$$

$$S = \frac{U - U(0)}{T} + nR(\ln q - \ln N + 1)$$

$$G - G(0) = -nRT \ln \left(\frac{q_m}{N_A} \right)$$

where q_m is the molar partition function. For distinguishable, independent particles $Q = q^N$

$$U - U(0) = -N \left(\frac{\partial \ln q}{\partial \beta} \right)_V$$

$$S = \frac{U - U(0)}{T} + nR \ln q$$

$$G - G(0) = -nRT \ln q$$

In general, for indistinguishable independent particles,

$$Q = \frac{(q_{\text{external}} q_{\text{internal}})^N}{N!}$$

$$= \frac{(q_{\text{external}})^N}{N!} \times (q_{\text{internal}})^N$$

The thermodynamic functions are then the sums of internal and external (translational) contributions.

where $\beta = 1/kT$. If the molecules are independent, we can go on to make the substitutions $Q = q^N$ (if the molecules are also distinguishable, as in a solid) or $Q = q^N/N!$ (if they are indistinguishable, as in a gas). All the thermodynamic functions introduced in Part 1 are related to U and S , so we have a route to their calculation from Q . For later convenience, the expressions we derive here are collected in Table 20.1.

(a) The Helmholtz energy

The Helmholtz energy, A , is defined as $A = U - TS$. This relation implies that $A(0) = U(0)$, so substitution for U and S by using eqn 1 leads to the very simple expression

$$A - A(0) = -kT \ln Q \quad (2)$$

(b) The pressure

It follows from classical thermodynamics, using an argument like that leading to eqn 5.10,¹ that the pressure, p , and the Helmholtz energy are related by

$$p = - \left(\frac{\partial A}{\partial V} \right)_T \quad (3)$$

Therefore,

$$p = kT \left(\frac{\partial \ln Q}{\partial V} \right)_T \quad (4)$$

This relation is entirely general, and may be used for any type of substance, including perfect gases, real gases, and liquids.

Example 20.1 Deriving an equation of state

Derive an expression for the pressure of a gas of independent particles.

Method We can suspect that the pressure is that given by the perfect gas law. To proceed systematically, substitute the explicit formula for Q for a gas of independent, indistinguishable molecules (see Table 19.1) into eqn 4.

Answer For a gas of independent molecules, $Q = q^N/N!$ with $q = V/\Lambda^3$:

$$p = kT \left(\frac{\partial \ln Q}{\partial V} \right)_T = \frac{kT}{Q} \left(\frac{\partial Q}{\partial V} \right)_T = \frac{NkT}{q} \left(\frac{\partial q}{\partial V} \right)_T \\ = \frac{NkT \Lambda^3}{V} \times \frac{1}{\Lambda^3} = \frac{NkT}{V} = \frac{nRT}{V}$$

To derive this relation, we have used

$$\left(\frac{\partial q}{\partial V} \right)_T = \left(\frac{\partial (V/\Lambda^3)}{\partial V} \right)_T = \frac{1}{\Lambda^3}$$

and $NkT = nN_A kT = nRT$.

Comment The calculation shows that the equation of state of a gas of independent particles is indeed the perfect gas law. This calculation can be regarded as yet another way of deducing that $\beta = 1/kT$.

¹ Specifically, from $A = U - TS$, it follows that $dA = -p dV - S dT$, so $(\partial A / \partial V)_T = -p$.

Self-test 20.1 Derive the equation of state of a sample for which $Q = q^N f/N!$, with $q = V/\Lambda^3$, where f depends on the volume.

$$[p = nRT/V + kT(\partial \ln f / \partial V)_T]$$

(c) The enthalpy

At this stage we can use the expressions for U and p in the definition $H = U + pV$ to obtain an expression for the enthalpy, H , of any substance:

$$H - H(0) = - \left(\frac{\partial \ln Q}{\partial \beta} \right)_V + kTV \left(\frac{\partial \ln Q}{\partial V} \right)_T \quad (5)$$

We have already seen that $U - U(0) = \frac{3}{2}nRT$ for a gas of independent particles (eqn 19.28a), and have just shown that $pV = nRT$. Therefore, for such a gas,²

$$H - H(0) = \frac{5}{2}nRT \quad (6)^\circ$$

(d) The Gibbs energy

One of the most important thermodynamic functions for chemistry is the Gibbs energy, $G = H - TS = A + pV$. We can now express this function in terms of the partition function by combining the expressions for A and p :

$$G - G(0) = -kT \ln Q + kTV \left(\frac{\partial \ln Q}{\partial V} \right)_T \quad (7)$$

This expression takes a simple form for a gas of independent molecules because pV in the expression $G = A + pV$ can be replaced by nRT :

$$G - G(0) = -kT \ln Q + nRT \quad (8)^\circ$$

Furthermore, because $Q = q^N/N!$, and therefore $\ln Q = N \ln q - \ln N!$, it follows that by using Stirling's approximation ($\ln N! \approx N \ln N - N$) we can write

$$\begin{aligned} G - G(0) &= -NkT \ln q + kT \ln N! + nRT \\ &= -nRT \ln q + kT(N \ln N - N) + nRT \\ &= -nRT \ln \left(\frac{q}{N} \right) \end{aligned} \quad (9)^\circ$$

with $N = nN_A$. Now we see another interpretation of the Gibbs energy: it is proportional to the logarithm of the average number of thermally accessible states per molecule.

It will turn out to be convenient to define the molar partition function, $q_m = q/n$ (with units mol^{-1}), for then

$$G - G(0) = -nRT \ln \left(\frac{q_m}{N_A} \right) \quad (10)^\circ$$

20.2 The molecular partition function

The energy of a molecule is the sum of contributions from its different modes of motion:

$$\varepsilon_i = \varepsilon_i^T + \varepsilon_i^R + \varepsilon_i^V + \varepsilon_i^E \quad (11)$$

where T denotes translation, R rotation, V vibration, and E the electronic contribution. This separation is only approximate (except for translation) because the modes are not completely independent, but in most cases it is satisfactory. The separation of the electronic and vibrational motions, for example, is justified by the Born–Oppenheimer approximation

² Recall from Part 1 that we use a superscript $^\circ$ on an equation number to denote a result valid only for a perfect gas.

(Chapter 14), and the separation of the vibrational and rotational modes is valid to the extent that a molecule can be treated as a rigid rotor.

Given that the energy is a sum of independent contributions, the partition function factorizes into a product of contributions (recall Section 19.2b):

$$q = \sum_i e^{-\beta \epsilon_i} = \sum_i e^{-\beta \epsilon_i^T - \beta \epsilon_i^R - \beta \epsilon_i^V - \beta \epsilon_i^E} \\ = \left(\sum_i e^{-\beta \epsilon_i^T} \right) \left(\sum_i e^{-\beta \epsilon_i^R} \right) \left(\sum_i e^{-\beta \epsilon_i^V} \right) \left(\sum_i e^{-\beta \epsilon_i^E} \right) = q^T q^R q^V q^E \quad (12)$$

This factorization means that we can investigate each contribution separately.

(a) The translational contribution

The translational partition function of a molecule of mass m in a container of volume V was derived in Section 19.2:

$$q^T = \frac{V}{\Lambda^3} \quad \Lambda = h \left(\frac{\beta}{2\pi m} \right)^{1/2} = \frac{h}{(2\pi m k T)^{1/2}} \quad (13)$$

Notice that $q^T \rightarrow \infty$ as $T \rightarrow \infty$ because an infinite number of states becomes accessible as the temperature is raised. Even at room temperature $q^T \approx 2 \times 10^{28}$ for an O_2 molecule in a vessel of volume 100 cm^3 .

The thermal wavelength, Λ , lets us judge whether the approximations that led to the expression for q^T are valid. The approximations are valid if many states are occupied, which requires V/Λ^3 to be large. That will be so if Λ is small compared with the linear dimensions of the container. For H_2 at 25°C , $\Lambda = 71 \text{ pm}$, which is far smaller than any conventional container is likely to be (but comparable to pores in zeolites or cavities in clathrates). For O_2 , a heavier molecule, $\Lambda = 18 \text{ pm}$.

(b) The rotational contribution

As demonstrated in Example 19.1, the partition function of a nonsymmetrical (AB) linear rotor is

$$q^R = \sum_J (2J+1) e^{-\beta h c B J(J+1)} \quad (14)$$

The direct method of calculating q^R is to substitute the experimental values of the rotational energy levels into this expression and to sum the series numerically.

Example 20.2 Evaluating the rotational partition function explicitly

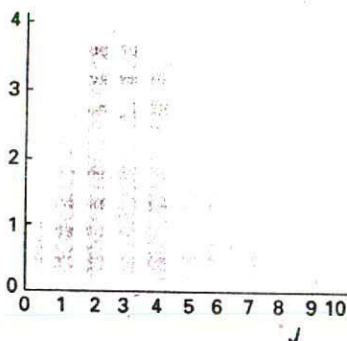
Evaluate the rotational partition function of $^1\text{H}^{35}\text{Cl}$ at 25°C , given that $B = 10.591 \text{ cm}^{-1}$.

Method We use eqn 14, and evaluate it term by term. A useful relation is $kT/hc = 207.22 \text{ cm}^{-1}$ at 298.15 K . The sum is readily evaluated using mathematical software.

Answer To show how successive terms contribute, we draw up the following table using $hcB/kT = 0.05111$ (Fig. 20.1).

J	0	1	2	3	4	...	10
$(2J+1)e^{-0.05111J(J+1)}$	1	2.71	3.68	3.79	3.24	...	0.08

The sum required by eqn 14 (the sum of the numbers in the last row of the table) is 19.9; hence $q^R = 19.9$ at this temperature. Taking J up to 50 gives $q^R = 19.902$.



20.1 The contributions to the rotational partition function of an HCl molecule at 25°C . The vertical axis is the value of $(2J+1)e^{-\beta hcB J(J+1)}$. Successive terms (which are proportional to the populations of the levels) pass through a maximum because the population of individual states decreases exponentially, but the degeneracy of the levels increases with J .

Comment Notice that about ten J -levels are significantly populated but the number of populated states is larger on account of the $(2J + 1)$ -fold degeneracy of each level. We shall shortly encounter the approximation that $q^R \approx kT/hcB$, which in the present case gives $q^R = 19.6$, in good agreement with the exact value, and with much less work.

Self-test 20.2 Evaluate the rotational partition function for HCl at 0°C .

[18.26]

At room temperature $kT/hc \approx 200 \text{ cm}^{-1}$. The rotational constants of many molecules are close to 1 cm^{-1} (Table 16.2) and often smaller. (The very light H_2 molecule, for which $B = 60.9 \text{ cm}^{-1}$, is one exception.) It follows that many rotational levels are populated at normal temperatures. When this is the case, the partition function may be approximated by

$$\begin{aligned} \text{Linear rotors: } q^R &= \frac{kT}{hcB} \\ \text{Nonlinear rotors: } q^R &= \left(\frac{kT}{hc}\right)^{3/2} \left(\frac{\pi}{ABC}\right)^{1/2} \end{aligned} \quad (15)$$

where A , B , and C are the rotational constants of the molecule. However, before using these expressions, read on (to eqns 17 and 20).

Justification 20.1

When many rotational states are occupied and kT is much larger than the separation between neighbouring states, the sum in the partition function can be approximated by an integral, much as we illustrated for translational motion in *Justification 19.4*:

$$q^R = \int_0^\infty (2J + 1)e^{-\beta hcBJ(J+1)} dJ$$

Although this integral looks complicated, it can be evaluated without much effort by noticing that it can also be written as

$$q^R = -\frac{1}{\beta hcB} \int_0^\infty \left(\frac{d}{dJ} e^{-\beta hcBJ(J+1)}\right) dJ$$

Then, because the integral of a derivative of a function is the function itself,

$$q^R = -\frac{1}{\beta hcB} e^{-\beta hcBJ(J+1)} \Big|_0^\infty = \frac{1}{\beta hcB}$$

The calculation for a nonlinear molecule is along the same lines, but slightly trickier (see *Further reading*).

Table 20.2* Rotational and vibrational temperatures

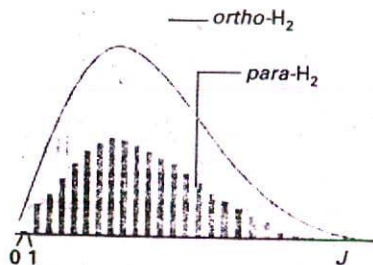
Molecule	Mode	θ_V/K	θ_R/K
H_2		6330	88
HCl		4300	9.4
I_2		309	0.053
CO_2	ν_1	1997	0.561
	ν_2	3380	
	ν_3	960	

*For more values, see Table 16.2 in the *Data section* at the end of this volume, and use $hc/k = 1.439 \text{ K cm}$.

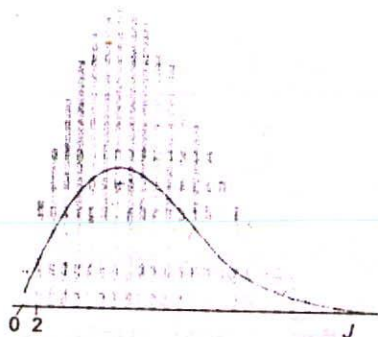
A useful way of expressing the temperature above which the approximation is valid is to introduce the rotational temperature, $\theta_R = hcB/k$. Then 'high temperature' means $T \gg \theta_R$. Some typical values are shown in Table 20.2. The value for H_2 is abnormally high and we must be careful with the approximation for this molecule.

The general conclusion at this stage is that molecules with large moments of inertia (and hence small rotational constants and low rotational temperatures) have large rotational partition functions. The large value of q^R reflects the closeness in energy (compared with kT) of the rotational levels in large, heavy molecules, and the large number of them that are accessible at normal temperatures.

We must take care, however, not to include too many rotational states in the sum. For a homonuclear diatomic molecule or a symmetrical linear molecule (such as CO_2 or $\text{HC}\equiv\text{CH}$), a



20.2 The values of the individual terms $(2J + 1)e^{-\beta hc B J(J+1)}$ contributing to the mean partition function of a 3 : 1 mixture of *ortho*- and *para*-H₂. The partition function is the sum of all these terms. At high temperatures, the sum is approximately equal to the sum of the terms over all values of J , each with a weight of $\frac{1}{2}$. This is the sum of the contributions indicated by the curve.



20.3 The relative populations of the rotational energy levels of CO₂. Only states with even J values are occupied. The full line shows the smoothed, averaged population of levels.

rotation through 180° results in an indistinguishable state of the molecule. Hence, the number of thermally accessible states is only half the number that can be occupied by a heteronuclear diatomic molecule, where rotation through 180° does result in a distinguishable state. Therefore, for a symmetrical linear molecule,

$$q^R = \frac{kT}{2hcB} \quad (16)$$

The equations for symmetrical and nonsymmetrical molecules can be combined into a single expression by introducing the symmetry number, σ , which is the number of indistinguishable orientations of the molecule. Then

$$q^R = \frac{kT}{\sigma hcB} \quad (17)$$

For a heteronuclear diatomic molecule $\sigma = 1$; for a homonuclear diatomic molecule or a symmetrical ($D_{\infty h}$) linear molecule, $\sigma = 2$.

Justification 20.2

The quantum mechanical origin of the symmetry factor is the Pauli principle, which forbids the occupation of certain states. We saw in Section 16.8, for example, that H₂ may occupy rotational states with even J only if its nuclear spins are paired (*para*-hydrogen), and odd J states only if its nuclear spins are parallel (*ortho*-hydrogen). There are three states of *ortho*-H₂ to each value of J (because there are three parallel spin states of the two nuclei).

To set up the rotational partition function we note that 'ordinary' molecular hydrogen is a mixture of one part *para*-H₂ (with only its even- J rotational states occupied) and three parts *ortho*-H₂ (with only its odd- J rotational states occupied). Therefore, the average partition function per molecule is

$$q^R = \frac{1}{4} \left\{ \sum_{\text{even } J} (2J + 1)e^{-\beta hc B J(J+1)} + 3 \sum_{\text{odd } J} (2J + 1)e^{-\beta hc B J(J+1)} \right\} \quad (18)$$

The odd- J states are more heavily weighted than the even- J states (Fig. 20.2). From the illustration we see that we would obtain approximately the same answer for the partition function (the sum of all the populations) if each J term contributed half its normal value to the sum. That is, the last equation can be approximated as

$$q^R = \frac{1}{2} \sum_J (2J + 1)e^{-\beta hc B J(J+1)} \quad (19)$$

and this approximation is very good when many terms contribute (at high temperatures).

The same type of argument may be used for linear symmetrical molecules in which identical bosons are interchanged by rotation (such as CO₂). As pointed out in Section 16.8, if the nuclear spin of the bosons is 0, then only even- J states are admissible. Because only half the rotational states are occupied, the rotational partition function is only half the value of the sum obtained by allowing all values of J to contribute (Fig. 20.3).

The same care must be exercised for other types of symmetrical molecule, and for a nonlinear molecule we write

$$q^R = \frac{1}{\sigma} \left(\frac{kT}{hc} \right)^{3/2} \left(\frac{\pi}{ABC} \right)^{1/2} \quad (20)$$

Some typical values of the symmetry numbers required are given in Table 20.2. The value $\sigma(\text{H}_2\text{O}) = 2$ reflects the fact that a 180° rotation about its C_2 axis interchanges two indistinguishable atoms. In NH₃, there are three indistinguishable orientations around its C_3

axis. For CH_4 , any of three 120° rotations about any of its four C–H bonds leaves the molecule in an indistinguishable state, so the symmetry number is $3 \times 4 = 12$. For benzene, any of six orientations around its C_6 axis leaves it apparently unchanged, as does a rotation of 180° around any of six C_2 axes in the plane of the molecule.

A more formal way of arriving at the value of the symmetry number is to note that σ is the order (the number of elements) of the rotational subgroup of the molecule, the point group of the molecule with all but the identity and the rotations removed. The rotational subgroup of H_2O is $\{E, C_2\}$, so $\sigma = 2$. The rotational subgroup of NH_3 is $\{E, 2C_3\}$, so $\sigma = 3$. This recipe makes it easy to find the symmetry numbers for more complicated molecules. The rotational subgroup of CH_4 is obtained from the T character table as $\{E, 8C_3, 3C_2\}$, so $\sigma = 12$. For benzene, the rotational subgroup of D_{6h} is $\{E, 2C_6, 2C_3, C_2, 3C_2', 3C_2''\}$, so $\sigma = 12$.

Example 20.3 Estimating a rotational partition function

Estimate the rotational partition function of ethene at 25°C given that $A = 4.828 \text{ cm}^{-1}$, $B = 1.0012 \text{ cm}^{-1}$, and $C = 0.8282 \text{ cm}^{-1}$.

Method Use eqn 20 with $kT/hc = 207.226 \text{ cm}^{-1}$. Next, identify the molecular point group (for example, by using the chart in Fig. 15.14 or the shapes in Fig. 15.15). The symmetry number is obtained by deciding on the rotational subgroup of the molecular point group, and counting the number of elements in the group.

Answer The point group of the molecule is D_{2h} . From that group's character table (see the *Data section*), the rotational subgroup of D_{2h} consists of the elements $\{E, C_{2x}, C_{2y}, C_{2z}\}$. The order of this subgroup is 4; therefore $\sigma = 4$. Then, because $ABC = 4.0033 \text{ cm}^{-3}$, it follows that $q^R = 661$.

Comment Ethene is quite a big molecule, the energy levels are close together (compared with kT at room temperature), and many are significantly populated at room temperature.

Self-test 20.3 Evaluate the rotational partition function of pyridine, $\text{C}_5\text{H}_5\text{N}$, at room temperature ($A = 0.2014 \text{ cm}^{-1}$, $B = 0.1936 \text{ cm}^{-1}$, $C = 0.0987 \text{ cm}^{-1}$).

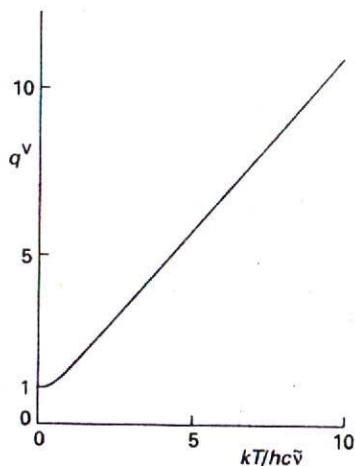
[4.3×10^4]

(c) The vibrational contribution

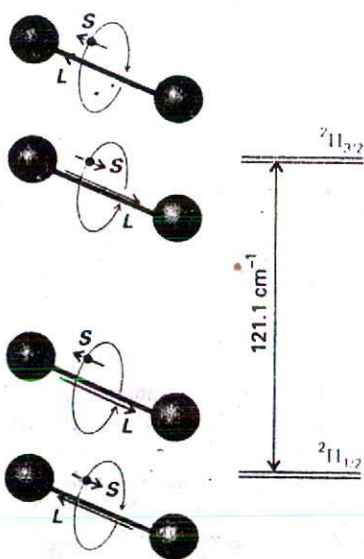
The vibrational partition function of a molecule is calculated by substituting the measured vibrational energy levels into the exponentials appearing in the definition of q^V , and summing them numerically. In a polyatomic molecule each normal mode (Section 16.14) has its own partition function (provided the anharmonicities are so small that the modes are independent). The overall vibrational partition function is the product of the individual partition functions, and we can write $q^V = q^V(1)q^V(2) \dots$, where $q^V(K)$ is the partition function for the K th normal mode and is calculated by direct summation of the observed spectroscopic levels.

Illustration

Given that a typical value of the vibrational partition function of one normal mode is about 1.14, and that a nonlinear molecule containing 10 atoms has $3N - 6 = 24$ normal modes (Section 16.14a), the overall vibrational partition function is approximately



20.4 The vibrational partition function of a molecule in the harmonic approximation. Note that the partition function is linearly proportional to the temperature when the temperature is high ($T \gg \theta_v$).



20.5 The doubly degenerate ground electronic level of NO (with the spin and orbital angular momentum around the axis in opposite directions) and the doubly degenerate first excited level (with the spin and orbital momenta parallel). The upper level is thermally accessible at room temperature.

$q^v \approx (1.1)^{24} = 9.8$. Even though each vibrational mode is not appreciably excited, there may be so many modes in a molecule that overall their excitation is significant.

If the vibrational excitation is not too great, the harmonic approximation may be made, and the vibrational energy levels written as

$$E_v = (v + \frac{1}{2})hc\tilde{\nu} \quad v = 0, 1, 2, \dots \quad (21)$$

If we measure energies from the zero-point level (our general rule), then the permitted values are $\epsilon_v = vhc\tilde{\nu}$ and the partition function is

$$q^v = \sum_v e^{-\beta h c \tilde{\nu} v} = \sum_v (e^{-\beta h c \tilde{\nu}})^v \quad (22)$$

(because $e^{ax} = (e^x)^a$). We met this sum in Example 19.2 (which is no accident: the ladder-like array of levels in Fig. 19.3 is exactly the same as that of a harmonic oscillator). The series can be summed in the same way, and gives

$$q^v = \frac{1}{1 - e^{-\beta h c \tilde{\nu}}} \quad (23)$$

This function is plotted in Fig. 20.4. In a polyatomic molecule, each normal mode gives rise to a partition function of this form.

Example 20.4 Calculating a vibrational partition function

The wavenumbers of the three normal modes of H_2O are 3656.7 cm^{-1} , 1594.8 cm^{-1} , and 3755.8 cm^{-1} . Evaluate the vibrational partition function at 1500 K.

Method Use eqn 23 for each mode, and then form the product of the three contributions. At 1500 K, $kT/hc = 1042.6 \text{ cm}^{-1}$.

Answer We can draw up the following table displaying the contributions of each mode:

Mode:	1	2	3
$\tilde{\nu}/\text{cm}^{-1}$	3656.7	1594.8	3755.8
$hc\tilde{\nu}/kT$	3.507	1.530	3.602
q^v	1.031	1.276	1.028

The overall vibrational partition function is therefore

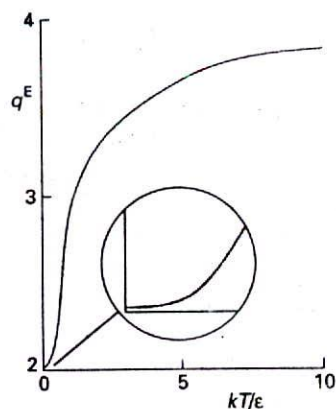
$$q^v = 1.031 \times 1.276 \times 1.028 = 1.353$$

Comment The vibrations of H_2O are at such high wavenumbers that even at 1500 K most of the molecules are in their vibrational ground state.

Self-test 20.4 Repeat the calculation for CO_2 , where the vibrational wavenumbers are 1388 cm^{-1} , 667.4 cm^{-1} , and 2349 cm^{-1} , the second being the doubly degenerate bending mode.

[6.79]

In many molecules the vibrational wavenumbers are so great that $\beta h c \tilde{\nu} > 1$. For example, the lowest vibrational wavenumber of CH_4 is 1306 cm^{-1} , so $\beta h c \tilde{\nu} = 6.3$ at room temperature. C-H stretches normally lie in the range 2850 to 2960 cm^{-1} , so for them $\beta h c \tilde{\nu} \approx 14$. In these cases, $e^{-\beta h c \tilde{\nu}}$ in the denominator of q^v is very close to zero (for example, $e^{-6.3} = 0.002$), and the vibrational partition function for a single mode is very close to 1



20.6 The variation with temperature of the electronic partition function of an NO molecule. Note that the curve resembles that for a two-level system (Fig. 19.5), but rises from 2 (the degeneracy of the lower level) and approaches 4 (the total number of states) at high temperatures.

($q^V = 1.002$ when $\beta hc\bar{\nu} = 6.3$), implying that only the zero-point level is significantly occupied.

Now consider the case of bonds so weak that $\beta hc\bar{\nu} \ll kT$. When this condition is satisfied, the partition function may be approximated by expanding the exponential ($e^x = 1 + x + \dots$):

$$q^V = \frac{1}{1 - (1 - \beta hc\bar{\nu} + \dots)} \quad (24)$$

That is, for weak bonds at high temperatures,

$$q^V = \frac{1}{\beta hc\bar{\nu}} = \frac{kT}{hc\bar{\nu}} \quad (25)$$

The temperatures for which eqn 25 is valid can be expressed in terms of the **vibrational temperature**, $\theta_V = hc\bar{\nu}/k$ (Table 20.2). In terms of the vibrational temperature, 'high temperature' means $T \gg \theta_V$. The value for H_2 is abnormally high because the atoms are so light and the vibrational frequency consequently high.

(d) The electronic contribution

Electronic energy separations from the ground state are usually very large, so for most cases $q^E = 1$. An important exception arises in the case of atoms and molecules having electronically degenerate ground states, in which case $q^E = g_0$, where g_0 is the degeneracy of the electronic ground state. Alkali metal atoms, for example, have doubly degenerate ground states (corresponding to the two orientations of their electron spin), so $q^E = 2$.

Some atoms and molecules have low-lying electronically excited states. (At high enough temperatures, all atoms and molecules have thermally accessible excited states.) An example is NO, which has a configuration of the form $\dots \pi^1$ (the molecule has one electron more than N_2). The orbital angular momentum may take two orientations with respect to the molecular axis (corresponding to circulation clockwise or counter-clockwise around the axis), and the spin angular momentum may also take two, giving four states in all (Fig. 20.5). The energy of the two states in which the orbital and spin momenta are parallel (giving the ${}^2\Pi_{3/2}$ term) is slightly greater than that of the two other states in which they are antiparallel (giving the ${}^2\Pi_{1/2}$ term). The separation, which arises from spin-orbit coupling (Section 13.8), is only 121 cm^{-1} . Hence, at normal temperatures, all four states are thermally accessible. If we denote the energies of the two levels as $E_{1/2} = 0$ and $E_{3/2} = \epsilon$, the partition function is

$$q^E = \sum_{\text{levels } j} g_j e^{-\beta \epsilon_j} = 2 + 2e^{-\beta \epsilon} \quad (26)$$

The variation of this function with temperature is shown in Fig. 20.6. At $T = 0$, $q^E = 2$, because only the doubly degenerate ground state is accessible. At high temperatures, q^E approaches 4 because all four states are accessible. At 25°C , $q^E = 3.1$.

(e) The overall partition function

The partition functions for each mode of motion of a molecule are collected in Table 20.3. The overall partition function is the product of each contribution. For a diatomic molecule with no low-lying electronically excited states and $T \gg \theta_R$,

$$q = g^E \left(\frac{V}{\Lambda^3} \right) \left(\frac{kT}{\sigma hcB} \right) \left(\frac{1}{1 - e^{-\beta hc\bar{\nu}}} \right) \quad (27)$$

Overall partition functions obtained in this way are approximate because they assume that the rotational levels are very close and that the vibrational levels are harmonic. These approximations are avoided by using the energy levels identified spectroscopically and evaluating the sums explicitly.

Table 20.3* Symmetry numbers

Molecule	σ
H_2O	2
NH_3	3
CH_4	12
C_6H_6	12

* For more values, see Table 16.2 in the Data section.

Example 20.5 Calculating a thermodynamic function from spectroscopic data

Calculate the value of $G_m^\ominus - G_m^\ominus(0)$ for $\text{H}_2\text{O}(\text{g})$ at 1500 K given that $A = 27.8778 \text{ cm}^{-1}$, $B = 14.5092 \text{ cm}^{-1}$, and $C = 9.2869 \text{ cm}^{-1}$ and the information in Example 20.4.

Method The starting point is eqn 10. For the standard value, we evaluate the translational partition function at p^\ominus (that is, at 10^5 Pa exactly). The vibrational partition function was calculated in Example 20.4. Use the expressions in Table 20.4 for the other contributions.

Answer For this C_{2v} molecule, $\sigma = 2$. Because $m = 18.015 \text{ u}$, $q_m^\ominus = 1.706 \times 10^8 \text{ mol}^{-1}$. For the vibrational contribution we have already found that $q^V = 1.352$. For the rotational contribution, $q^R = 486.7$. Therefore,

$$\begin{aligned} G_m^\ominus - G_m^\ominus(0) &= -(8.3145 \text{ J K}^{-1} \text{ mol}^{-1}) \times (1500 \text{ K}) \\ &\quad \times \ln \left(\frac{(1.706 \times 10^8 \text{ mol}^{-1}) \times 486.7 \times 1.352}{6.02214 \times 10^{23} \text{ mol}^{-1}} \right) \\ &= -365.6 \text{ kJ mol}^{-1} \end{aligned}$$

Self-test 20.5 Repeat the calculation for CO_2 . The vibrational data are given in Self-test 20.4; $B = 0.3902 \text{ cm}^{-1}$.

[$-366.6 \text{ kJ mol}^{-1}$]

Table 20.4 Contributions to the molecular partition function*

Translation

$$\begin{aligned} q &= \frac{V}{\Lambda^3} \quad \Lambda = \left(\frac{h^2 \beta}{2\pi m} \right)^{1/2} \\ \Lambda/\text{pm} &= \frac{1749}{(T/\text{K})^{1/2} (M/\text{g mol}^{-1})^{1/2}} \\ \frac{q_m^\ominus}{N_A} &= \frac{kT}{p^\ominus \Lambda^3} = 2.561 \times 10^{-2} (T/\text{K})^{5/2} (M/\text{g mol}^{-1})^{3/2} \end{aligned}$$

Rotation

(a) Linear molecules

$$q = \frac{1}{\sigma hcB\beta} = \frac{0.6950}{\sigma} \times \frac{T/\text{K}}{(B/\text{cm}^{-1})}$$

(b) Non-linear molecules

$$q = \frac{1}{\sigma} (1/hc\beta)^{2/3} \left(\frac{\pi}{ABC} \right)^{1/2} = \frac{1.0270}{\sigma} \times \frac{(T/\text{K})^{3/2}}{(ABC/\text{cm}^{-3})^{1/2}}$$

Vibration

$$q = \frac{1}{1 - e^{-hc\tilde{\nu}\beta}} = \frac{1}{1 - e^{-a}} \quad a = \frac{1.4388(\tilde{\nu}/\text{cm}^{-1})}{T/\text{K}}$$

Electronic

$$q = g_0$$

where g_0 is the degeneracy of the electronic ground state (when that is the only accessible level); at high temperatures, evaluate q explicitly.

* $\beta = 1/kT$. It is often useful to note that

$$\frac{hc}{k} = 1.43879 \text{ cm K}$$

See also inside front cover for further information.

Using statistical thermodynamics

Any thermodynamic quantity can now be calculated from a knowledge of the energy levels of molecules: we have merged thermodynamics and spectroscopy. In this section, we indicate how to do the calculations for a number of important properties.

20.3 Mean energies

It is often useful to know the mean energy, $\langle \epsilon \rangle$, of various modes of motion. When the molecular partition function can be factorized into contributions from each mode, the mean energy of each mode M is

$$\langle \epsilon^M \rangle = -\frac{1}{q^M} \left(\frac{\partial q^M}{\partial \beta} \right)_V \quad M = T, R, V, \text{ or } E \quad (28)$$

(a) The mean translational energy

To see a pattern emerging, we consider first a one-dimensional system of length X, for which $q^T = X/\Lambda$, with $\Lambda \approx h(\beta/2\pi m)^{1/2}$. Then, if we note that Λ is a constant times $\beta^{1/2}$,

$$\langle \epsilon^T \rangle = -\frac{A}{X} \left(\frac{\partial X}{\partial \beta \Lambda} \right)_V = -\beta^{1/2} \frac{d}{d\beta} \left(\frac{1}{\beta^{1/2}} \right) = \frac{1}{2\beta} = \frac{1}{2}kT \quad (29)$$

For a molecule free to move in three dimensions, the analogous calculation leads to

$$\langle \epsilon^T \rangle = \frac{3}{2}kT \quad (30)$$

Both conclusions are in agreement with the classical equipartition theorem (see the *Introduction*), that the mean energy of each quadratic contribution to the energy is $\frac{1}{2}kT$. Furthermore, the fact that the mean energy is independent of the size of the container is consistent with the thermodynamic result that internal energy of a perfect gas is independent of its volume (Section 5.1b).

(b) The mean rotational energy

The mean rotational energy of a linear molecule is obtained from the partition function given in eqn 14. When the temperature is low ($T < \theta_R$), the series must be summed term by term, which gives

$$q^R = 1 + 3e^{-2\beta hcB} + 5e^{-6\beta hcB} + \dots$$

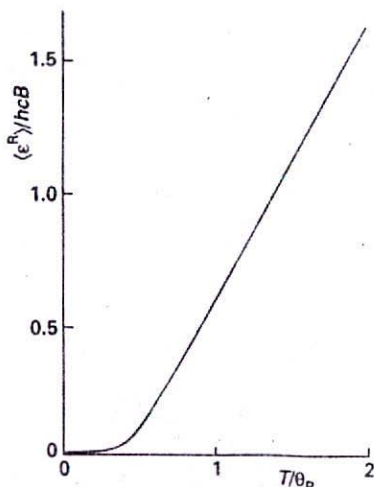
Hence

$$\langle \epsilon^R \rangle = \frac{hcB(6e^{-2\beta hcB} + 30e^{-6\beta hcB} + \dots)}{1 + 3e^{-2\beta hcB} + 5e^{-6\beta hcB} + \dots} \quad (31)$$

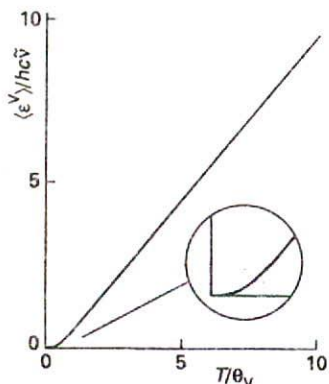
This function is plotted in Fig. 20.7. At high temperatures ($T \gg \theta_R$), q^R is given by eqn 17, and

$$\langle \epsilon^R \rangle = -\frac{1}{q^R} \frac{dq^R}{d\beta} = -\sigma hc\beta B \frac{d}{d\beta} \frac{1}{\sigma hc\beta B} = \frac{1}{\beta} = kT \quad (32)$$

(q^R is independent of V , so the partial derivatives have been replaced by complete derivatives.) The high-temperature result is also in agreement with the equipartition theorem, for the classical expression for the energy of a linear rotor is $E_K = \frac{1}{2}I_{\perp}\omega_a^2 + \frac{1}{2}I_{\perp}\omega_b^2$. (There is no rotation around the line of atoms.) It follows from the equipartition theorem that the mean rotational energy is $2 \times \frac{1}{2}kT = kT$.



20.7 The mean rotational energy of a nonsymmetrical linear rotor as a function of temperature. At high temperatures ($T \gg \theta_R$), the energy is linearly proportional to the temperature, in accord with the equipartition theorem.



20.8 The mean vibrational energy of a molecule in the harmonic approximation as a function of temperature. At high temperatures ($T \gg \theta_V$), the energy is linearly proportional to the temperature, in accord with the equipartition theorem.

(c) The mean vibrational energy

The vibrational partition function in the harmonic approximation is given in eqn 23. Because q^V is independent of the volume, it follows that

$$\frac{dq^V}{d\beta} = \frac{d}{d\beta} \left(\frac{1}{1 - e^{-\beta hc\tilde{\nu}}} \right) = -\frac{hc\tilde{\nu}e^{-\beta hc\tilde{\nu}}}{(1 - e^{-\beta hc\tilde{\nu}})^2} \quad (33)$$

and hence that

$$\langle \epsilon^V \rangle = \frac{hc\tilde{\nu}}{e^{\beta hc\tilde{\nu}} - 1} \quad (34)$$

The zero-point energy, $\frac{1}{2}hc\tilde{\nu}$, can be added to the right-hand side if the mean energy is to be measured from 0 rather than the lowest attainable level (the zero-point level). The variation of the mean energy with temperature is illustrated in Fig. 20.8.

At high temperatures, when $T \gg \theta_V$, or $\beta hc\tilde{\nu} \ll 1$, the exponential functions can be expanded ($e^x = 1 + x + \dots$) and all but the leading terms discarded. This approximation leads to

$$\langle \epsilon^V \rangle = \frac{hc\tilde{\nu}}{(1 + \beta hc\tilde{\nu} + \dots) - 1} \approx \frac{1}{\beta} = kT \quad (35)$$

This result is in agreement with the value predicted by the classical equipartition theorem, because the energy of a one-dimensional oscillator is $E = \frac{1}{2}mv_x^2 + \frac{1}{2}kx^2$ and the mean value of each quadratic term is $\frac{1}{2}kT$.

20.4 Heat capacities

The constant-volume heat capacity is defined as $C_V = (\partial U / \partial T)_V$. The derivative with respect to T is converted into a derivative with respect to β by using

$$\frac{d}{dT} = \left(\frac{d\beta}{dT} \right) \frac{d}{d\beta} = -\frac{1}{kT^2} \frac{d}{d\beta} = -k\beta^2 \frac{d}{d\beta} \quad (36)$$

It follows that

$$C_V = -k\beta^2 \left(\frac{\partial U}{\partial \beta} \right)_V \quad (37)$$

Because the internal energy of a perfect gas is a sum of contributions, the heat capacity is also a sum of contributions from each mode. The contribution of mode M is

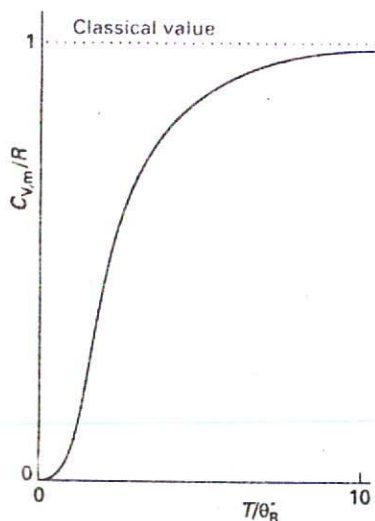
$$C_V^M = N \left(\frac{\partial \langle \epsilon^M \rangle}{\partial T} \right)_V = -Nk\beta^2 \left(\frac{\partial \langle \epsilon^M \rangle}{\partial \beta} \right)_V \quad (38)$$

(a) The individual contributions

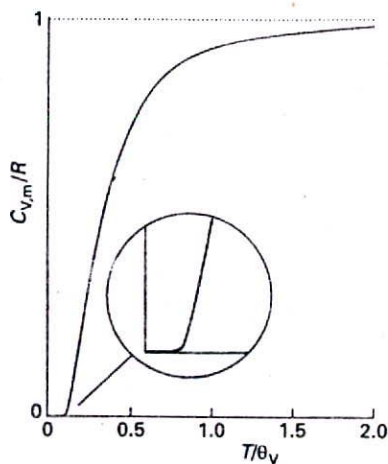
The temperature is always high enough (provided the gas is above its condensation temperature) for the mean translational energy to be $\frac{3}{2}kT$, the equipartition value. Therefore, the molar constant-volume heat capacity is

$$C_{V,m}^T = N_A \frac{d(\frac{3}{2}kT)}{dT} = \frac{3}{2}R \quad (39)$$

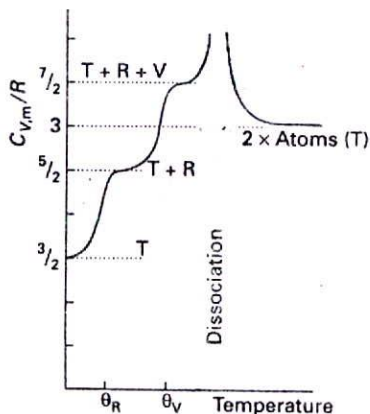
Translation is the only mode of motion for a monatomic gas, so for such a gas $C_{V,m} = \frac{3}{2}R = 12.47 \text{ J K}^{-1} \text{ mol}^{-1}$. This result is very reliable: helium, for example, has this



20.9 The temperature dependence of the rotational contribution to the heat capacity of a linear molecule.



20.10 The temperature dependence of the vibrational heat capacity of a molecule in the harmonic approximation calculated by using eqn 41. Note that the heat capacity is within 10 per cent of its classical value for temperatures greater than θ_V .



20.11 The general features of the temperature dependence of the heat capacity of diatomic molecules are as shown here. Each mode becomes active when its characteristic temperature is exceeded. The heat capacity becomes very large when the molecule dissociates because the energy is used to cause dissociation and not to raise the temperature. Then it falls back to the translational value of the atoms.

value over a range of 2000 K. We saw in Section 3.3a that $C_{p,m} - C_{v,m} = R$, so for a monatomic perfect gas $C_{p,m} = \frac{5}{2}R$, and therefore

$$\gamma = \frac{C_p}{C_v} = \frac{5}{3} \quad (40)^\circ$$

When the temperature is high enough for the rotations of the molecules to be highly excited (when $T \gg \theta_R$), we can use the equipartition value kT for the mean rotational energy (for a linear rotor) to obtain $C_{v,m} = R$. For nonlinear molecules, the mean rotational energy rises to $\frac{3}{2}kT$, so the molar rotational heat capacity rises to $\frac{3}{2}R$ when $T \gg \theta_R$. Only the lowest rotational state is occupied when the temperature is very low, and then rotation does not contribute to the heat capacity. We can calculate the rotational heat capacity at intermediate temperatures by differentiating the equation for the mean rotational energy (eqn 31). The resulting (untidy) expression, which is plotted in Fig. 20.9, shows that the contribution rises from zero (when $T = 0$) to the equipartition value (when $T \gg \theta_R$). Because the translational contribution is always present, we can expect the molar heat capacity of a gas of diatomic molecules ($C_{v,m}^T + C_{v,m}^R$) to rise from $\frac{3}{2}R$ to $\frac{5}{2}R$ as the temperature is increased above θ_R .

Molecular vibrations contribute to the heat capacity, but only when the temperature is high enough for them to be significantly excited. The equipartition mean energy is kT for each mode, so the maximum contribution to the molar heat capacity is R . However, it is very unusual for the vibrations to be so highly excited that equipartition is valid, and it is more appropriate to use the full expression for the vibrational heat capacity, which is obtained by differentiating eqn 34:

$$C_{v,m}^V = Rf^2 \quad f = \frac{\theta_V}{T} \left(\frac{e^{-\theta_V/2T}}{1 - e^{-\theta_V/T}} \right) \quad (41)$$

where $\theta_V = hc\bar{\nu}/k$ is the vibrational temperature. The curve in Fig. 20.10 shows how the vibrational heat capacity depends on temperature. Note that even when the temperature is only slightly above the vibrational temperature the heat capacity is close to its equipartition value.³

(b) The overall heat capacity

The total heat capacity of a molecular substance is the sum of each contribution (Fig. 20.11). When equipartition is valid (when the temperature is well above the characteristic temperature of the mode, $T \gg \theta_M$) we can estimate the heat capacity by counting the numbers of modes that are active. In gases, all three translational modes are always active, and contribute $\frac{3}{2}R$ to the molar heat capacity. If we denote the number of active rotational modes by ν_R^* (so for most molecules at normal temperatures $\nu_R^* = 2$ for linear molecules, and 3 for nonlinear molecules), then the rotational contribution is $\frac{1}{2}\nu_R^*R$. If the temperature is high enough for ν_V^* vibrational modes to be active, the vibrational contribution to the molar heat capacity is ν_V^*R . In most cases $\nu_V^* \approx 0$. It follows that the total molar heat capacity is

$$C_{v,m} = \frac{1}{2}(3 + \nu_R^* + 2\nu_V^*)R \quad (42)$$

Example 20.6 Estimating the molar heat capacity of a gas

Estimate the molar constant-volume heat capacity of water vapour at 100°C. Vibrational wavenumbers are given in Example 20.4; the rotational constants of an H_2O molecule are 27.9, 14.5, and 9.3 cm^{-1} .

³ Equation 41 is essentially the same as the Einstein formula for the heat capacity of a solid (eqn 11.9) with θ_V the Einstein temperature, θ_E . The only difference is that vibrations can take place in three dimensions in a solid.

Method We need to assess whether the rotational and vibrational modes are active by computing their characteristic temperatures from the data (to do so, use $hc/k = 1.439 \text{ cm K}$).

Answer The characteristic temperatures (in round numbers) of the vibrations are 5300 K, 2300 K, and 5400 K; the vibrations are therefore not excited at 373 K. The three rotational modes have characteristic temperatures 40 K, 21 K, and 13 K, so they are fully excited, like the three translational modes. The translational contribution is $\frac{3}{2}R = 12.5 \text{ JK}^{-1} \text{ mol}^{-1}$. Fully excited rotations contribute a further $12.5 \text{ JK}^{-1} \text{ mol}^{-1}$. Therefore, a value close to $25 \text{ JK}^{-1} \text{ mol}^{-1}$ is predicted.

Comment The experimental value is $26.1 \text{ JK}^{-1} \text{ mol}^{-1}$. The discrepancy is probably due to deviations from perfect gas behaviour.

Self-test 20.6 Estimate the molar constant-volume heat capacity of gaseous I_2 at 25°C ($B = 0.037 \text{ cm}^{-1}$; see Table 16.2 for more data).

[$21 \text{ JK}^{-1} \text{ mol}^{-1}$]

20.5 Equations of state

The canonical partition function, Q , is a function of the volume and the temperature of the system and the number of molecules it contains. Therefore, eqn 4 for the pressure in terms of the partition function has the form $p = f(n, V, T)$. That is, eqn 4 is an equation of state. The relation between p and Q is a very important route to the equations of state of real gases in terms of intermolecular forces, for the latter can be built into Q .

We have already seen (Example 20.1) that the partition function for a gas of independent particles leads to the perfect gas equation of state, $pV = nRT$. Real gases differ from perfect gases in their equations of state and we saw in Section 1.4b that their equations of state may be written

$$\frac{pV_m}{RT} = 1 + \frac{B}{V_m} + \frac{C}{V_m^2} + \dots \quad (43)$$

where B is the second virial coefficient and C is the third virial coefficient.

The total kinetic energy of a gas is the sum of the kinetic energies of the individual molecules. Therefore, even in a real gas the canonical partition function factorizes into a part arising from the kinetic energy, which is the same as for the perfect gas, and a factor called the **configuration integral**, Z , which depends on the intermolecular potentials. We therefore write

$$Q = \frac{Z}{\Lambda^{3N}} \quad (44)$$

By comparing this equation with eqn 19.46b ($Q = q^N/N!$, with $q = V/\Lambda^3$), we see that for a perfect gas

$$Z = \frac{V^N}{N!} \quad (45)$$

For a real gas, Z is related to the total potential energy \mathcal{V} of interaction of all the particles by

$$Z = \frac{1}{N!} \int e^{-\beta\mathcal{V}} dr_1 dr_2 \dots dr_N \quad (46)$$

Illustration

When the molecules do not interact with one another, $\mathcal{V} = 0$, and hence $e^{-\beta\mathcal{V}} = 1$. Then

$$Z = \frac{1}{N!} \int d\mathbf{r}_1 d\mathbf{r}_2 \cdots d\mathbf{r}_N = \frac{V^N}{N!}$$

because $\int d\mathbf{r} = V$, where V is the volume of the container. This result coincides with eqn 45.

When we consider only interactions between pairs of particles the configuration integral simplifies to

$$Z = \frac{1}{2} \int e^{-\beta\mathcal{V}} d\mathbf{r}_1 d\mathbf{r}_2 \quad (47)$$

The second virial coefficient then turns out to be

$$B = -\frac{1}{2} \frac{N_A}{V} \int f d\mathbf{r}_1 d\mathbf{r}_2 \quad f = e^{-\beta\mathcal{V}} - 1 \quad (48)$$

The quantity f is the Mayer f -function: it goes to zero when the two particles are so far apart that $\mathcal{V} = 0$. When the intermolecular interaction depends only on the separation r of the particles and not on their relative orientation, as in the interaction of closed-shell atoms and tetrahedral and octahedral molecules, eqn 48 simplifies to

$$B = -2\pi N_A \int_0^\infty f r^2 dr \quad (49)$$

The integral can be evaluated (usually numerically) by substituting an expression for the intermolecular potential energy.

Intermolecular potential energies are discussed in more detail in Chapter 22, where several expressions are developed for them. At this stage, we can illustrate how eqn 49 is used by considering the **hard-sphere potential**, which is infinite when the separation of the two molecules, r , is less than or equal to a certain value σ , and is zero for greater separations. Then

$$\begin{aligned} e^{-\beta\mathcal{V}} &= 0 & f &= -1 & \text{when } r \leq \sigma \text{ (and } \mathcal{V} = \infty) \\ e^{-\beta\mathcal{V}} &= 1 & f &= 0 & \text{when } r > \sigma \text{ (and } \mathcal{V} = 0) \end{aligned} \quad (50)$$

It follows from eqn 49 that the second virial coefficient is

$$B = 2\pi N_A \int_0^\sigma r^2 dr = \frac{2}{3}\pi N_A \sigma^3 \quad (51)$$

This calculation of B raises the question as to whether a potential can be found which, when the virial coefficients are evaluated, gives the van der Waals equation of state. Such a potential can be found: it consists of a hard-sphere repulsive core and a long-range, shallow attractive region. A further point is that, once a second virial coefficient has been calculated for a given intermolecular potential, it is possible to calculate other thermodynamic properties that depend on the form of the potential. For example, it is possible to calculate the isothermal Joule-Thomson coefficient, μ_T (Section 3.2c), from the thermodynamic relation

$$\lim_{p \rightarrow 0} \mu_T = B - T \frac{dB}{dT} \quad (52)$$

and from the result calculate the Joule-Thomson coefficient itself by using eqn 3.19.

20.6 Residual entropies

Entropies may be calculated from spectroscopic data; they may also be measured experimentally (Section 4.3d). In many cases there is good agreement, but in some the experimental entropy is less than the calculated value. One possibility is that the experimental determination failed to take a phase transition into account (and a term of the form $\Delta_{\text{trs}}H/T_{\text{trs}}$ incorrectly omitted from the sum). Another possibility is that some disorder is present in the solid even at $T = 0$. The entropy at $T = 0$ is then greater than zero, and is called the **residual entropy**.

The origin and magnitude of the residual entropy can be explained by considering a crystal composed of AB molecules, where A and B are similar atoms (such as CO, with its very small electric dipole moment). There may be so little energy difference between ...AB AB AB AB..., ...AB BA BA AB..., and other random arrangements that the molecules adopt either orientation at random in the solid. We can readily calculate the entropy arising from residual disorder by using the Boltzmann formula $S = k \ln W$. To do so, we suppose that two orientations are equally probable, and that the sample consists of N molecules. Because the same energy can be achieved in 2^N different ways (because each molecule can take either of two orientations), the total number of ways of achieving the same energy is $W = 2^N$. It follows that

$$S = k \ln 2^N = Nk \ln 2 = nR \ln 2 \quad (53)$$

We can therefore expect a residual molar entropy of $R \ln 2 = 5.8 \text{ J K}^{-1} \text{ mol}^{-1}$ for solids composed of molecules that can adopt either of two orientations at $T = 0$. If s orientations are possible, the residual molar entropy will be

$$S_m = R \ln s \quad (54)$$

An FCIO_3 molecule, for example, can adopt four orientations with about the same energy, and the calculated residual molar entropy of $R \ln 4 = 11.5 \text{ J K}^{-1} \text{ mol}^{-1}$ is in good agreement with the experimental value ($10.1 \text{ J K}^{-1} \text{ mol}^{-1}$). For CO, the measured residual entropy is $5 \text{ J K}^{-1} \text{ mol}^{-1}$, which is close to $R \ln 2$, the value expected for a random structure of the form ...CO CO OC CO OC OC...

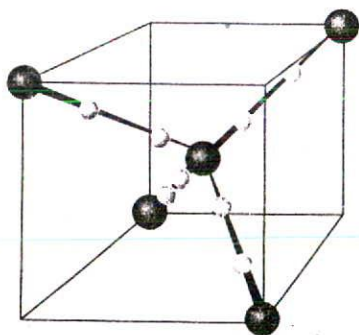
The residual entropy of ice is $3.4 \text{ J K}^{-1} \text{ mol}^{-1}$. This value can be explained in terms of the hydrogen-bonded structure of the solid. Each O atom is surrounded tetrahedrally by four H atoms, two of which are attached by short σ bonds, the other two being attached by long hydrogen bonds (Fig. 20.12). The randomness lies in which two of the four bonds are short, and an approximate analysis (see the *Justification* below) leads to $S_m(0) \approx R \ln \frac{3}{2} = 3.4 \text{ J K}^{-1} \text{ mol}^{-1}$, in good agreement with the experimental value.

Justification 20.3

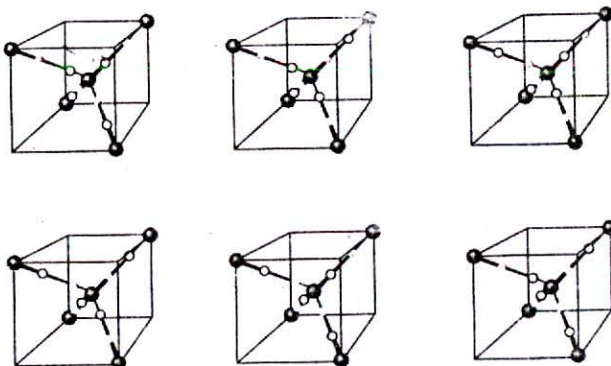
Consider a sample of ice that consists of N H_2O molecules. Each of the $2N$ H atoms can be in one of two positions: either close to or far from an O atom (Fig. 20.13). There are therefore 2^{2N} possible arrangements. However, not all these arrangements are acceptable. Indeed, of the $2^4 = 16$ ways of arranging four H atoms around one O atom, only six have two short and two long OH distances and hence are acceptable. Therefore, the number of permitted arrangements is

$$W = 2^{2N} \left(\frac{6}{16}\right)^N = \left(\frac{3}{2}\right)^N$$

It then follows that the residual molar entropy is $R \ln(3/2)$, as stated in the text.



20.12 The possible locations of H atoms around a central O atom in an ice crystal are shown by the spheres. Only one of the locations on each bond may be occupied by an atom, and two H atoms must be close to the O atom and two H atoms must be distant from it.



20.13 The six possible arrangements of H atoms in the locations identified in Fig. 20.12.

20.7 Equilibrium constants

The Gibbs energy of a gas of independent molecules is given by eqn 10 in terms of the molar partition function, $q_m = q/n$. The equilibrium constant K of a reaction is related to the standard Gibbs energy of reaction by $\Delta_r G^\ominus = -RT \ln K$. To calculate the equilibrium constant, we must combine these two equations. We shall consider gas-phase reactions in which the equilibrium constant is expressed in terms of the partial pressures of the reactants and products.

(a) The relation between K and the partition function

To find an expression for the standard reaction Gibbs energy we need expressions for the standard molar Gibbs energies, G^\ominus/n , of each species. For these expressions, we need the value of the molar partition function when $p = p^\ominus$ (where $p^\ominus = 1$ bar): we denote this standard molar partition function q_m^\ominus . Because only the translational component depends on the pressure, we can find q_m^\ominus by evaluating the partition function with V replaced by V_m^\ominus , where $V_m^\ominus = RT/p^\ominus$. For a species J it follows that

$$G_{J,m}^\ominus = G_{J,m}^\ominus(0) - RT \ln \left(\frac{q_{J,m}^\ominus}{N_A} \right) \quad (55)$$

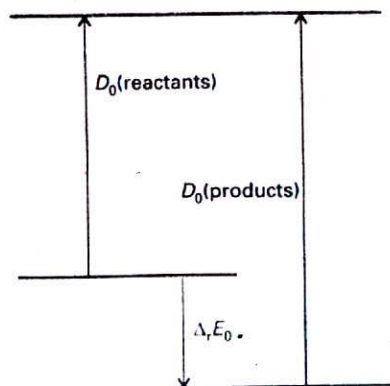
where $q_{J,m}^\ominus$ is the standard molar partition function of J . By combining expressions like this one (as shown in the *Justification* below), it turns out that the equilibrium constant for the reaction



is given by the expression

$$K = \frac{(q_{C,m}^\ominus/N_A)^c (q_{D,m}^\ominus/N_A)^d}{(q_{A,m}^\ominus/N_A)^a (q_{B,m}^\ominus/N_A)^b} e^{-\Delta_r E_0/RT} \quad (56)$$

where $\Delta_r E_0$ is the difference in molar energies of the ground states of the products and reactants (this term is defined more precisely in the *Justification*), and is calculated from the bond dissociation energies of the species (Fig. 20.14).



20.14 The definition of $\Delta_r E_0$ for the calculation of equilibrium constants.

Justification 20.4

The standard molar reaction Gibbs energy for the reaction is

$$\begin{aligned}\Delta_r G^\ominus &= cG_{C,m}^\ominus + dG_{D,m}^\ominus - aG_{A,m}^\ominus - bG_{B,m}^\ominus \\ &= cG_{C,m}^\ominus(0) + dG_{D,m}^\ominus(0) - aG_{A,m}^\ominus(0) - bG_{B,m}^\ominus(0) \\ &\quad - RT \left\{ c \ln \left(\frac{q_{C,m}^\ominus}{N_A} \right) + d \ln \left(\frac{q_{D,m}^\ominus}{N_A} \right) - a \ln \left(\frac{q_{A,m}^\ominus}{N_A} \right) - b \ln \left(\frac{q_{B,m}^\ominus}{N_A} \right) \right\}\end{aligned}$$

Because $G(0) = U(0)$, the first term on the right is

$$\Delta_r E_0 = cU_{C,m}^\ominus(0) + dU_{D,m}^\ominus(0) - aU_{A,m}^\ominus(0) - bU_{B,m}^\ominus(0) \quad (57)$$

the reaction internal energy at $T = 0$ (a molar quantity).

Now we can write

$$\begin{aligned}\Delta_r G^\ominus &= \Delta_r E_0 - RT \left\{ \ln \left(\frac{q_{C,m}^\ominus}{N_A} \right)^c + \ln \left(\frac{q_{D,m}^\ominus}{N_A} \right)^d \right. \\ &\quad \left. - \ln \left(\frac{q_{A,m}^\ominus}{N_A} \right)^a - \ln \left(\frac{q_{B,m}^\ominus}{N_A} \right)^b \right\} \\ &= \Delta_r E_0 - RT \ln \left\{ \frac{(q_{C,m}^\ominus/N_A)^c (q_{D,m}^\ominus/N_A)^d}{(q_{A,m}^\ominus/N_A)^a (q_{B,m}^\ominus/N_A)^b} \right\} \\ &= -RT \left\{ -\frac{\Delta_r E_0}{RT} + \ln \left\{ \frac{(q_{C,m}^\ominus/N_A)^c (q_{D,m}^\ominus/N_A)^d}{(q_{A,m}^\ominus/N_A)^a (q_{B,m}^\ominus/N_A)^b} \right\} \right\}\end{aligned}$$

At this stage we can pick out an expression for K by comparing this equation with $\Delta_r G^\ominus = -RT \ln K$, which gives

$$\ln K = -\frac{\Delta_r E_0}{RT} + \ln \left\{ \frac{(q_{C,m}^\ominus/N_A)^c (q_{D,m}^\ominus/N_A)^d}{(q_{A,m}^\ominus/N_A)^a (q_{B,m}^\ominus/N_A)^b} \right\}$$

This expression is easily rearranged into eqn 56 by taking antilogarithms of both sides.⁴

(b) A dissociation equilibrium

We shall illustrate the application of eqn 56 to an equilibrium in which a diatomic molecule X_2 dissociates into its atoms:



According to eqn 56 (with $a = 1$, $b = 0$, $c = 2$, and $d = 0$):

$$K = \frac{(q_{X,m}^\ominus/N_A)^2}{q_{X_2,m}^\ominus/N_A} e^{-\Delta_r E_0/RT} = \frac{(q_{X,m}^\ominus)^2}{q_{X_2,m}^\ominus N_A} e^{-\Delta_r E_0/RT} \quad (59)$$

with

$$\Delta_r E_0 = 2U_{X,m}^\ominus(0) - U_{X_2,m}^\ominus(0) = D_0(X-X) \quad (60)$$

where $D_0(X-X)$ is the dissociation energy of the $X-X$ bond.

⁴ In terms of the general chemical equation for a reaction, eqn 2.40, we would write

$$K = \left\{ \prod_i \left(\frac{q_i^\ominus}{N_A} \right)^{\nu_i} \right\} e^{-\Delta_r E_0/RT}$$

The standard molar partition functions of the atoms X are

$$q_{X,m}^{\ominus} = g_X \left(\frac{V_m^{\ominus}}{A_X^3} \right) = \frac{RTg_X}{p^{\ominus} A_X^3}$$

because $V_m^{\ominus} = RT/p^{\ominus}$; g_X is the degeneracy of the electronic ground state of X. The diatomic molecule X_2 also has rotational and vibrational degrees of freedom, so its standard molar partition function is

$$q_{X_2,m}^{\ominus} = g_{X_2} \left(\frac{V_m^{\ominus}}{A_{X_2}^3} \right) q_{X_2}^R q_{X_2}^V = \frac{RTg_{X_2} q_{X_2}^R q_{X_2}^V}{p^{\ominus} A_{X_2}^3}$$

where g_{X_2} is the degeneracy of the electronic ground state of X_2 . It follows that the equilibrium constant is

$$K = \frac{kTg_X^2 A_X^3}{p^{\ominus} g_{X_2} q_{X_2}^R q_{X_2}^V A_X^6} e^{-D_0/RT} \quad (61)$$

where we have used $R/N_A = k$, the Boltzmann constant. All the quantities in this expression can be calculated from spectroscopic data. The A s are defined in Table 20.4 and depend on the masses of the species and the temperature; the expressions for the rotational and vibrational partition functions are also available in Table 20.4 and depend on the rotational constant and vibrational wavenumber of the molecule.

Example 20.7 Evaluating an equilibrium constant

Evaluate the equilibrium constant for the dissociation $\text{Na}_2(\text{g}) \rightleftharpoons 2\text{Na}(\text{g})$ at 1000 K from the following data: $B = 0.1547 \text{ cm}^{-1}$, $\tilde{\nu} = 159.2 \text{ cm}^{-1}$, $D_0 = 70.4 \text{ kJ mol}^{-1}$. The Na atoms have doublet ground terms.

Method The partition functions required are specified in eqn 61. They are evaluated by using the expressions in Table 20.4. For a homonuclear diatomic molecule, $\sigma = 2$. In the evaluation of kT/p^{\ominus} use $p^{\ominus} = 10^5 \text{ Pa}$ and $1 \text{ Pa m}^3 = 1 \text{ J}$.

Answer The partition functions and other quantities required are as follows:

$$\begin{aligned} A(\text{Na}_2) &= 8.14 \text{ pm} & A(\text{Na}) &= 11.5 \text{ pm} \\ q^R(\text{Na}_2) &= 2246 & q^V(\text{Na}_2) &= 4.885 \\ g(\text{Na}) &= 2 & g(\text{Na}_2) &= 1 \end{aligned}$$

Then, from eqn 61

$$\begin{aligned} K &= \frac{(1.38 \times 10^{-23} \text{ J K}^{-1}) \times (1000 \text{ K}) \times 4 \times (8.14 \times 10^{-12} \text{ m})^3}{(10^5 \text{ Pa}) \times 2246 \times 4.885 \times (1.15 \times 10^{-11} \text{ m})^6} \times e^{-\epsilon} \\ &= 2.42 \end{aligned}$$

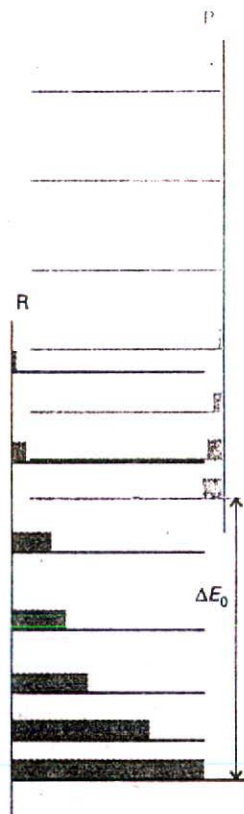
Comment For conversion to an equilibrium constant in terms of molar concentrations, use $[J] = p_J/RT$.

Self-test 20.7 Evaluate K at 1500 K.

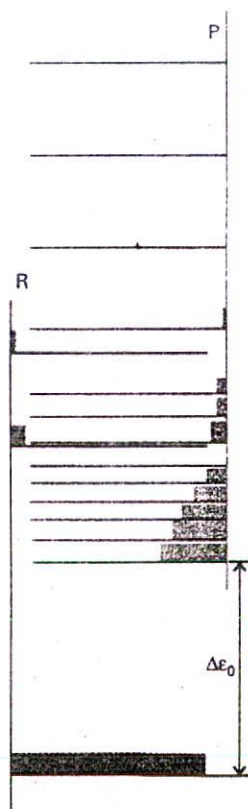
(c) Contributions to the equilibrium constant

We are now in a position to appreciate the physical basis of equilibrium constants. To see what is involved, consider a simple $R \rightleftharpoons P$ gas-phase equilibrium (R for reactants, P for products).

Figure 20.15 shows two sets of energy levels; one set of states belongs to R, and the other belongs to P. The populations of the states are given by the Boltzmann distribution, and are independent of whether any given state happens to belong to R or to P. We can therefore imagine a single Boltzmann distribution spreading, without distinction, over the two sets of states. If the spacings of R and P are similar (as in Fig. 20.15), and P lies above R, the diagram indicates that R will dominate in the equilibrium mixture. However, if P has a high density of states (a large number of states in a given energy range, as in Fig. 20.16) then, even though its zero-point energy lies above that of R, the species P might still dominate at equilibrium.



20.15 The array of R(ectants) and P(roducts) energy levels. At equilibrium all are accessible (to differing extents, depending on the temperature), and the equilibrium composition of the system reflects the overall Boltzmann distribution of populations. As ΔE_0 increases, R becomes dominant.



20.16 It is important to take into account the densities of states of the molecules. Even though P might lie well above R in energy (that is, ΔE_0 is large and positive), P might have so many states that its total population dominates in the mixture. In classical thermodynamic terms, we have to take entropies into account as well as enthalpies when considering equilibria.

It is quite easy to show (see the *Justification* below) that the ratio of numbers of R and P molecules at equilibrium is given by

$$\frac{N_P}{N_R} = \frac{q_P}{q_R} e^{-\Delta_r E_0/RT} \quad (62)$$

and therefore that the equilibrium constant for the reaction is

$$K = \frac{q_P}{q_R} e^{-\Delta_r E_0/RT} \quad (63)$$

just as would be obtained from eqn 56.⁵

Justification 20.5

The population in a state i of the composite (R, P) system is

$$n_i = \frac{N e^{-\beta \epsilon_i}}{q}$$

where N is the total number of molecules. The total number of R molecules is the sum of these populations taken over the states belonging to R; these states we label r with energies ϵ_r . The total number of P molecules is the sum over the states belonging to P; these states we label p with energies ϵ'_p (the prime is explained in a moment):

$$N_R = \sum_r n_r = \frac{N}{q} \sum_r e^{-\beta \epsilon_r} \quad N_P = \sum_p n_p = \frac{N}{q} \sum_p e^{-\beta \epsilon'_p}$$

The sum over the states of R is its partition function, q_R , so

$$N_R = \frac{N q_R}{q}$$

The sum over the states of P is also a partition function, but the energies are measured from the ground state of the *combined* system, which is the ground state of R. However, because $\epsilon'_p = \epsilon_p + \Delta \epsilon_0$, where $\Delta \epsilon_0$ is the separation of zero-point energies (as in Fig. 20.16),

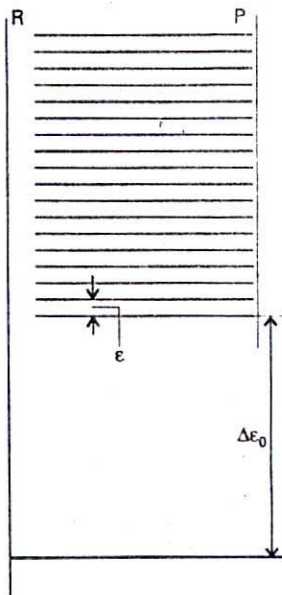
$$N_P = \frac{N}{q} \sum_p e^{-\beta(\epsilon_p + \Delta \epsilon_0)} = \frac{N}{q} \left(\sum_p e^{-\beta \epsilon_p} \right) e^{-\beta \Delta \epsilon_0} = \frac{N q_P}{q} e^{-\Delta_r E_0/RT}$$

The switch from $\Delta \epsilon_0/k$ to $\Delta_r E_0/R$ in the last step is the conversion of molecular energies to molar energies.

The equilibrium constant of the $R \rightleftharpoons P$ reaction is proportional to the ratio of the numbers of the two types of molecule. Therefore,

$$K = \frac{N_P}{N_R} = \frac{q_P}{q_R} e^{-\Delta_r E_0/RT}$$

as in eqn 63.



20.17 The model used in the text for exploring the effects of energy separations and densities of states on equilibria. The products P can dominate provided $\Delta \epsilon_0$ is not too large and that P has an appreciable density of states.

The content of eqn 63 can be seen most clearly by exaggerating the molecular features that contribute to it. We shall suppose that R has only a single accessible level, which implies that $q_R = 1$. We also suppose that P has a large number of evenly, closely spaced levels (Fig. 20.17). The partition function of P is then $q_P = kT/\epsilon$. In this model system, the

5 For an $R \rightleftharpoons P$ equilibrium, the V factors in the partition functions cancel, so the appearance of q in place of q^\ominus has no effect. In the case of a more general reaction, the conversion from q to q^\ominus comes about at the stage of converting the pressures that occur in K to numbers of molecules.

equilibrium constant is

$$K = \frac{kT}{\varepsilon} e^{-\Delta_r E_0/RT} \quad (64)$$

When $\Delta_r E_0$ is very large, the exponential term dominates and $K \ll 1$, which implies that very little P is present at equilibrium. When $\Delta_r E_0$ is small but still positive, K can exceed 1 because the factor kT/ε may be large enough to overcome the small size of the exponential term. The size of K then reflects the predominance of P at equilibrium on account of its high density of states. At low temperatures $K \ll 1$, and the system consists entirely of R. At high temperatures the exponential function approaches 1 and the pre-exponential factor is large. Hence P becomes dominant. We see that, in this endothermic reaction (endothermic because P lies above R), a rise in temperature favours P, because its states become accessible. This behaviour is what we saw, from the outside, in Chapter 9.

The model also shows why the Gibbs energy, G , and not just the enthalpy, determines the position of equilibrium. It shows that the density of states (and hence the entropy) of each species as well as their relative energies controls the distribution of populations and hence the value of the equilibrium constant.

Checklist of key ideas

Fundamental relations

20.1 The thermodynamic functions

- see Table 20.1
- molar partition function (10)

20.2 The molecular partition function

- see Table 20.4

- rotational temperature
- symmetry number
- rotational subgroup
- vibrational temperature

Using statistical thermodynamics

20.3 Mean energies

- mean energy of a mode (28)

20.4 Heat capacities

- heat capacity of a mode (38)
- overall heat capacity (42)

20.5 Equations of state

- configuration integral
- Mayer f -function (48)
- hard-sphere potential (50)

20.6 Residual entropies

- residual entropy (54)

20.7 Equilibrium constants

- standard molar partition function
- equilibrium constant (56)

Further reading

Articles of general interest

- C.W. David, A tractable model for studying solution thermodynamics. *J. Chem. Educ.* **64**, 484 (1987).
- R.A. Alberty, The effect of a catalyst on the thermodynamic properties and partition functions of a group of isomers. *J. Chem. Educ.* **65**, 409 (1988).
- M. Ross, Equations of state. In *Encyclopedia of applied physics* (ed. G.L. Trigg), **6**, 291. VCH New York (1993).

- T.L. Hill, *An introduction to statistical mechanics*. Dover, New York (1986).
- N. Davidson, *Statistical thermodynamics*. McGraw-Hill, New York (1962).
- K. Lucas, *Applied statistical thermodynamics*. Springer-Verlag, New York (1991).
- D. Chandler, *Introduction to statistical mechanics*. Oxford University Press (1987).
- C.E. Hecht, *Statistical mechanics and kinetic theory*. W.H. Freeman & Co, New York (1990).

Texts and sources of data and information

- A. Ben-Naim, *Statistical thermodynamics for chemists and biologists*. Plenum, New York (1992).

Exercises

- 20.1 (a)** Use the equipartition theorem to estimate the constant-volume molar heat capacity of (a) I_2 , (b) CH_4 , (c) C_6H_6 in the gas phase at 25°C.
- 20.1 (b)** Use the equipartition theorem to estimate the constant-volume molar heat capacity of (a) O_3 , (b) C_2H_6 , (c) CO_2 in the gas phase at 25°C.
- 20.2 (a)** Estimate the value of $\gamma = C_p/C_v$ for gaseous ammonia and methane. Do this calculation with and without the vibrational contribution to the energy. Which is closer to the expected experimental value at 25°C?
- 20.2 (b)** Estimate the value of $\gamma = C_p/C_v$ for carbon dioxide. Do this calculation with and without the vibrational contribution to the energy. Which is closer to the expected experimental value at 25°C?
- 20.3 (a)** Estimate the rotational partition function of HCl at (a) 25°C and (b) 250°C.
- 20.3 (b)** Estimate the rotational partition function of O_2 at (a) 25°C and (b) 250°C.
- 20.4 (a)** Give the symmetry number for each of the following molecules: (a) CO, (b) O_2 , (c) H_2S , (d) SiH_4 , and (e) $CHCl_3$.
- 20.4 (b)** Give the symmetry number for each of the following molecules: (a) CO_2 , (b) O_3 , (c) SO_3 , (d) SF_6 , and (e) Al_2Cl_6 .
- 20.5 (a)** Calculate the rotational partition function of H_2O at 298 K from its rotational constants 27.878 cm^{-1} , 14.509 cm^{-1} , and 9.287 cm^{-1} . Above what temperature is the high-temperature approximation valid?
- 20.5 (b)** Calculate the rotational partition function of SO_2 at 298 K from its rotational constants 2.02736 cm^{-1} , 0.34417 cm^{-1} , and 0.293535 cm^{-1} . Above what temperature is the high-temperature approximation valid?
- 20.6 (a)** From the results of Exercise 20.5a, calculate the rotational contribution to the molar entropy of gaseous water at 25°C.
- 20.6 (b)** From the results of Exercise 20.5b, calculate the rotational contribution to the molar entropy of sulfur dioxide at 25°C.
- 20.7 (a)** Calculate the rotational partition function of CH_4 (a) by direct summation of the energy levels at 298 K and 500 K, and (b) by the high-temperature approximation. Take $B = 5.2412 \text{ cm}^{-1}$.
- 20.7 (b)** Calculate the rotational partition function of CH_3CN (a) by direct summation of the energy levels at 298 K and 500 K, and (b) by the high-temperature approximation. Take $A = 5.28 \text{ cm}^{-1}$ and $B = 0.307 \text{ cm}^{-1}$.
- 20.8 (a)** The bond length of O_2 is 120.75 pm. Use the high-temperature approximation to calculate the rotational partition function of the molecule at 300 K.
- 20.8 (b)** The NOF molecule is an asymmetric rotor with rotational constants 3.1752 cm^{-1} , 0.3951 cm^{-1} , and 0.3505 cm^{-1} . Calculate the rotational partition function of the molecule at (a) 25°C, (b) 100°C.
- 20.9 (a)** Plot the molar heat capacity of a collection of harmonic oscillators as a function of T/θ_v , and predict the vibrational heat capacity of ethyne at (a) 298 K, (b) 500 K. The normal modes (and their degeneracies in parentheses) occur at wavenumbers 612(2), 729(2), 1974, 3287, and 3374 cm^{-1} .
- 20.9 (b)** Plot the molar entropy of a collection of harmonic oscillators as a function of T/θ_v , and predict the standard molar entropy of ethyne at (a) 298 K, (b) 500 K. For data, see the preceding exercise.
- 20.10 (a)** A CO_2 molecule is linear, and its vibrational wavenumbers are 1388.2 cm^{-1} , 667.4 cm^{-1} , and 2349.2 cm^{-1} , the last being doubly degenerate and the others non-degenerate. The rotational constant of the molecule is 0.3902 cm^{-1} . Calculate the rotational and vibrational contributions to the molar Gibbs energy at 298 K.
- 20.10 (b)** An O_3 molecule is angular, and its vibrational wavenumbers are 1110 cm^{-1} , 705 cm^{-1} , and 1042 cm^{-1} . The rotational constants of the molecule are 3.553 cm^{-1} , 0.4452 cm^{-1} , and 0.3948 cm^{-1} . Calculate the rotational and vibrational contributions to the molar Gibbs energy at 298 K.
- 20.11 (a)** The ground level of Cl is $^2P_{3/2}$ and a $^2P_{1/2}$ level lies 881 cm^{-1} above it. Calculate the electronic contribution to the heat capacity of Cl atoms at (a) 500 K and (b) 900 K.
- 20.11 (b)** The first electronically excited state of O_2 is $^1\Delta_g$ and lies 7918.1 cm^{-1} above the ground state, which is $^3\Sigma_g^-$. Calculate the electronic contribution to the molar Gibbs energy of O_2 at 400 K.
- 20.12 (a)** The ground state of the Co^{2+} ion in $CoSO_4 \cdot 7H_2O$ may be regarded as $^4T_{9/2}$. The entropy of the solid at temperatures below 1 K is derived almost entirely from the electron spin. Estimate the molar entropy of the solid at these temperatures.
- 20.12 (b)** Estimate the contribution of the spin to the molar entropy of a solid sample of a d -metal complex with $S = \frac{5}{2}$.
- 20.13 (a)** Calculate the residual molar entropy of a solid in which the molecules can adopt (a) three, (b) five, (c) six orientations of equal energy at $T = 0$.
- 20.13 (b)** Suppose that the hexagonal molecule $C_6H_nF_{6-n}$ has a residual entropy on account of the similarity of the H and F atoms. Calculate the residual for each value of n .
- 20.14 (a)** An average human DNA molecule has 5×10^8 binucleotides (rungs on the DNA ladder) of four different kinds. If each rung were a random choice of one of these four possibilities, what would be the residual entropy associated with this typical DNA molecule?
- 20.14 (b)** Calculate the standard molar entropy of $N_2(g)$ at 298 K from its rotational constant $B = 1.9987 \text{ cm}^{-1}$ and its vibrational wavenumber $\tilde{\nu} = 2358 \text{ cm}^{-1}$. The thermochemical value is 192.1 $J K^{-1} \text{ mol}^{-1}$. What does this suggest about the solid at $T = 0$?
- 20.15 (a)** Calculate the equilibrium constant of the reaction $I_2(g) \rightleftharpoons 2I(g)$ at 1000 K from the following data for I_2 : $\tilde{\nu} = 214.36 \text{ cm}^{-1}$, $B = 0.0373 \text{ cm}^{-1}$, $D_e = 1.5422 \text{ eV}$. The ground state of the I atoms is $^2P_{3/2}$, implying fourfold degeneracy.
- 20.15 (b)** Calculate the value of K at 298 K for the gas-phase isotopic exchange reaction $2^{79}Br^{81}Br \rightleftharpoons ^{79}Br^{79}Br + ^{81}Br^{81}Br$. The Br_2 molecule has a non-degenerate ground state, with no other electronic states nearby. Base the calculation on the wavenumber of the vibration of $^{79}Br^{81}Br$, which is 323.33 cm^{-1} .

Problems

Numerical problems

20.1 The NO molecule has a doubly degenerate electronic ground state and a doubly degenerate excited state at 121.1 cm^{-1} . Calculate the electronic contribution to the molar heat capacity of the molecule at (a) 50 K, (b) 298 K, and (c) 500 K.

20.2 Explore whether a magnetic field can influence the heat capacity of a paramagnetic molecule by calculating the electronic contribution to the heat capacity of an NO_2 molecule in a magnetic field. Estimate the total constant-volume heat capacity using equipartition, and calculate the percentage change in heat capacity brought about by a 5.0 T magnetic field at (a) 50 K, (b) 298 K.

20.3 The energy levels of a CH_3 group attached to a larger fragment are given by the expression for a particle on a ring, provided the group is rotating freely. What is the high-temperature contribution to the heat capacity and the entropy of such a freely rotating group at 25°C ? The moment of inertia of CH_3 about its C_3 axis is $5.341 \times 10^{-47} \text{ kg m}^2$.

20.4 Calculate the temperature dependence of the heat capacity of $p\text{-H}_2$ (in which only rotational states with even values of J are populated) at low temperatures on the basis that its rotational levels $J = 0$ and $J = 2$ constitute a system that resembles a two-level system except for the degeneracy of the upper level. Use $B = 60.864 \text{ cm}^{-1}$ and sketch the heat capacity curve. The experimental heat capacity of $p\text{-H}_2$ does in fact show a peak at low temperatures.

20.5 The pure rotational microwave spectrum of HCl has absorption lines at the following wavenumbers (in cm^{-1}): 21.19, 42.37, 63.56, 84.75, 105.93, 127.12, 148.31, 169.49, 190.68, 211.87, 233.06, 254.24, 275.43, 296.62, 317.80, 338.99, 360.18, 381.36, 402.55, 423.74, 444.92, 466.11, 487.30, 508.48. Calculate the rotational partition function at 25°C by direct summation.

20.6 Calculate and plot as a function of temperature, in the range 300 K to 1000 K, the equilibrium constant for the reaction $\text{CD}_4(\text{g}) + \text{HCl}(\text{g}) \rightleftharpoons \text{CHD}_3(\text{g}) + \text{DCI}(\text{g})$ using the following data (numbers in parentheses are degeneracies): $\bar{\nu}(\text{CHD}_3)/\text{cm}^{-1} = 2993(1), 2142(1), 1003(3), 1291(2), 1036(2)$; $\bar{\nu}(\text{CD}_4)/\text{cm}^{-1} = 2109(1), 1092(2), 2259(3), 996(3)$; $\bar{\nu}(\text{HCl})/\text{cm}^{-1} = 2991$; $\bar{\nu}(\text{DCI})/\text{cm}^{-1} = 2145$; $B(\text{HCl})/\text{cm}^{-1} = 10.59$; $B(\text{DCI})/\text{cm}^{-1} = 5.445$; $B(\text{CHD}_3)/\text{cm}^{-1} = 3.28$; $A(\text{CHD}_3)/\text{cm}^{-1} = 2.63$; $B(\text{CD}_4)/\text{cm}^{-1} = 2.63$.

20.7 The exchange of deuterium between acid and water is an important type of equilibrium, and we can examine it by using spectroscopic data on the molecules. Calculate the equilibrium constant at (a) 298 K and (b) 800 K for the gas-phase exchange reaction $\text{H}_2\text{O} + \text{DCI} \rightleftharpoons \text{HDO} + \text{HCl}$ from the following data: $\bar{\nu}(\text{H}_2\text{O})/\text{cm}^{-1} = 3656.7, 1594.8, 3755.8$; $\bar{\nu}(\text{HDO})/\text{cm}^{-1} = 2726.7, 1402.2, 3707.5$; $A(\text{H}_2\text{O})/\text{cm}^{-1} = 27.88$, $B(\text{H}_2\text{O})/\text{cm}^{-1} = 14.51$, $C(\text{H}_2\text{O})/\text{cm}^{-1} = 9.29$; $A(\text{HDO})/\text{cm}^{-1} = 23.38$, $B(\text{HDO})/\text{cm}^{-1} = 9.102$, $C(\text{HDO})/\text{cm}^{-1} = 6.417$; $B(\text{HCl})/\text{cm}^{-1} = 10.59$; $B(\text{DCI})/\text{cm}^{-1} = 5.449$; $\bar{\nu}(\text{HCl})/\text{cm}^{-1} = 2991$; $\bar{\nu}(\text{DCI})/\text{cm}^{-1} = 2145$.

Theoretical problems

20.8 Derive the Sackur-Tetrode equation for a monatomic gas confined to a two-dimensional surface, and hence derive an expression for the standard molar entropy of condensation to form a mobile surface film.

20.9 Derive expressions for the internal energy, heat capacity, entropy, Helmholtz energy, and Gibbs energy of a harmonic oscillator. Express the results in terms of the vibrational temperature, θ_v and plot graphs of each property against T/θ_v .

20.10 Although expressions like $\langle \epsilon \rangle = -d \ln q / d\beta$ are useful for formal manipulations in statistical thermodynamics, and for expressing thermodynamic functions in neat formulas, they are sometimes more trouble than they are worth in practical applications. When presented with a table of energy levels, it is often much more convenient to evaluate the following sums directly:

$$q = \sum_j e^{-\beta \epsilon_j}, \quad \bar{q} = \sum_j \beta \epsilon_j e^{-\beta \epsilon_j}, \quad \bar{q}^2 = \sum_j (\beta \epsilon_j)^2 e^{-\beta \epsilon_j}$$

(a) Derive expressions for the internal energy, heat capacity, and entropy in terms of these three functions. (b) Apply the technique to the calculation of the electronic contribution to the constant volume molar heat capacity of magnesium vapour at 5000 K using the following data:

Term	1S	3P_0	3P_1	3P_2	1P_1	3S
Degeneracy	1	1	3	5	3	3
$\bar{\nu}/\text{cm}^{-1}$	0	21850	21870	21911	35051	41197

20.11 Determine whether a magnetic field can influence the value of an equilibrium constant. Consider the equilibrium $\text{I}_2(\text{g}) \rightleftharpoons 2\text{I}(\text{g})$ at 1000 K, and calculate the ratio of equilibrium constants $K(B)/K$, where $K(B)$ is the equilibrium constant when a magnetic field B is present and removes the degeneracy of the four states of the $^2P_{3/2}$ level. Data on the species are given in Exercise 20.15a. The electronic g -value of the atoms is $\frac{4}{3}$. Calculate the field required to change the equilibrium constant by 1 per cent.

20.12 The heat capacity ratio of a gas determines the speed of sound in it through the formula

$$c_s = \left(\frac{\gamma RT}{M} \right)^{1/2}$$

where $\gamma = C_p/C_v$ and M is the molar mass of the gas. Deduce an expression for the speed of sound in a perfect gas of (a) diatomic, (b) linear triatomic, (c) nonlinear triatomic molecules at high temperatures (with translation and rotation active). Estimate the speed of sound in air at 25°C .

Additional problems supplied by Carmen Giunta and Charles Trapp

20.13 For H_2 , at very low temperatures, only the translational contribution to the heat capacity is observed. At temperatures above $\theta_R = hcB/k$, the rotational contribution to the heat capacity becomes significant. At still higher temperatures, above $\theta_V = hv/k$, the vibrations contribute. But at this latter temperature, dissociation of the molecule into the atoms must be considered. (a) Explain the origin of the expressions for θ_R and θ_V , and calculate their values for hydrogen. (b) Obtain an expression for the molar constant-pressure heat capacity of hydrogen at all temperatures taking into account the dissociation of hydrogen. (c) Make a plot of the molar constant-pressure heat capacity as a function of temperature in the high-temperature region where dissociation of the molecule is significant.

20.14 J.G. Dojahn, E.C.M. Chen, and W.E. Wentworth (*J. Phys. Chem.* 100, 9649 (1996)) characterized the potential energy curves of the ground and electronic states of homonuclear diatomic halogen anions. The ground state of F_2^- is $^2\Sigma_u^+$ with a fundamental vibrational wavenumber of 450.0 cm^{-1} and equilibrium internuclear distance of 190.0 pm . The first two excited states are at 1.609 and 1.702 eV above the ground state. Compute the standard molar entropy of F_2^- at 298 K .

20.15 R. Viswanathan, R.W. Schmude, Jr, and K.A. Gingerich (*J. Phys. Chem.* 100, 10784 (1996)) studied thermodynamic properties of several boron-silicon gas-phase species experimentally and theoretically. These species can occur in the high-temperature chemical vapour deposition of silicon-based semiconductors. Among the computations they reported was computation of the Gibbs function of $BSi(g)$ at several temperatures based on a $^4\Sigma^-$ ground state with equilibrium internuclear distance of 190.5 pm and fundamental vibrational wavenumber of 772 cm^{-1} and a 2P_0 first excited level 8000 cm^{-1} above the ground level. Compute the standard molar Gibbs function $G_m^\ominus(2000\text{ K}) - G_m^\ominus(0)$.

20.16 In a spectroscopic study of the fullerene C_{60} , F. Negri, G. Orlandi, and F. Zerbetto (*J. Phys. Chem.* 100, 10849 (1996))

reviewed the wavenumbers of all the vibrational modes of the molecule. The wavenumber for the single A_g mode is 976 cm^{-1} ; wavenumbers for the four threefold degenerate T_{1u} modes are 525 , 578 , 1180 , and 1430 cm^{-1} ; wavenumbers for the five threefold degenerate T_{2g} modes are 354 , 715 , 1037 , 1190 , and 1540 cm^{-1} ; wavenumbers for six fourfold degenerate G_g modes are 345 , 757 , 776 , 963 , 1315 , and 1410 cm^{-1} ; and wavenumbers for the seven fivefold degenerate H_u modes are 403 , 525 , 667 , 738 , 1215 , 1342 , and 1566 cm^{-1} . How many modes have a vibrational temperature θ_V below 1000 K ? Estimate the molar constant-volume heat capacity of C_{60} at 1000 K , counting as active all modes with θ_V below this temperature.

20.17 J. Hutter, H.P. Lüthi, and F. Diederich (*J. Amer. Chem. Soc.* 116, 750 (1994)) examined the geometric and vibrational structure of several carbon molecules of formula C_n . Given that the ground state of C_3 , a molecule found in interstellar space and in flames, is a bent singlet with moments of inertia 39.340 , 39.032 , and 0.3082 u \AA^2 and with vibrational wavenumbers of 63.4 , 1224.5 , and 2040 cm^{-1} , compute $G_m^\ominus(10.00\text{ K}) - G_m^\ominus(0)$ and $G_m^\ominus(1000\text{ K}) - G_m^\ominus(0)$ for C_3 .

20.18 The molecule Cl_2O_2 , which is believed to participate in the seasonal depletion of ozone over Antarctica, has been studied by several means. M. Birk, R.R. Friedl, E.A. Cohen, H.M. Pickett, and S.P. Sander (*J. Chem. Phys.* 91, 6588 (1989)) report its rotational constants (actually cB) as $13\,109.4$, 2409.8 , and 2139.7 MHz . They also report that its rotational spectrum indicates a molecule with a symmetry number of 2.19 . J. Jacobs, M. Kronberg, H.S.P. Möller, and H. Willner (*J. Amer. Chem. Soc.* 116, 1106 (1994)) report its vibrational wavenumbers as 753 , 542 , 310 , 127 , 646 , and 419 cm^{-1} . Compute $G_m^\ominus(200\text{ K}) - G_m^\ominus(0)$ of Cl_2O_2 .

20.19 (a) Show that the number of molecules in any given rotational state of a linear molecule is given by $N_J = C(2J + 1)e^{-hcBJ(J+1)/kT}$, where C is a constant. (b) Use this result to prove eqn 16.45 for the J value of the most highly populated rotational energy level. (c) Estimate the temperature at which the spectrum of HCl shown in Fig. 16.40 was taken.